DISS. ETH NO. 26539

The Multifaceted Functions of TDP-43 in Schwann Cells and Oligodendrocytes

A thesis submitted to attain the degree of
DOCTOR OF SCIENCES of ETH ZURICH
(Dr. sc. ETH Zurich)

presented by
Sven Bachofner

MSc ETH Biology,
ETH Zurich

born on 23.02.1989

citizen of
Zurich ZH, Switzerland

accepted on the recommendation of

Prof. Dr. Ueli Suter
Prof. Dr. Sabine Werner
Prof. Dr. Claire Jacob

2020

to my family

to Katja

Acknowledgment

First and foremost, I express my special gratitude to *Prof. Dr. Ueli Suter* for giving me the opportunity to perform this project in his group. I deeply appreciate his support and the scientific freedom he provided me to contribute shaping the project.

I would like to thank my co-referees *Prof. Dr. Sabine Werner* and *Prof. Dr. Claire Jacob* for providing support and give valuable feedback to the project.

I was lucky to share the lab with great colleagues: *Jorge Pereira* already supervised my master thesis, and continued to be a teacher and pillar of support throughout my doctoral studies. *Joanne Gerber*, a brilliant technician who performed countless quantifications. *Jennifer Keller*, a talented former master student who joined my project and delivered a great mood to the lab. *Cristina Fimiani* provided support at any occasion although it took me a long time to learn how to correctly spell her name (it's not C**h**ristina!). I would like to express my appreciation to *Monica Ghidinelli*, my long-term bench-neighbour. I learned a lot from her expertise, and it was a pleasure to work next to her while sharing the good (and sometimes bad) mood. *Ned Mantei*, an expert in molecular biology, provided his experienced advice, and shared great stories from earlier times in the lab. I thank all the present and past members of the Suter lab for giving their support and good company. My special thanks go to *Dr. Klaus Toyka*, an expert in electrophysiology.

I am also grateful to the following members of the ETH phenomics center (EPIC), the infrastructure team of the institute and the functional genomics centre (FGCZ): *Alex Cajamarca*, *Roger Staub*, *Sabrina Isler*, *Sanja Vasic* and *Susanne Freedrich* spent a lot of time and energy to take care of the animals. *Rolf Huber*, *Claudia Stucki*, *Giorgio Giordano*, *Ruth Kugler* and *Rita Ziörjen* for handling all the work "behind the curtains". *Catharine Aquino*, *Lennart Opitz*, *Emilio Yángüez* and *Ge Tan* provided their expertise and support for the transcriptomic analysis.

I was lucky to share my time outside of ETH with great people. I thank all members of the *Turnverein Effretikon* for keeping me (as good as possible) in shape and provide excellent company. I have to thank my fellow officers and sergeants for the time I experienced during four weeks in every year of my doctoral studies, which not only provided job variation and sleep deprivation, but also great comradeship.

Finally, I am deeply thankful for the most important people: My parents *Christoph* and *Karin Bachofner* unconditionally supported me throughout my entire life, my big brother *Marc Bachofner* for being a role model and great friend, and my grandparents *Oskar* and *Lilly Rahm* for their love and care. I can not express my gratitude enough for *Katja Brancher*, who closely accompanied me during my journey with all her love and selfless support.

Contributions

The presented work was accomplished as a team effort, here I report the major scientific and experimental contributions by collaborating colleagues. Most notably I received a lot of support by colleagues in the Suter Lab: *Jorge Pereira* performed the preparation and acquisition by SEM, supported the electrophysiological analysis, substantially contributed to scientific discussions and provided feedback for the thesis. *Ned Mantei* provided valuable feedback and proofread the thesis. *Joanne Gerber* contributed to many experiments throughout the thesis, including behavioural assessments, dissections, sample processing and image analysis. *Cristina Fimiani* provided support for tissue dissection and substantially contributed to the analysis of *mpz*-iKO experiments including nerve regeneration. *Jennifer Keller* mainly contributed to the analysis of *cnp*-cKO and *plp*-iKO mice, but also supported the examination of *mpz*-cKO mice. The electrophysiological experiments were performed and analysed by *Dr. Klaus Toyka*. The function genomics center Zurich (FGCZ) provided the platform and experts for the RNA sequencing analysis: Bulk RNA sequencing was performed by *Catharine Aquino* (wet-lab, supported by *Jay Tracy*) and *Lennart Opitz* (bioinformatic analysis and support). Single-cell RNA sequencing was performed by *Emilio Yángüez* (wet-lab, supported by *Dahlia Schatzmann*) and *Ge Tan* (raw bioinformatic processing and support).

Contents

Part I

Summary, Introduction and Methods

1. Summary

TAR-DNA binding protein 43 (TDP-43) is an RNA binding protein, which regulates a broad spectrum of RNA biology. It is mainly implicated in alternative splicing, transcript stability and transport. In the past years, TDP-43 has emerged as a guardian against aberrant retention of intronic sequences into the mature transcript (cryptic splicing). Pathological aggregation of TDP-43 in the cytoplasm of motor neurons, along with its nuclear clearance, is a hallmark of amyotrophic lateral sclerosis (ALS), a fast progressing, fatal neurodegenerative disease. There are indications that TDP-43 is required in myelination-competent glial cells, and these cells are known to modulate neuronal health. In this study, we investigated the functional role of TDP-43 in both myelination-competent glia, Schwann cells (SCs) and oligodendrocytes (OLs), during development and in adult mice using the Cre/loxP-system.

We show that TDP-43 is required in SCs for timely-onset of developmental myelination and remyelination after injury. Functionally, TDP-43 is required to repress cryptic splicing in glial *neurofascin*, which enables proper formation of paranodal domains and healthy electrophysiological nerve function. In adult SCs, TDP-43 protects the SC myelinated state and axonal health, with particular emphasis on large calibre axons. Sciatic nerves are less dependent on TDP-43 in SCs than spinal root nerves, particularly in those containing motor axons, and inducible loss of TDP-43 in SCs resulted in milder deterioration than congenital loss. Taken together, we provide evidence that TDP-43 in SCs is essential for the correct organisation of paranodal domains and the long-term integrity of the myelin-axon unit.

In strong contrast, TDP-43 in OLs is critical during CNS development. It ensures progression of differentiated OLs along the correct transcriptional program during early maturation, and proper myelination and protection of the axon-myelin unit in fully mature OLs of the white matter. However, after induced deletion of TDP-43, mature OLs and myelin remained remarkably pertinacious in the white matter of adult mice, at least within the timeframe of our analysis. Furthermore, the dependence of OLs on TDP-43 is region-specific, leading to rapid demyelination and loss of mature OLs in the spinal cord grey matter, which is accompanied by mild reduction in the numbers of motor neurons. Our study collectively indicates that TDP-43 in OLs is indispensable for developmental maturation and – specifically in the spinal cord grey matter – for OL survival and potentially for support of motor neurons in adult mice. Beyond the spinal cord, TDP-43 deletion also impacts OLs residing in various brain regions.

Altogether, our study provides detailed insight into the multi-faceted requirement of TDP-43 in SCs and OLs. The broad spectrum of influence that TDP-43 exerts on SC and OL biology should be taken into consideration in order to thoroughly understand TDP-43 function and dysfunction in the nervous system health and disease.

2. Zusammenfassung

TAR-DNA bindendes Protein 43 (TDP-43) ist ein RNA bindendes Protein, welches ein breites Spektrum der RNA-Biologie reguliert. Seine Hauptfunktionen beinhalten die Regulation von alternativem Spleissen, die Regulation von Transkript-Stabilität und dessen Transport. In den letzten Jahren wurde diese Palette erweitert, in welcher TDP-43 zusätzlich als Schutz-Element gegen die fehlerhafte Beibehaltung von intronischen Sequenzen in das verarbeitete Transkript (kryptisches Spleissen) wirkt. In den meisten Fällen von amyotropher Lateralsklerose (ALS), einer tödlichen neurodegenerativen Erkrankung, wird TDP-43 als Teil von pathologischen Anhäufungen im Zytoplasma von Motorneuronen vorgefunden. Es gibt Anzeichen, dass TDP-43 in Schwann Zellen (SZ) und Oligodendrozyten (OL) unabdingbar ist und man weiss, dass diese Zellen einen Einfluss auf das Wohlergehen von Neuronen haben. In dieser Studie untersuchen wir die Funktion von TDP-43 in SZ und OL in Mäusen während der Entwicklung und in erwachsenen Tieren mit dem Cre/loxP-System. Wir zeigen hier, dass TDP-43 in SZ für den rechtzeitigen Start der Myelinisierung während Entwicklung und Regeneration benötigt wird. Funktionell unterdrückt TDP-43 das kryptische Spleissen von *neurofascin* in Glia-Zellen, was für die Organisation der paranodalen Region und Reizleiter-Funktion von peripheren Nerven entscheidend ist. Des Weiteren ist TDP-43 in SZ über längere Zeit unverzichtbar für die Aufrechterhaltung der Myelinisierung und der axonalen Gesundheit, besonders in Axonen mit grossem Durchmesser. Dieser Aspekt war im Vergleich zu Ischiasnerven stärker in den Wurzelnerven ausgeprägt, insbesondere in jenen mit Motor-Axonen. Die genannten Auswirkungen waren drastischer, wenn TDP-43 in SZ von Geburt an fehlte, als wenn die Rekombination in erwachsenen Mäusen herbeigeführt wurde. Zusammengefasst zeigen wir auf, dass TDP-43 in SZ für die korrekte Etablierung der paranodalen Region und die Langzeiterhaltung der funktionellen Axon-Myelin Einheit essentiell ist. TDP-43 ist in OL unverzichtbar für die Entwicklung des zentralen Nervensystems. Es stellt den korrekten Verlauf von differenzierten OL entlang des transkriptionellen Programs während der frühen Reifung sicher und ist in ausgereiften OL in der weissen Materie sowohl entscheidend für die Vollendung der Myelinisierung, als auch für die Erhaltung der Myelin-Axon Einheit. Nach induzierter Rekombination von TDP-43 in erwachsenen Mäusen sind ausgereifte OL und Myelin der weissen Materie jedoch stabil, zumindest innerhalb des analysierten Zeitrahmens. Zusätzlich ist die Abhängigkeit von TDP-43 in OL regionen-spezifisch. Induzierte Rekombination bewirkt Demyelinisierung und den Verlust von ausgereiften OL in der grauen Materie des Rückenmarks, was mit einer leichten Verminderung der Motorneuronen einhergeht. Insgesamt ist TDP-43 essentiell für die OL-Reifung und in erwachsenen Tieren – speziell in der grauen Materie des Rückenmarks – für das Überleben von OL und möglicherweise die Unterstützung von Motorneuronen. Darüber hinaus hat die Elimination von TDP-43 in OL ebenfalls Auswirkungen in verschiedenen Hirn-Regionen.

Im Ganzen bietet diese Studie einen detaillierten Einblick in die facettenreiche Wirkung von TDP-43 in SZ und OL. Das breite Einfluss-Spektrum von TDP-43 auf die Biologie von SZ und OL zeigt, dass diese Zellen für ein umfassendes Verständnis der Funktion von TDP-43 im gesunden und erkrankten Nervensystem in jedem Fall berücksichtigt werden müssen.

3. Introduction

3.1. The Nervous System

Metazoan organisms require efficient strategies for intercellular communication. Acquiring and transporting signals, processing these signals to extract useful information and derive appropriate actions, and sending the suitable signals to the correct location of an organism are vital functions for survival. An efficient way of signal transmission is achieved by nerve cells. At a basic level, nerve cells are able to detect incoming stimuli, to integrate and transfer information from one nerve cell to another, or to trigger actions (*e.g.* muscle contraction). Therefore, signals are not only transmitted to a target cell but can additionally be integrated and processed in a complex network to generate the desired output. Networks of nerve cells can be found in most metazoan organisms, albeit with dramatic differences in complexity ranging from simple nerve nets in Cnidaria up to the intricate neuronal network in mammals. In basal organisms such as the Hydra, ganglion cells are found in a net-like pattern with a process length between 30-200 µm (David, 1973). Several circuits have been identified that react to external stimuli and trigger simple motor actions that lead to radial or longitudinal contraction of the Hydra (Dupre and Yuste, 2017). The transmitted electrical signals are generated by a local depolarization of the axonal membrane, termed the action potential. It is triggered by opening voltage-gated ion channels and propagates along the axons, triggering other voltage-gated channels along the way to sustain itself. In a complex environment, where predators seek prey and prey must escape from predators, the speed of signal transmission becomes decisive for survival and success. Fast signal transmission is especially pivotal for highly complex nervous systems as well as large organisms. The giant squid has an average mantle length of more than a meter (Roper and Shea, 2013), and some motor neurons in mammals project their axons from the spinal cord down to the muscles of the feet, resulting in enormous dimensions of a single cell. Basal forebrain cholinergic neurons in mice have a total axon length of up to 50 cm and are thought to have a mean axon length of around 100 m in humans (Wu et al., 2014). Evolution has met the need for speed over potentially long distances by two major adaptions. The first we will discuss is a drastic increase to the axonal diameter, designated axon gigantism. The gain in conduction velocity is proportional to the square root of the axon diameter (Hodgkin, 1954). This strategy has been

adopted by most of the more advanced Bilateria. Among them, pencil squids (*Loliginidae*) have axons with a diameter up to 800 µm, larger than most pencil leads (Pumphrey and Young, 1938; Young, 1938). This is an effective solution but requires a lot of space. Given the high numbers of neurons in the mammalian central nervous system that require fast signal transmission, axonal gigantism would not be feasible without drastic anatomical changes. The second and much more space-efficient solution is to increase the conduction velocity by myelination. Myelin consists of a compacted, lipid-rich membrane wrapped around and insulating long segments of the axon, leaving only small gaps in between. The gain in conduction velocity of a myelinated fiber is proportional to its diameter, which is more efficient when axons are larger than 1 µm (Fig. 3.1).

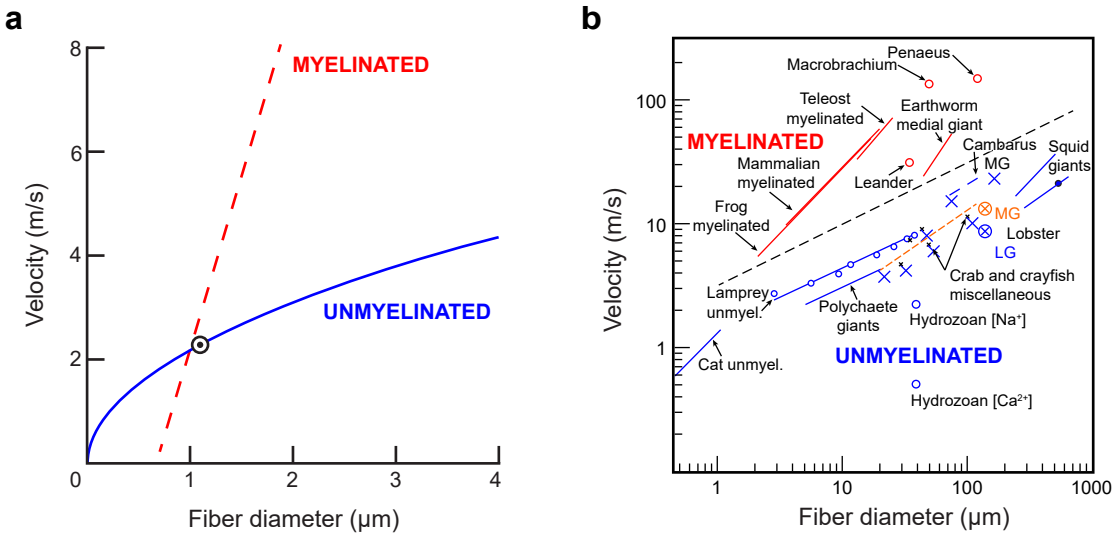

Figure 3.1: Conduction velocity and myelin **(a)** Relation between fiber diameter and conduction velocity of myelinated (solid line) and nonmyelinated fibers (dashed line). **(b)** Collection of "intrinsic" conduction velocities for various nerve fibers by Castelfranco and Hartline, assuming standard conditions. Lines indicate general relation over a range of fiber diameters. MG/LG: medial/lateral giants from lobster. (a) reproduced from Rushton (1951), (b) reproduced from Castelfranco and Hartline (2016)

Myelin has been "invented" several times during evolution, which is a testimony to its strategical importance. It is found in some invertebrates and in almost all vertebrates (Holmes, 1942; Heuser and Doggenweiler, 1966; Gunther, 1976; Bullock et al., 1984; Davis et al., 1999). The vertebrate nervous system is divided into two compartments, the central nervous system (CNS) and the peripheral nervous system (PNS). The brain and the spinal cord are part of the CNS, while all emerging nerves except the optic nerves belong to the PNS. The PNS acquires information through the afferent sensory fibers and transmits it to the CNS, and also sends processed signals back to the effectors through efferent motor fibers.

The motor division is further divided into two systems: The somatic nervous system controls skeletal muscles and is responsible for voluntary body movements. Contrariwise, the autonomic nervous system controls the visceral functions. The myelinating cells in mammals are the Schwann cells (SCs) in the PNS and oligodendrocytes (OLs) in the CNS.

3.1.1. Impulse Conduction

The signal travelling along the axon, irrespective of the presence of myelin, is an electrical impulse (action potential). The action potential is generated by local depolarization of the axonal membrane (axolemma). The membrane potential is influenced by all ions in the intracellular and extracellular space, but mainly sodium and potassium ions are involved. The kinetics vary between species and different types of neurons, depending on the types and composition of the ion channels. When no signal is being transmitted, the axonal membrane has a resting potential of -60 to -75 mV. ATP-dependent $Na^+\backslash K^+$ pumps export three Na^+ ions in exchange for two K^+ ions. K^+ ions can also leave the cytoplasm through other specialized channels and the potential equilibrates at its resting state. Two main types of voltage gated channels are responsible for the conduction of the electric impulse, *i.e.* the action potential. Voltage-gated Na^+ channels are closed in the resting state, but get quickly opened in an all-or-none fashion when the membrane depolarization is increased beyond -55 mV. Na^+ ions stream into the axonal cytoplasm and depolarize the membrane, reaching a peak action potential above 30 mV. The local depolarization is spread as graded potential along the axon by passive ion diffusion, which further triggers the opening of closed, voltage-gated Na^+ channels in the downstream vicinity, and thereby reinforces and transmits the impulse along the axon. The voltage-gated Na^+ channels are inactivated and enter a refractory period shortly after their opening. While inactive, voltage-gated Na^+ do not allow flow of Na^+ ions. The depolarization in turn opens voltage-gated K^+ channels and K^+ ions flow out of the axonal cytoplasm and reduce the membrane potential to a hyperpolarized state. Hyperpolarization changes the K^+ voltage gated channel to the closed state. Finally the membrane potential reaches the resting potential and Na^+ channels return to the closed but active state, ready to elicit a new action potential. The whole cycle of one action potential takes less than a few milliseconds, allowing fast firing rates. Due to the inactivation of voltage-gated Na^+ channels after depolarization, it is not possible that an impulse elicits an action potential “upstream” towards the signal that led to the action potential.

3.1.2. Nodes of Ranvier

In myelinated axons, voltage-gated ion channels and pumps are highly concentrated in and around small gaps between the long (300-2000 µm) myelinated internodal segments, and act there to reinforce the graded potential in order to relay the action potential downstream to the synaptic terminal. These gaps, known as nodes, have been prominently described in the 19th century by the French histologist Louis-Antoine Ranvier (Ranvier, 1878) , and are named after him. As a result of having nodes of Ranvier located between myelinated segments, the action potential is not gradually reinforced along the axon, but passively diffuses along internodes and is only strengthened at the nodes of Ranvier. This saltatory conduction of the action potential improves conduction velocity, reaching over 100$^{m}/_{s}$ (Hursh, 1939; Gordon et al., 1987). Consequentially, an electrical impulse in such an axon will cover a distance of 100 mm in one millisecond. Given the short duration required to generate an action potential (few ms), the potential is being reinforced simultaneously in multiple nodes of Ranvier rather than in a strictly sequential manner.

Morphological Organization

The nodal region of an axon is longitudinally organized into specific, distinct domains: The node of Ranvier, the axoglial paranodal junctions and the juxtaparanode, which are located at the edge of adjacent myelinated internodes (Fig. 3.2a). Kv1 K^+ channels are mainly localized in the axolemma of the juxtaparanode and are thought to serve as rectifiers for the resting potential and action potential thresholds (Brew et al., 2003; Brew et al., 2007; Higgs and Spain, 2011). SCs and OLs form several paranodal cytoplasmic loops and are connected to the axolemma with septate-like junctions in the paranodal region (Bargmann and Lindner, 1964; Andres, 1965). These interactions are mediated by the transmembrane protein Caspr1 and the GPI-anchored protein Contactin1 on the axonal side and Neurofascin 155 (NF155) on the glial side (Fig. 3.2b). Another isoform derived from the *Nfasc* gene is NF186, which is expressed by neurons and located in the nodal region. The node of Ranvier, where the action potential is reinforced, is dependent on rapid de- and repolarization of the membrane and therefore harbors a high density of voltage gated Na^+ and K^+ channels. Ankyrin-G, Ankyrin-B and 4.1B link the transmembrane proteins in the axolemma to the cytoskeleton via spectrins. Based on the clustering of the major ion channels for Na^+ and K^+, the vast majority of nodes of Ranvier form postnatally with different dynamics in the PNS and the CNS, respectively.

In sciatic nerves of mice, most nodes of Ranvier display clustering of Na^+ channels within the first two postnatal days (Custer et al., 2003) and K^+ channels first appear around one week post birth, but are only gradually clustering until P60 (Vabnick et al., 1999). In the optic nerve, Na^+ channel clusters are first detected at P9-P10 (Rasband et al., 1999a), whereas clusters of K^+ channels first appear after two weeks and occur throughout by P40 (Rasband et al., 1999b).

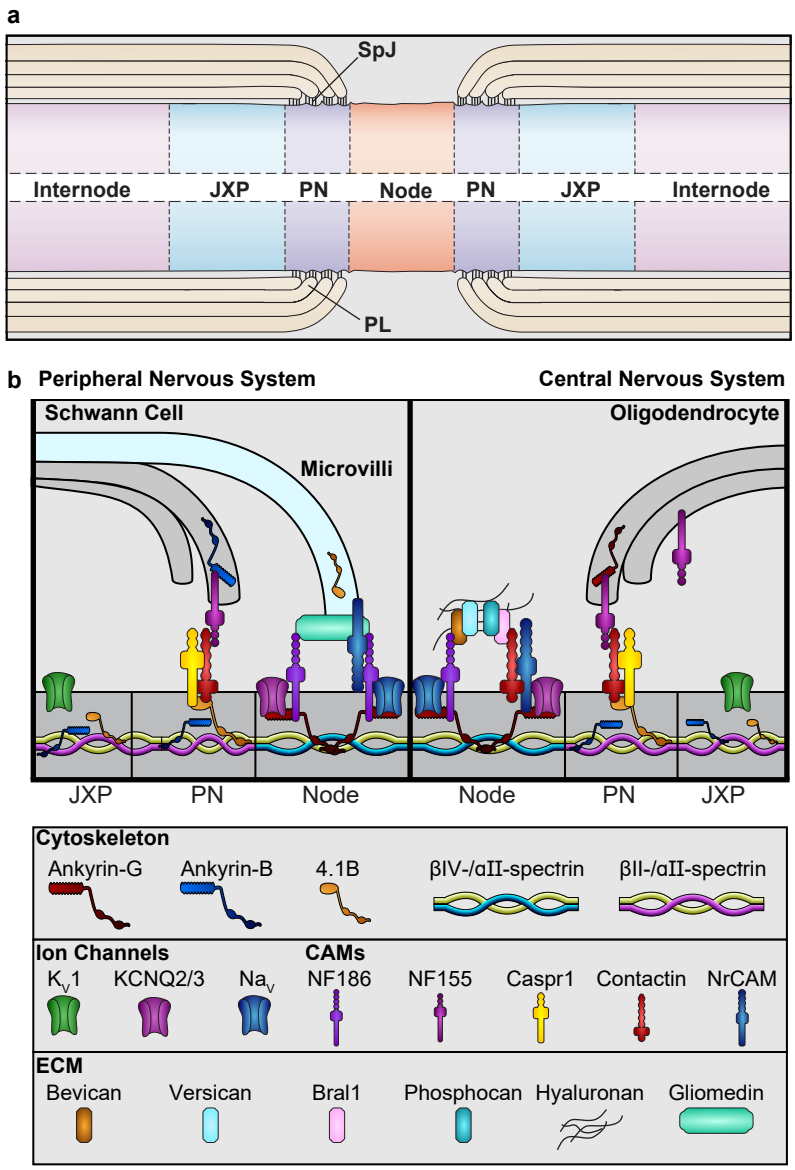

Figure 3.2: Architecture of a node of Ranvier and adjacent domains. (a) Longitudinal domains include the node of Ranvier and the neighboring paranode (PN), where paranodal loops (PL) of myelinating glia cells contact the axolemma through septate-like junctions (SpJ). The juxtaparanode (JXP) is the myelinated segment in close proximity to the paranode. Internodes are the myelinated segments between nodes of Ranvier. **(b)** Major molecular components and their localization in the nodal region of the PNS (left) and the CNS (right). K_V1 channels are located in the axolemma of the JXP, while KCNQ2/3 potassium channels and Na_V channels are concentrated in the node. Contactin/Caspr1 interact with NF155 in the PN. NrCAM in the node is located in SC microvilli and the axolemma, and interacts either with NF186 or components of the ECM. Transmembrane proteins interact with Ankyrin-G, Ankyrin-B or 4.1B. Instead of βIV-spectrin, βII-spectrin is the prevalent variant in the nodal region of the axon. The paranodal junctions attach the myelin sheath to the axolemma and serve as barrier to prevent longitudinal diffusion of nodal or juxtaparanodal transmembrane proteins of the axon. Illustrations were modified from Poliak and Peles (2003), Rasband and Peles (2015), and Nelson and Jenkins (2017).

Proper expression and localization of ion channels are major determinants of fast conduction properties of axons. To achieve the saltatory conduction from node to node, it is pivotal that internodal segments are correctly myelinated. Intriguingly, myelin protein zero (MPZ), a known key protein of peripheral myelin, is also required in paranodal loops and SC microvilli to maintain paranodal and nodal integrity through interaction with Neurofascins in the PNS (Brugger et al., 2015).

Myelin

Myelin is formed by a highly compact, lipid-rich membrane wrapped multiple times around an axon. In adult rat sciatic nerves, 72-94 layers are reported for some axons (Webster, 1971). Regarding the impulse-conducting properties of a nerve fiber, myelin acts as an insulating layer and decreases the membrane's capacitance, preventing the rapid decay of the graded potential. The thickness of the myelin sheath is proportional to the axon diameter (Donaldson and Hoke, 1905; Schmitt and Bear, 1937; Gasser and Grundfest, 1939; Sanders and Whitteridge, 1946). Schmitt and Bear coined the term "g-ratio", the ratio of the inner axonal diameter to the outer fiber diameter. Already early on, basic theoretical considerations suggested that there is an optimal thickness of the myelin sheath for a myelinated fiber with a given diameter (Rushton, 1951): Not too thin, to prevent fast and extensive leaking of the current before it reaches the next node, and not too thick so the same geometric space can accommodate enough axoplasm that allows the current to flow along the axon. Rushton (1951) defined an optimum g-ratio of ~0.61. OLs create myelin sheaths around multiple axonal segments, whereas SCs establish a one-to-one relationship with axons and myelinate a single internodal segment. Myelination by SCs is restricted to axons with a large caliber (~>1 μm), while smaller axons are engaged with non-myelinating SCs to form Remak bundles (reviewed by Jessen and Mirsky, 2005). Remak bundles may contain, amongst others, nociceptive sensory axons (reviewed by Harty and Monk, 2017). The experimentally observed g-ratio in the sciatic nerve centers around 0.67 (Chen et al., 2006; Friede, 1986; Michailov et al., 2004). The myelin sheath is considerably thinner in the CNS, resulting in a g-ratio between 0.7 and 0.8 (Benninger et al., 2006; Hildebrand and Hahn, 1978; Lunn et al., 1997; Xin et al., 2005). The higher g-ratio in the CNS may be a consequence of a higher pressure for space efficiency compared to the peripheral nerves (Chomiak and Hu, 2009). Moreover, myelination in the CNS not only aims to maximize conduction velocity, but is adaptive and takes part in the complex coordination of the CNS neuronal network (perspective by Bechler and Constant, 2014).

Composition of Myelin

Myelin of the PNS and the CNS consists of over 70 % lipids in dry weight and a substantial fraction of cholesterol (~40 $\%_{mol}$ of lipids, Laatsch et al., 1962; Norton and Autilio, 1965; Obrien and Sampson, 1965; Norton and Autilio, 1966; O'Brien et al., 1967; Horrocks, 1967; Smith, 1968; Spritz et al., 1973; Oulton and Mezei, 1976; Smith and Curtis, 1979). Myelin from SCs and OLs differs in its molecular composition, including myelin proteins that are specific to each cell type, and other proteins that are common. A common major myelin protein is the myelin basic protein (MBP, Jahn et al., 2009; Patzig et al., 2011). It is a peripheral, positively charged membrane protein found in compact myelin (Han et al., 2013). MBP neutralizes the negative charge of phospholipids, forms a cohesive mesh-like network, and brings the membrane bilayer close together in a zipper-like manner (Aggarwal et al., 2013). The *shiverer* mouse is a natural MBP null mutant and is unable to form compact myelin in the CNS (Bird et al., 1978; Privat et al., 1979; Roach et al., 1985). MBP-deficient mice still have compacted myelin in the peripheral nerves, as myelin protein zero (MPZ/P0) can partially compensate due to its positively charged cytoplasmic domain (Kirschner and Ganser, 1980; Ding and Brunden, 1994; Martini et al., 1995). MPZ is the most abundant myelin protein in the PNS, adding up to 21% of the total myelin content (Patzig et al., 2011), and is not found in oligodendrocyte myelin. PMP22 is another myelin protein of the PNS (Snipes et al., 1992). Remarkably, 80% of the protein are readily degraded via the proteasome after translation (Pareek et al., 1997; Notterpek et al., 1999), and a finely balanced expression is essential for successful myelination (Adlkofer et al., 1995; Thomas, 1999; Robaglia-Schlupp et al., 2002). In the CNS, the X-linked proteolipid protein (PLP1) is the major myelin protein (Jahn et al., 2009). PLP1 is a part of compact myelin, and can even be detected at lower levels in SCs, while MPZ is exclusively found in PNS myelin (Jahn et al., 2009; Patzig et al., 2011). OLs express two alternatively spliced isoforms, PLP1 and DM20. PLP1 is required for cholesterol accumulation in the myelin membrane and its deletion leads to marked pathological changes in adult mice (Luders et al., 2019, reviewed by Edgar and Garbern, 2004), but does not lead to severe hypomyelination (Rosenbluth et al., 2006; Werner et al., 2013). Only when another tetraspan proteolipid protein – M6B – is knocked out along with PLP1, axons in the CNS are severely hypomyelinated (Werner et al., 2013). Both PLP1 and M6B have a high affinity for cholesterol and are likely to have a function in providing cholesterol in the secretory pathway during myelin biogenesis (Werner et al., 2013).

Contrary to PLP1, M6B is only found in negligible amounts in the myelin sheath (Werner et al., 2013). 2',3'-cyclic nucleotide phosphodiesterase (CNP1) and Myelin associated glycoprotein (MAG) are two further proteins found in non-compact myelin of the CNS and to a lesser extent also in the PNS (Jahn et al., 2009; Patzig et al., 2011). CNP1 is a peripheral membrane enzyme (Braun et al., 1991; Agrawal et al., 1990) and required for axonal support in the CNS (Lappe-Siefke et al., 2003; Edgar et al., 2009). MAG is a type-1 single-span transmembrane protein like MPZ and has five extracellular Ig domains (reviewed by Trapp, 1990). At least in the PNS, MAG is required for long term axonal support, although it is apparently dispensable for developmental myelination (Montag et al., 1994; Fruttiger et al., 1995). MAG mediates axon-glial signaling and is part of an inhibitory signaling to repress axonal regeneration in the CNS (reviewed by McKerracher and Rosen, 2015).

3.1.3. Schwann Cells (SCs)

The SC lineage entails four major developmental stages. The SC precursors give rise to immature SCs. At this stage, they either differentiate to non-myelinating SCs or to pro-myelinating SCs, which finally mature to myelinating SCs (Fig. 3.3).

Schwann Cell Precursors

SC precursors (SCPs), the earliest stage in the SC lineage, originate from migrating neural crest cells, which delaminate from the neural folds at the dorsal side of the developing neural tube and migrate ventrally (reviewed by Jessen and Mirsky, 2005). SCPs are interdigitated between the axons in developing peripheral nerves. They are fully dependent on axon-derived survival signals, most importantly Neuregulin1 (Nrg1), which is also essential for migration (Dong et al., 1995; Lyons et al., 2005). SPCs express desert hedgehog (dhh), which is widely used as an SCP-marker and has a role in the formation of the epi-, peri- and endoneurium (Parmantier et al., 1999). SCPs display multipotent, stem-cell-like features, and have the potential to generate non-glial cell lineages including neurons, melanocytes, mesenchymal stem cells and fibroblasts (Espinosa-Medina et al., 2014; Dyachuk et al., 2014; Adameyko et al., 2009; Kaukua et al., 2014; Joseph et al., 2004), comprehensive review by Furlan and Adameyko, 2018).

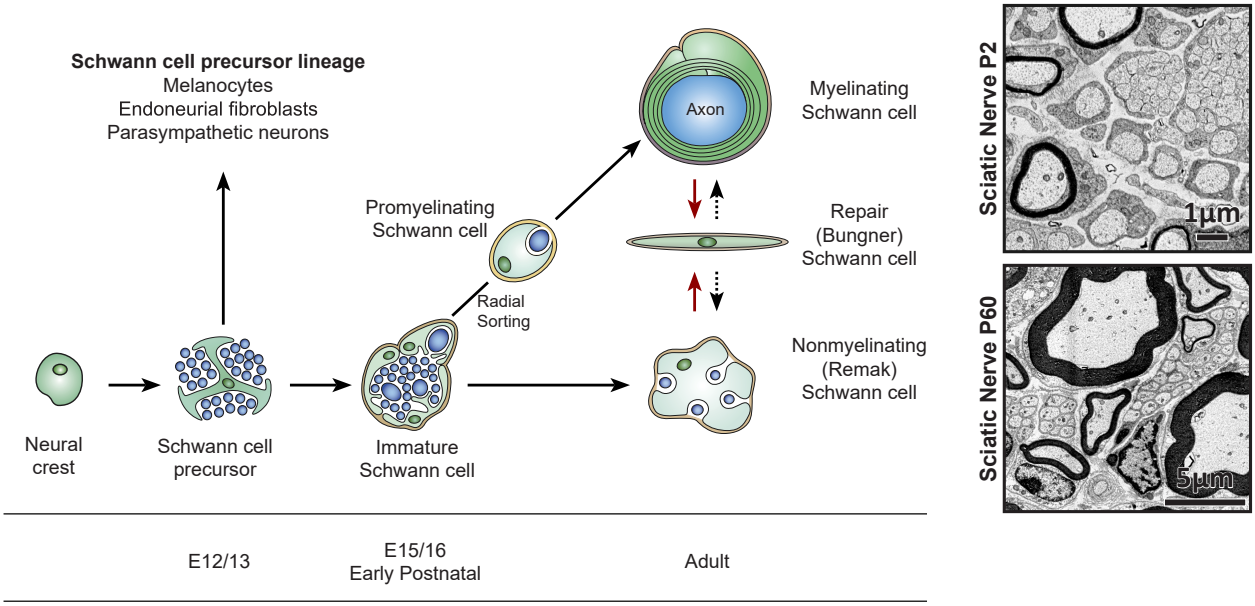

Figure 3.3: Differentiation of the SC Lineage (a) Neural crest cells ventrally migrate from the folding fringes of the neural tube and give rise to numerous cell types including the SC lineage. Neural crest cells can differentiate into SC precursors (SCPs), which proliferate and distribute along the axons from E12 to E13 in mice. SPCs differentiate into immature SCs, which are widely abundant in peripheral nerves by E16. Several immature SCs surround bundles of axons and provide mutual trophic support. Multiple small caliber axons remain engaged by single immature SCs, which will later develop into non-myelinating SCs to form Remak bundles. As immature SCs engage with larger caliber axons (~>1 µm in diameter when measured in adult animals) in a 1:1 relation in a process called radial sorting, they progress to the pro-myelinating stage. The promyelinating SC activates the myelination program and quickly begins wrapping myelin around the axon segment. Radial sorting and onset of myelination therefore gradually progress during the first weeks after birth in a mouse, and radial sorting is virtually complete before mice reach 2 weeks of age. Illustration modified from Jessen et al. (2015) **(b)** Exemplary electron micrographs of mouse sciatic nerves at P2 and P60. At P2, nerves display bundles of unsorted axons (B), sorted, but not yet myelinated axons (S) and few myelinated axons (M). At P60, larger caliber axons are myelinated (M). Smaller axons appear embedded in SC cytoplasma as Remak bundles (R)

Immature & Pro-Myelinating SCs

Promoted by Notch1-signalling (Woodhoo et al., 2009), SCPs further differentiate into immature SCs (iSCs) in mice, which ensheath large groups of axons. iSCs produce a basal lamina and develop autocrine survival circuits (Dong et al., 1995; Meier et al., 1999; Weiner and Chun, 1999; Dowsing et al., 1999). Numbers of iSCs are finely adjusted by proliferation, survival and cell death (reviewed by Jessen and Mirsky, 2019). ECM-activated cAMP signaling through G-protein coupled receptor 126 (Gpr126) stimulates iSC proliferation (Monk et al., 2009; Arthur-Farraj et al., 2011; Guo et al., 2013a). Axon-mediated Notch1 signaling promotes proliferation of iSCs (Woodhoo et al., 2009). The mitogenic impact of Nrg-1 signaling has been demonstrated *in vitro* but not fully resolved *in vivo* (Morrissey et al., 1995; Dong et al., 1995; Garratt et al., 2000).

Transforming growth factor beta (TGFβ) performs a dual function. It induces cell death by itself, but promotes proliferation in combination with Nrg1 signaling (Parkinson et al., 2001; D'Antonio et al., 2006). iSCs extend processes and selectively engage with a single large-caliber axons (>1 µm in diameter when measured in adult mice) in a one-to-one relationship – referred to as radial sorting – and become promyelinating SCs. Radial sorting requires a drastic cytoskeletal reorganization, and largely depends on the integration of signaling derived from the ECM with signals presented by the axon (reviewed by Feltri et al., 2016). Zeb2 is a transcriptional repressor of inhibitors of maturation, which is essential for SC differentiation and radial sorting to occur (Quintes et al., 2016). Small caliber axons that are not sorted remain in the bundle. iSCs and the remaining axons subsequently mature to a Remak bundle. Remak SCs individually ensheath multiple axons such that each axon in a Remak bundle is separated from the surrounding axons by the Remak SC.

Myelination

Axonal Nrg1-III (membrane-bound form of Nrg1) triggers myelination in a threshold-dependent manner by activating ErbB2/3 signaling, and thus controls myelin growth (Michailov et al., 2004). Early growth response-2 (Krox20/Egr2) is the central transcription factor that activates myelin gene expression in SCs (Topilko et al., 1994). Myelination is strictly controlled by positive and negative regulators. SRY-related HMG-box-10 (Sox10), an essential transcription factor for SC generation (Britsch et al., 2001), is also required during myelination (Finzsch et al., 2010), and acts together with several other regulators to promote the myelination program. POU class 3 homeobox 1/2 (Oct-6/Brn-2) and Sox10 synergistically induce the expression of Krox20 and suppresses expression of negative regulators of myelination (Jaegle et al., 1996; Bermingham et al., 1996; Jaegle et al., 2003; Ghislain and Charnay, 2006; Jagalur et al., 2011). Nuclear factor of activated T cells, cytoplasmic, calcineurin-dependent-4 (NFATc4) activates Krox20 expression also in association with Sox10 (Kao et al., 2009). Ying Yang (YY1) is another transcriptional activator of Krox20 (He et al., 2010). Histone deacetylase 2 (HDAC2) promotes expression of genes driving myelination, including Sox10, Krox20 and MPZ (Jacob et al., 2011). Krox20 transcriptionally activates NGFI-A binding protein 1/2 (Nab1/2), an essential set of transcription factors to start myelination (Le et al., 2005b). Myelination is a metabolically demanding process and is inherently dependent on massive membrane synthesis. Sterol regulatory element binding proteins (SREBPs) are a group of transcription factors that regulate lipid metabolism.

SREBPs are essential for proper myelination (Verheijen et al., 2009), and in synergy with Krox20 promote transcription of genes that are part of the cholesterol biosynthesis pathway (Leblanc et al., 2005). Anabolic regulation by mTORC1 has a dual role in SCs. High mTORC1 activity negatively regulates Krox20 to suppress differentiation before the onset of myelination, and is later required for correct myelin growth (Norrmen et al., 2014; Figlia et al., 2017; Beirowski et al., 2017; Jiang et al., 2018). Negative regulators of myelination include SRY-Box 2 (Sox2, Le et al., 2005a; Florio et al., 2018; Roberts et al., 2017), inhibitor of DNA binding 2 (Id2, Florio et al., 2018) and Notch1 signaling (Woodhoo et al., 2009).

Maintenance

Adult myelinating and Remak SCs remain highly adaptive. In consequence, their differentiated state must be actively maintained. Additionally, myelin is not an inert structure and requires active maintenance by the myelinating SCs. Krox20 (Decker et al., 2006) and Sox10 (Bremer et al., 2011) are required beyond development, including in adult SCs, to prevent demyelination and de-differentiation in adult mice. Yap/Taz is another key factor for myelin maintenance, as conditional double knockout mice displayed demyelination and abnormal, vacuole-containing myelin profiles (Grove et al., 2017). HDAC1/2 regulate expression of MPZ, which interacts with Neurofascins and is ultimately required to maintain the nodal integrity (Brugger et al., 2015). Adult myelinating and Remak SCs also have to provide sustained trophic support to the axons they are engaged with. Liver kinase B1 (LKB1), a metabolic regulator, is essential for the long-term support of axons (Beirowski et al., 2014). Interestingly, non-myelinated sensory axons are most affected, which emphasizes the necessity of axonal support by both myelinating and Remak SCs.

Regeneration after Injury

Peripheral nerves have an outstanding regenerative capacity, as differentiated SCs remain remarkably plastic. In case of an injury, regeneration is not dependent on a nerve-resident stem cell niche, but instead is mediated by trans-differentiation of myelinating and Remak SCs (Stierli et al., 2018). In both crush injuries and nerve transections, axons degenerate and elicit a similar repair program in the distal nerve segment. Injury-mediated axonal degeneration triggers an adaptive cellular re-programming of myelinating and Remak SCs into repair SCs, a specialized cell type to encourage axonal regeneration before remyelination can occur.

c-Jun is a major regulator of the cellular reprogramming of myelinating and Remak SCs to repair SCs and the subsequent repair program (Arthur-Farraj et al., 2012; Arthur-Farraj et al., 2017). c-Jun is rapidly upregulated in SCs upon injury (Shy et al., 1996; Norrmen et al., 2018), and is in a cross-antagonistic relationship with Krox20 to switch between the myelinating and repair programs (Parkinson et al., 2004; Parkinson et al., 2008). c-Jun directly decreases expression of myelin genes (Parkinson et al., 2008) and promotes expression of neurotrophic factors (Fontana et al., 2012). The injury response is also shaped by HDAC2, which is highly expressed shorty after injury (Brugger et al., 2017). HDAC2 delays the initial cellular reprogramming of SCs and axonal regrowth, but is later required for efficient remyelination (Brugger et al., 2017).

Shortly after the injury, axons locally translate placental growth factor (PlGF, distal to the lesion site) and promote the formation of constricting actin spheres in SCs via vascular endothelial growth factor receptor (VEGFR)-signaling, which ultimately accelerates the disintegration of injured axons (Catenaccio et al., 2017; Vaquie et al., 2019). Cytokines such as interleukin-1α (Il-1α), Il-1β and tumor necrosis factor α (TNFα) are highly expressed in SCs at 1 day after injury to attract macrophages and promote an innate immune response (Rotshenker, 2011) to support myelin phagocytosis (myelinophagy, reviewed by Hirata and Kawabuchi, 2002). Myelinophagy by SCs and macrophages peaks around 5 days after injury (Gomez-Sanchez et al., 2015). In response to the injury, repair SCs undergo dramatic morphological changes, during which they elongate by 2- to 3-fold in comparison with myelinating or Remak SCs (Gomez-Sanchez et al., 2017), and align in columns inside the basal lamina tubes to form regeneration tracks (bands of Büngner, Büngner, 1890). These tracks provide a supportive environment and guidance for regenerating axons, in part due to the expression of neurotrophic factors that promote axon survival and regeneration (Eggers et al., 2010). These factors include glial-derived neurotrophic factor (GDNF), brain-derived neurotrophic factor (BDNF) and neurotrophin-3 (NT3).

3.1.4. Oligodendrocytes (OLs)

Origin

OLs are one of the glial cell types in the CNS. Glia (from Greek "γλια", glue) were first described as neural connective tissue ("cement") until its cellular components were identified. OLs belong to the class of macroglia along with astrocytes. Macroglia are generated from neuroepithelial cells, which are of ectodermal origin. Neuroepithelial-derived neural stem cells are the primary progenitors of neurons and macroglia. Neurogenesis starts around embryonic day 9 (E9) and largely finishes at E13 in the mouse spinal cord. Remaining neural stem cells give rise to OLs and astrocytes. Dorsoventral morphogenic gradients and their cross-regulatory signaling activities initiate the domain-patterning and consequently the specification of the differentiating neurons and macroglia. Wingless-type MMTV integration site family proteins (WNTs) and bone morphogenic proteins (BMPs) are highly expressed by dorsal roof plate cells, while sonic hedgehog (SHH) is highly expressed by cells in the floor plate (Wilson and Maden, 2005; Ulloa and Marti, 2010; Briscoe and Novitch, 2008; Chizhikov and Millen, 2005; Liu and Niswander, 2005). SHH signaling is required to specify the ventral domains, including the pMN domain harboring cells expressing the bHLH transcription factors Olig1 and Olig2 (Lu et al., 2000, Fig. 3.4a). Olig2 is essential for further differentiation of these cells to either motor neuron progenitors or oligodendrocyte precursors (OPCs, Lu et al., 2000; Zhou et al., 2000; Zhou et al., 2001). Among other factors, Notch-signaling is permissive to drive the cells into the oligodendroglial fate (reviewed by Rowitch and Kriegstein, 2010). These OPCs are generated around E12.5, after which they migrate and populate the whole neural tube (reviewed by Rowitch and Kriegstein, 2010). It is known that OPCs arise from two subsequent waves in the embryonic spinal cord (Cai et al., 2005; Vallstedt et al., 2005; Fogarty et al., 2005; Tripathi et al., 2011, Fig. 3.4a). OPCs emerging in the second wave at E15.5 from dorsal domains are less numerous than the ventrally derived OPCs, but are most prevalent in the dorsal funiculus in adult mice (Tripathi et al., 2011). In the brain, OPCs arise during three waves in the telencephalic ventricular zone (Kessaris et al., 2006, Fig. 3.4b): The first wave starts at E12.5, the second at E15.5 and the third at birth. OPCs from the first wave are largely replaced by those generated in later waves (Kessaris et al., 2006).

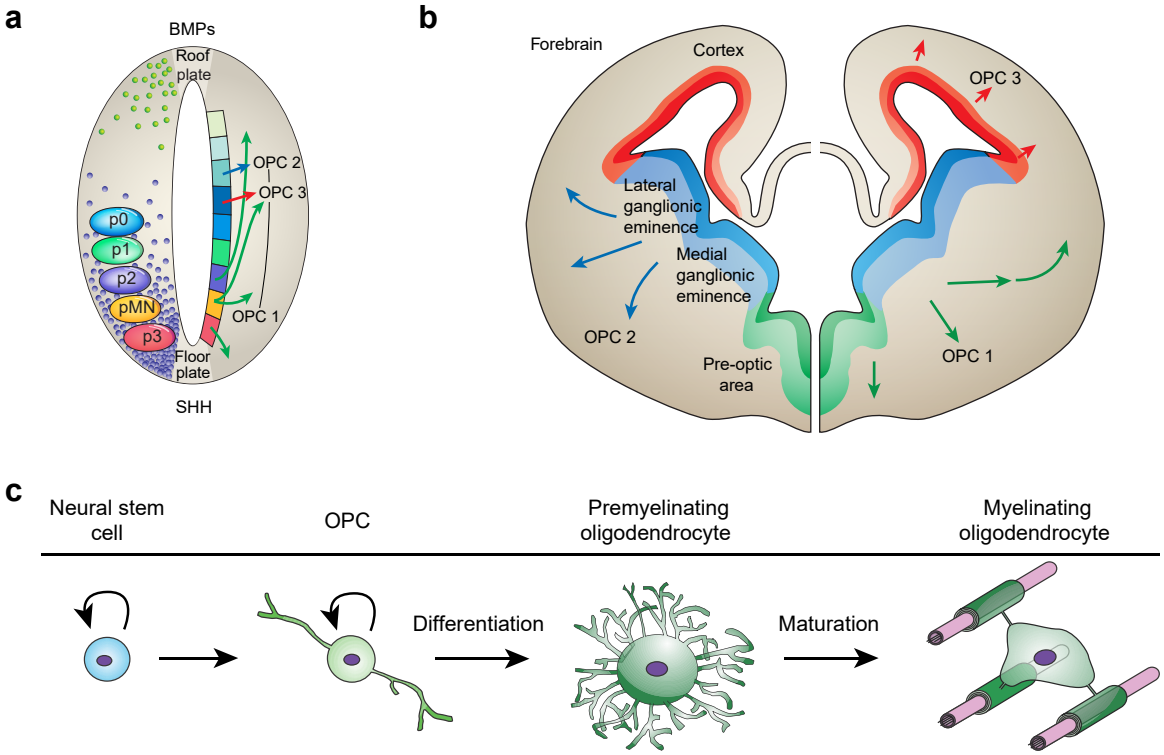

Figure 3.4: Oligodendrocyte lineage (a) Domain organization of the spinal cord and origin of OPCs. Dorsoventral domains are largely defined by SHH and BMP/WNT from cells at ventral and dorsal roof plates, respectively. Progenitor cells in the pMN domain give rise to OPCs in a first wave at E12.5. A second wave of OPCs is generated from dorsal domains at E15.5. **(b)** Three waves of OPC generation in the telencephalic ventricular zone have been identified: At E12.5, E15.5 and at birth. **(c)** Stages of the oligodendrocyte lineage. OPCs initially arise from neural stem cells, migrate, and proliferate. Cell numbers are matched by limited availability of growth factors and self repulsion. Most OPCs differentiate postnatally to premyelinating oligodendrocytes, which reach out to axons by multiple processes in a dynamic manner. During the process of maturation, selected axonal internodes finally become myelinated by myelinating oligodendrocytes. Illustrations in (a) & (b) modified from Rowitch and Kriegstein (2010), (c) modified from Goldman and Kuypers (2015)

Oligodendrocyte Precursors

OPCs are migratory and highly proliferative precursors of the oligodendrocyte lineage (Fig. 3.4c), identified by their expression of Olig2, Sox10 and Pdgfrα. Within the oligodendrocyte lineage only OPCs express Pdgfrα, which mediates mitogenic signaling together with $\alpha v\beta 3$ integrins (Baron et al., 2002). OPC numbers are partially matched to the requirement in the tissue by the limited availability of growth factors like PDGF-A, IGF-1, NT-3 and CNTF (Calver et al., 1998; Barres et al., 1993; Ye et al., 1995; Zeger et al., 2007; Barres et al., 1994; Cohen et al., 1996; Barres et al., 1996; Louis et al., 1993). In addition, neuronal activity has been shown to positively stimulate OPC proliferation (Barres and Raff, 1993; Gibson et al., 2014). Excess OPCs are subsequently eliminated by apoptosis (Trapp et al., 1997; reviewed by Raff et al., 1993; Barres and Raff, 1994).

The correct density of OPCs is further achieved by density-dependent feedback inhibition and self-repulsion (Zhang and Miller, 1996; Kirby et al., 2006; Hughes et al., 2013). Starting around E18.5 in mice, OPCs start to differentiate into OLs. OL generation peaks in mice at ~2-3 weeks after birth (Kang et al., 2010). It continues up to 8 months in the mouse corpus callosum and cortex, although at a low rate (Rivers et al., 2008). Intrinsic and extrinsic signals are responsible for OPC differentiation. Chromatin remodeling by BRG1/SMARCA4 and HDAC1/2 are essential for OPC differentiation (Marin-Husstege et al., 2002; Shen et al., 2005; Lyssiotis et al., 2007; Ye et al., 2009; Wu et al., 2012b; Yu et al., 2013). HDAC activity is required to repress the repressors of differentiation and thereby 'release the brakes' for differentiation (Swiss et al., 2011, reviewed by Zuchero and Barres, 2013). Among others, HDACs are required to relieve β-Catenin mediated repression of differentiation, likely by interacting with the transcription factor Tcf7l2 (Fancy et al., 2009; Ye et al., 2009). Another binding partner of Tcf7l2 is Kaiso, a repressor of β-Catenin dependent activation of transcription (Zhao et al., 2016). Furthermore Tcf7l2 is required in cooperation with Sox10 to promote myelination in a Wnt/β-Catenin independent manner (Hammond et al., 2015; Zhao et al., 2016). Differentiation (transition from OPCs to postmitotic OLs) is repressed by a reciprocal repression of Olig2 and Nkx2.2 (Sun et al., 2001; Sun et al., 2003; Weider et al., 2018). NFAT proteins are dephosphorylated by Calcineurin, which allows them to translocate into the nucleus and relieve the reciprocal repression between Olig2 and Nkx2.2 (Weider et al., 2018). Nkx2.2 then represses PDGFRα expression and promotes differentiation (Qi et al., 2001; Zhu et al., 2014). Remarkably, Olig2, NFAT and NKX2.2 are under the transcriptional control of Sox10 (Weider et al., 2015; Weider et al., 2018).

Postmitotic OLs and CNS Myelination

The transition from OPCs to postmitotic OLs ("differentiation") is followed by pronounced changes in morphology and protein expression, upon which OLs reach out with their cytoplasmic processes and finally myelinate up to 60 axons ("maturation", Matthews and Duncan, 1971; Chong et al., 2012). OLs do not require molecular cues from axons to initiate myelination. They can ensheath chemically fixed axons (Rosenberg et al., 2008) as well as artificial fibers (Bullock and Rome, 1990; Howe, 2006; Lee et al., 2012a; Mei et al., 2014; Bechler et al., 2015). OLs produce MBP^+ sheaths around fibers larger than 0.4 µm and adjust the sheath length according to the fiber diameter (Lee et al., 2012a; Bechler et al., 2015). Extrinsic signals that adapt myelination include Neuregulin and BDNF (Lundgaard et al., 2013), as well as electrical activity of axons, at least in part via Ca^{2+}

transients in the OLs (Wake et al., 2011; Baraban et al., 2018; Krasnow et al., 2018). Transcriptionally active myelin regulatory factor (MYRF) trimers that act synergistically with Sox10 are a key factor promoting the myelination program (Emery et al., 2009; Bujalka et al., 2013; Hornig et al., 2013; Muth et al., 2016). MYRF is expressed in postmitotic OLs and initially anchored to the ER by a transmembrane domain (Emery et al., 2009; Li et al., 2013). It associates to homotrimers and forms the transcriptionally active form by autoproteolytic cleavage (Bujalka et al., 2013; Muth et al., 2016; Kim et al., 2017).

Analysis and Convention

Differentiation and maturation are two separate, consecutive processes in the OL lineage progression (Fig. 3.4c). In this thesis, I will refer to OLs in different developmental stages according to the following convention. All Olig2-expressing cells are considered as cells of the OL lineage. Expression of Pdgfrα defines OPCs and Pdgfrα^{neg} cells delineate differentiated OLs. Pdgfrα^{neg} cells that are not positively labelled using the CC1 antibody comprise early stages of differentiated OLs (referred to by others as *pre-myelinating* or *intermediate* OLs, Kang et al., 2010; Gonzalez-Fernandez et al., 2018; Kirby et al., 2019). Differentiated OLs in later stages of maturation, including fully mature myelinating OLs, are CC1^{pos}.

Metabolic Support

The main energy source metabolized by the TCA cycle in the central nervous system is glucose (Hui et al., 2017). Neural activity is maintained with different metabolites including glucose, pyruvate and lactate (Brown et al., 2001; Wyss et al., 2011), but lactate metabolism and oxidative phosphorylation are essential for neurons themselves (Trevisiol et al., 2017; Fukui et al., 2007; Funfschilling et al., 2012). Astrocytes do not depend on oxidative phosphorylation and play an important role in the metabolic support of neurons via lactate shuttling (Supplie et al., 2017; Jha and Morrison, 2018; Barros and Weber, 2018). Moreover it has become clear that OLs are largely glycolytic and can also metabolically support axons by providing lactate through the monocarboxylate transporter 1 (MCT1, Funfschilling et al., 2012; Lee et al., 2012b). This concept of metabolic support has been also shown in *Drosophila* (Volkenhoff et al., 2015), suggesting it is a conserved mechanism.

The axonal metabolic demand may be sensed by glutamate release through oligodendroglial NMDA receptors as a surrogate signal for electrical activity, which triggers the incorporation of additional glucose transporters (Glut-1) in the plasma membrane of OLs (Saab et al., 2016).

3.1.5. Neuropathies and Neurodegenerative Diseases

A number of diseases of the central and peripheral nervous system directly involve SCs or OLs. For example, the demyelinating form of Charcot-Marie-Tooth neuropathy (CMT1) is the most prevalent peripheral neuropathy (Fridman et al., 2015). Most frequently, patients with CMT1 display a duplication of the *Pmp22* gene or a mutation in the *Mpz* gene (Saporta et al., 2011; Cornett et al., 2017). Neurodegenerative disorders in the central nervous systems also display a potential link to OL function: Spinal muscular atrophy (SMA) is characterized by selective motor neuron dysfunction and loss, with *Smn1* deletions or loss-of-function mutations as the underlying cause of SMA (Lefebvre et al., 1995). In SMA, the role of OLs remains controversial (O'Meara et al., 2017; Ohuchi et al., 2019). Multiple systems atrophy (MSA) is a rapidly progressing, fatal neurodegenerative disorder. Glial cytoplasmic inclusions containing α-Synuclein have been identified in OLs and are causative for the pathology, leading to demyelination and eventually secondary axonal degeneration (reviewed by Stefanova and Wenning, 2016). Multiple Sclerosis is an CNS-specific disabling disease, leading to demyelination, oligodendrocyte loss and finally axonal degeneration (reviewed by Compston and Coles, 2008; Dobson and Giovannoni, 2019).

Amyotrophic Lateral Sclerosis

Amyotrophic lateral sclerosis (ALS, also known as Charcot's disease or Lou Gehrig's disease) is a neurodegenerative disease mainly affecting motor neurons (reviewed by Swinnen and Robberecht, 2014). The main feature of ALS is a progressive evolution of motor deficits. The clinical presentation is heterogenous, as any voluntary muscle can be affected (reviewed by Swinnen and Robberecht, 2014). Initially affected regions are either bulbar upper motor neurons or lower spinal motor neurons (reviewed by Es et al., 2017). ALS is not a pure motor neuron disease, but rather a multisystem condition. Neurons in the brain may also be affected and patients display characteristics on a spectrum from classical ALS to frontotemporal dementia (FTD; Rippon et al., 2006; Burrell et al., 2011; Rascovsky et al., 2011; Mioshi et al., 2014, reviewed by Ling et al., 2013; Swinnen and Robberecht, 2014).

ALS is a fatal disease, with a mean survival time of about 3 years from diagnosis and with respiratory failure being the most common cause of death (reviewed by Swinnen and Robberecht, 2014). ALS is slightly more common in men than in women, and symptoms usually appear between 65 to 74 years of age (Logroscino et al., 2010). Historically, ALS has been classified as sporadic (sALS) or, if a family history has been identified, familial (fALS). fALS accounts for 5-10% of all cases, but may be underestimated. In most cases of fALS, mutations in four genes have been identified. Most commonly *C9orf72*, *Sod1*, *Fus* and *Tardbp* (protein: TDP-43). Regional differences are observed between European and Asian patients (Zou et al., 2017): For example, mutations in *Sod1* are most common in Asia (30%) but not Europe (14.8%). Conversely, mutations of *C9orf72* are found in 34% of fALS cases in Europe and only 2% in Asian cases. Also, mutations in *Tardbp* are more common in Europe (4% vs 1.5%). With modern sequencing technologies, a plethora of potentially causative genes has been identified (reviewed by Mathis et al., 2019). Prominently affected processes involve axonal transport, protein turnover, RNA metabolism, and mitochondrial function (reviewed by Robberecht and Philips, 2013; Turner et al., 2013; Mathis et al., 2019). Among the discovered genes, a substantial number encode RNA-binding proteins, including those encoded by *Tardbp*, *Fus*, *Atxn2* (Ataxin-2), *Taf15*, *Tia1*, *Hnrnpa1* and *Hnrnpa2/b1* (reviewed by Kapeli et al., 2017; Zhao et al., 2018): Most of these proteins contain an arginine/glycine-rich domain, in which most mutations have been discovered. This largely unstructured, prion-like region is suspected to mediate the formation of toxic aggregates (Wang et al., 2012a; Hergesheimer et al., 2019). Intriguingly, TDP-43 has been identified as a major component of pathological aggregates in FTD and ALS even if not mutated (Arai et al., 2006; Neumann et al., 2006; Davidson et al., 2007). In many cells containing these pathological aggregates, TDP-43 is efficiently cleared from the nucleus, where it is mostly located in healthy conditions (Neumann et al., 2006; Davidson et al., 2007; Mackenzie et al., 2007). This peculiar finding leads to the question of whether loss of nuclear TDP-43 function or aggregate-mediated toxicity is detrimental in the context of the pathology (reviewed by Lee et al., 2011). Numerous studies have bolstered the hypothesis that TDP-43 aggregates are toxic. However, cytotoxic effects have also been observed in the absence of aggregates, even when mutated forms of TDP-43 still displayed nuclear localization (Hergesheimer et al., 2019). This points out the multifaceted pathological mechanisms involving TDP-43. One notable exception among the variety of underlying mutations in ALS patients is the group of cases harboring mutations in the *Sod1* gene, where TDP-43 is absent in aggregates (Mackenzie et al., 2007).

Although a lot of research has been carried out to unravel the genetic and molecular basis of ALS, available drugs are scarce and at best delay the progression of the disease: Riluzole is the most common and only widely approved drug (first preclinical study by Mizoule et al., 1985). Clinical studies have shown that Riluzole prolongs the survival of ALS patients by two to three months (Miller et al., 2012). Edaravone is a free radical scavenger and delays the progression of functional decline (Rothstein, 2017, reviewed by Es et al., 2017). The drug has been approved consecutively by South Korea, U.S., Canada, Switzerland and China from 2015 onwards, but has not been submitted for approval in the European Union (EU). Nuedexta does not extend the lifespan but appears to improve the quality of life due to dampened pseudobulbar affects, *i.e.* episodes of uncontrolled laughing or crying, in ALS (Brooks et al., 2004). Finally, antisense-oligonucleotides for *sod1* have emerged as promising treatment, as they extended the lifespan in the $SOD1^{G93A}$ mouse model of ALS (McCampbell et al., 2018).

Role of Schwann cells & Oligodendrocytes in ALS

Although the major affected cell types are motor neurons, glial cells potentially modulate the disease or directly contribute to neuronal cell death (reviewed by Valori et al., 2014; Philips and Rothstein, 2014; Trias et al., 2017; Gentile et al., 2019). Based on presence of aggregates positive for (phosphorylated) TDP-43, OLs are also affected in ALS patients (Tan et al., 2007; Nishihira et al., 2008; Philips et al., 2013; Brettschneider et al., 2014; Rohan et al., 2014; Fatima et al., 2015; Takeuchi et al., 2016a; Takeuchi et al., 2016b). Moreover, it has been shown that OLs modulate the pathogenesis in the $SOD1^{G93A}$ mouse model (Kang et al., 2013): Ablation of $SOD1^{G93A}$ specifically in $NG2^{+}$ OPCs delayed the disease progression and extended survival. Contribution of non-neuronal cell types in ALS mouse models is further reflected by the extended lifespan of wt/mutant SOD1 chimeras (Clement et al., 2003). SOD1-based mouse models are the first and most studied models of ALS (reviewed by Tan et al., 2017). In $SOD1^{G93A}$ mice, axonal pathology including denervation and axonal loss preceded behavioral symptoms or loss of motor neurons (Fischer et al., 2004; Verheijen et al., 2014). These studies each analyzed post-mortem biopsies from ALS patients and confirmed their observations, suggesting that peripheral, non-cell autonomous neurotoxicity is involved. Conditional deletion of transgenic expression of mutant SOD1 in SCs further suggested a contribution specifically by SCs: Dismutase inactive $SOD1^{G85R}$ transgenic mice displayed delayed pathology and extended survival in mice with conditionally diminished transgene expression in SCs (Wang et al., 2012b).

Conversely, deletion of dismutase active $SOD1^{G37R}$ transgene expression accelerated the disease progression and shortened the life expectancy of mice (Lobsiger et al., 2009). The authors concluded that both SOD1 gain or loss of function in SCs modulates ALS pathogenesis. In summary, there is evidence that both OLs and SCs might be involved in the pathogenesis of amyotrophic lateral sclerosis.

3.2. RNA-binding proteins

RNA-biology is largely governed by RNA-binding proteins (RBPs), assembling to ribonucleoproteins (RNPs) together with RNA. Heteronuclear ribonucleoproteins (hnRNPs) are an evolutionary conserved, major subclass of RNPs and primarily found in the nucleus. The hnRNPs assemble with (pre-)mRNA and provide a processing center for many aspects of RNA biology, such as splicing, polyadenylation, nuclear export, localization, stability, and translation. Historically, RBPs are classified as hnRNPs when they are in complex with RNA Polymerase II derived RNA and not part of other known stable RNP complexes such as small nuclear ribonucleoproteins (snRNPs, reviewed by Dreyfuss et al., 1993). This classification of hnRNPs has thereby been largely based on the availability of experimental techniques. However, a strict distinction from other RNP classes like splicing factors is not fully established (reviewed by Dreyfuss et al., 2002). Most hnRNPs contain a conventional nuclear localization signal and are usually composed of an RNA binding domain (RBD) and an auxiliary domain (reviewed by Bandziulis et al., 1989; Geuens et al., 2016). The most notable RBD is the RNA recognition motif (RRM): It contains two highly conserved RNP consensus sequences termed RNP-1 and RNP-2 (Adam et al., 1986; Swanson et al., 1987). The RRM forms a $\beta\alpha\beta$-$\beta\alpha\beta$ domain structure (β: β-sheets, α: α-helix), positioning RNP-1 and RNP-2 into close proximity to each other and the nucleic acid (Wittekind et al., 1992; Oubridge et al., 1994). Some hnRNPs are also able to interact with single-stranded DNA (ssDNA, reviewed by Dreyfuss et al., 1993; Dickey et al., 2013). Auxiliary, *i.e.* non-RBD, domains add another layer of diversity to the interactions with other proteins. The combination of two RRMs and glycine-rich auxiliary domain has been identified as a prevalent eukaryotic structure of hnRNPs (Matunis et al., 1992). More complexity is added by post-translational modifications.

The hnRNPs are known to be post-translationally modified by phosphorylation (Wilk et al., 1983; Karn et al., 1977; Holcomb and Friedman, 1984; Dreyfuss et al., 1984; Habelhah et al., 2001; Ostareck-Lederer et al., 2002), methylation (Beyer et al., 1977; Karn et al., 1977; Williams et al., 1985; Merrill et al., 1986; Kim et al., 1997; Ostareck-Lederer et al., 2006) and sumoylation (Li et al., 2004; Vassileva and Matunis, 2004).

3.2.1. TDP-43

TDP-43 is an hnRNP-like protein with multifaceted functions in RNA biology. It was discovered in HeLa cells as a protein of 43 kDa binding to HIV-1 TAR DNA sequence motifs (Ou et al., 1995). Mouse and human TDP-43 protein have 96% sequence identity (from mouse transcript NM_145556.4 and human transcript NM_007375.3).

Structure

The main isoform of human and mouse TDP-43 consists of 414 amino acids (Fig. 3.6a). The protein can be roughly separated into three regions: 1) The N-terminal domain consists of a ubiquitin-like fold and is able to interact with ssDNA (Qin et al., 2014). The first ten N-terminal residues are required for homodimerization, which is vital for splicing activity (Fig. 3.6b-1, Zhang et al., 2013; Jiang et al., 2017). 2) Two RNA recognition motifs (Fig. 3.6b-2, Ou et al., 1995; Buratti and Baralle, 2001). 3) The C-terminal sequence is an amyloidogenic, prion-like region that consists of a glycine-rich, low complexity domain (Ou et al., 1995) with a transient α-helix in the middle (Fig. 3.6b-3, Jiang et al., 2013; Mompean et al., 2014; Mompean et al., 2015). TDP-43 is widely detected in the cell nucleus and bears two nuclear localization signals between the N-terminal domain and the RNA-binding domain (Ayala et al., 2008; Winton et al., 2008). Although a putative nuclear export signal has been identified, nuclear export is predominantly driven by passive diffusion independent of exportins 1 and 5 (Pinarbasi et al., 2018; Ederle et al., 2018). TDP-43 is generally expressed at high levels during embryonic development and is essential for early embryonic development (Sephton et al., 2010; Wu et al., 2010). It regulates itself post-transcriptionally though binding to its own 3'UTR and destabilizing the transcript (Ayala et al., 2011; Polymenidou et al., 2011; Avendano-Vazquez et al., 2012).

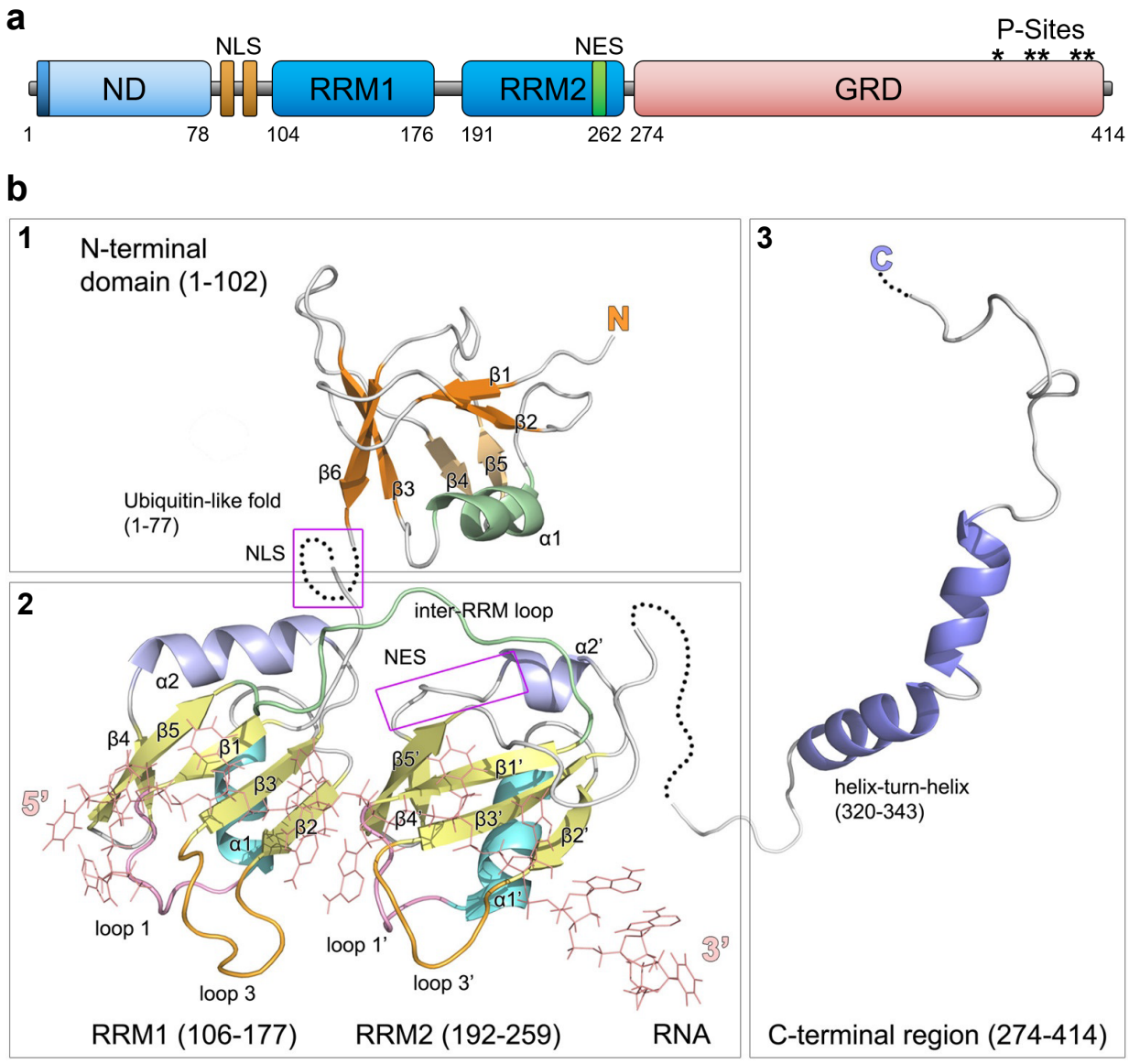

Figure 3.5: TAR-DNA Binding Protein 43 - TDP-43 (a) Domains of TDP-43. The N-terminal domain (ND) is required for dimerization, particularly the first 10 amino acids (dark blue). Two nuclear localization signals (NLS) are located between the ND and the tandem RNA recognition motifs (RRMs). The second RRM contains a putative nuclear export signal (NES). The C-terminal, glycine-rich domain (GRD) is largely unstructured and mediates interactions with other proteins. **(b)** Protein structure of TDP-43. Resolved molecular structures of the N-terminal domain (1), the RRM domains (2) and the C-terminal domain (3). Separate domains are connected by dashed lines. NLS and NES sequences are shown in purple boxes. The N-terminal domain harbors an ubiquitin-like fold. The structure of the RRMs is shown in complex with RNA (pink line drawing). Illustration modified from Sun and Chakrabartty (2017).

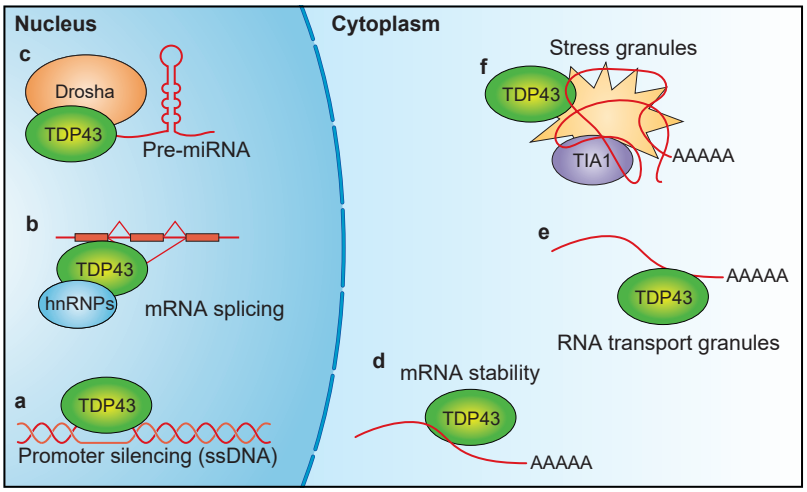

Figure 3.6: Functional spectrum of TDP-43 TDP-43 is mostly located in the nucleus (a-c), but also influences RNA metabolism in the cytoplasm (d-f). **(a)** TDP-43 is located in transcriptionally active nuclear regions and in one case reportedly binds to the promoter region and represses transcription. **(b)** The most-studied function of TDP-43 entails alternative splicing and repression of non-canonical, cryptic splicing. **(c)** TDP-43 interacts with proteins of the microprocessor and is involved of miRNA biogenesis of selected miRNAs. **(d)** The stability of some mRNAs is either promoted or lowered through binding of TDP-43 to their 3'UTR. TDP-43 binds to its own transcript and promotes destabilization, in order to regulate its own expression in a negative feedback-loop. **(e)** In neurons, TDP-43 is also located in RNA transport granules. ALS-related mutations impair the transport function of TDP-43. **(f)** Upon diverse cellular conditions, TDP-43 locates to stress granules and influences their assembly.

Function

TDP-43 is well described as RNA-binding protein that is involved in several functional aspects of RNA biology. It binds to UG-rich repeats of intronic pre-mRNAs in the nucleus or to 3'UTRs of mRNAs in the cytoplasm (Buratti and Baralle, 2001; Buratti et al., 2001; Buratti et al., 2004; Polymenidou et al., 2011; Tollervey et al., 2011; Xiao et al., 2011; Sephton et al., 2011; Narayanan et al., 2013). TDP-43 interacts with transcripts of up to several thousand protein-coding genes, which represent a substantial part (~30%) of the transcriptome (Polymenidou et al., 2011; Tollervey et al., 2011; Sephton et al., 2011). To a minor extent TDP-43 additionally interacts with long non-coding RNAs (lncRNA, Tollervey et al., 2011). In the nucleus, TDP-43 co-localizes with sites of active transcription and associates with nascent transcripts (Casafont et al., 2009). Interaction with genomic DNA has been reported for the *acrv1* gene, where TDP-43 binds to the promoter region and represses transcription (Lalmansingh et al., 2011). Most notably, TDP-43 globally regulates splicing, particularly alternative and non-canonical, cryptic splicing (Buratti and Baralle, 2001; Buratti et al., 2001; Buratti et al., 2004; Polymenidou et al., 2011; Tollervey et al., 2011; Ling et al., 2015; Vogler et al., 2018).

Nuclear functions of TDP-43 are further reflected by its protein interactome: In the nucleus it mainly interacts with hnRNPs and splicing complexes (Freibaum et al., 2010; Ling et al., 2010; Sephton et al., 2011). In addition, TDP-43 interacts at least *in vitro* with Drosha/Dicer and other miRNA processing associated proteins, and is involved in miRNA biogenesis (Gregory et al., 2004; Ling et al., 2010; Kawahara and Mieda-Sato, 2012; Di Carlo et al., 2013). In the cytoplasm, TDP-43 binds to the 3'UTR of mRNAs and either promotes or lowers their stability to regulate expression (Ayala et al., 2011; Colombrita et al., 2012; Costessi et al., 2014; Strong et al., 2007). Interestingly, TDP-43 destabilizes its own transcript and thereby regulates its protein levels in a negative feedback loop (Ayala et al., 2011). TDP-43 in the cytoplasm interacts with proteins largely involved in translation and localizes to RNP granules (Elvira et al., 2006; Freibaum et al., 2010; Blokhuis et al., 2016). RNP granules are membrane-less organelles and differently influence post-transcriptional regulation, including storage of translationally repressed transcripts (stress granules, processing bodies) or transport of transcripts to specific sites (transport granules, reviewed by Anderson and Kedersha, 2009). As demonstrated in neurons, TDP-43 forms RNP granules in association with bound mRNA and is transported along axons (Alami et al., 2014, not yet peer-reviewed: Wong and Tsai, 2019). TDP-43 is found in stress granules under acute cellular stress inductions and potentially contributes to their formation (Freibaum et al., 2010; Dewey et al., 2011; Colombrita et al., 2009; McDonald et al., 2011). Stress granules transiently form and store a particular set of transcripts in the cytoplasm under a variety of stress conditions (Anderson and Kedersha, 2008).

Post-translational Modifications

A variety of post-translational modifications have been reported for TDP-43 and include phosphorylation, ubiquitinylation, cysteine oxidation, proteolytic cleavage, and acetylation (Buratti, 2018). Most of these modifications have been studied in a disease-focused manner due to the prominent manifestation of aggregated TDP-43 in neurodegenerative diseases (see subsection 3.1.5). Several phosphorylation sites have been identified (Neumann et al., 2009; Kametani et al., 2016), most notably S48 (Wang et al., 2018a) and S409/410 (Hasegawa et al., 2008; Inukai et al., 2008; Kim et al., 2015). A phosphomimetic S48E mutation impaired the oligomerization and consequently the splicing function of TDP-43 (Wang et al., 2018a), while phosphomimetic mutants of S408/409 are toxic to cells (Kim et al., 2015). The E3 ligase Parkin ubiquitinylates TDP-43 (Hebron et al., 2013) and a variety of targeted lysine residues have been identified in diverse contexts (Seyfried et al., 2010; Dammer et al., 2012; Wagner et al., 2011; Kim et al., 2011).

TDP-43 is mainly degraded via the ubiquitin-proteasome system (UPS, Scotter et al., 2014). Ubiquilin-2, an ubiquitin-like protein involved in UPS and autophagy (Ko et al., 2004; N'Diaye et al., 2009a; N'Diaye et al., 2009b), binds with high affinity to the C-terminus of TDP-43 and was suggested to mediate the degradation of TDP-43 (Cassel and Reitz, 2013). Remarkably, mutations in the *Ubqln2* gene cause ALS and FTD (Deng et al., 2011; Daoud et al., 2012; Synofzik et al., 2012; Williams et al., 2012). Oxidative stress can lead to cysteine oxidation and result in both both inter- and intra-molecular disulphide bonds (Cohen et al., 2012). Cysteine oxidation located within the RRMs generally leads to loss of function and aggregation (Chang et al., 2013; Rabdano et al., 2017). Oxidation of N-terminal cysteines (C39,C50) reduces TDP-43 tetramerization and may influence aggregation (Jiang et al., 2017; Bozzo et al., 2016).

Although it remains controversial and most likely depends on the exact experimental system, aggregation is also observed when TDP-43 is overexpressed (Igaz et al., 2011; Shan et al., 2010; reviewed by Hergesheimer et al., 2019). Aggregates contain C-terminal fragments (CTF) of approximately 25 and 35 kDa. These cytoplasmic fragments lack the NLS and when generated in the nucleus are efficiently exported (Pesiridis et al., 2011). These fragments are most likely generated proteolytically, e.g. upon cellular stress (Dormann et al., 2009; Wobst et al., 2017), and are closely related to pathology. Potential proteases include caspases 3,4 and 7 (Zhang et al., 2007; Huang et al., 2017; Li et al., 2015), but also AEP (Herskowitz et al., 2012) and calpain (Yamashita et al., 2012) have been reported to cleave TDP-43.

TDP-43 in Myelination-Competent Glia

TDP-43 (TBPH) knockdown in *Drosophila* glial cells results in age-dependent motor deficits, premature lethality, and defects in motor neuron wrapping (Ghosh et al., 2013; Diaper et al., 2013; Romano et al., 2015). These data suggest that TDP-43 might be essential also in glia cells of other species. As elaborated above, mutations in TDP-43 have also been associated with severe human disorders like ALS, and OLs have also been implicated in TDP-43 ALS/FTLD pathology (subsection 3.1.5). Furthermore, mice harboring TDP-43 deficient OLs display progressive motor deficits and premature lethality, at least in part associated with the death of differentiated oligodendrocytes (Wang et al., 2018b).

3.3. RNA splicing

Transcribed pre messenger RNA (pre-mRNA) undergoes three major modifications in eukaryotes: 5' capping, splicing and 3' polyadenylation. During splicing, separated blocks of coding or regulatory sequences are joined and the separating sequences (introns) are removed (Berget et al., 1977; Chow et al., 1977). While introns do not contribute to the mRNA, they can contain functional non-coding RNA species such as miRNAs and snoRNAs, or serve functions amongst others as regulatory sequences for transcription factors at the genomic level or for splicing regulatory factors at the transcript level (reviewed by Jo and Choi, 2015). There are some forms of non-canonical splicing generating retained introns, recursive splicing, circular RNAs, microexons and cryptic exons. The latter will be subsequently explained in more detail.

3.3.1. RNA Splicing by the Spliceosome

Splicing mediated by the spliceosome is a widely conserved process among eukaryotes, although the proportion of pre-mRNAs having introns is highly variable among different eukaryotic organisms: Unicellular eukaryotes, as for example trypanosomes, have an extremely low prevalence for intron-containing genes. In yeast (S. Cerevisiae), it is estimated that only 5 % of all pre-mRNAs contain introns (~300 genes, Liang et al., 2003; Morgan et al., 2019). On the other hand, pre-mRNAs of mammalian organisms are widely spliced (mice ~85 %, humans ~90 %; Cunningham et al., 2019). The spliceosome is a ribozyme that mediates splicing dependent on two catalytic divalent metal ions (Fica et al., 2013; Steitz and Steitz, 1993). It is assembled stepwise and changes composition along with the splicing process, which essentially consists of two subsequent S_N2-type transesterifications (reviewed by Shi, 2017): First, the phosphoester bond at the 5' splice site (5'SS) is broken and the free 5'end of the intron is linked to the branch site located on the same intron, resulting in a free 3'end of the 5' exon and an intron-lariat 3' exon intermediate. Second, the intron-lariat is detached and the exons are ligated. The core of the spliceosome consists of five small nuclear ribonucleoproteins (snRNPs), containing uridine-rich small nuclear RNAs (snRNAs U1, U2, U4, U5 and U6) and their associated proteins. The snRNAs interact with the pre-mRNA and position it for the splicing. In addition, U2, U5 and U6 form the active site together with the two associated Mg^{2+} ions. The spliceosome is a complex and protein-rich ribozyme, containing ~45 snRNP-associated proteins and a total of ~170 spliceosome-associated proteins (Wahl et al., 2009).

3.3.2. Alternative splicing

The presence of introns not only gives rise to additional regulatory features, but also allows to differently combine the exons from one gene and thereby increase the genome coding capacity. Another evolutionary benefit is the possibility to combine exons from different ancestor genes to form new genes, commonly referred to as exon shuffling (Hynes, 2012). In line with the low prevalence of introns in Yeast (*S. Cerevisiae*), there are only very few reported cases of alternative splicing (Morgan et al., 2019). Conversely, it is estimated that about 95 % of human multi-exon genes are alternatively spliced (mice ~79 %, Pan et al., 2008; Cunningham et al., 2019). However, the contribution of alternative splicing events towards functionally distinct isoforms is controversial, and is estimated to only hold true for a minority of genes (Bhuiyan et al., 2018; Saudemont et al., 2017). Differential usage of exons is controlled by regulatory elements, their associated proteins and the splice sites themselves. A strong splice site is very similar to the consensus sequence and thereby has a higher affinity to splicing factors than a weak splice site with lower consensus. Usually, strong splice sites are used constitutively, whereas the usage of weak splice sites is variable. The alternative use of splice sites involves alternative cassette exons (sometimes mutually exclusive), alternative 5' or 3' splice sites, or retention of alternative introns. Cis-acting splicing regulatory elements (SREs) are found on exons or introns to both promote (enhancers) or repress (silencers) splicing. These elements are often targeted by trans-acting factors (regulatory RBPs), such as Ser-Arg-rich (SR) proteins as well as proteins of the hnRNP family. Regulatory RBPs always exert their function via the core splicing machinery through regulating snRNP assembly, recruitment of limited core components to the splice site, or modulating key steps of the splicing cycle (Fu and Ares, 2014). Despite the identification of many trans-acting factors and regulatory sequences, a 'splicing code' to predict the splicing outcome could not be deciphered and the specific context matters (Fu and Ares, 2014): The decision between competing splice sites may be reached due to relatively more efficient interaction with the splicing machinery. In many cases SR proteins are positive splicing factors promoting exon inclusion, and hnRNPs repress splicing. The location of the SRE also changes the outcome, and it is decisive whether it is located in the exon or intron, and where exactly. For example, the position of an intronic SRE relative to the exon determines whether a trans-acting factor either promotes or inhibits exon inclusion. Splicing factors may bind cooperatively or compete for the same binding site.

3.3.3. Non-canonical splicing

Non-canonical splicing is a collection of various kinds of splicing events. Some are likely physiological and constitute a post-transcriptional regulation of gene expression, while others have detrimental effects and have to be generally suppressed. As an example discovered in Arabidopsis, exonic introns (exitrons) are introns within protein coding exons and affect protein structure (Marquez et al., 2015). If splice sites are weak or introns are very short, it may be retained in the mRNA (retained introns). Retained introns are proposed to be another global layer of regulation to tune gene expression (Yap et al., 2012; Wong et al., 2013; Braunschweig et al., 2014; Boutz et al., 2015). These transcripts are either directly degraded in the nucleus (Yap et al., 2012) or after export in the cytoplasm by nonsense-mediated mRNA decay (NMD, Wong et al., 2013). NMD is one of the quality control systems of a cell and typically targets mRNAs with a termination codon within the open reading frame, commonly referred to as premature termination codon (PTC, one form of NMD-activating codons; reviewed by Lykke-Andersen and Jensen, 2015). To efficiently trigger NMD, PTCs must be located 50-55 nucleotides upstream of the last exon-exon junction (reviewed by Lykke-Andersen and Jensen, 2015).

AS-NMD and Cryptic Splicing

Introns comprises a large sequence space, so it is not unlikely that a canonical splice site motif appears by pure chance. These cryptic splice sites do not necessarily lead to efficient splicing and mostly only appear once a repressive RBP is removed or the site has become stronger due to genomic mutations. If cryptic splice sites are used by the splicing machinery, intronic sequence is incorporated as a cryptic exon. Cryptic exons often result in a frameshift and emergence of pre-termination codons (PTCs), finally leading to the degradation of the transcript by NMD (Eom et al., 2013; Ling et al., 2015; Ling et al., 2016; Humphrey et al., 2017). Cryptic exons are usually defined as non-annotated exons that impair the function of the mRNA sequence, *e.g.* by introducing frameshifts (Sibley et al., 2016). However there are also functional NMD exons or poison cassettes (Jangi et al., 2014), which introduce PTCs as a regulatory mechanism to tune the transcript levels. Interestingly, splicing regulatory RBPs themselves are not only part of the splicing dynamics but also prominent members of proteins regulated by AS-NMD (Lewis et al., 2003; Mendell et al., 2004; Baek and Green, 2005; Lareau et al., 2007; Ni et al., 2007; Jangi et al., 2014; Yan et al., 2015).

A distinct feature of alternatively spliced NMD exons is their high conservation, indicating a physiological function (Lareau et al., 2007; Ni et al., 2007). Less conserved exonization (emergence of cryptic exons) occurs due to transposable elements (TEs, Sorek et al., 2002; Vorechovsky, 2010; Lin et al., 2009; Sela et al., 2010; Shen et al., 2011). Alu elements, which are short interspersed elements (SINEs) found in primates, are strikingly numerous and cover about 11% of the whole human genome (Lander et al., 2001). Their incorporation into the genome often creates polypyrimidine tracts and few mutations generate potential splice sites (Sorek, 2007; Keren et al., 2010). The polypyrimidine tracts (poly-U) serves as binding site for regulatory factors such as U2AF2 and TIA proteins, which thereby promote the cryptic splicing (Gal-Mark et al., 2009; Zarnack et al., 2013). If mutations lead to a weak splice site, it may remain without deleterious effect as the majority of the transcripts are still properly spliced. hnRNP C has been identified as a safeguard against unwanted exonization (Zarnack et al., 2013): It binds to the Alu element derived polypyrimidine tracts (poly-U) and thereby directly competes with U2AF65, an essential factor for recruitment of the U2 snRNP. Other RNA binding proteins that act as safeguards of the transcriptome have been described in the last years: TDP-43 (Ling et al., 2015), PTBP1/2 (Ling et al., 2016), hnRNP L (McClory et al., 2018) and RBM17 (Tan et al., 2016). hnRNP L represses cryptic splicing of exons containing $(CA)_n$ repeats. TDP-43 and PTBP1/2 act via intronic, U-rich repeats of $(UG)_n$ and $(CU)_n$ respectively. While these proteins do have conserved targets not associated with cryptic splicing, cryptic exons are only poorly conserved (Ling et al., 2015; Ling et al., 2016; Humphrey et al., 2017). Due to the complex mechanism of alternative splicing itself and incidentally its low predictability, it is not surprising that also cryptic splicing events are highly variable depending on the cellular context (Jeong et al., 2017). Two recent studies focused on motor neurons have identified an essential TDP-43-mediated repression of cryptic splicing of *stmn2* (stathmin-2) pre-mRNA, which encodes a microtubulin-associated protein required for normal axonal outgrowth and regeneration (Melamed et al., 2019; Klim et al., 2019): Cryptic splicing produced a ten times shorter transcript due to an alternative 3'UTR in the second, cryptic exon. Remarkably, reconstitution of Stathmin-2 expression could restore the impairments in cells without TDP-43 function, indicating that TDP-43 is required in these cells to a large extent to safeguard against cryptic splicing of *stmn2*.

3.4. Motivation and Aim of the Study

There is evidence from *Drosophila* that TDP-43 performs a vital function in glial cells, and recently evidence regarding mouse oligodendrocytes. TDP-43 is mutated in some cases of ALS, and is a hallmark component of pathological aggregates in the vast majority of ALS patients. Possibly due to its implication in ALS, previous studies of TDP-43 have been highly focused on neurons, and the current available literature on the relationship between myelinating cells and TDP-43 is limited and fragmentary. Most mouse models of ALS are based on mutations of the *Sod1* gene (Tan et al., 2017) and mouse models based on TDP-43 disease mutations have not been very successful in entirely mimicking the disease. OLs and SCs are known to modulate the pathological progression in a $SOD1^{mutant}$ ALS mouse models, emphasizing that these cells have a potential impact in neurodegenerative diseases like ALS, which might also include the majority of ALS cases with aggregates containing TDP-43. Functionally, TDP-43 is involved in many aspects of RNA biology and interacts with a plethora of transcripts in mouse and human cells. Considering the available findings, we hypothesize that TDP-43 plays a fundamental role in myelination-competent glia.

In this study, we want to elucidate the physiological function of TDP-43 in myelination-competent glia. In our analysis, we will investigate the function of TDP-43 during cell differentiation and homeostasis. To this end, we will conditionally delete TDP-43 in both OLs and SCs separately during development and after developmental myelination. Ultimately, we aim to gain knowledge about the cell-intrinsic functional role of TDP-43, and further consider potential non-cell autonomous impact on other cells in the nervous system, including neurons.

Our findings will help in understanding the basic function of this globally acting RNA-binding protein in myelination-competent glia. Moreover, the knowledge gained could feed into our understanding of the loss-of-function component of TDP-43 proteinopathies such as ALS.

3.5. Frequently used Abbreviations & Genes

SC	Schwann cell
OL	oligodendrocyte
SN	sciatic nerve
SpC	spinal cord
CC	corpus callosum
CB	cerebellum
WM	white matter
GM	grey matter

TAR-DNA Binding Protein 43

gene	*Tardbp*
mRNA	*tardbp* or TDP-43 mRNA
Protein	TDP-43

Neurofascin

gene	*Nfasc*
mRNA	*nfasc*
Protein	NFASC

Glial Isoform

mRNA	*nfasc155*
protein	NF155 (or glial Neurofascin)

Neuronal Isoform

mRNA	*nfasc186*
protein	NF186

4. Methods

Parts of the methods described here were already described in my master thesis "RNAi in Schwann Cell Development: The Role of the Lin28/let-7 Axis, 2014" and were partly transferred to this section.

4.1. Animal Procedures

4.1.1. Transgenic Mice

Mice harboring floxed alleles of TDP-43 (*B6(SJL)-Tardbptm1.1Pcw/J*; Chiang et al., 2010) were obtained from The Jackson Laboratory (stock no 017591). Mice carrying a Cre transgene under control of the *Dhh* (Jaegle et al., 2003), *Mpz* (Feltri et al., 1999), *Cnp* (Lappe-Siefke et al., 2003) or *Olig2* (Schuller et al., 2008) promoter regulatory sequences were used to delete TDP-43 during development. To induce recombination in a temporally controlled manner, mice carrying a Cre^{ERT2} transgene under control of the *Plp1* or *Mpz* promoter regulatory sequences (Leone et al., 2003) were used. Mice expressing EGFP under control of the *Pdgfrα* promoter (*B6.129S4-Pdgfratm11(EGFP)Sor/J*; Hamilton et al., 2003) were obtained from The Jackson Laboratory (stock no 007669), as well as mice carrying a lox-Stop-lox-tdTomato cassette in the Rosa26 locus (*B6.Cg-Gt(ROSA)26Sortm9(CAG-tdTomato)Hze/J*, stock no 007909; Madisen et al., 2010).

To conditionally delete TDP-43 in Schwann cells, *dhh*Cre or *mpz*Cre positive mice were crossed with TDP-43 floxed mice (*dhh*-cKO and *mpz*-cKO). Deletion of TDP-43 in oligodendrocytes was achieved through crossing *cnp*Cre or *olig2*Cre positive mice with TDP-43 floxed mice (*cnp*-cKO and *olig2*-cKO). *mpz*Cre^{ERT2} and *plp*Cre^{ERT2} positive mice were crossed with TDP-43 floxed mice to investigate the inducible deletion of TDP-43 in Schwann cells (*mpz*-iKO) and oligodendrocytes (*plp*-iKO), respectively. Reporter lines were crossed in for some experiments to label recombined cells. *cnp*Cre TDP-43 mice were crosses with LSL-tdTomato and *pdgfrα*H2B-EGFP mice. *plp*Cre^{ERT2} and *mpz*Cre^{ERT2} TDP-43 mice were crossed with LSL-tdTomato mice. Recombination of *plp*Cre^{ERT2} and *mpz*Cre^{ERT2} mice was induced between 8 to 10 weeks of age by daily intraperitoneal injections of tamoxifen (2 mg, MERCK) dissolved in 10% Ethanol and sunflower seed oil (MERCK) over five consecutive days. Control mice for experiments were Cre^{neg} TDP-$43^{fl/fl\ or\ fl/wt}$, and Cre^{pos} TDP-$43^{wt/wt}$ $tdTomato^{tg/wt}$ if tdTomato was additionally used. Animals were maintained on a C57BL/6 inbred background. Experimental animals were on a mixed background between C57BL/6 and B6SJL due to the generation of the TDP-43 floxed mice. Mice of either sex were used in the experiments. A maximum of five animals were housed together in individually ventilated cages (type II long, TECNIPLAST) in a 12 h light-dark cycle with standard chow *ad libitum*. Experimental mice were euthanized using one of the following methods: a) a lethal intraperitoneal injection of pentobarbital (150 $\mu g/_{gBW}$, Esconarkon, Streuli Pharma SA), b) inhalation of CO_2 (only for animals older than 2 weeks) or d) decapitation of young mice (P0 – P10). All animal experiments were performed with the approval of the Zurich Cantonal Veterinary Office (permits ZH161/2014, ZH090/2017 and ZH234/2015).

4.1.2. Genotyping

Biopsies from non-genotyped mice were obtained by clipping either a toe or an ear-cookie in older animals. Alkaline lysis buffer (200 µl; 25 mM NaOH, 0.2 mM EDTA, pH 12) was added and the toe-clipped biopsies were quickly spun down (1 min at 17'000 rcf, Heraeus Pico 17 Centrifuge, Thermo). All samples were boiled on a heatblock (Thermomixer Compact, 25 min at 95 °C, 800 rpm). Neutralization buffer was added (200 µl; 40 mM Tris-HCl, pH 5) at the end. The solution was used as source for the genomic DNA. Primer pairs indicated in Tab. 4.1 were used in the reaction mix (Tab. 4.2), and the reaction was performed in a thermal cycler (Tab. 4.4, T3000, Biometra). Agarose gels (2-2.5 %) were prepared using 1x TAE buffer (100 ml; 40 mM Tis Base, 11 % acetic acid, 1 mM EDTA). SYBR Safe DNA Gel Stain (7.5µl, Invitrogen) was added to the cooled, hand-warm solution. The gel was poured into a standard gel cast (PerfectBlue Gelsystem Mini L, Peqlab). PCR samples were mixed with appropriate amounts of 6x orange-G loading buffer (Tab. 4.3) before loading into the wells. 6 µl of Log2 DNA ladder (New England Biolabs) were used. PCR samples were separated at 100 V (5 V/cm) using either a PowerPac 3000 or 300 (BioRad) and fluorescent signals were acquired (E-box, Vilber Lourmat).

Name		Forward (5′–3′)	Reverse (3′–5′)
Tardbp		AACTTCAAGATCTGACACCCTCCCC	GGCCCTGGCTCATCAAGAACTG
Cre	***unspecific***	ACCAGGTTCGTTCACTCATGG	AGGCTAAGTGCCTTCTCTACA
	cnp	GATGGGGCTTACTCTTGC	CATAGCCTGAAGAACGAGA
	dhh	ATACCGGAGATCATGCAAGC	GGTGGTGTGGTAGAGCAGGT
	mpz	ACCACCACCTCTCCATTGCAC	GCTGGCCCAAATGTTGCTGG
CreERT2	***plp***	CACTCTGTGCTTGGTAACATGG	TCGGATCCGCCGCATAACC
	mpz	CTGCACAGACATGAGACCATAGG	TCGGATCCGCCGCATAACC
Rosa26	***wt***	AAGGGAGCTGCAGTGGAGTA	CCGAAAATCTGTGGGAAGTC
	LSLtdtomato	GGCATTAAAGCAGCGTATCC	CTGTTCCTGTACGGCATGG
Pdgfrα	***wt***	CCCTTGTGGTCATGCCAAAC	GCTTTTGCCTCCATTACACTGG
	egfp	CCCTTGTGGTCATGCCAAAC	ACGAAGTTATTAGGTCCCTCGAC

Table 4.1: Mouse Genotyping Primer Sequences

Substance	Amount	Final
10x PCR Buffer (Gibco)	3 µl	1 x
$MgCl_2$ 50mM	0.9 µl	1.5 mM
Primers, each 5µM	3 µl	0.5 µM
dNTPs, each 25mM	0.24 µl	200 µM
Taq (LifeTech, 5 U/µl)	0.09 µl	1.5 U/100µl
ddH_2O	20.77 µl	
Sample (DNA)	2 µl	
Total Reaction Volume	30 µl	

Table 4.2: PCR Reaction Mix

Substance	Concentration
Ficoll 400	2.5 %
EDTA	11 mM
Tris-HCl	3.3 mM
SDS	0.017 %
Orange G	0.15 %

Table 4.3: 6x Orange-G Loading Buffer

a regular

Cycles	**Time** (s)	**Target** (°C)
1	120	94
30	45	94
	30	60
	60	72
1	300	72
	∞	4

b Rosa26 tdTomato

Cycles	**Time** (s)	**Target** (°C)	**Δ°C/cycle**
1	120	94	
10	45	94	
	30	65	-0.5
	60	72	
30	45	94	
	30	60	
	60	72	
1	300	72	
	∞	4	

Table 4.4: Program for genotyping PCRs. (a) Cre, TDP-43, *pdgfrα*$^{\text{H2B-EGFP}}$. For *plp*Cre$^{\text{ERT2}}$ and *mpz*Cre$^{\text{ERT2}}$, the annealing temperature was set to 53 °C. **(b)** Program used for the tdTomato reporter line.

4.1.3. Behavioural Analysis

To assess the motor performance of mice, we applied the inverted grid hanging test (Deacon, 2013 from Kondziella, 1964). Mice were placed on the lower side of a suspended wire mesh (28x28cm, mesh-size of 13 mm, mounted on a 28x28cm frame). The hanging time until mice fell into a padded landing zone 30 cm below the wire mesh was recorded. Three trials with at least 30 min inbetween trials were performed. The maximum score was set to 10 min, mice holding onto the grid beyond this time were removed from the grid.

4.1.4. *In vivo* electrophysiological analysis

The sciatic and the tibial nerve were used for analysis as described (Zielasek et al., 1996). Anaesthesia was induced by injection of ketamine (Ketanest, 90 µg/gBW) and xylazine (Rompun, 9 µg/gBW). Anaesthesia was controlled and adjusted by the loss of the pedal withdrawal reflex. The body-temperature was continuously controlled and maintained at 32-34 °C using a heat-lamp. One pair of near-nerve electrodes (proximal stimulation) were inserted into the left sciatic notch, a second pair of near-nerve electrodes (distal stimulation) was inserted subcutaneously along the tibial nerve just above the ankle. The distance between proximal and distal electrodes was used to calculate the nerve conduction velocity (NCV). A third pair of electrodes (muscle recording) was inserted in the skin close to the hallux and between the second and third digit of the left foot. Waves were recorded and processed using a Neurosoft Evidence 3102 electromyograph (Schreiber and Tholen Medizintechnik, Germany) upon supramaximal stimulation. See Tab. 4.5 for used values and calculations.

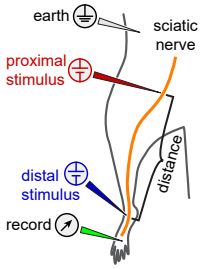

Type/Calculation	Stimulating	Recording	Derived Parameter
motor proximal	proximal	recording	H-wave
motor distal	distal	recording	cMAP
cs latency	distal	proximal	cSNAP
$\frac{\Delta latency_{\text{motor}}(prox.-dist.)}{distance}$			motor NCV
$\frac{latency_{\text{cs}}(dist.\ to\ prox.)}{distance}$			csNCV

Table 4.5: Electrophysiology.
(left) Schematic of electrode placement. **(right)** Settings for recordings, calculations of NCVs and parameters used.

4.1.5. Surgical procedures (nerve crush)

Mice were subjected to unilateral sciatic nerve crush two months post tamoxifen injection. Mice were injected with buprenorphine for analgesia (0.1 mg/kg; Temgesic). A first pre-emptive injection was given before the procedure and two daily injections 4-6 h apart in the following 48 hours. In the same peridod, drinking water was supplemented with buprenorphine (0.3 mg/ml) during the nights. Anesthesia was induced and maintained with isoflurane (Provet AG) inhalation. After blunt dissection to reveal the sciatic nerve, it was crushed for 30 s with blunt forceps (S&T JF-5 TC, FST). Bupivacaine (0.025 %) was administered for local anesthetic treatment. The wound was subsequently closed and the skin incisure was closed with histoacryl tissue adhesive (B.Braun-SSC AG). Morphological analysis was performed~2 mm distal to the crush site.

4.2. Cell Sorting

Mice were either directly decapitated (P5 – P10) or after euthanasia using pentobarbital (>P10), and the spine was cut in the proximal sacral segments of the spinal cord. A syringe filled with cold PBS was inserted into the sacral spinal cavity using eroded 21G canules, and the spine was straightened using mild pressure with a finger. The spinal cord was subsequently extruded by hydraulic pressure. Spinal cords are shortly transferred to dishes with cold PBS and gently tapped on a dry surface to remove excess liquids. Using straight scalpel blades (233-5474, VWR), the spinal cord was finely minced and dissociation buffer was added (490 µl, Tab. 4.6). The mix was subsequently transferred to 15ml tubes and incubated at 37 °C for 20 min with occasional shaking (1'000 rpm for 15 sec per 4 min, ThermoMixer C, Eppendorf). The dissociated tissue was triturated by carefully pipetting 30x with a 1ml pipette tip followed by 20x with a 200µl pipette tip. The digestion was stopped by adding 9.5 ml cold 'stop buffer' (10 % FBS, 5 mM EGTA, DMEM GLutamax). The suspension was centrifuged at 4 °C (5 min at 450 g, for single-cell sequencing 100 g) and the supernatant was carefully aspirated. The pellet containing cells was carefully resuspended in FACS flow buffer (400 µl; 0.5 % BSA, 5 mM EGTA in PBS). For protein analysis, only 0.1 % BSA was used in the flow buffer. Up to 20 min before sorting, the suspension was passed through a 50 µm filter (CellTrics, Sysmex). Sorting itself was performed on a Sony SH800 sorter. A pressure of 3 to 5 was applied to use cells for OPC cultures and single-cell RNA sequencing, for collection of cells in lysis buffers we used a pressure of 6 to 7. Gating was performed according to the specific experiment, however the last gate always positively selected single cells determined by the forward scatter area versus height. Sorting was performed in purity mode.

Substance	Amount
Trypsin[a]	0.15 %
Collagenase, Typ II[b]	0.29 %
Hyaluronidase[c]	1 $^{U}/_{µl}$
DNaseI[d]	80 $^{µ}/_{ml}$

in HBSS

Table 4.6: Dissociation Buffer [a]T9201, Merck; [b]LS004174 and [c]LS005477, Worthington; [d]D4527, Merck

4.3. Biochemical Analysis

4.3.1. RNA Extraction and Analysis

We used the AllPrep RNA/DNA Kit in combination with precedent use of QIAshredder tubes (Qiagen) for peeled – *i.e.* maximum removal of the epi- & perineurium – P5 sciatic nerves which were analysed by RNA sequencing. Total RNA from all other samples was extracted using Qiazol (Qiagen). Whole tissue was ground at -80 °C (metal tube rack on dry ice) in 1.5ml plastic tubes using pre-cooled plastic pestles (Argos Technologies). Triazol was added the suspension, which was further mixed until the tissue dissolved completely. Cells from culture were washed once with cold PBS. Qiazol (1 $^{mL}/_{cm^2}$) was added, and transferred to tubes after gentle shaking.

Samples were left at room temperature for 5 min before chloroform (200 µL/mL Qiazol) was added. Samples were vortexed (15 s) and placed at room temperature for 2 min for phase separation. The supernatant was collected after centrifugation (15 min at 17'000 rcf, 4 °C, Heraeus Fresco 17 Centrifuge, Thermo) in a new tube. Glycogen (40 µg/ml Qiazol, Life Technologies) was added as a co-precipitant along with one volume of isopropanol (-20 °C). After shortly vortexing (15 s) and incubation (10 min at RT), the precipitated RNA was spun down (30 min at 17'000 rcf, 4 °C). Subsequently, the supernatant was removed by aspiration, and the pellet was washed twice with pre-cooled 70% ethanol. Finally, the pellet was allowed to air-dry at room temperature (5-10 min) and resuspended in nuclease-free H_2O (20 µl). The RNA concentration was measured using a spectrophotometer (Nanodrop Lite, Thermo Scientific) or the Qubit RNA HS Assay (Thermo Scientific). RNA was stored at -80 °C.

cDNA was prepared using the "Maxima First Strand cDNA Synthesis Kit for RT-qPCR" (Thermo Scientific). The reagent mix was prepared according to the manufacturer's instructions (Tab. 4.7), and the reverse transcription was performed in a thermal cycler (TProfessional TRIO, Biometra) with the indicated temperature program (Tab. 4.8). cDNA was diluted to 4 µl/ng RNA input with nuclease-free H_2O and stored at -20 °C. The relative abundance of specific transcripts was analysed by real-time quantitative polymerase chain reactions (qPCR). Primers were designed using PrimerBlast (Tab. 4.9, Ye et al., 2012).

Samples were always analyzed in technical triplicates. cDNA and the reaction mix were filled 384-well plates (Tab. 4.10). The plates were sealed afterwards with adhesive foil and the plate was shortly centrifuged (max. 2800 rpm, Centrifuge 5804 R, eppendorf). The qPCR itself was performed in a Light Cycler 480 II (Roche, Tab. 4.11). C_t values were normalized to *gapdh* or *β-actin* (4.1). Linearized ΔC_t values were further normalized to the average of all control samples (4.2). Statistics were performed on the normalized linear ΔC_t values.

Substance	Amount
5x Reaction Mix	4 µl
Maxima Enzyme Mix	2 µl
RNA	100 ng*
H_2O, nuclease-free: fill up to	20 µl
Total Reaction Volume	20 µl

Table 4.7: Reverse Transcription Reaction Mix
*min. amount, up to 1 µg was used.

Time	Temperature
10 min	25 °C
15 min	50 °C
5 min	85 °C
Pause	4 °C

Table 4.8: Reverse Transcription Temperature Program

$$\text{linear } \Delta C_{t,\,x} = 2^{-\Delta C_{t,\,x}} = 2^{-(C_{t,\,x} - C_{t,\,\text{housekeeper}})} \tag{4.1}$$

$$\text{normalized linear } \Delta C_{t,\,x} = \frac{\text{linear } \Delta C_{t,\,x}}{<\text{linear } \Delta C_{t,\,x,\text{control}}>} \tag{4.2}$$

Gene	*Forward (5'–3')*	*Reverse (3'–5')*
actb	CTTTGCAGCTCCTTCGTTGC	CCTTCTGACCCATTCCCACC
enpp6	GGATGGTTTTCGCTCAGACTACA	GTTGCCGATCATCTGGTGGA
gapdh	GAGAGTGTTTCCTCGTCCCG	ATGAAGGGGTCGTTGATGGC
heyl	AGAGAAACGGCGCAGAGAC	GTGATCCACGGTCATCTGCAA
itpr2	CCAGCTTCCTCTACATTGGGG	TTCTTGGGTGGGTTGGCAAG
klk6	CCTGGCAAGATCACCCAGAG	GAGGCGACCCCCACATACTA
lgr4	TCGTGGACTGAGTGCTTTGC	AGATGCCGCAACTGAACGAG
mag	CTGCCTTCAACCTGTCTGTG	CTGCCTTCAACCTGTCTGTG
mog	CGTGCAGAAGTAGAGAATCTCCAT	ATCACTCAAAAGGGGTTTCTTAGCT
nfasc155	GGAGAGAGACCCGAGAGACTT	CGGATTTTAACTTCAGTGGGCG
olig2	ACAGACCGAGCCAACACCAG	ATCATCGGGTTCTGGGGACG
pdgfra	CACAATAACGGGAGGCTGGT	TATACACAGTCTGGCGTGCG
plp1	GCAAGGTTTGTGGCTCCAAC	GCGAAGTTGTAAGTGGCAGC
pnpla3	GCTATCGCTGCAGTCCACA	ACACCCTGGGCCCAAGTATT
tardbp	CTGTGCTTCCTCCTTGTGCT	CAACACCGTCCCATCGTCTT
tardbp$^{exon\ 3}$	TCCCCTGGAAAACAACTGAGC	TTACAGTCACACCATCGCCC
tcf7l21	CCTCCGCACCCTCCAGATAT	CCTAGACATAGATGCGTTGACTGT
tdp43	CTGTGCTTCCTCCTTGTGCT	CAACACCGTCCCATCGTCTT
tmem199	CGGCAGTACGTGATGCTCAT	TTCAGGGAACGAGGATGGGT
wwp2	CGGAAGTGGAGCGGAGTTAG	GCTGACACCACTTTCAGGGT

Table 4.9: qPCR Primer Sequences

Substance	**Amount**
FastStart Essential DNA Green Master	5 µl
Primer Forward (5 µM)	0.5 µl
Primer Reverse (5 µM)	0.5 µl
cDNA (4 $^{\mu l}/_{\mu g\ \text{RNA input}}$)	4 µl
Total Reaction Volume	10 µl

Table 4.10: qPCR Reaction Mix

Name	**Cycles**	**Time** (mm:ss)	**Target** (°C)	**Ramp Rate** ($\frac{°C}{s}$)
Preincubation	1	10:00	95	4.4
Amplification	50	00:10	95	4.4
		00:20	60	2.2
+HRM Dye Detection*		00:20	72	4.4
Melting Curve	1	00:05	95	4.4
		01:00	60	2.2
		-	95	0.11
Cooling	1	00:30	40	2.2

Table 4.11: Temperature Program for qPCR *High resolution melting dye

4.3.2. Western Blotting

Frozen mouse tissue (peeled sciatic nerves or spinal cords) was ground before and after adding lysis buffer (Tab. 4.12). Cells were washed with cold PBS before lysis buffer (PN2 Tab. 4.12 or 1x Laemmli Tab. 4.13) was added. The large end of a pipette tip was used to scrape the cells and the obtained lysate was afterwards transferred into 1.5ml tubes. The protein concentration of lysates in PN2 buffer was determined using the Micro BCA Protein Assay Kit (Thermo Scientific) and measurement of the absorption at 560 nm on a microplate reader (GloMax Discover, Promega). Afterwards, 10x Laemmli buffer (Tab. 4.13) was added to these lysates in appropriate volumes to get a 1x dilution. The lysates were stored at -20 °C.

Substance	Amount
SDS	0.1 %
Tris-HCl[a]	25 mM
NaCl	95 mM
EDTA[b]	10 mM
Inhibitors[c]	1 x

Table 4.12: PN2 Protein Lysis Buffer [a]from 1 M stock solution, pH7.4 [b]from 500 mM stock solution, pH8 [c] c0mplete protease inhibitor and phosphor-Stop (11844600, 04906837001, Roche)

Substance	Amount
Tris-HCl pH 6.8	62.5 mM
glycerol	10 %
β-mercaptoethanol	5 %
SDS	2 %
1% Bromophenol Blue	2 ‰

Table 4.13: 1x Laemmli Buffer

Separation by SDS-PAGE

Separation and blotting were performed using the Mini Trans-Blot Cell system (BioRad). Protein lysates in 1x Laemmli buffer were boiled (5 min at 95 °C, 800 rpm) and subsequently loaded into an SDS-PAGE gel (Mini-Protean TGX, 4-15%, BioRad). All empty wells were filled with 1x Laemmli buffer. Electrophoretic separation was performed at 110 mA using SDS running buffer (Tab. 4.14). PVDF membranes (Merck) were activated in methanol for 30 s. Membranes, filter paper and sponges were equilibrated in transfer buffer (Tab. 4.15) before they were used for assembling. The gel with the membrane directed towards the anode was inserted into a sandwich of thick filter paper and sponges on the outside. A 50ml tube was used to roll over the stack and thereby remove air bubbles. The whole mount was filled with transfer buffer and tapped until no more air bubbles appeared. Blotting was performed at 70 V for 90 min at 4 °C.

Substance	Amount
Tris Base	30.2 g
Glycine	144 g
SDS	10 g
H_2O: fill up to	1 l

Table 4.14: 10x SDS running buffer

Substance	Amount
Tris Base	2.4 g
Glycine	24.4 g
MeOH	200 ml
H_2O: fill up to	1 l

Table 4.15: Transfer buffer

Verification of Transfer

To confirm that proteins were successfully blotted onto the membrane or to make them visible for cutting the membrane, they were stained with staining solution (0.5%$_{w/v}$ Ponceau S, 1%$_{v/v}$ acetic acid). The membranes were incubated with staining solution (20 ml for 5 min at RT) and washed with distilled H_2O until the background was removed. Before proceeding with detection, the membranes were washed once with H_2O followed by TBS-T (20 mM TrisBase, 137 mM NaCl, 0.05 % Tween-20 in H_2O) until the staining largely disappeared.

Protein Detection

The membranes were washed once with TBS-T (20 ml, 5 min at RT) and incubated in blocking buffer (5 ml TBS-T containing 5% BSA, Sigma) for 1 h at RT. Membranes were subsequently incubated with 3 ml blocking buffer containing the primary antibody (Tab. 4.16) in 15 or 50ml tubes on a roller mixer (overnight at 4°C). The membranes were washed three times (20 ml TBS-T, 5 min at RT) and subsequently incubated with 3ml milk blocking buffer (5% skimmed milk powder instead of BSA) containing the secondary antibody (1 h at RT). Incubation with antibodies against loading control proteins (β-Actin, α-Tubulin & GAPDH) and the corresponding secondary antibody were reduced to 30 min, and performed in milk blocking buffer. Membranes were washed three times (20 ml TBS-T, 5 min at RT). Detection reagent (ECL Prime, VWR or CDP-Star, Merck; 1 ml per full membrane) was added and membranes were imaged after 5 min at room temperature using a FusionFX7 (Vilber Lourmat). If membranes were used to further detect proteins, they were washed three times (20 ml TBS-T with 0.1 % NaN_3, 5 min at RT) before proceeding.

Target	Species	Dilution	Company	Catalog Nr
αTubulin	m	1/10'000	Sigma	T5168
βActin	m	1/10'000	Sigma	A5316
Cont-1	gt	1/1'000	R&D	AF904
H3	rb	1/2'000	Cell Signaling Technology	4499
KV1.2	m	1/1'000	abcam	ab192758
MBP	rt	1/500	Serotec	MCA409s
Nfasc	rb	1/5'000	R&D	AF3235
Pdgfrα	rb	1/1'000	Cell Signaling Technology	3174
TDP-43	rb	1/1'000	ProteinTech	12892-1-AP

Table 4.16: Primary Antibodies used for western blots.
Species include mouse (m), rat (rt), rabbit (rb) and goat (gt).

Computational Analysis

The quantification was performed using ImageJ. The background of the bands was optionally subtracted (Rolling ball, no smoothing) to avoid bias from manual border determinations. The quantification was performed using the gel analysis tool as described in the software manual. Values were normalized individually to the selected loading control signal and to the average of control samples.

4.4. Immunofluorescent Analysis

Tissue Preparation

Animals were euthanized and dissected. For spinal cords, mice were first perfused with PBS and subsequently 4 % paraformaldehyde (PFA, Electron Microscopy Sciences) in PBS. Sciatic nerves were dissected immediately after euthanization and fixed for one hour at room temperature, followed by one hour in 10 % sucrose in PBS, and finally over night 20 % sucrose in PBS at 4 °C, before embedding in O.C.T (Tissue-Tek). Spinal cords were post-fixed over night in 4 % PFA in PBS at 4 °C and cryo-protected in 30 % sucrose in PBS for 24 h at 4 °C before embedding in OCT. Blocks with embedded tissues were sectioned (sciatic nerves: 5 µm, spinal cord: 10 µm) with at least 100 µm in between cross-sections. Sections were incubated in PBS for 5 min before using.

Antigen Retrieval

When using TDP-43 or CC1 antibodies, sections were incubated in alkaline antigen retrieval buffer (10 mM Tris-Base, 1 mM EDTA, 0.05 % Tween-20; in $_{dd}H_2O$, pH 9) for 20 min at 95 °C and another 20 min at to cool down to room temperature.

Staining and Imaging

Sciatic nerve sections were permeabilized prior to blocking (20 min in 0.5 % TX-100 in PBS). Blocking buffer (spinal cords: 10 % goat/donkey serum, 1 % TX-100 in PBS; sciatic nerves: 10 % goat/donkey serum, 1 % BSA, 0.1 % TX-100 in PBS) was added for one hour before incubating slides with primary antibodies (Tab. 4.16) in blocking buffer at 4 °C over night. Thereafter, slides were washed 3 times in PBS before adding fluorophore-coupled secondary antibodies (1:300 in blocking buffer) for one hour at room temperature. DAPI (2 µg/ml in PBS) was added for 10 min. After three times washing in PBS for 5 min, few drops of Immumount (Fisher Scientific) were added and covered with a glass coverslip for imaging. Immunofluorescence stainings of tissue cross-sections were imaged using a widefield microscope (Axio Imager-M2, Carl Zeiss). Longitudinal sections (sciatic nerves) for nodal analysis were imaged on a confocal microscope (SP8, Leica) using a 40x water objective.

Analysis

Nodes of Ranvier: A minimum of 43 control and 65 *mpz*-cKO nodes of Raniver were counted per animal (Fig. 5.6f).
Sciatic nerves: 3 sciatic nerve cross-sections were quantified for each animal (Fig. 5.11d,e).
Spinal cords: Analysis entailed the quantification of hemi-sections from 3 spinal cord cross-sections (>100 µm apart from each other) per animal.
Spinal cord motor neuron analysis: At least 84 control and 63 *plp*-iKO motor neurons wer counted per animal in at least three cross-sections (>100 µm apart from each other, Fig. 6.13i).

Target	Species	Dilution	Company	Catalog Nr
CC1	m	1/500	ab16794/OP80	abcam/Calbiochem
ChAT	gt	1/200	ab144P	Millipore
Contactin-1	gt	1/80	AF904	R&D
GFAP	ch	1/300	ab5541	Chemicon
hSox10	gt	1/200	AF2864	R&D
Iba1	rb	1/300	019-19741	Wako
KV1.2	m	1/300	75-008	NeuroMab
NF186	rb	1/300	ab31719	abcam
Olig2	m	1/600	MABN50	Millipore
Olig2	rb	1/500	ab9610	Millipore
Pdgfrα	rb	1/400	3174	Cell Signalling Technology
TDP43	rb	1/1000	12892-1-AP	ProteinTech

Table 4.17: Primary Antibodues used for immunofluorescence.
Species included mouse (m), rabbit (rb) and goat (gt).

4.5. Morphological Analysis

4.5.1. Preparation of Specimens

Sciatic nerves were placed on a thick paper and fixed with PFA (4 %, Electron Microscopy Sciences) and glutaraldehyde (2.5 %, MERCK) in PBS. For root nerves, spinal cords and brain tissue animals were perfused with PBS followed by fixative before dissection. Tissues were post-fixed for at least 12 hours. They were further treated with osmium tetroxide (2 %, EMS), dehydrated over a series of acetone gradients, infiltrated and embedded in Spurr's resin (EMS). Ultrathin sections (99 nm) were used to contrast with uranyl acetate and lead citrate, and imaged with a Zeiss Merlin SEM. Quantification was performed on whole cross sections of sciatic nerves and root nerves and random fields in CNS areas (Tab. 4.18).

Tissue	Feature	Quantification	Total Area
SN		Whole cross-section	
L4 Root Nerves		Whole cross-section	
SpC ventral WM		3 random fields	2'700 μm^2
SpC ventral GM		3 random fields	2'700 μm^2
SpC dorsal GM	Myelinated axons	3 random fields	2'700 μm^2
SpC dorsal GM	Vacuoles	3 random fields	27'000 μm^2
CC	% Myelinated axons	3 random fields	675 μm^2
CC	% Vacuolar Area	2 random fields	2'500 μm^2
Cortical GM	Myelinated axons	5 random fields	2'000 μm^2

Table 4.18: EM Analysis Sciatic nerve (SN), spinal cord (SpC), corpus callosum (CC). Features are only indicated if analysed differently within the same tissue. Random fields were placed in order to include similarly composed regions regarding axon calibres, cell bodies and in brains the density of myelinated axons.

4.5.2. g-ratio - Analysis of Myelin Thickness

The g-ratio was quantified as ratio of axon diameter to fiber diameter. The axon area was measured to calculate the axon diameter in assumption of a perfect circle. Myelin thickness was measured and added to the axon diameter to get the fiber diameter. For manual quantification of spinal cord white matter fibers, the myelin thickness was averaged from measurements at two different loci of compact, well-preserved myelin. At least 100 fibers were measured per animal. Automated quantification was performed on peripheral nerves using a modified version of AxonSeg (Zaimi et al., 2016). Main changes include the calculation of g-ratio as described above and implementing a more robust measurement of myelin thickness. To this end the average of the second sextile of myelin measurements from at least 180 radial projections was used for further calculations. Measurements were computationally and manually filtered, yielding at least 1'200 g-ratio measurements for sciatic nerves.

4.6. RNA-Sequencing

Bulk RNA sequencing (RNAseq) experiments were performed using four samples per condition. Peeled sciatic nerves were sequenced at P5 from control and *mpz*-cKO mice. Oligodendrocytes (*cnp*Cre^{+} TDP-43$^{wt/wt\ or\ f/f}$ tdTomato$^{T/wt}$) were sorted by FACS (section 4.2) and collected separately according to their size (Fig. A.6). Without splitting by size, the same genotypes and strategy were used to collect oligodendrocytes for single-cell RNA sequencing (scRNAseq) of one control and one *cnp*-cKO mouse. To this end, a target number of 5'000 cells was used for the scRNAseq library preparation. Total RNA or cells used for sequencing experiments and processed according to specified parameters of each experiment (Tab. 4.19). Initial number of reads are enlisted in Tab. 4.20.

Bioinformatic processing of RNAseq experiments

Reads were pre-processed using Trimmomatic (Bolger et al., 2014) as built-in part of the pipeline. Reads were further either aligned to the genome using STAR (Dobin et al., 2013) and counts were subsequently extracted using FeatureCounts (Liao et al., 2019), or processed using the more recent tool Kallisto (Bray et al., 2016) was used. Except for specific purposes, we used the ensembl mouse genome annotation (GRCm38.p5). Specifications of the processing are given in Tab. 4.21. For whole gene level analysis, counts were analysed with edgeR (Robinson et al., 2010) using a generalized linear model (glm) and quasi-likelyhood (QL) test for differentially expressed genes. Background expression was set to 10. Counts were normalized using the TMM (trimmed mean of M values, Robinson and Oshlack, 2010). To analyse the sequencing data on junction- and exon-level, we used JunctionSeq (Hartley and Mullikin, 2016) with fdr-threshold 0.05 and minimal count 6.

Experiment	P5 *mpz*-cKO sciatic nerves RNAseq	P10 *cnp*-cKO oligodendrocytes RNAseq	P10 *cnp*-cKO oligodendrocytes scRNAseq
Type	total RNA	total RNA	single cell sequencing
RNA extraction	Qiagen Allprep RNA/DNA	Trizol	-
Library	TruSeq RNA stranded	TruSeq RNA stranded	10X Genomics Single Cell, V3
Enrichment	Ribosomal Depletion, Ribo Zero	Ribosomal Depletion, Ribo Zero Gold	-
Instrument	HiSeq 4000	HiSeq 4000	NovaSeq
Sequencing	2x150bp	2x150bp	90bp

Table 4.19: Parameters of RNA sequencing experiments "2x" indicates paired-end sequencing.

Condition	Sample	Mio. Reads
P5 mpz-cKO sciatic nerves RNAseq		
Control	Ctl 1	82
	Ctl 2	85
	Ctl 3	63
	Ctl 4	44
mpz-cKO	cKO 1	76
	cKO 2	69
	cKO 3	88
	cKO 4	81
P10 cnp-cKO oligodendrocytes RNAseq		
Control	Ctl 1 FSC^{low}	98
	Ctl 2 FSC^{low}	107
	Ctl 3 FSC^{low}	100
	Ctl 4 FSC^{low}	108
	Ctl 1 FSC^{High}	95
	Ctl 2 FSC^{High}	65
	Ctl 3 FSC^{High}	107
	Ctl 4 FSC^{High}	87
cnp-cKO	cKO 1 FSC^{low}	118
	cKO 2 FSC^{low}	109
	cKO 3 FSC^{low}	102
	cKO 4 FSC^{low}	126
	cKO 1 FSC^{High}	96
	cKO 2 FSC^{High}	208
	cKO 3 FSC^{High}	90
	cKO 4 FSC^{High}	82
P10 cnp-cKO oligodendrocytes scRNAseq		
Control	Ctl 1	516
cnp-cKO	*cnp*-cKO 1	422

Table 4.20: Total reads from RNA sequencing experiments

Options for	Parameter	Value
Trimmomatic	trimAdapter	TRUE
	trimLeft	4
	trimRight	4^a, 20^b
	minTailQuality	10^a, 0^b
	minAvgQuality	10
	minReadLength	80
STAR Mode	twopassMode	TRUE
Alignments and Seeding	alignIntronMax	1e6
	alignMatesGapMax	1e6
	alignSJDBoverhangMin	1
	alignSJoverhangMin	8
Chimeric Alignments	chimJunctionOverhangMin	15
	chimScoreMin	15
	chimScoreSeparation	10
	chimSegmentMin	15
Output: Filtering	outFilterMatchNmin	30
	outFilterMismatchNmax	10
	outFilterMismatchNoverLmax	0.05
	outFilterMultimapNmax	50
	outFilterType	BySJout
Output: SAM/BAM	outSAMstrandField	intronMotif

Table 4.21: Parameters of RNA alignment using STAR [a]used for FeatureCounts and EdgeR, [b]used for JunctionSeq

Processing of Single cell sequencing

The analysis was performed using the Seurat R package (version 3, Butler et al., 2018; Stuart et al., 2019) and DoubleFinder (McGinnis et al., 2019). Counting matrices from CellRanger count were used as input. Cells having more than 15% mitochondrial genes or less than 2'500 identified genes were removed from the analysis. Gene counts were further log-normalized: For each cell, counts were divided by the total counts for that cell and multiplied by 10^4. The numbers were subsequently natural-log transformed using log1p (calculates log(1+x)). Control and *cnp*-cKO data sets were integrated and merged using the first 20 dimensions of the canonical correlation analysis. Data was scaled and clustered at high resolution. Duplicate cells were identified using DoubletFinder (McGinnis et al., 2019). We removed these duplicates as well as clusters containing more than 50% duplicate cells. The resulting data-set was considered as final filtered set and used for the analysis. First, the data set was scaled, clustered and used to calculate a UMAP projection. Marker genes for each cluster were extracted and used to assign a cell type and state. Clusters were subsequently merged to a minimum of biological clusters. *FindMarkers* was further used to determine differentially expressed genes between cells from different genotypes in each cluster separately.

4.7. OPC Cultures

Preparation of Medium and Culture Dishes

Stock solutions were prepared as described (Emery and Dugas, 2013) with few changes: N-acetyl cysteine, putrescine, progesterone and sodium selenite were prepared as 100x concentrated stock, Transferrin and BSA were stored as separate 100x concentrated stock at -80 °C. 1x Sato medium was freshly prepared and stored at 4 °C for maximum two weeks (Tab. 4.22). Growth factors were added immediately before use: CNTF (10 $^{ng}/_{ml}$; AF-450-13, Peprotech) for every condition. For OPCs, Sato medium was further supplemented with Pdgfα (10 $^{ng}/_{ml}$; 100-13A, Peprotech). In differentiating conditions, T_3 (3 $^{\mu g}/_{ml}$; T6397, Merck) was added. Cell culture dishes were coated with PDL (20 min with 0.1 $^{mg}/_{ml}$; P6407, Merck), washed twice with water and dried.

Substance	Catalog-Serial	Concentration
Human apo-Transferrin	T1147[a]	0.1 $^{mg}/_{ml}$
BSA	A4161[a]	0.1 $^{mg}/_{ml}$
N-acetyl-cysteine	A8199[a]	368 µM
Putrescine	P5780[a]	100 µM
Progesterone	P8783[a]	200 nM
Sodium Selenite	S5261[a]	300 nM
Insulin	I6634[a]	50 $^{\mu g}/_{ml}$
Trace Elements B 1'000x	15343641[b]	0.1 %
Forskolin	F6886[a]	10 µM
B27 50X	17504044[c]	1 x
Penicillin-Streptomycin	P0781[a]	1 %
In DMEM Glutamax	31966[c]	

Table 4.22: 1x Sato Buffer for oligodendrocyte cultures Suppliers: [a]Merck, [b]Corning, [c]ThermoFisher

Generation and Manipulation of OPC Cultures

Mice expressing the tdTomato reporter were used around P7 (P5-P8) to generate OPC cultures. OPCs were isolated from spinal cords using FACS (section 4.2, Fig. A.6) and collected in FACS flow buffer containing 1-1.5e5 tdTomato^{pos} OPCs ('small' fraction of cells; see Fig. A.6a) were seeded per 3.5cm-dish and allowed to attach for 20-30 min. Subsequently, the FACS flow buffer was replaced by freshly prepared Sato medium with double concentration of Pdgfα. 50% of the medium was exchanged every 2-3 days with full supplement of growth factors.

For passaging, OPCs were detached for 5 min at 37 °C using Trypsin (0.25% plus EDTA diluted 10x in EBSS, Life Technologies) after one wash with EBSS (Gibco). Trypsinisation was stopped by adding 30 % FBS (in PBS, 16000044, Gibco; 150 % of the added volume of Trypsin buffer). Cell suspensions were subsequently centrifuged at room temperature (10 min at 200 rpm) and the supernatant was aspirated. OPCs were resuspended in 1x Sato medium and plated (6'600 $^{cells}/_{cm^2}$).

OPC Differentiation

For differentiation experiments, OPCs were collected from expanded cultures as described above and seeded at a density of 26'500 $^{cells}/_{cm^2}$. Cells were cultures for 4 days under differentiating conditions (T_3 instead of Pdgfα).

4.8. Data Processing and Statistical Analysis

4.8.1. Replicates and Statistical Analysis

Replicates are indicated in the corresponding figure legends. If not further specified, they correspond to the number of analysed tissues from independent mice per group (*e.g.* per genotype). Tests used to determine statistical significance are indicated individually for each analysis in the corresponding figure legend. Significance is displayed on graphs as described in the corresponding figure legend. Generally, the following criteria were used to determine which test should be applied:

two-tailed, unpaired Student's t-test:
Generally used simple comparison of two conditions

Mann Whitney test:
Non-parametric comparison of two conditions, applied when values of one group were close to 0.

one sample t-test with hypothetical mean of zero:
Applied, when the majority of values in the control group were equal to 0

Variants of the **two-way ANOVA** using multiple comparisons

two-way ANOVA with Šídák's multiple comparisons test:
Specific comparison between groups (*e.g.* genotypes) within the same factor (*e.g.* axon-caliber bin, timepoint)

two-way ANOVA with Tukey's multiple comparisons test:
Comparison between all groups and factors

4.8.2. Software

Image quantification: Adobe Photoshop
Densiometry (western blot): ImageJ
Automated g-ratio: Matlab
Analysis of RNA sequencing data: R-Studio
Sequence analysis: CLC genomics workbench
Table calculations: Microsoft Excel
Statistical tests and graph generation: Graphpad Prism
Illustrations: Adobe Illustrator
Figure Panels: Adobe Indesign

Part II

Results

5. TDP-43 in Schwann cells

5.1. Function of TDP-43 in Schwann Cells during PNS Development

TDP-43 is widely expressed in cells from various tissues of adult mice and in a more restricted pattern during embryonic development (Sephton et al., 2010). In mouse brains, TDP-43 protein levels are highest during embryonic development and decrease within the first weeks of age (Sephton et al., 2010). So far, there are no coherent data about the expression of TDP-43 in the Schwann cell (SC) lineage. Therefore, we collected sciatic nerves (SNs) from wild-type mice at different timepoints after birth and analyzed TDP-43 mRNA and protein levels. TDP-43 was highly expressed during the first postnatal days. While protein levels were gradually reduced, mRNA levels at P30 were still around 50 % of its maximum expression at P1 (Fig. 5.1a-c). In order to study the function of TDP-43 in SCs, we employed a mouse model deleting TDP-43 specifically in the Schwann cell lineage. To this end, mice harboring a floxed allele of the TDP-43 gene (*Tardbp*) were crossed with mice expressing Cre recombinase under control of the regulatory sequences of the *Mpz* promoter (*mpz*TDP-43^{cKO}, hereafter *mpz*-cKO; Fig. 5.1d). The *mpz*Cre transgene mostly drives recombination of immature Schwann cells between E13.5 and E16 (Feltri et al., 2002; Yu et al., 2005; Woodhoo et al., 2009). First, we assessed the efficiency of the mouse model in ablating expression of TDP-43. The mRNA and protein levels of TDP-43 in SNs of P5 *mpz*-cKO animals were strongly reduced compared to controls, indicating efficient recombination and protein degradation (Fig. 5.1e-g). Using this mouse model, we first asked to what extent Schwann cells depend on TDP-43 to perform their function during postnatal development, *i.e.* radial sorting, and myelination. We analyzed control and *mpz*-cKO mice between the first postnatal day and P60, when developmental myelination is expected to be largely finished. Within the timeframe of the analysis, no behavioral differences could be qualitatively observed between *mpz*-cKO mice and their control littermates. Moreover, *mpz*-cKO mice had normal bodyweights and similar motor performance assessed by the inverted grid hanging test (Fig. 5.1h,i).

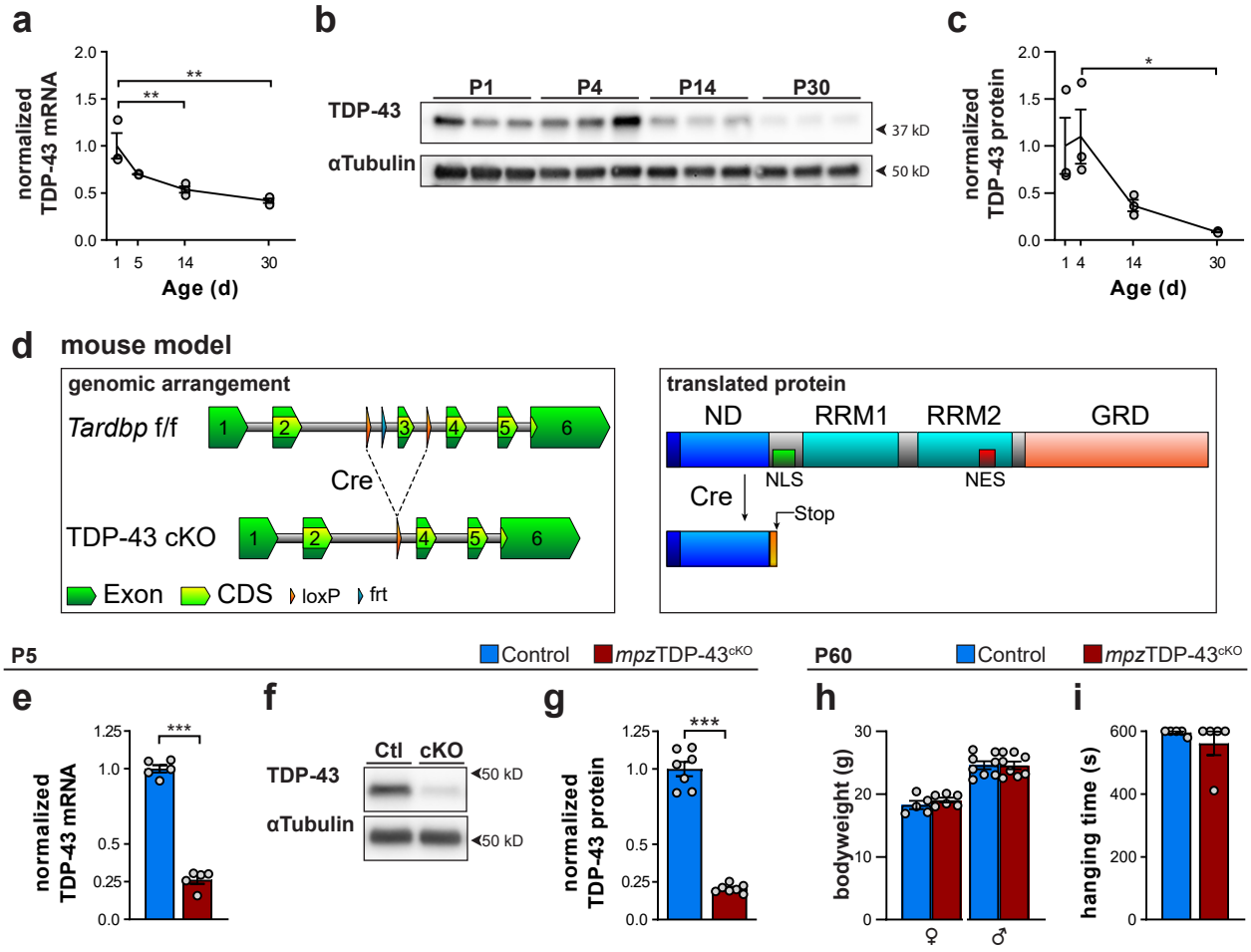

Figure 5.1: TDP-43 is expressed by Schwann cells and efficiently ablated in the *mpz*-cKO mouse. (a-c) Expression profile of TDP-43 in wild-type SNs at various timepoints between P1 and P30, showing higher expression in early postnatal life. **(a)** Quantification of TDP-43 mRNA by RT-qPCR. **(b)** Profile of TDP-43 protein abundance. **(c)** Quantification of (b). **(d)** Schematic representation of the floxed allele of *TDP-43* and the consequences for the expressed protein after recombination. Excision of exon 3 results in a frameshift and numerous emerging stop codons more than 50 nucleotides upstream from the next exon-exon junctions (first such stop codon in exon 4), suggesting that recombined transcripts are readily routed to degradation via NMD. **(e-g)** Validation of TDP-43 deletion in *mpz*-cKO mice compared to controls, analyzed at P5. **(e)** RT-qPCR reveals a strong reduction of TDP-43 mRNA in *mpz*-cKO compared to control SNs. **(f)** Detection of TDP-43 protein on western blots from control and *mpz*-cKO SN lysates. **(g)** Quantification of (f) displays a strong reduction of TDP-43 protein in *mpz*-cKO compared to control SNs. **(h)** Bodyweights of control and *mpz*-cKO mice at P60 are comparable. **(i)** Hanging time on inverted grid of control and *mpz*-cKO mice at P60. **(Statistics)** Bar graphs represent mean±SEM; *p<0.05, **p<0.01, ***p<0.001. (a,c) n = 3 mice, two-way ANOVA with Tukey's multiple comparisons test. (e,i) n = 5 mice, two-tailed, unpaired Student's t-test. (g) n = 7 mice, two-tailed, unpaired Student's t-test. (h) n = 5 ♀ ctl, 6 ♀ *mpz*-cKO; 8 ♂ ctl and *mpz*-cKO, two-tailed, unpaired Student's t-test

Developmental Myelination Is Marginally Affected in TDP-43^{cKO} Mice

Cells of the SC lineage are tightly involved in several processes during development, including radial sorting, onset of myelination, and myelin growth. To learn more about the function of TDP-43 in SCs during postnatal PNS development, SN cross sections from control and *mpz*-cKO mice were analyzed by electron microscopy (EM) at P1, P5 and P60. Morphological analysis of EM micrographs of control and *mpz*-cKO SNs from postnatal day one to sixty did not reveal a major failure during development (Fig. 5.2a). At postnatal day one and five, the number of sorted axons in a 1:1 relation with SCs with or without myelin was not detectably changed between control and *mpz*-cKO animals, indicating a normal progression of radial sorting upon loss of TDP-43 (Fig. 5.2b). Despite comparable numbers of total sorted axons, there were proportionally fewer fibers already myelinated in *mpz*-cKO SNs compared to controls (Fig. 5.2c). Among the myelinated population, we detected axons that were not in complete contact with the myelinating SC, leading to the impression that the axon and myelin ring blistered from each other. These structures are further referred to as "blistered axons" and sometimes they contained myelin debris in the space that separates the axon from the compact myelin ring. Blistered axons were prominently enriched in *mpz*-cKO, but not in control nerves at P5 (Fig. 5.2d), or at other timepoints analyzed (not shown). After onset of myelination, SCs produce consecutive wraps to create compact myelin that is proportional in thickness to the axonal diameter. In order to assess whether deletion of TDP-43 impacts myelin growth in SCs, we quantified the g-ratio in SNs at P60. Overall, no major differences could be detected (Fig. 5.2e), although detailed inspection of different axon calibers revealed mild hypomyelination of large diameter axons (≥5 µm) and minor hypermyelination of very small axons (1-2 µm) in *mpz*-cKO SNs compared to controls (Fig. 5.2f). Taken together, our data suggests that TDP-43 is required for the timely onset of Schwann cell myelination, and potentially also influences the correct proportions of the myelin sheath.

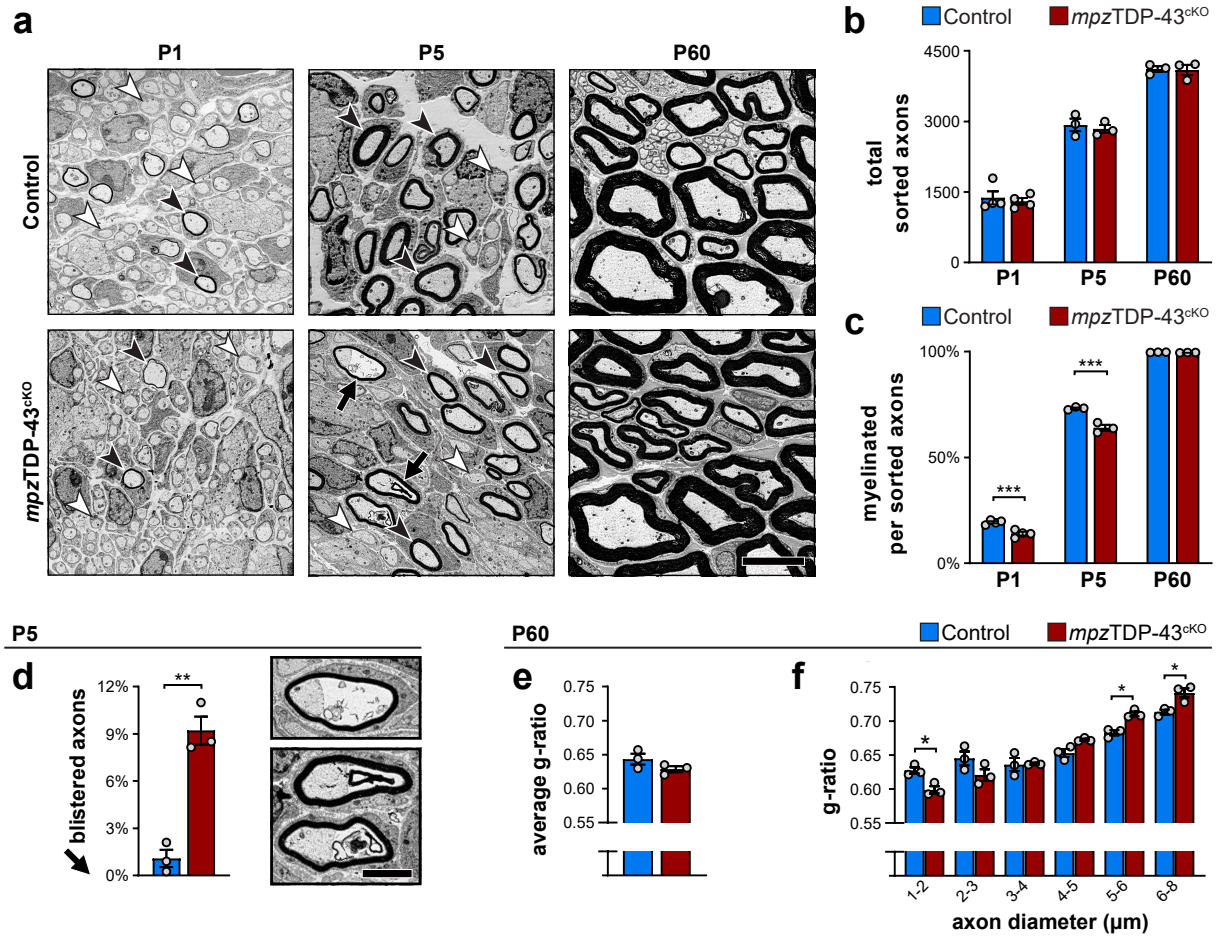

Figure 5.2: TDP-43 is required for a timely onset of myelination. (a) Exemplary electron micrographs of control and *mpz*-cKO sciatic nerves at different timepoints, showing sorted, non-myelinated (white arrowheads) and myelinated axons (black arrowheads). Moreover, *mpz*-cKO nerves contain blistered axons (black arrows). scalebar 5 µm **(b)** Quantification of total sorted axons (includes myelinated and 1:1 non-myelinated SC-axon units) reveals no significant changes between *mpz*-cKO and control nerves. **(c)** Ratio of myelinated over the total number of sorted axons reveals fewer myelinated axons in *mpz*-cKO compared to control nerves at P1 and P5. **(d)** Occurrence of blistered axons at P5 is significantly elevated in *mpz*-cKO compared to control nerves. Exemplary EM images depict blistered axons (magnified and rotated) of *mpz*-cKO SNs at P5 shown in panel (a). scalebar 2 µm **(e)** Average g-ratio in sciatic nerves at P60 is not significantly different between *mpz*-cKO and control nerves. **(f)** Histogram showing mild differences between P60 *mpz*-cKO and control SNs in the g-ratio of axons at specific diameter bins. **(Statistics)** Bar graphs represent mean±SEM; *p<0.05, **p<0.01, ***p<0.001. (b,c) P1 n = 4 mice (all animals are littermates), P5/P60 n = 3 mice, two-way ANOVA with Šídák's multiple comparisons test. (d,e) n = 3 mice, two-tailed, unpaired Student's t-test. (f) n = 3 mice, two-way ANOVA with Šídák's multiple comparisons test.

Our observations in *mpz*-cKO mice did not indicate radial sorting defects. However, they also did not rule out the possibility that TDP-43 does play a functional role in the regulation of radial sorting in SCs, which might be revealed if recombination was induced earlier in embryonic development. To tackle this hypothesis, and to provide orthogonal evidence for our findings in *mpz*-cKO nerves, mice expressing Cre under control of the *Dhh* regulatory sequences were used to generate conditional knockout mice (*dhh*TDP-43^{cKO}, hereafter *dhh*-cKO), in which recombination is already observed at E12.5 (Jaegle et al., 2003). *dhh*-cKO animals were kept until ~35 days age, but not for longer due to animal welfare considerations. The aggravated impact in *dhh*-cKO mice might be related to potential off target recombination in cell types other than SCs (Jaegle et al., 2003). As the *dhh*-cKO mice did not reach P60, we focused our analysis on P5 using EM (Fig. 5.3a). The morphological findings in the *dhh*-cKO SNs were largely in line with those in the *mpz*-cKO animals: the number of sorted axons was comparable to that in control animals, while the fraction of myelinated axons was reduced (Fig. 5.3b,c). Excitingly, we also observed blistered axons significantly enriched in *dhh*-cKO SNs compared to controls (Fig. 5.3d). Considering our findings in both *mpz*-cKO and *dhh*-cKO mice, we conclude that TDP-43 is required for the onset of myelination, and to protect the axon-myelin units from aberrant blistering at P5. However, we could not detect evidence for a critical requirement of TDP-43 during radial sorting.

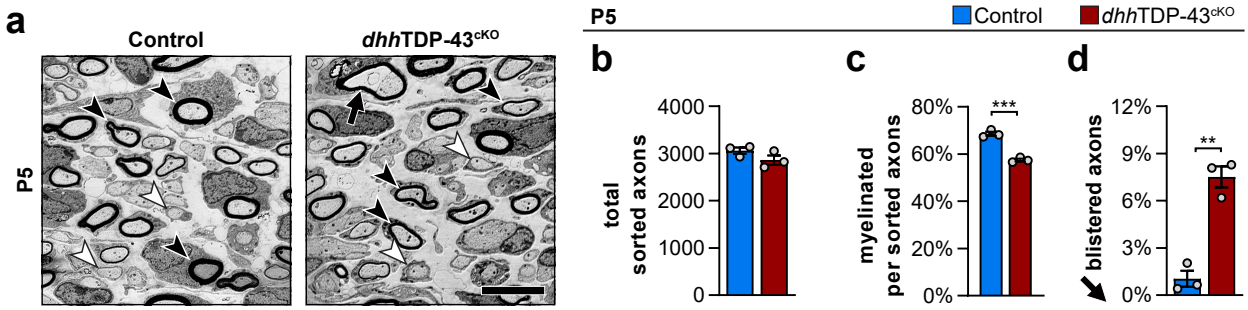

Figure 5.3: ***dhh*-cKO mice confirm that TDP-43 is dispensable for radial sorting (a)** Exemplary electron micrographs of sciatic nerve cross sections of *dhh*-cKO and control SNs showing non-myelinated sorted axons (white arrowheads) and myelinated sorted axons (black arrowheads). A blistered axon (black arrow) is highlighted in the *dhh*-cKO image. scalebar 5 µm **(b)** Quantification of sorted axons (includes myelinated axons and 1:1 non-myelinated SC-axon profiles) at P5 shows no significant difference between controls and *dhh*-cKO nerves. **(c)** Ratio of myelinated per the total number of sorted axons reveals a lower fraction of myelinated axons in *dhh*-cKO nerves compared to controls. **(d)** Occurrence of blistered axons is significantly higher in *dhh*-cKO nerves compared to controls. **(Statistics)** Bar graphs represent mean±SEM; **p<0.01, ***p<0.001. (b-d) n = 3 mice, two-tailed, unpaired Student's t-test.

Impact of TDP-43 on the Transcriptome of Schwann Cells

TDP-43 is an RNA binding protein, widely described as a regulator of alternative splicing and a repressor of cryptic splicing. We therefore hypothesized that TDP-43 also acts to regulate RNA splicing in SCs. To evaluate the extent of transcriptome dysregulation upon loss of TDP-43 in SCs, we compared total bulk RNA sequencing data obtained from control and *mpz*-cKO SNs at P5 (Fig. 5.4). We selected P5 for analysis, as it was the timepoint with the most pronounced phenotypic changes observed thus far in *mpz*-cKO animals compared to controls. Globally, loss of TDP-43 did not dramatically affect the levels of gene expression, and only few genes were significantly (pValue < 0.01) increased or decreased by a greater factor than 1.5 fold (Fig. 5.4a). Gene ontology analysis of biological processes in *mpz*-cKO SNs over controls revealed mainly proliferation as the affected process among the significantly upregulated genes, and lipid metabolic transport among the significantly downregulated genes (Fig. 5.4b). Inspection of selected genes known to act as transcriptional regulators of SC differentiation did not indicate a clear coherent change in transcript abundance in *mpz*-cKO nerves compared to controls (Fig. 5.4c). As we observed fewer myelinated fibers in *mpz*-cKO nerves at P1 and P5, we wondered whether transcript levels of genes related to myelin proteins and lipid biosynthesis, which are key structural components of the myelin sheath, were reduced in *mpz*-cKO mice. Except for *pmp2*, transcripts related to all selected myelin protein genes were detected at lower levels in *mpz*-cKO SNs compared to controls (Fig. 5.4d). Along with fatty acid synthase (*fasn*), transcripts derived from genes of the cholesterol biosynthetic pathway were also less abundant in *mpz*-cKO compared to control SNs (Fig. 5.4e). Taken together, the transcriptional profile of *mpz*-cKO SNs corroborates the fewer myelinated axons quantified in EM micrographs, but the plain assessment of transcript abundance did not resolve or indicate changes in transcript variants.

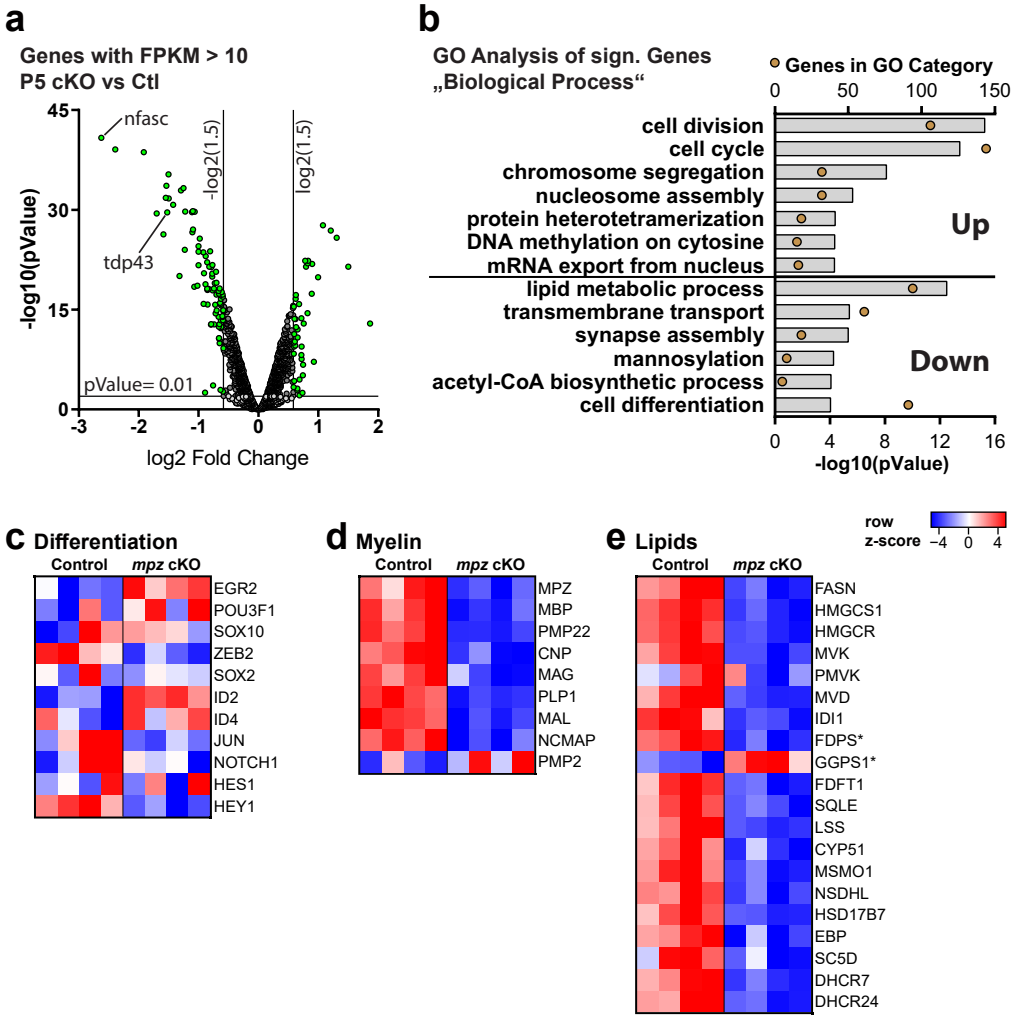

Figure 5.4: Differentially regulated transcripts in *mpz*-cKO SNs compared to controls mainly reflect delayed onset of myelination. Total RNA from peeled P5 control and *mpz*-cKO SNs was sequenced. **(a)** Volcano plot displaying edgeR quantified gene levels of *mpz*-cKO versus control SNs. For reasons of clear presentation, only genes with an average coverage of at least 10 FPKM in control or *mpz*-cKO nerves are shown (n = 4 littermates). **(b)** Gene ontology analysis of biological processes of significantly changed genes ($p \leq 0.01$, log ratio ≥ 0.5). Bars represent significance ($-\log_{10}$(p-Value)) and points display the number of significant genes that are contained in each category. **(c-e)** Heatmap representation of row z-score-processed normalized counts. The color key applies to all three graphs. **(c)** Genes involved in regulation of Schwann cell differentiation do not show coherent differences between genotypes. **(d)** Expression of genes encoding myelin proteins except *pmp2* is reduced in *mpz*-cKO SNs compared to controls. **(e)** Expression of fatty acid synthase (*fasn*) and genes of the cholesterol biosynthesis pathway is lower in *mpz*-cKO SNs compared to controls. *fdps* and *ggps1* (asterisks) perform the same enzymatic reactions within the cholesterol biosynthetic pathway. Based on FPKM values, *fdps* is expressed >11-fold than *ggps1* in controls and >6-fold in *mpz*-cKO SNs.

TDP-43 Guards Against Cryptic Splicing in Schwann Cells

Beyond regulating canonical alternative splicing, TDP-43 is a well described repressor of cryptic splicing (Fig. 5.5a, Ling et al., 2015). UG-rich intronic sequences act as recognition sites, where TDP-43 binds and suppresses the aberrant retention of neighboring intronic sequences in mature mRNAs. These cryptic splicing events often result in malicious changes in the mature transcript and may ultimately result in frameshifts and premature termination codons (Humphrey et al., 2017). To identify these cryptic splicing events in a global manner, we analyzed individual exons and splice junctions in the RNA sequencing data with the JunctionSeq package (Hartley and Mullikin, 2016, Fig. 5.5b). We focused our analysis on splice junctions that meet the following 3 criteria: They are *1)* not yet annotated, *i.e.* 'novel', which is expected for cryptic incorporation; *2)* only detected in control nerves at very low levels, since they are predicted to be suppressed in the presence of TDP-43; and *3)* highly upregulated in *mpz*-cKO nerves (red box in Fig. 5.5b). We hypothesized that those 'novel' events comprise cryptic splice junctions due to the relief of TDP-43 mediated repression. Manual inspection of these candidates revealed cryptic splicing events to variable degrees (Fig. 5.5c). For *cyth3* and *wtip*, coverage of the cryptic exon (*i.e.* retained intronic sequences) was clearly lower than that of the canonical exons, indicating that only part of the transcripts have been spliced aberrantly. Conversely, coverage of the cryptic exon in *ube2d1* and *adnp2* was only slightly lower to that of the canonical exons, indicating that most transcripts have been spliced aberrantly.

Among the cryptic splicing events, we also identified *neurofascin* (*nfasc*), which also displayed similar abundance of the cryptic exon and of canonical exons. When cDNA was used to amplify a segment covering parts of the neighboring exons by PCR, the resulting amplicons from P5 and P60 *mpz*-cKO SNs were consistently longer than expected from canonically spliced *nfasc* (Fig. 5.5d). Moreover, the expected amplicon was observed in control samples, but was barely detectable when using *mpz*-cKO cDNA. To learn more about the identity of the cryptic exon retained in *nfasc* upon TDP-43 deletion, we sequenced the shifted amplicon from *mpz*-cKO cDNA. The sequence properly aligned to the flanking exons and exposed an additional 104bp of intronic sequence retained in between. The retained sequence causes a frameshift of 2bp. As a consequence of the frameshift, 9 premature termination codons emerge in the CDS, of which 5 are more than 50 nucleotides upstream from the next exon-exon junction, likely routing the transcript to nonsense-mediated RNA decay (NMD).

Beyond our observations with cryptic incorporation, we also noted that *nfasc* was the most strongly reduced gene in *mpz*-cKO SNs compared to controls (Fig. 5.4a). Taken together, these findings indicate that the majority of *nfasc* transcripts had been cryptically spliced and were consequently degraded.

TDP-43 represses cryptic splicing through direct interaction with transcripts. To find potential evidence that cryptic splicing of *nfasc* is a direct consequence of TDP-43 deletion, we analyzed the intronic sequence flanking the identified cryptic exon. The cryptic sequence aligned with the highly covered intronic region in the sequencing data and was located directly upstream of a stretch of 19 UG-repeats, which comprises a *bona fide* binding motif of TDP-43 (Fig. 5.5e). Transcripts directly interacting with TDP-43 have been previously identified in brain tissue of mice (Polymenidou et al., 2011). Neurofascin is expressed in SCs in the PNS, and by both neurons and oligodendrocytes in the CNS. Therefore, we could use the public TDP-43 UV-CLIP data (Polymenidou et al., 2011) to find a potential direct interaction. Indeed, the UG-rich, downstream flanking region of the cryptic exon displayed high coverage in the TDP-43 UV-CLIP data (Fig. 5.5e). Collectively, our findings indicate that *nfasc* was almost entirely incorrectly spliced due to loss of TDP-43 mediated repression of cryptic splicing in *mpz*-cKO mice. These findings support the conclusion that TDP-43 normally binds to UG-repeats in the intronic regions of *nfasc* and prevents the retention of deleterious cryptic exons on its mature mRNA.

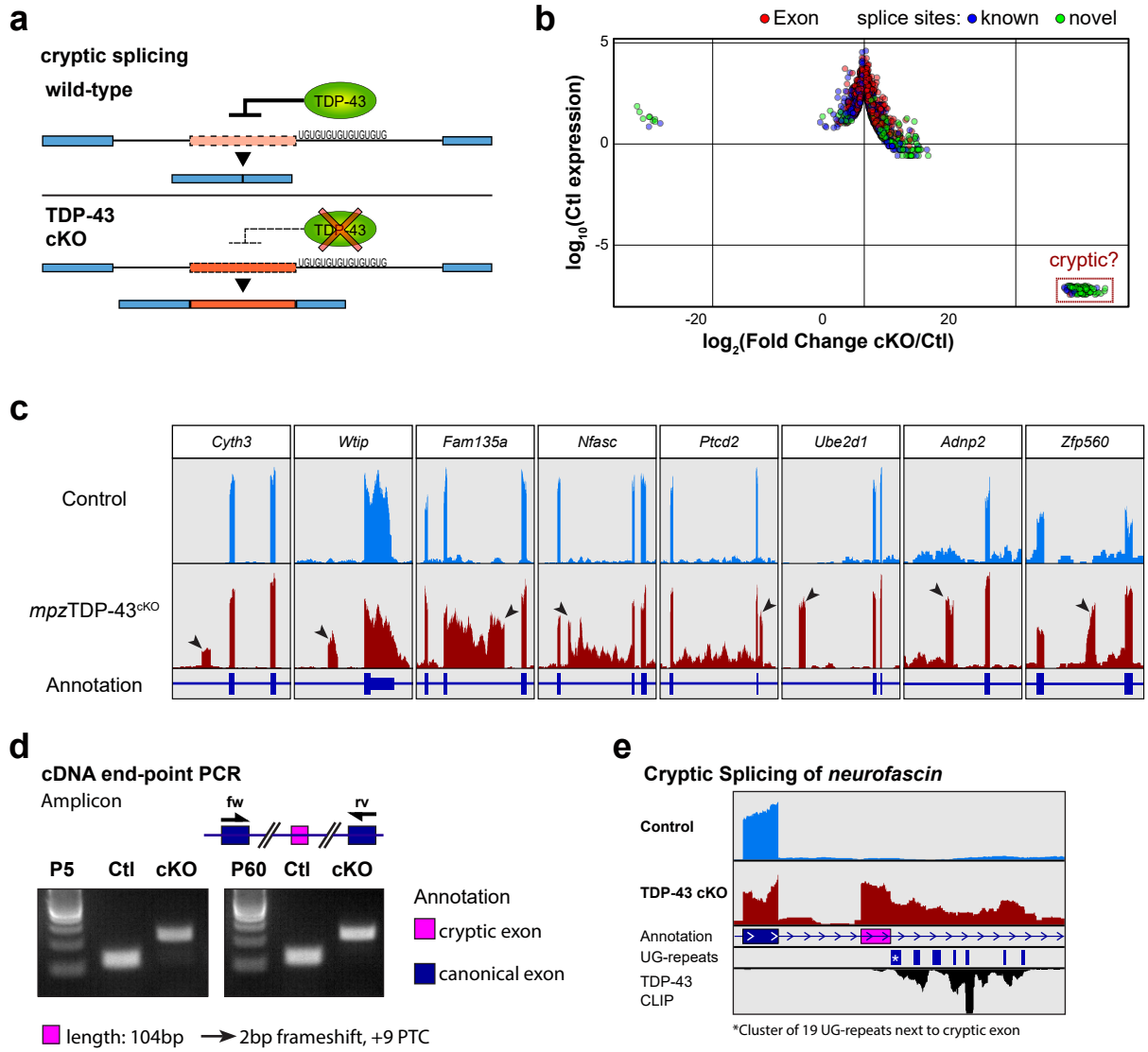

Figure 5.5: Neurofascin as a major target of TDP-43 in Schwann cells among identified cryptic splicing events. **(a)** Schematic showing the function of TDP-43 as a repressor of cryptic splicing events, modified from (Ling et al., 2015). Intronic UG-repeats serve as binding sites for TDP-43, allowing it to suppress incorporation of neighboring intronic sequences into mRNA. **(b)** Quantification of exons and splice sites from RNA-sequencing data. Novel splice sites that are only present in *mpz*-cKO nerves served as candidate events of cryptic splicing (red box). **(c)** Confirmed cryptic splicing events in *mpz*-cKO SNs but not in controls (black arrowheads). Bars represent coverage aligned to genomic sequence. Height of bars is scaled individually. Annotation shows exons (thick bars) and 3' UTRs (thin bars). All genes are presented in *sense* orientation. **(d)** PCR amplification confirms presence of cryptic *nfasc* exons in SNs of *mpz*-cKO but not of control mice at both P5 and P60. Sequencing of the resulting amplicon confirms the incorporation of 104bp intronic sequence, leading to a frameshift and nine premature termination codons in the coding sequence. **(e)** Detailed analysis of cryptic splicing of *neurofascin* transcripts. Sequences of $(UG)_{\geq 4}$ are considered as UG-repeats (blue boxes). A stretch of 19 consecutive UG-repeats is located directly downstream of the cryptic exon. TDP-43 CLIP represents coverage of TDP-43 from re-analyzed UV-CLIP data from brain tissue of 8-week old mice (Polymenidou et al., 2011), indicating direct interaction between TDP-43 and the transcript.

Altered Nodes of Ranvier in *mpz*TDP-43^{cKO} Mice

Neurofascin is expressed by neurons and myelination-competent glia (SCs and oligodendrocytes) as different isoforms. Neurons express NF186 (186kDa) while SCs and oligodendrocytes express NF155 (155kDa). In spite of the evidence presented so far, cryptic splicing of *nfasc* could potentially also have appeared due to secondary events, leading to expression of aberrant transcripts in neurons. Isoform-specific qPCR and protein analysis confirmed an immense reduction of *nfasc155* and its protein NF155 already at P5 (Fig. 5.6a-c). Conversely, neuronal NF186 was not reduced in *mpz*-cKO SNs compared to controls at P5 and P60 (Fig. 5.6b,d). Together, these results indicate that the reduction in the bulk sequencing data was due to SC-specific changes in *nfasc* expression.

Considering that NF155 is required to interact with Contactin-1 in the paranodal regions (Pillai et al., 2009), the reduction of NF155 could lead to defective paranodal junctions, which might further disturb the organization of the nodal area, comprising the node of Ranvier, the paranodal region, and the juxtaparanodes. To test this hypothesis, we analyzed nerves from control and *mpz*-cKO mice at P60, when developmental myelination is mature and nodal region organization well established (Vabnick et al., 1999; Custer et al., 2003). Longitudinal sections of control and *mpz*-cKO SNs were labelled with KV1.2 to mark the juxtaparanode, Contactin-1 to mark the paranode, and NF186 to mark the node of Ranvier. Nerves from *mpz*-cKO mice consistently displayed incorrectly localized KV1.2 and Contactin-1 immunofluorescence (Fig. 5.6e,f). The immunofluorescence signal-intensity of KV1.2 and Contactin-1 also appeared to be lower in *mpz*-cKO nerves than in control nerves, although total protein levels analyzed by western blotting were not markedly different (Fig. 5.6g,h). This indicates that the lower staining intensity of KV1.2 and Contactin-1 seen in Fig. 5.6e in *mpz*-cKO nerves was not because the proteins were overall less abundant, but rather they were improperly localized and not concentrated in the specific domains. A higher density of nodes in *mpz*-cKO mice with lower levels of both KV1.2 and Contactin-1, could potentially also explain the observed lack of change on the overall levels on western blots. However, two independent findings did not lend support to this hypothesis. *First*, NF186 protein levels were not significantly upregulated in *mpz*-cKO SNs at P60 (Fig. 5.6d). *Second*, the fraction of nuclei of myelinating SCs compared to the total number of myelinated axons (*i.e.* among SCs myelinating each internode), was only trendwise marginally higher (and not statistically significant) in cross-sections from *mpz*-cKO compared to control SNs analyzed by EM (Fig. A.1).

This indicates that the overall internodal length cannot be drastically shorter in *mpz*-cKO nerves, which is consequently not consistent with a pronounced increase in the number of nodes.

Electrophysiological Properties are Impaired in *mpz*-cKO Nerves

According to previous studies, deleting components of the nodal region (including NF155) impairs the conduction properties of myelinated axons (Pillai et al., 2009; Boyle et al., 2001; Saifetiarova et al., 2017). We therefore hypothesized that the reduction of NF155, and consequential disturbance of the nodal region domains, would lead to electrophysiological defects in *mpz*-cKO SNs. To test this hypothesis, we evaluated the electrophysiology of *mpz*-cKO and control SNs *in vivo* at P60 (Fig. 5.6i). The compound muscle action potential (cMAP) peak-amplitude (Fig. 5.6j,k), as well as the compound sensory nerve action potential (cSNAP) amplitude (Fig. 5.6m) were both significantly reduced in *mpz*-cKO mice compared to controls. In addition to the amplitude defects, *mpz*-cKO nerves also displayed a reproducible reduction of the nerve conduction velocity (NCV) by roughly 50 % compared to controls. The reduced NCV was evident in the specific analysis of motor fibers (motor NCV, Fig. 5.6j,l) as well as in the compound sensory NCV (csNCV, Fig. 5.6n), which includes orthodromic sensory conduction and antidromic motor conduction. The H-reflex, which consists of the motor response elicited via the reflex arch upon co-stimulation of sensory fibers in the SN, was very consistently delayed in *mpz*-cKO animals compared to controls (Fig. 5.6o). In summary, the coherently impaired conduction velocity and amplitude signals observed in the nerves of *mpz*-cKO mice at P60 contrasts with the near-normal appearance of the myelinated axon profiles at this age. Thus, such electrophysiology defects in the absence of prominent demyelination or of drastically thinner myelin, and without detectable loss of axons, are very likely related to the changes in the nodal region present in these mice.

Overall, we propose the interpretation that TDP-43 normally interacts with UG-repeats in intronic regions of *nfasc* and thereby prevents the retention of cryptic exons on the mature mRNA form of *nfasc155* in SCs. This TDP-43-mediated protection of *nfasc155* is essential for the proper expression of NF155, and consequently the appropriate localization of components of the paranodal and juxtaparanodal regions, which in turn is essential for proper electrophysiological conduction of action potentials along axons.

Figure 5.6 *(facing page)*: Neurofascin 155 is strongly reduced in TDP-43^{cKO} Schwann cells, leading to impaired nodal architecture and impulse conduction properties. (a-d) RNA and protein analysis of Neurofascin isoforms in control and *mpz*-cKO sciatic nerves at P5 and P60. **(a)** qRT-PCR analysis of *nfasc155* transcripts shows a reduction in the sciatic nerve of *mpz*-cKO mice compared to controls at both ages. **(b)** Protein detection of Neurofascin (NF) isoforms and αTubulin by western blotting shows a reduction of NF155 in *mpz*-cKO compared to control SNs at both ages. **(c)** Quantification of NF155 and **(d)** quantification of NF186 in sciatic nerves at P5 and P60 normalized to αTubulin revealed a significant reduction of NF155 but not NF186 in *mpz*-cKO SNs compared to controls. **(e)** Longitudinal sections of control and *mpz*-cKO sciatic nerves. Immunofluorescent images display potassium channel KV1.2 (green) in the juxtaparanode, Contactin-1 (white) in the paranode and NF186 (red) in the node of Ranvier. Note the abnormal localization of KV1.2 and Contactin-1 in *mpz*-cKO mice. scalebar: 20 µm **(f)** Quantification of the nodal architecture. Proportion of quantified nodes that display a clear separation of the KV1.2 signal from NF186 by a gap, indicating that KV1.2 is located in close proximity to the node of Ranvier in *mpz*-cKO nerves. **(g)** Protein detection of KV1.2 and Contactin-1 (Cont-1) by western blotting in control and *mpz*-cKO sciatic nerves at P60. **(h)** Quantification of (g), displaying no evidence for differences between genotypes for each protein. **(i)** Schematic of *in vivo* electrophysiological analysis setup. For motor unit and H reflex analysis, proximal and distal stimuli were recorded by the recording electrode in the foot muscle. For compound sensory analysis, the proximal stimulating electrode was repurposed to record stimuli from the distal stimulating electrode. **(j-o)** Electrophysiological analysis of control and *mpz*-cKO mice at P60. **(j)** Representative electrophysiological traces of the compound muscle response upon proximal and distal stimulation of the sciatic nerve in control and *mpz*-cKO mice. Traces show the direct motor response (M-wave, first peak) and the H-reflex (H-wave, second peak marked by 'H'). The colored columns illustrate the difference in latency between distal and proximal stimuli. The y-axis represents the compound muscle potential (cMAP) and the x-axis represents time. **(k)** The cMAP peak-amplitude evoked by distal stimulation is reduced in *mpz*-cKO mice compared to controls. **(l)** Nerve conduction velocity (NCV) in motor axons innervating the foot muscle is decreased in *mpz*-cKO mice compared to controls. **(m)** Compound sensory action potential (cSNAP) peak-amplitude is variable but significantly reduced in *mpz*-cKO SNs compared to controls. **(n)** Compound sensory nerve conduction velocity (csNCV) is decreased *mpz*-cKO SNs compared to controls. **(o)** Latency of H-reflex evoked by proximal stimulation, displaying a consistent increase in *mpz*-cKO compared to control mice. **(Statistics)** Bar graphs represent mean±SEM; *p<0.05, **p<0.01, ***p<0.001. (a) P5 n = 5 mice, P60 n = 4 mice, two-tailed, unpaired Student's t-test. (c,d) P5 n = 7 mice, P60 n = 5 mice, two-tailed, unpaired Student's t-test. (h) n = 5 mice, two-tailed, unpaired Student's t-test. (k-o) n = 9 mice, two-tailed, unpaired Student's t-test.

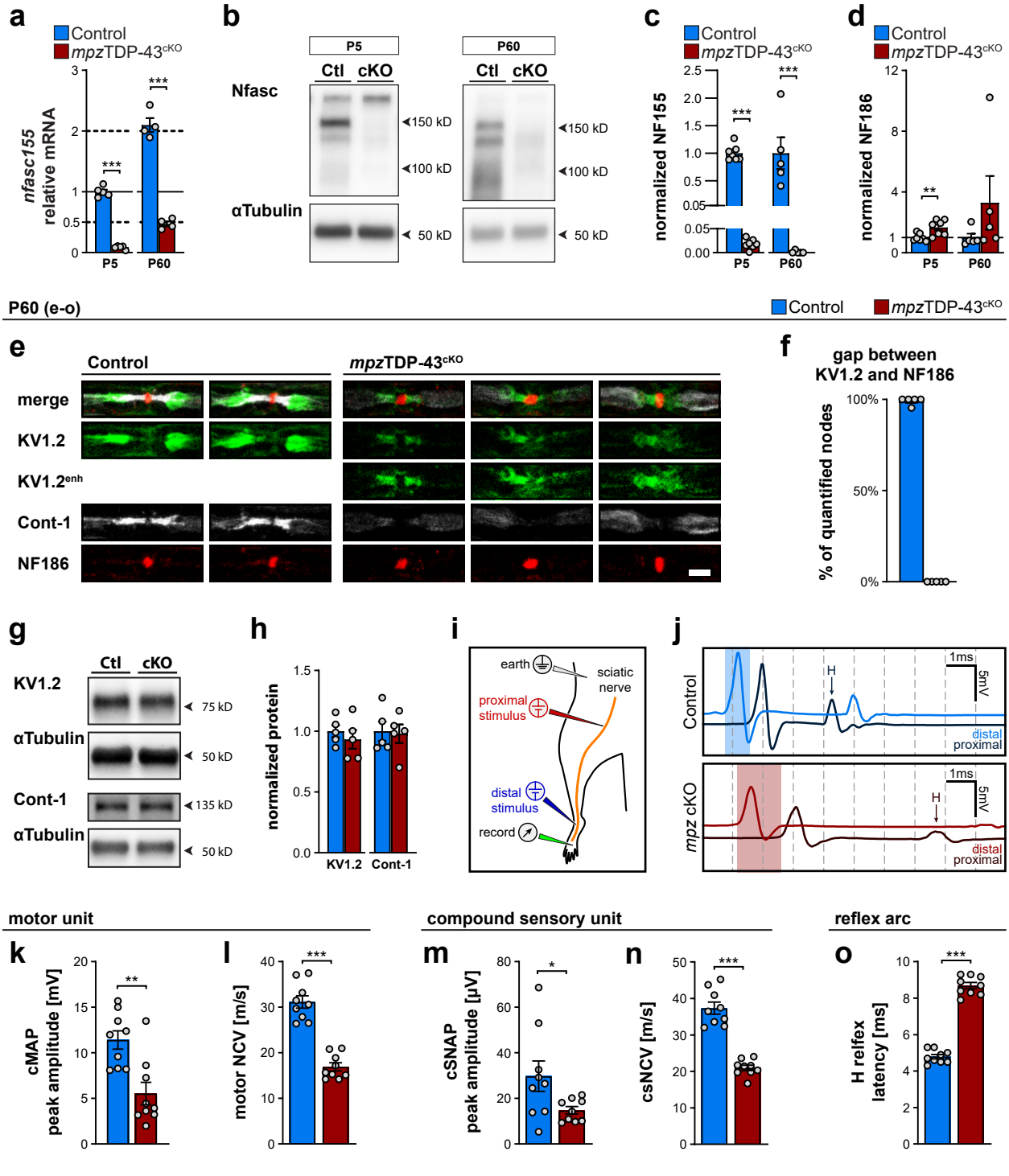
a
Control
mpzTDP-43cKO
nfasc155 relative mRNA
P5
P60
b
P5
P60
Ctl
cKO
Nfasc
αTubulin
150 kD
100 kD
50 kD
c
normalized NF155
d
normalized NF186
P60 (e-o)
e
Control
mpzTDP-43cKO
merge
KV1.2
KV1.2enh
Cont-1
NF186
f
gap between KV1.2 and NF186
% of quantified nodes
100%
50%
0%
g
KV1.2
αTubulin
Cont-1
75 kD
50 kD
135 kD
h
normalized protein
KV1.2
Cont-1
i
earth
sciatic nerve
proximal stimulus
distal stimulus
record
j
Control
mpz cKO
H
1ms
5mV
distal
proximal
motor unit
compound sensory unit
reflex arc
k
cMAP peak amplitude [mV]
l
motor NCV [m/s]
m
cSNAP peak amplitude [µV]
n
csNCV [m/s]
o
H reflex latency [ms]

5.2. Long-Term Impact of Loss of TDP-43 in Aging Animals

The analysis of *mpz*-cKO mice up to P60 revealed the functional impact of TDP-43 during developmental myelination. Past this stage, continuous neuroglial interaction is still required to maintain the healthy myelinated state and protect both glial cells and axons from damage and degeneration. We therefore asked whether TDP-43 in Schwann cells continues to contribute towards homeostasis in the PNS as the mice age. To this end, we analyzed *mpz*-cKO and control mice beyond 60 days of age.

Aging *mpz*-cKO Mice Develop Severe Abnormalities in Large Caliber Axons

For several months after P60, *mpz*-cKO mice appeared normal in gross appearance, and without an evident impairment in free cage behavior. Since we did not observe additional signs pointing to a striking phenotype progression, we allowed the mice to age further to 12 months of age. At this age, *mpz*-cKO mice developed a pronounced motor dysfunction and consistently clasped their hind limbs when lifted by the tail (Fig. 5.7a). Weight measurements revealed a lower body mass of *mpz*-cKO mice compared to controls (Fig. 5.7b). Assessment of motor performance with the inverted grid hanging test displayed clearly decreased performance of *mpz*-cKO mice compared to controls (Fig. 5.7c). This contrasts with the assessment at P60, in which *mpz*-cKO mice and controls did not differ on this test. In order to evaluate histological features in peripheral nerves that could be related to the worsening condition of *mpz*-cKO mice, we investigated the SN morphology at 12 months of age by EM. Through qualitative appreciation, SNs of *mpz*-cKO mice did not appear dramatically affected when compared to control nerves (Fig. 5.7d). However, detailed quantifications of EM panoramas scanning the whole nerve section area revealed an approximate reduction of 300 myelinated axons (-7 %) in *mpz*-cKO SNs compared to controls (Fig. 5.7e). The g-ratio analysis showed comparable values between control and *mpz*-cKO mice in small and larger caliber axons, however it also revealed that axons between 2 and 5 microns in diameter were enveloped by myelin that was apparently too thick for the corresponding axonal caliber (Fig. 5.7f). Detailed inspection of all measurements did not reveal a segregated population of thinly myelinated axons (Fig. A.2a). Remarkably, during g-ratio analysis, we consistently observed fewer large caliber axons in *mpz*-cKO SNs than in control SNs.

The g-ratio analysis in peripheral nerves including SNs was performed using automated identification and axon segregation of myelinated fibers in whole nerve cross sections, providing at least several hundred individual measurements per animal without a potential limitation by the selection of random fields. To assess whether this observation indicated a genuine reduction of large diameter axons in *mpz*-cKO SNs, the diameters of all myelinated axons in EM cross-sections were quantified (Fig. 5.7g,h). The number of myelinated axons with small calibers (1-3 µm) were obviously higher in *mpz*-cKO SNs compared to controls, while axons larger than 4 µm in diameter were consistently reduced in the same cKO mice (Fig. 5.7h). The reduction in axon numbers seemed proportionally more drastic with increasing axon diameter, and axons larger than 8 µm in diameter were almost absent in *mpz*-cKO SNs. In summary, *mpz*-cKO animals aged to one year display an impaired motor performance and dysfunction when compared to controls, concomitant with an overall reduction of myelinated large caliber axons in SNs. Besides a marginal effective reduction of the total number of axons, SNs from *mpz*-cKO animals additionally display an evident shift on the diameter of remaining myelinated axons, with an enrichment of small caliber and a reduction of large caliber axons. When further considering that myelin was apparently too thick on intermediate diameter axons of *mpz*-cKO animals, we favor the interpretation that some degree of axonal atrophy might occur in large caliber axons, surrounded by correspondingly thick myelin, ultimately causing a reduction of their diameter and giving the appearance as being hypermyelinated after shrinking.

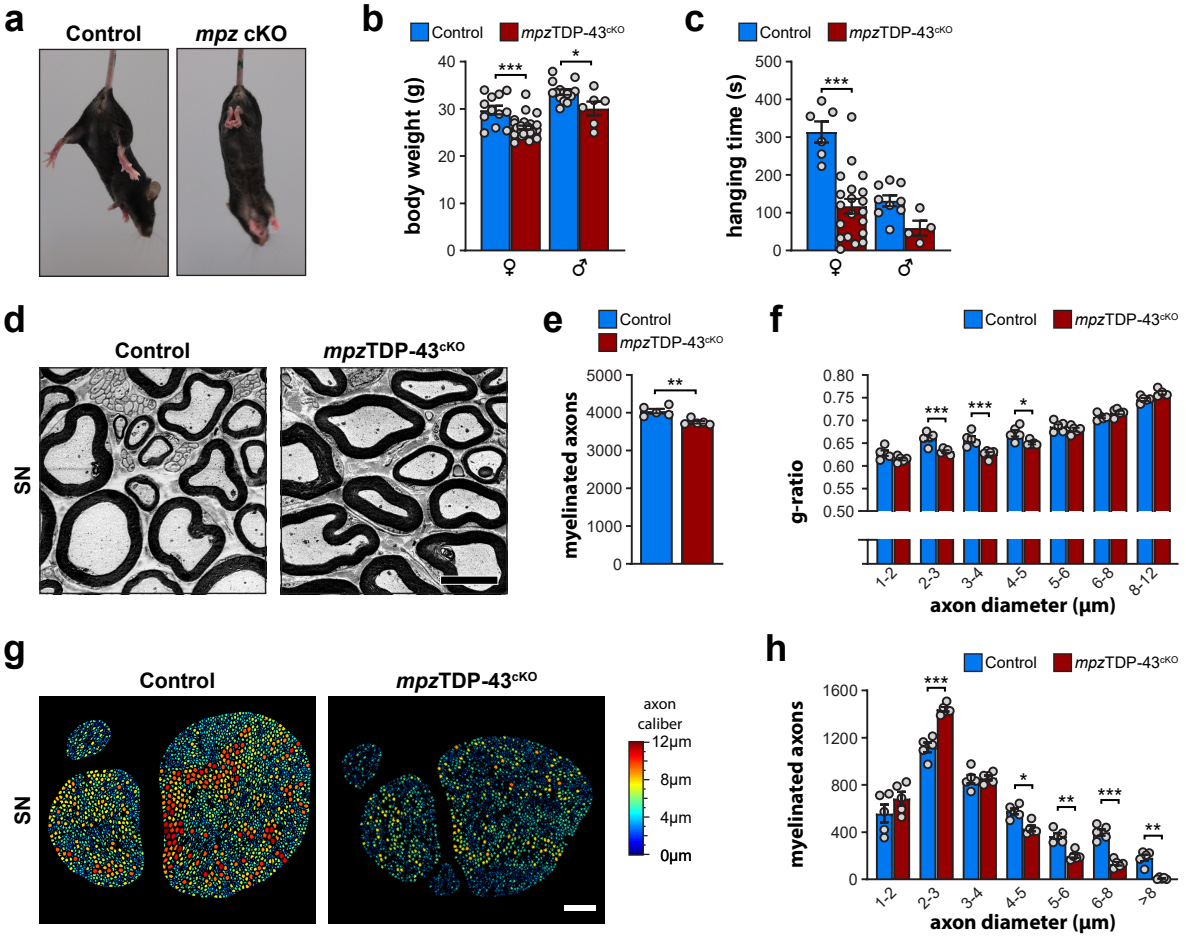

Figure 5.7: Deletion of TDP-43 in Schwann cells results in motor dysfunction and loss of large caliber axons in one-year-old *mpz*-cKO mice. **(a)** Tail-suspension test showing an example of consistent hind paw clasping by *mpz*-cKO mice. **(b)** Bodyweight of control and *mpz*-cKO mice at one year of age, depicting lower weight in *mpz*-cKO mice of both sexes. **(c)** Hanging time in the inverted grid test reveals a decreased motor performance of *mpz*-cKO mice compared to controls. **(d)** Representative EM micrographs of control and *mpz*-cKO SNs in one-year-old mice. scalebar: 5 µm. **(e)** Quantification of total myelinated axons in SN cross sections. SNs from *mpz*-cKO mice have approximately 7 % fewer myelinated axons than control SNs. **(f)** Quantification of the myelin thickness in relation to the axon diameter (g-ratio), showing apparently too thick myelin in middle-caliber axons of *mpz*-cKO mice compared to controls. **(g)** Exemplary visualizations of axon caliber analysis of a control and *mpz*-cKO sciatic nerve. Axons are colored individually according to their diameter (scale on right side). scalebar 100 µm. **(h)** Diameter measurements of all axons in EM micrographs of entire SN cross sections reveal a decrease in axons with larger diameters and a concomitant enrichment of smaller caliber axons in *mpz*-cKO mice compared to controls. Axons smaller than 1 µm occur only seldom and are not displayed. **(Statistics)** Bar graphs represent mean±SEM; *p<0.05, **p<0.01, ***p<0.001 (b) ♀ n = 12 control and 27 *mpz*-cKO mice, ♂ n = 14 control and 6 *mpz*-cKO mice, two-way ANOVA with Šídák's multiple comparisons test. (c) ♀ n = 6 control and 20 *mpz*-cKO mice, ♂ n = 9 control and 4 *mpz*-cKO mice, two-way ANOVA with Šídák's multiple comparisons test. (e) n = 5 mice, two-tailed, unpaired Student's t-test. (f,h) n = 5 mice, two-way ANOVA with Šídák's multiple comparisons test.

The axonal impact detected in *mpz*-cKO animals at one year of age raises intriguing possibilities in light of the established literature relationship between TDP-43 and motor neurons. At least in the context of ALS, retention of TDP-43 in cellular aggregates is thought to contribute towards motor neuron degeneration. Considering these premises, and that sciatic nerves contain axons from both sensory and motor neurons, we entertained the possibility that motor axons were particularly affected in the *mpz*-cKO SNs. In order to analyze sensory and motor axons separately, we harvested the fourth lumbar (L4) root nerves from control and *mpz*-cKO mice at 12 months of age. L4 root nerves provide two advantages: *First*, root nerves consist of pairs and exit the spinal cord ventrally and dorsally. Ventral root nerves contain only motor fibers and dorsal root nerves are solely composed of sensory fibers. *Second*, the L4 root nerve is the largest root nerve contributing to the sciatic nerve and thereby it is likely the most representative to compare with our previous results.

In *mpz*-cKO mice, both ventral and dorsal root nerves were robustly affected (Fig. 5.8a). Ventral root nerves from *mpz*-cKO mice displayed fewer myelinated and fewer total axons compared to controls, indicating axonal loss (Fig. 5.8b,c). Two prominent features were almost uniquely observed in *mpz*-cKO mice relative to controls: *First*, the occurrence of highly vacuolated fibers, mostly splitting the myelin sheath (Fig. 5.8d). *Second*, being a pure motor nerve, L4 ventral roots only contain myelinated axons and no Remak bundles. Nevertheless, non-myelinated fibers were present in *mpz*-cKO L4 ventral roots but virtually absent in controls, which is highly indicative of motor axon demyelination (Fig. 5.8d). In dorsal root nerves, myelinated and total axons (>1 µm in diameter) also tended to be less numerous in *mpz*-cKO mice compared to controls, but without statistical significance (Fig. 5.8e,f). Vacuolated fibers and nonmyelinated axons (>1 µm in diameter) were also found in *mpz*-cKO dorsal root nerves, but virtually absent in controls (Fig. 5.8g). We considered the dorsal phenotype substantially milder than the one in the ventral roots, given that the occurrence of vacuolated or nonmyelinated fibers was less frequent in absolute numbers, and even fewer if related to the total numbers of axons in each respective nerve. The different extent of phenotypic features was also reflected in the myelin sheath thickness analysis: The *mpz*-cKO ventral roots were consistently hypomyelinated across axons of all diameters compared to controls (Fig. 5.8h, Fig. A.2b). Myelinated axons in the *mpz*-cKO dorsal roots were globally hypomyelinated in small caliber axons, with statistical significance up to 2 µm in diameter (Fig. 5.8i). However, sporadic axons with thin myelin (high g-ratio) were also detected in the *mpz*-cKO mice up to approximately 6 µm in diameter (Fig. A.2c).

As previously shown, the sciatic nerve in *mpz*-cKO mice lost mainly large caliber axons compared to controls. Diameter analysis of all myelinated axons in *mpz*-cKO ventral and dorsal root nerves revealed that myelinated axons larger than 6 µm were also substantially reduced compared to controls (Fig. 5.8j-l), even though we acknowledge that this impact might be more pronounced in the ventral roots. Similar results were obtained when vacuolated and non-myelinated axons were included in the analysis (Fig. A.3). The observations in root nerves are therefore consistent with the SN, and further indicate that both sensory and motor nerves are in principle affected due to loss of TDP-43 in SCs. In summary, *mpz*Cre-mediated deletion of TDP-43 also has an impact during moderate aging, and most strikingly affected ventral root nerves. The motor dysfunction in *mpz*-cKO mice developed only gradually and was not completely evident without performing behavioral experiments at one year of age. This potentially indicates that, besides the developmental defects depicted in our analysis up to P60, SCs ultimately fail to maintain myelination and axonal support over the course of longer periods of time.

Figure 5.8 ***(facing page)*****: Ventral root nerves are particularly affected in one-year-old *mpz*-cKO mice.** L4 ventral and dorsal root nerves were analyzed in one-year-old control and *mpz*-cKO mice. **(a)** EM micrographs displaying typical morphological features of control and *mpz*-cKO root nerves. Ventral and dorsal *mpz*-cKO root nerves display myelinated fibers with vacuoles, sometimes splitting the myelin sheath (black arrowheads). In control mice, non-myelinated axons are not expected in ventral root nerves and only expected in dorsal root nerves for axons in Remak bundles (below 1 µm in diameter). However, *mpz*-cKO dorsal and ventral L4 root nerves display non-myelinated axons, some of which larger than 1 µm in diameter (white arrowheads). scalebar 10 µm. **(b-d)** Quantification of features per ventral root nerve cross section. The number of myelinated axons (b) and total axons (c) were both decreased in *mpz*-cKO ventral roots compared to controls. Vacuole-containing fibers as well as non-myelinated axons were both elevated in *mpz*-cKO ventral roots compared to controls (d). **(e-g)** Quantification of features per dorsal root nerve cross section. Similar to the ventral root nerves, the number of myelinated axons (e) and total axons (f) trend towards a reduction in *mpz*-cKO dorsal roots compared to controls, albeit without statistical significance. The vacuole-containing fibers as well as non-myelinated axons (g) were also increased in *mpz*-cKO dorsal roots compared to controls. A minimum caliber-cut-off of 1 µm was applied when non-myelinated axons were counted. **(h)** Quantification of the myelin sheath thickness in ventral root nerves, plotted as a function of g-ratio versus axon diameter. Axons in *mpz*-cKO are robustly hypomyelinated across all axon calibers compared to controls. **(i)** g-ratio of myelinated fibers in dorsal root nerves mainly highlight thinner myelin on small diameter axons in *mpz*-cKO mice compared to controls, among other minor changes. **(j)** Exemplary visualizations of axon caliber analysis of control and *mpz*-cKO root nerves. Axons are colored individually according to their caliber (scale on bottom). scalebar 100 µm. **(k,l)** Quantification of calibers from all intact, *i.e.* non-vacuolated, myelinated fibers in the ventral (k) and dorsal (l) root nerves, generally depicts a reduction of axons with large diameters and an increase of axons with small diameters in *mpz*-cKO mice compared to controls. Axons smaller than 1 µm occur only seldom in ventral root nerves (k) and are not displayed. **(Statistics)** Bar graphs represent mean±SEM; *p<0.05, **p<0.01, ***p<0.001. (b,c,e,f) n = 5 mice, two-tailed, unpaired Student's t-test. (e) p=0.06, (f) p=0.07. (d,g) n = 5 mice, Mann Whitney test. (h,i,k,l) n = 5 mice, two-way ANOVA with Šídák's multiple comparisons test.

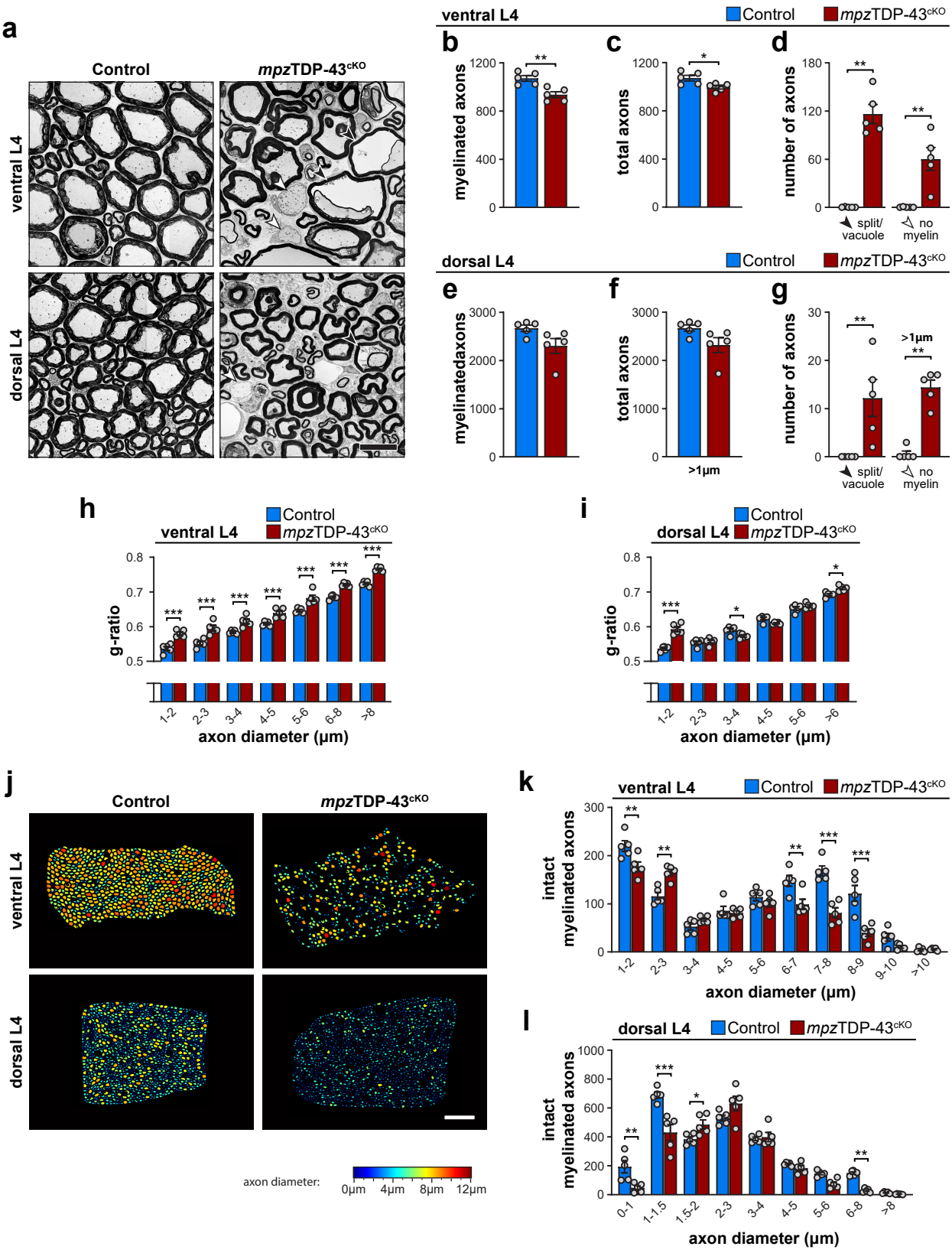
a
Control
mpzTDP-43cKO
ventral L4
dorsal L4
ventral L4
Control
mpzTDP-43cKO
b
myelinated axons
c
total axons
d
number of axons
split/ vacuole
no myelin
dorsal L4
Control
mpzTDP-43cKO
e
myelinatedaxons
f
total axons
>1µm
g
number of axons
>1µm
split/ vacuole
no myelin
h
ventral L4
Control
mpzTDP-43cKO
g-ratio
axon diameter (µm)
i
dorsal L4
Control
mpzTDP-43cKO
g-ratio
axon diameter (µm)
j
Control
mpzTDP-43cKO
ventral L4
dorsal L4
axon diameter:
0µm 4µm 8µm 12µm
k
ventral L4
Control
mpzTDP-43cKO
intact myelinated axons
axon diameter (µm)
l
dorsal L4
Control
mpzTDP-43cKO
intact myelinated axons
axon diameter (µm)

TDP-43^{cKO} Leads to a Progressively Aggravated Condition Without Recovery

Our data at one year showed an aggravated phenotype of *mpz*-cKO mice relative to P60. However, it was not clear whether this phenotype at one year represented a stable steady peak of symptoms, or whether it could further deteriorate in older animals. To evaluate whether the phenotype progresses further, mice were allowed to age beyond one year. We performed our analysis at 16 months of age and mainly focused on histological analysis of EM micrographs, since these enable a detailed evaluation of the phenotype. An overview over these micrographs immediately indicated widespread changes in *mpz*-cKO SNs when compared to controls (Fig. 5.9a), apparently more severe than features observed at one year. The SNs, ventral nerve roots, and also dorsal nerve roots from *mpz*-cKO mice exhibited an even greater reduction in the total number of axons than was seen at one year (Fig. 5.9b,d,f). In addition to the missing axons, we observed striking accumulation of axons without myelin, suggestive of widespread demyelination in all tissues assessed (Fig. 5.9c,e,g). Among the myelinated fibers in *mpz*-cKO L4 root nerves, a significant fraction displayed aberrant vacuolated profiles (Fig. 5.9e,g). A distinct feature of *mpz*-cKO dorsal root nerves was the presence of onion bulb profiles, i.e. multiple layers of cells and matrix surrounding a central axon that may or not be myelinated, which were not detected in control nerves (Fig. 5.9h). The reduction of motor axons in *mpz*-cKO mice likely reflects axonal degeneration. Together with the potentially persistent impairment of impulse conduction in *mpz*-cKO nerves, we hypothesized that TDP-43 deletion in SCs might result in reduced innervation of muscles or reduced neuronal signaling through the present neuromuscular junctions. Both of these conditions are expected to lead to muscle wasting, as it was previously shown in experimental models (Sacheck et al., 2007) or neuropathies, *e.g.* spinal muscular atrophy (SMA) and Charcot-Marie-Tooth neuropathy type 1 (CMT1A) (reviewed by Thomas, 1999; Kolb and Kissel, 2011). To this end, we analyzed gastrocnemius (GN), tibialis anterior (TA) and soleus (Sol) muscles of *mpz*-cKO and control mice at 16 months of age. Qualitatively, all muscles appeared smaller in *mpz*-cKO mice compared to controls (Fig. 5.9i). The mass of GN muscles from *mpz*-cKO mice was at about 50 % of the mass of GN muscles from control mice (Fig. 5.9j).

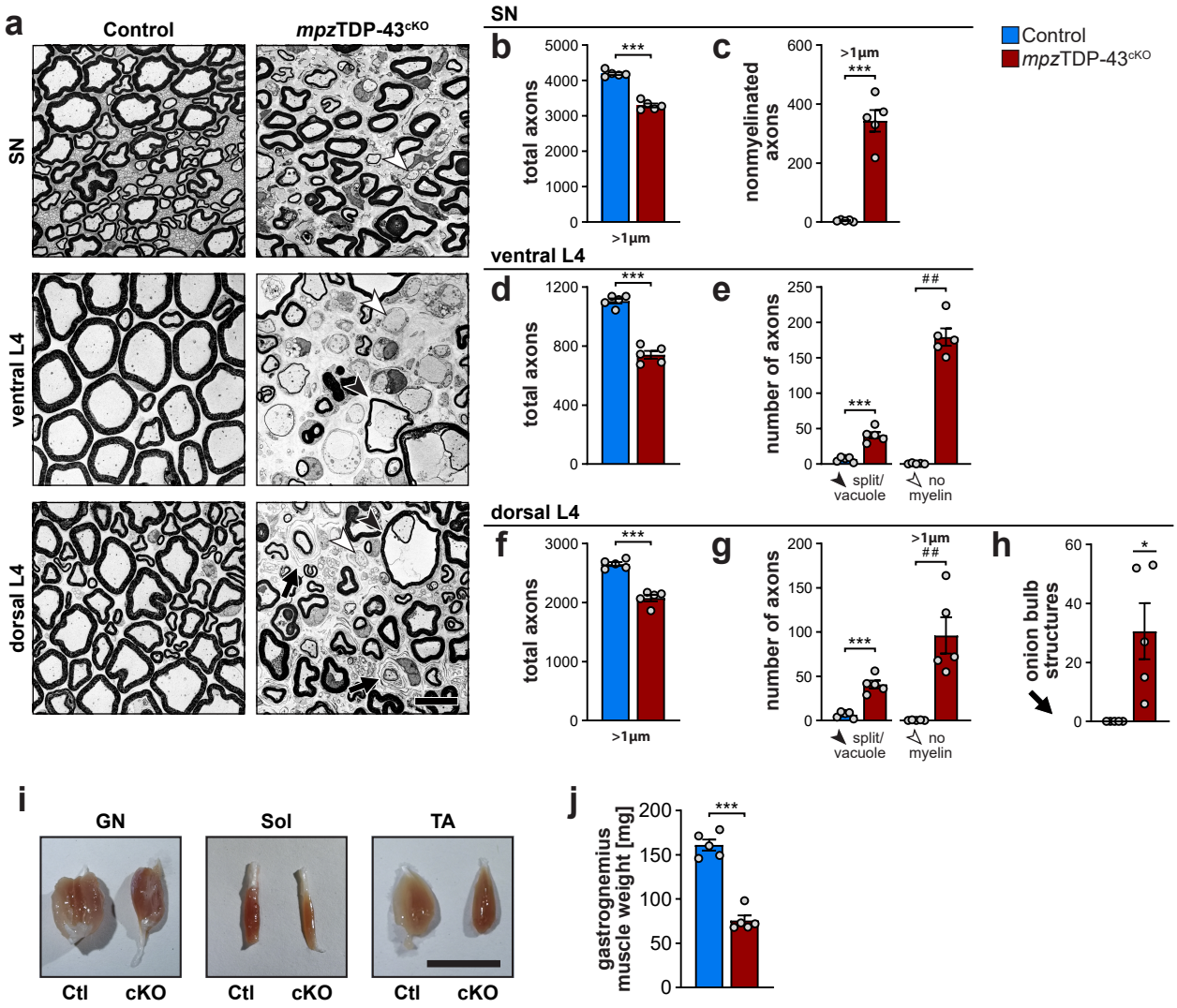

Figure 5.9: Loss of TDP-43 ultimately leads to widespread demyelination and axonal loss. Control and *mpz*-cKO mice were analyzed at 16 months of age by electron microscopy. **(a)** Exemplary EM micrographs illustrating the morphology of sciatic and L4 root nerves. *mpz*-cKO nerves display nonmyelinated axons (white arrowheads) and highly vacuolated myelinated fibers (black arrowheads). Onion bulb structures (black arrows) are observed in *mpz*-cKO dorsal roots. scalebar: 10 µm **(b,c)** Quantification of the sciatic nerve, displaying reduced numbers of total axons >1 µm (b) and increased numbers of nonmyelinated axons (c) in *mpz*-cKO mice compared to controls. **(d-h)** Quantification of ventral L4 root nerves (d,e) and of L4 dorsal root nerves (f-h). The total numbers of axons are reduced (d,f), whereas the numbers of axons without myelin and the occurrence of vacuoles in myelinated fibers is increased (e,g) in *mpz*-cKO nerves compared to controls. Furthermore, onion bulb structures were prominently observed in dorsal root nerves of *mpz*-cKO mice but virtually absent in controls (h). **(i,j)** Muscular atrophy in *mpz*-cKO mice compared to controls. Exemplary pictures of the gastrocnemius (GN), Soleus (Sol) and tibialis anterior (TA) muscle (i). The *mpz*-cKO gastrocnemius muscle weight is strongly reduced compared to controls (j). **(Statistics)** Bar graphs represent mean±SEM; $^{\#\#}$p<0.01, *p<0.05, **p<0.01, ***p<0.001. (all graphs) **n = 5 mice**; (b,c,d,f,j) two-tailed, unpaired Student's t-test. (e,g) *two-tailed, unpaired Student's t-test, $^{\#}$Mann Whitney test. (h) one sample t-test with hypothetical mean of zero.

Taken together, we reason that the condition of peripheral nerves continuously worsened in *mpz*-cKO mice, ultimately resulting in severe axonal loss in all nerve tissues assessed and concomitant muscular wasting. Furthermore, remaining axons were partially demyelinated and highly vacuolated in the root nerves. Based on these observations, we concluded that loss of TDP-43 during development also impairs adult SC biology such that emerging signs of damage (including failure to prevent axonal degeneration and failure to protect the myelinated state) appear slowly, but progressively worsen as the mice age. When conceptually considering the stage of SC life impacted by TDP-43 that could result in the late defects described above, we can enumerate three speculative possibilities. *First*, *mpz*-cKO Schwann cells may not develop properly in the first place, carrying impairments not covered or identified by our analysis that ultimately lead to late-onset defects. *Second*, SCs may also be susceptible to an impairment specifically in the adult stage, thereby failing to maintain myelination and axonal support due to the lack of TDP-43 in their fully differentiated, myelinating state. *Third*, when SCs fail to maintain their stable myelinated state in the absence of TDP-43, the process of de- and re-myelination may also in itself be further impaired due to the lack of TDP-43, leading to formation of myelin aberrations and lack of efficient myelin repair.

5.3. Regeneration and Maintenance in *mpz*TDP-43^{iKO} Mice

Nerve Regeneration Is Largely Successful in *mpz*-iKO Mice

Our analysis on *mpz*-cKO mice revealed problems with the protection of axonal survival, altered myelin proportions, and also widespread presence of demyelinated axons. These observations raise the question of whether TDP-43 expressed by SCs is specifically required for nerve repair following nerve injury in adult animals, especially considering that following a PNS injury healthy SCs normally play key roles in promoting regeneration, and subsequent remyelination. To specifically address this question we utilized the *mpz*Cre^{ERT2} mouse line (Leone et al., 2003), in which the ablation of TDP-43 can be temporally controlled and only induced after developmental myelination is complete. In this setup, *mpz*-iKO (*mpz*TDP-43^{iKO}) and control mice were injected with tamoxifen between 8-10 weeks of age to induce recombination, and 2 additional months were allowed for recombination and protein depletion (Fig. 5.10a).

The recombination was assessed by RT-qPCR for TDP-43 mRNA, designed such that one primer binds to exon 3 in order to only amplify non-recombined TDP-43 transcripts and serve as a sensitive indicator of TDP-43 recombination. Abundance of TDP-43 exon 3 mRNA was reduced in *mpz*-iKO SN cDNA at 2mpT compared to controls (Fig. 5.10b), suggesting successful recombination of TDP-43. To further control for loss of TDP-43 function, we evaluated *nfasc155* levels, which are potentially under direct protection by TDP-43-mediated repression of cryptic splicing. Abundance of *nfasc155* was also reduced in *mpz*-iKO compared to control SNs (Fig. 5.10c), which is in agreement with reduced expression of TDP-43 and suggests a loss of function in recombined *mpz*-iKO SCs at 2mpT. To induce demyelination, a crush injury was performed two months after the tamoxifen injection (2mpT) in both control and *mpz*-iKO mice. The key repair phases following peripheral nerve injury follow a well-established temporal pattern, and we tuned the timing of the analysis to evaluate the progression of these main stages. We selected 5 days post crush (dpc) to investigate myelin breakdown, 12dpc to evaluate the onset of remyelination and 30dpc to assess complete remyelination including myelin growth (Fig. 5.10a,d).

The number of intact appearing myelin rings was comparable between control and *mpz*-iKO mice, although we noted considerable variation within each genotype (Fig. 5.10e). At 12 days post crush, control and *mpz*-iKO SNs contained similar numbers of axons, but fewer were already remyelinated in *mpz*-iKO mice (Fig. 5.10f,g). These observations suggest a defect in the timely onset of remyelination without evidence for differential axon regrowth in *mpz*-iKO mice compared to controls. To evaluate whether the impairment at the onset of remyelination consists of a transient delay or a more durable defect, we analysed *mpz*-iKO mice at 30dpc, a time point in which controls should be fully remyelinated. Surprisingly, *mpz*-iKO animals showed a very slight but significant increase in the number of myelinated axons (Fig. 5.10h), indicating that the impairment at 12dpc was a transient delay. Analysis of myelin thickness towards axonal diameter revealed a nearly identical g-ratio for control and *mpz*-iKO mice (Fig. 5.10i,j). The diameter distribution of the axons analyzed was also very similar between *mpz*-iKO and control mice (Fig. 5.10k). In summary, *mpz*-iKO mice displayed a capacity to regenerate after a nerve crush injury, at least in the main events up to 30 days post nerve crush, similar to that seen in control mice. Nonetheless, our observations indicate that TDP-43 in SCs is required for timely onset of remyelination, and we cannot exclude that late-onset defects would arise in *mpz*-iKO nerves at later time points after remyelination.

Figure 5.10 ***(facing page)*****: Schwann cell TDP-43 contributes to a timely onset of remyelination following nerve crush injury.** **(a)** Schematic representation of the experimental design. Tamoxifen was injected in 8-10 week-old control and *mpz*-iKO mice to induce TDP-43 deletion. Two months later, mice were subjected to a sciatic nerve crush injury and analyzed at different days post crush injury (dpc). **(b)** Abundance of TDP-43 exon 3 (*i.e.* nonrecombined) mRNA is reduced in SNs of *mpz*-iKO mice at 2mpT compared to controls. **(c)** Abundance of *nfasc155*, a transcript potentially protected via TDP-43-mediated repression of cryptic splicing, is reduced in *mpz*-iKO SNs compared to controls, consistent with a loss of TDP-43 function in SCs. **(d)** Representative EM micrographs of control and *mpz*-iKO sciatic nerves at 5, 12 and 30 dpc. Contralateral nerves were also extracted from mice at 30dpc. White arrowheads point at two exemplary intact myelin profiles. scalebar: 10 µm. **(e)** Quantification of intact appearing myelin rings at 5dpc to analyze myelin breakdown following the injury reveals no significant changes between control and *mpz*-iKO mice. **(f,g)** Analysis of numbers of regenerated axons and onset of remyelination at 12dpc. For this purpose, the number of axons larger than 1 µm (f) as well as their proportion with myelin sheaths (g) was quantified. No changes were detected in the number of regenerated axons, but *mpz*-iKO mice contain proportionally fewer remyelinated fibers than controls. **(h)** Total numbers of myelinated axons per SN cross section at 30dpc reveal no significant reduction in *mpz*-iKO compared to controls mice at a stage of expected complete remyelination. **(i-k)** Analysis of myelin thickness and axonal diameters at 30dpc. The average g-ratio (i) and the g-ratio plotted against different bins of axon diameters (j) was not detectably changed between control and *mpz*-iKO mice. The axonal diameter measurements used in the quantification of (j) were also used to assess the frequency distribution of axon diameters (k), which did not reveal major differences between the different genotypes. **(Statistics)** Bar graphs represent mean±SEM; *p<0.05, **p<0.01, ***p<0.001. (a,b) n = 5 mice, (e) n = 3 mice, (f,g) n = 5 mice, (h-k) n = 4 mice; (b,c,e-i) two-tailed, unpaired Student's t-test. (j,k) two-way ANOVA with Šídák's multiple comparisons test.

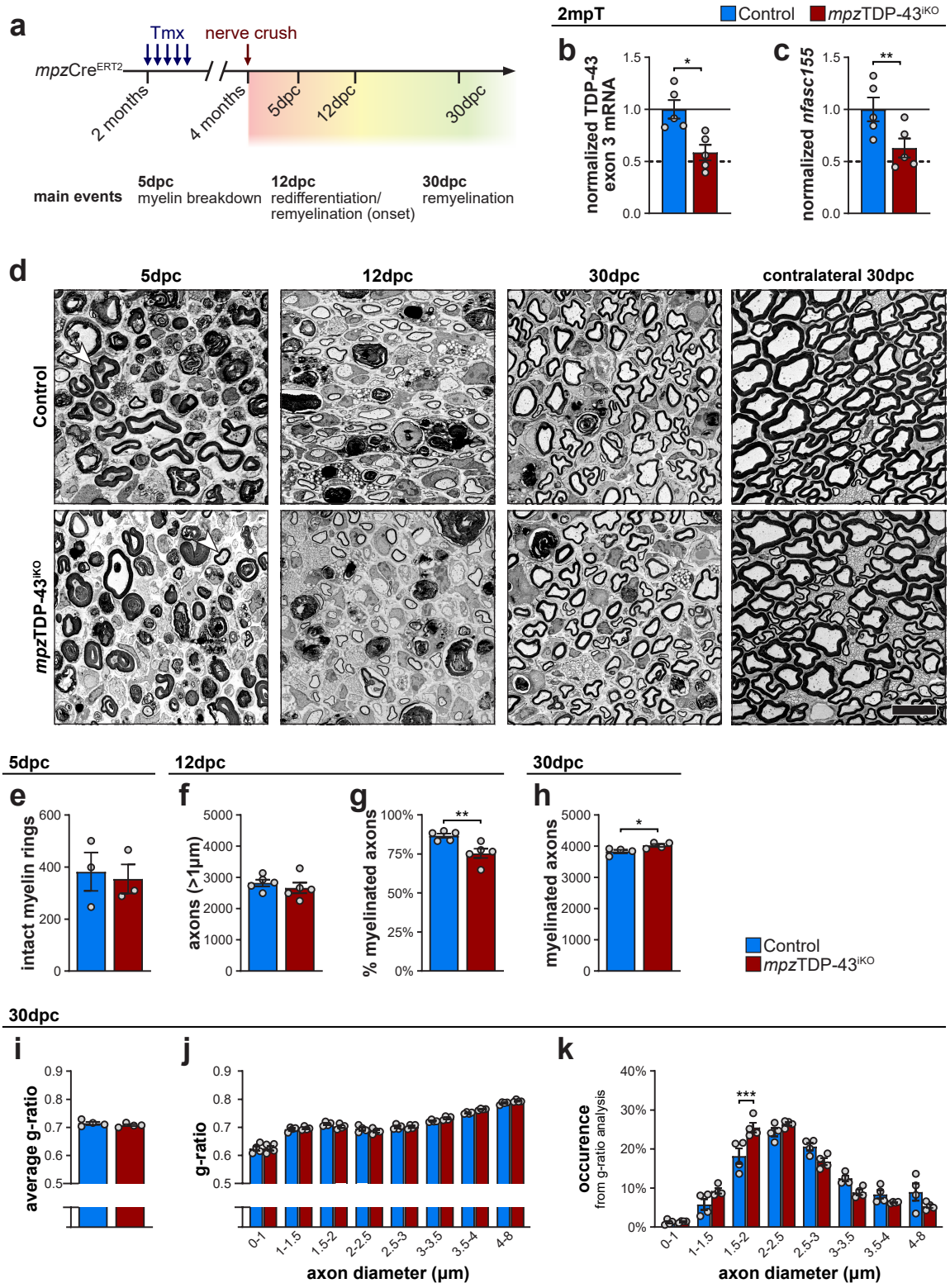
a
Tmx
nerve crush
mpzCreERT2
2 months
4 months
5dpc
12dpc
30dpc
main events
5dpc myelin breakdown
12dpc redifferentiation/ remyelination (onset)
30dpc remyelination
2mpT
Control
mpzTDP-43iKO
b
normalized TDP-43 exon 3 mRNA
c
normalized nfasc155
d
5dpc
12dpc
30dpc
contralateral 30dpc
Control
mpzTDP-43iKO
e
intact myelin rings
f
axons (>1µm)
g
% myelinated axons
h
myelinated axons
i
average g-ratio
j
g-ratio
axon diameter (µm)
k
occurence
from g-ratio analysis
axon diameter (µm)

Maintenance in *mpz*-iKO Mice

Our previous observations revealed major defects in the peripheral nerves of *mpz*-cKO mice during aging, clearly detectable at one year and substantially aggravated at 16 months of age. This phenotype might derive from a specific role of TDP-43 in adult myelinating SCs, but alternatively they could derive from molecular defects triggered much earlier in SC development, but only translated to a phenotype in later life. To evaluate whether TDP-43 is required to maintain myelination and axonal support specifically in adult SCs, we induced the recombination of TDP-43 after developmental myelination is largely completed. To this end, we used the aforementioned *mpz*-iKO mouse line and age-matched control animals, and performed tamoxifen injections between 8 and 10 weeks of age. Due to the observations in the *mpz*-cKO animals, we hypothesized that a phenotype would develop slowly, and possibly only become detectable several months after induction. In addition, inducible systems such as the one we employ are known not to trigger 100% recombination (Ribeiro et al., 2013; Brugger et al., 2015), and therefore nonrecombined Schwann cells might replace some of the recombined Schwann cells over time, further dampening the possibility of these animals developing strong impairments. Consequently, we analyzed control and *mpz*-iKO mice six and twelve months after the tamoxifen injection (Fig. 5.11a). To investigate the recombination and degree of turnover of Schwann cells in sciatic nerves, animals were bred with the Cre-dependent tdTomato reporter line (Madisen et al., 2010), and the SNs were analyzed by immunofluorescence at 6 and 12mpT (Fig. 5.11b,c). Using Sox10 as marker, no obvious differences in SC numbers were detected between genotypes (Fig. 5.11b-d). The proportion of recombined, tdTomato^{pos} Schwann cells was similar at 6mpT and then reduced in *mpz*-iKO mice compared to controls at 12mpT (Fig. 5.11b,c,e). This suggests that some of the recombined, tdTomato^{pos} SCs were lost in *mpz*-iKO SNs, potentially via apoptosis, and were in the meantime replaced by the pool of non-recombined SCs. At 6mpT, when recombined SCs are not yet reduced, we evaluated to which extent TDP-43 was functionally lost in *mpz*-iKO SNs by investigating the previously identified cryptic splicing of *nfasc155*. cDNA end-point PCR analysis indicated that a part of the *nfasc* transcripts incorporated the cryptic exon in *mpz*-iKO mice (Fig. 5.11f). Since cryptic *nfasc* transcripts are likely degraded by NMD, band intensities of canonical and cryptic amplicons cannot be compared to infer the total proportion of mis-spliced transcripts. However, we could screen for a reduction of total *nfasc155* mRNA in SNs, which provides an indication regarding the contribution of cryptic splicing due to loss of TDP-43 in recombined SCs (Fig. 5.11g).

Our observations confirm that *mpz*-iKO SNs displayed significantly reduced levels of *nfasc155* compared to controls, indicating that a major fraction of *nfasc155* has been cryptically spliced. Nevertheless, *mpz*-iKO animals appeared normal and not distinguishable from controls at 6mpT. By 12mpT, 8 out of 12 *mpz*-iKO mice showed hindlimb-clasping when suspended by the tail, indicative of PNS dysfunction (Fig. 5.11h). Nevertheless, the body weight and motor performance on the inverted grid hanging test did not significantly differ from that of control mice (Fig. 5.11i,j). Collectively, SCs derived from *mpz*-iKO mice efficiently recombine and functionally lose TDP-43, based on the evidence at 2 and 6 mpT. As expected, a phenotypic impact on the animals develops slowly, and only by 12mpT could we detect a partial turnover of recombined SCs in SNs of *mpz*-iKO mice, along with aberrant hindlimb spreading (a symptom of PNS dysfunction) in some of these mutant mice.

The initial assessment described above prompted us to focus our subsequent analysis of nerve morphology at 12mpT, when the phenotype is detectable. The overview electron micrographs depict SNs that appear largely normal in control and *mpz*-iKO mice (Fig. 5.12a). Numbers of myelinated axons were not reduced in *mpz*-iKO SNs, and the myelin sheath thickness was highly comparable to that in control SNs (Fig. 5.12b,c). Inspection of scatter plots with all individual g-ratio measurements plotted against the axonal diameter did not reveal a noteworthy number of thinly myelinated axons in *mpz*-iKO SNs, which would indicate remyelination (Fig. A.4). We previously observed a clear reduction of large caliber axons in one-year-old *mpz*-cKO SNs and wondered whether this could be detected in *mpz*-iKO mice as well. The g-ratio analysis in *mpz*-iKO mice at 12mpT provided a minimum of 1'200 measurements per SN, which we consider as a robust sampling to estimate the axon diameter composition in the analyzed SNs (Fig. 5.12d). The thickest axons (>8 µm in diameter) were only trendwise, marginally reduced in *mpz*-iKO mice compared to controls, suggesting that the function of TDP-43 specifically in adult SCs is not crucial to protect axons from degeneration within the timeframe of analysis. In summary, SNs of *mpz*-iKO mice at 12mpT do not recapitulate the defects seen in *mpz*-cKO mice at one year of age. We reason that there are two possible explanations contributing to these observations: *First*, the lack of TDP-43 during SC development may somehow compromise myelinated fibers, resulting in substantial loss and atrophy of axons much later in life. *Second*, it is possible that the non-recombined SCs in SNs of *mpz*-iKO mice provide enough support to prevent axonal degeneration.

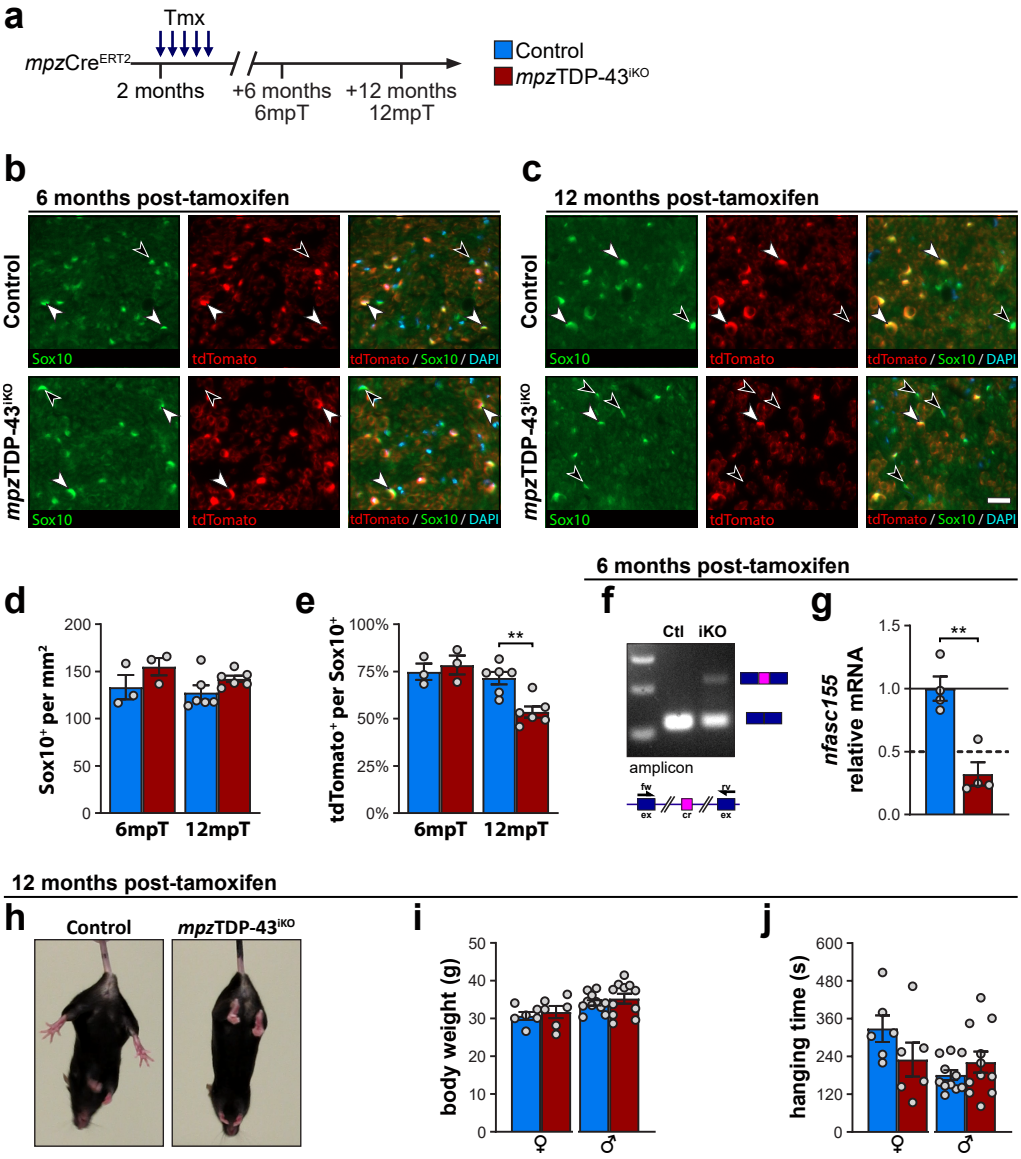

Figure 5.11: Induced deletion of TDP-43 mildly affects motor function and elicits turnover of Schwann cells (a) Schematic representation of the experimental design. Tamoxifen was injected in 8-10 week-old control and *mpz*-iKO mice to induce recombination. For immunofluorescent analysis, transgenic mice additionally harboring the Cre-dependent tdTomato reporter were used to label recombined cells. Mice were analyzed after 6 and 12 months post-tamoxifen (mpT). **(b,c)** Exemplary immunofluorescence images of SNs at 6mpT (b) and 12mpT (c). Sox10 was selected to label all Schwann cells and tdTomato was used as an indicator for their recombined state (white arrowheads). Black arrowheads indicate exemplary tdTomato^{neg} SCs. scalebar: 20 µm. **(d)** Density of Sox10^{pos} Schwann cells in control and *mpz*-iKO sciatic nerve cross sections at 6 and 12mpT reveals no significant changes between genotypes. **(e)** Proportion of tdTomato^{pos} Schwann cells among all Schwann cells quantified in (d) depicts a specific reduction of tdTomato^{pos} SCs in *mpz*-iKO SNs at 12mpT. **(f,g)** Analysis of *nfasc* cryptic splicing in control and *mpz*-iKO mice at 6mpT. **(f)** End-point PCR analysis after amplifying from exons neighboring the cryptic exon reveal the occurrence of cryptic splicing in *mpz*-iKO but not in control mice. **(g)** Expression of *nfasc155* is reduced in *mpz*-iKO sciatic nerves at 6mpT, in line with the detection of cryptic *nfasc* shown in (f). **(h)** Tail-suspension triggered hindlimb spreading in control but not *mpz*-iKO mice at 12mpT, which is indicative of a PNS dysfunction. **(i)** Bodyweight of control and *mpz*-iKO mice at 12mpT, displaying very similar body mass between genotypes. **(j)** Performance of control and *mpz*-iKO mice in inverted grid hanging test at 12mpT. Mice from both genotypes show a similar performance without statistical differences, despite a slight trend for reduced performance in *mpz*-iKO ♀ mice. **(Statistics)** Bar graphs represent mean±SEM; **p<0.01. (d,e) 6mpT n = 3 mice, 12mpT n = 6 mice, two-way ANOVA with Šídák's multiple comparisons test. (g) n = 4 mice, two-tailed, unpaired Student's t-test. (i,j) (♀ n = 6, ♂ n = 11 mice, two-tailed, unpaired Student's t-test.

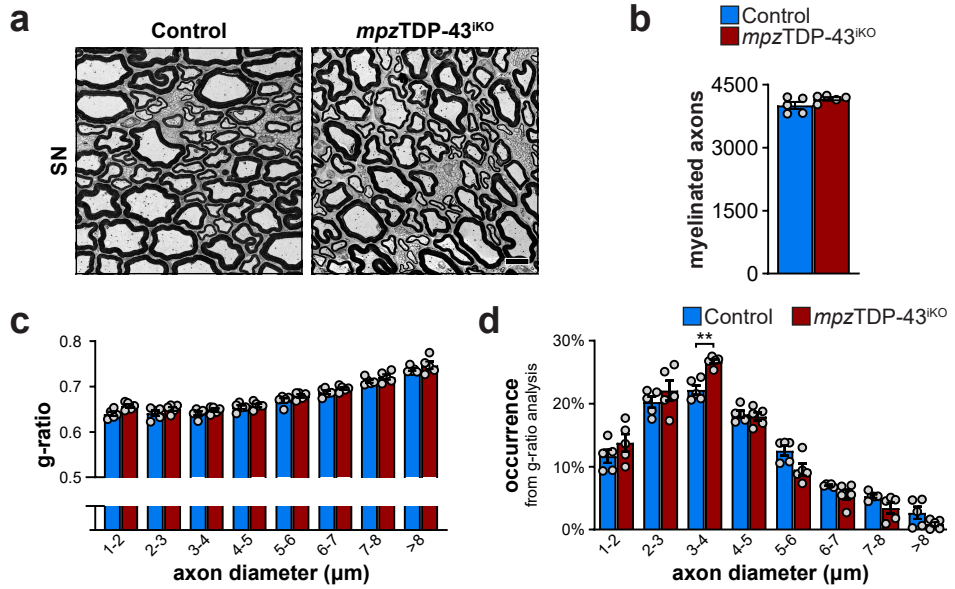

Figure 5.12: ***mpz*-iKO sciatic nerves do not display overt defects at 12 months post-tamoxifen.** SN cross sections of control and *mpz*-iKO mice were analyzed by electron microscopy at 12 months post-tamoxifen (12mpT). **(a)** Exemplary EM micrographs do not display evident differences between genotypes. scalebar: 5 µm. **(b)** Number of myelinated axons per sciatic nerve cross section. **(c)** Quantification of the g-ratio does not indicate significant changes between genotypes. **(d)** Axon diameter distribution of axons quantified in (c) reveals no major shift in the frequency distribution of axonal diameters in *mpz*-iKO SNs compared to controls. **(Statistics)** Bar graphs represent mean±SEM; **p<0.01. (all graphs) n = 5 mice; (b) two-tailed, unpaired Student's t-test, (c,d) two-way ANOVA with Šídák's multiple comparisons test.

Besides SNs, we had also previously analyzed nerve roots in one-year-old *mpz*-cKO and control mice, in an attempt to separately evaluate potential phenotypes related to sensory and motor axons. The motor nerve roots appeared more affected than the sensory roots, but surprisingly both root nerves were histologically more affected than the SNs (Fig. 5.7 & 5.8). In order to evaluate whether nerve roots were also particularly sensitive to TDP-43 deletion in adult SCs, we included these tissues in our EM analysis of *mpz*-iKO and control mice at 12mpT. Qualitative inspection of electron micrographs revealed clear differences between *mpz*-iKO roots and controls (Fig. 5.13a), due to the presence of vacuolated myelin profiles and axons without myelin. Despite containing similar numbers of myelinated and total axons (Fig. 5.13b,c) compared to controls, ventral root nerves from *mpz*-iKO mice appeared the most affected, with widespread presence of fibers harboring vacuolated myelin, and of axons lacking myelin altogether (Fig. 5.13d). Dorsal roots from *mpz*-iKO mice compared to controls also contained fibers with vacuolated myelin, and rarely some nonmyelinated fibers (>1 µm in diameter, Fig. 5.13g). However, these features were much less abundant than in ventral roots of the same mice. Unexpectedly, we detected a small but statistically significant increase in the numbers of myelinated and total axons (>1 µm in diameter) in the dorsal root nerves

of *mpz*-iKO mice compared to controls (Fig. 5.13e,f). We currently have no conclusive explanation for this tantalizing observation in *mpz*-iKO mice, but one possibility is the potential presence of multiple myelinated axonal regenerative sprouts, which are known to occur in nerves of some human patients with peripheral neuropathies (Said et al., 1983; Hattori et al., 2003; Vital et al., 2008). However, we also cannot fully exclude the possibility that technical or experimental factors lead to the observed difference. Taken together, the induced deletion of TDP-43 resulted in vacuolation of myelinated fibers and demyelination in nerve roots, but not to a detectable loss of axons. These findings agree with the interpretation that TDP-43 in adult myelinating SCs is required for myelin stability and maintenance of the myelinated state.

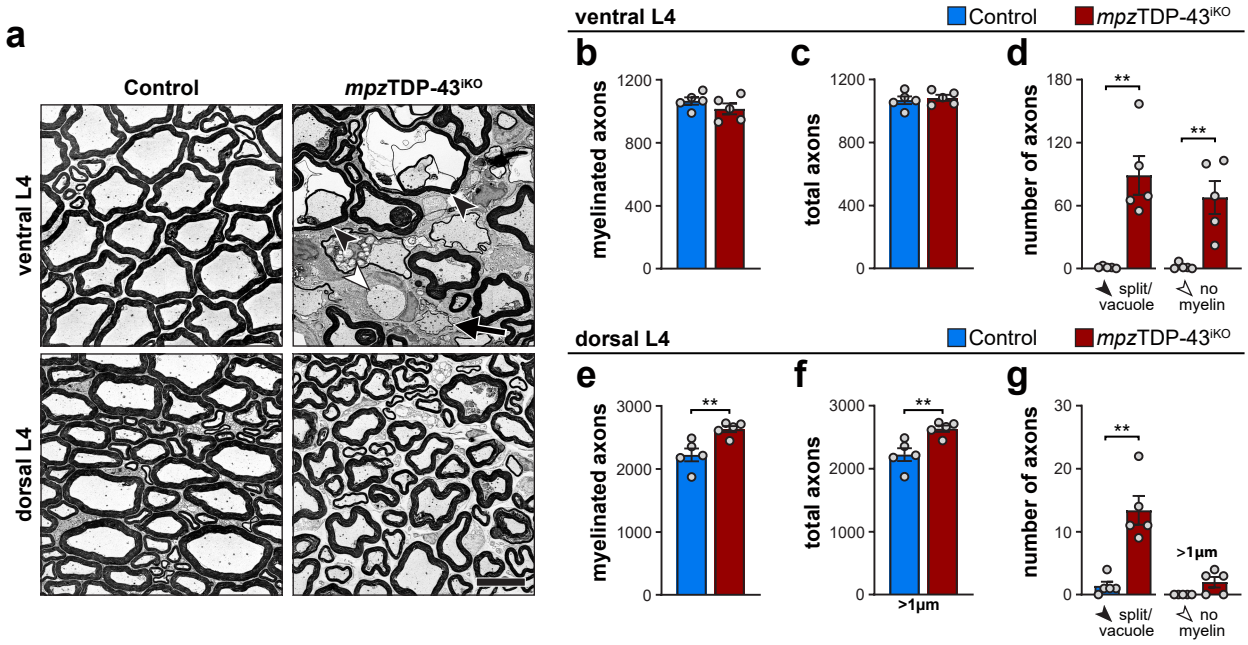

Figure 5.13: ***mpz*-iKO root nerves exhibit vacuolation and demyelination at 12 months post-tamoxifen.** Analysis of cross sections from control and *mpz*-iKO L4 root nerves at 12 month post-tamoxifen (mpT). **(a)** Exemplary electron micrographs of dorsal and ventral root nerves. Ventral *mpz*-iKO root nerves are evidently affected, harboring vacuolated fibers (black arrowheads), non-myelinated axons (white arrowheads) and thinly myelinated axons (black arrow). scalebar: 10 µm. **(b-g)** Quantitative analysis of control and *mpz*-iKO root nerves at 12mpT. Numbers represent the occurrence per cross section. **(b,c)** Numbers of myelinated (b) and total (c) axons in ventral root nerves are not detectably different between genotypes. **(d)** Numbers of myelinated fibers harboring vacuoles and number of non-myelinated axons are both significantly higher in *mpz*-iKO ventral root nerves compared to controls. **(e,f)** Analysis of dorsal root nerves reveals slightly increased numbers of myelinated (e) and total (f) axons in *mpz*-iKO mice compared to controls. **(g)** The number of myelinated fibers with vacuoles are significantly enriched in *mpz*-iKO dorsal roots compared to controls, but the number of axons without myelin only shows a marginal trend towards elevation in the same mutants. **(Statistics)** Bar graphs represent mean±SEM; **p<0.01 (all graphs) n = 5 mice. (b,c,e,f) two-tailed, unpaired Student's t-test. (d,g) Mann Whitney test.

The enrichment in axons without myelin suggests some degree of demyelination in *mpz*-iKO root nerves, and ongoing demyelination could be followed by remyelination, which might be detected through the presence of very thin myelin sheaths. To address this possibility, root nerves have been further analyzed for myelin thickness and distribution of axons diameters. The average myelin thickness was not changed significantly for any range of axon calibers, but the presence of thinly myelinated axons in *mpz*-iKO root nerves was evident in the EM micrographs (Fig. 5.13a). Inspection of all individual measurements in g-ratio versus axonal diameter scatter plots of both ventral and dorsal root nerves revealed that a substantial number of fibers in *mpz*-iKO harbored thinner myelin compared to the respective controls (Fig. 5.14a,b). A cut-off has been defined to incorporate most fibers from control nerves and thereby isolate a group of hypomyelinated axons (lines in Fig. 5.14a,b). An evidently enriched number of fibers from *mpz*-iKO root nerves was thereby classified as hypomyelinated, while only very few axons from control nerves were represented in this category (Fig. 5.14c). If further considering that dorsal roots have more myelinated axons than ventral roots, there are proportionally more hypomyelinated (presumably remyelinated) axons in ventral than dorsal root nerves. The variability was overall high, especially in *mpz*-iKO ventral root nerves, but the very low numbers in controls consolidate the significance of these changes.

Another key finding in *mpz*-cKO nerve roots was a marked reduction in the number of axons with large diameters. Even though axons were not detectably lost in *mpz*-iKO nerve roots, we reasoned that the representation of large diameter axons might be reduced. To test this hypothesis, we analyzed the diameters of all axons per cross section of root nerves, and exemplary color-coded profiles for controls and *mpz*-iKO root nerves are shown (Fig. 5.14d). As previously noted in the quantifications of hypomyelinated axons, the high variability of *mpz*-iKO ventral root nerve was further reflected in the axonal diameter distributions of myelinated fibers (compare the two *mpz*-iKO examples shown in Fig. 5.14d). Nevertheless myelinated fibers with axon diameters larger than 8 µm were greatly diminished (Fig. 5.14e). In contrast, the induced deletion of TDP-43 had no influence on the number of axons with large diameters in dorsal root nerves (Fig. 5.14f). The surplus of myelinated axons in *mpz*-iKO dorsal roots (see Fig. 5.13e) might relate to more axons between 1.5 and 3 µm in diameter, as axons of these diameters were substantially more numerous in *mpz*-iKO mice compared to controls. Similar results were obtained when vacuolated and non-myelinated axons were included in the analysis (Fig. A.5).

Taken together, our data suggests that TDP-43 expressed by SCs in adult nerve roots is required to maintain healthy myelin and prevent demyelination. Furthermore, although no effective reduction of total axon numbers were detected, we speculate that the action of TDP-43 in adult SCs is also required to preserve the proper abundance of motor axons with large diameters.

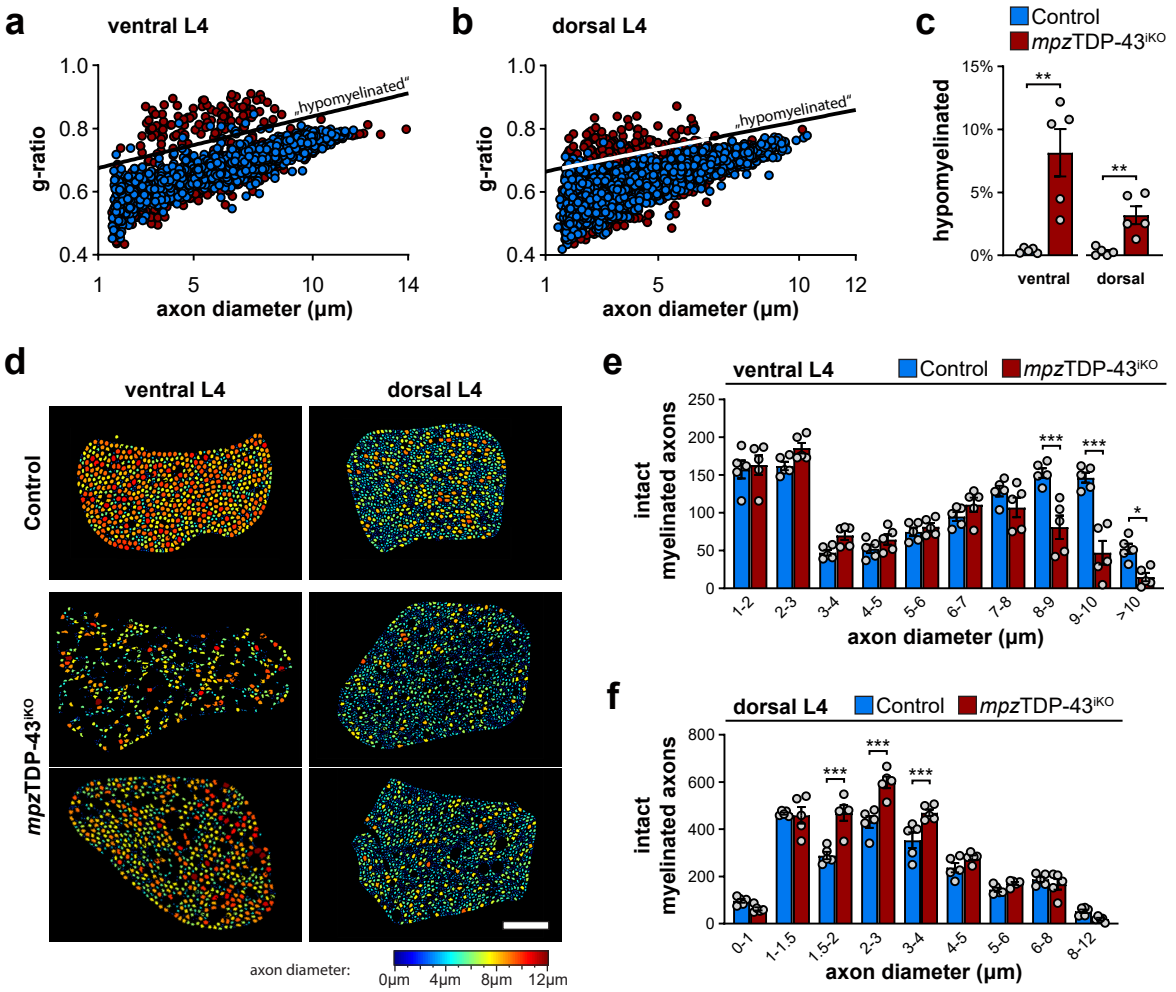

Figure 5.14: Induced deletion of TDP-43 provokes sparse hypomyelination and loss of large caliber axons in the ventral root nerves. Dorsal and ventral L4 root nerves from control and *mpz*-iKO mice were analyzed at 12 mpT. **(a,b)** g-ratio analysis plotted as axons caliber vs g-ratio for ventral (a) and dorsal (b) root nerves. To gate for evidently hypomyelinated axons, a line was plotted at the edge of bulk measurements from control animals. Note that both dorsal and ventral roots are enriched in measurements from *mpz*-iKO mice in the region above this line. **(c)** Percentage of axons from measurements in (a,b) that fall into the hypomyelinated region. **(d)** Exemplary visualizations of axon caliber analysis of control and *mpz*-iKO root nerves. Axons are colored individually according to their caliber (scale at bottom). Two *mpz*-iKO root nerves are shown to represent the variability in their appearance. **(e,f)** Quantification of calibers from all intact, *i.e.* non-vacuolated, myelinated fibers in the ventral (e) and dorsal (f) root nerves. Note that axons with diameter greater than 8 µm are prominently reduced specifically in *mpz*-iKO ventral roots. Axons smaller than 1 µm occur only seldom in ventral roots (e) and are not displayed. **(Statistics)** Bar graphs represent mean±SEM; *p<0.05, **p<0.01, ***p<0.001. (all graphs) n = 5 mice. (c) two-tailed, unpaired Student's t-test. (e,f) two-way ANOVA with Šídák's multiple comparisons test

5.4. Summary of the Function of TDP-43 in SCs

We have studied the function of TDP-43 in SCs by conditional deletion during embryonic development and after developmental myelination. We have shown that TDP-43 is strictly required for the timely onset of myelination in the SN during early postnatal development and potentially influences the correct proportions of the myelin sheath. However, developmental myelination in the SN was largely successful in *mpz*-cKO mice compared to controls. Strikingly, we found that TDP-43 function is crucial for protection of *nfasc155* from cryptic splicing in mice, a function of TDP-43 that is very likely required for proper expression of NF155. In *mpz*-cKO mice, the definition of the paranodal and juxtaparanodal regions was strongly impaired and the mutant nerves displayed striking electrophysiological abnormalities. At 12 and 16 months of age, *mpz*-cKO mice display increasing failure to maintain myelin and protect axons from degeneration, which was most evident in ventral root nerves. Moreover, aged *mpz*-cKO mice displayed impaired motor function and reduced body mass. This long-term phenotype upon loss of TDP-43 in SCs suggests that TDP-43 function during development and/or in adult mice is required to protect PNS integrity in aging animals.

Beyond development, we show that TDP-43 is required for the timely onset of remyelination after sciatic nerve crush injury, even though these defects are transient and eventually recover. To elucidate the function of TDP-43 specifically in adult SCs, we induced recombination in control and *mpz*-iKO mice after developmental myelination largely finished. A phenotypic impact was evident in *mpz*-iKO mice at 12mpT and we observed partial turnover of SCs in SNs of these mutants. In contrast to *mpz*-cKO SNs at one year of age, we did not find evidence for demyelination or shift of the axon diameter distribution in *mpz*-iKO SNs at 12mpT. Further analysis at 12mpT did reveal that TDP-43 is essential to maintain the myelinated state in some axons of the L4 root nerves, based on the occurrence of non-myelinated axons and vacuoles in myelinated axons. Additionally, *mpz*-iKO root nerves displayed myelinated axons with unexpectedly thin myelin compared to controls, suggesting that some axons were remyelinated. Axon diameter analysis revealed that motor axons of large diameters (>8 µm) were significantly reduced in ventral root nerves when compared to controls. Altogether, the analysis of aged *mpz*-iKO mice indicates that TDP-43 in adult SCs is crucial to maintaining myelination, and potentially has a distinct impact on big motor axons.

The broad spectrum of influence that TDP-43 exerts on SC biology should be taken into consideration in order to thoroughly understand TDP-43 function and dysfunction in the nervous system health and disease.

6. TDP-43 in Oligodendrocytes

6.1. Function of TDP-43 in Oligodendrocytes During Development

In the brain of young mice (P7 and P17, cerebral cortex), TDP-43 is expressed in neurons, astrocytes, cells of the oligodendrocyte (OL) lineage, and, to a lesser extent, in endothelial cells and microglia (Zhang et al., 2014). While OL precursor cells (OPCs) display highest TDP-43 levels in the OL lineage according to the study of Zhang et al. (2014), single-cell RNA sequencing data from various CNS tissues at P20-30 and P50-60 revealed a more diffuse pattern of TDP-43 abundance (Marques et al., 2016). From these datasets we assumed that TDP-43 is expressed at all stages of the OL lineage and might be functionally relevant at any stage of OL differentiation and maturation. In order to investigate the function of TDP-43 in the OL lineage, we deleted functional TDP-43 using a Cre-line specific for OLs and SCs (*cnp*Cre) and a flox-line in which exon 3 of the *Tardbp* gene is flanked by loxP sites (TDP-43$^{f/f}$, Fig. 6.1a). Cre positive, TDP-43$^{f/f}$ animals were used as conditional knockout animals (*cnp*TDP-43^{cKO}, hereafter *cnp*-cKO). The CNS is composed of many different cell types, and unlike for SCs in the SN, OLs do not comprise the large majority of cells in the spinal cord (SpC) or brain. Therefore, biochemical analysis on whole SpCs or brain biopsies is not feasible to specifically investigate OLs. To circumvent this issue, we used transgenic mice to mark OLs by fluorescent protein expression, and collected these OLs by fluorescence-activated cell sorting (FACS). In this study, we employed two independent transgenic reporter lines. Cre-dependent tdTomato expression (Madisen et al., 2010) was used to label all recombined cells, and endogenously knocked-in *pdgfrα*H2B-EGFP (histone H2B-EGFP fusion protein, Hamilton et al., 2003) was used to mark all OLs. Collectively, we were able to purify OLs from SpC tissue at P10, while the H2B-EGFP protein was highly stable and still detected in mature OLs. The latter is not unexpected, as EGFP is fused to H2B, and histones are very long-lived proteins (Toyama et al., 2013). Fractions enriched in OPCs or in differentiated OLs could be collected in a reproducible manner by additionally separating small and large cells during sorting (Fig. A.6).

Unexpectedly, we identified a minor tdTomato^{pos}EGFP^{neg} population that did not display expression of typical OL lineage genes, suggesting a small contamination of other cell types among tdTomato^{pos} cells (Fig. A.6a). To generate offspring of the desired genotpyes with a reasonable efficiency, we only used the tdTomato reporter line and accepted this bias when cells were collected for protein analysis, cell cultures, or single-cell RNA sequencing. To assess the reduction of TDP-43 in *cnp*-cKO mice, we collected OLs from P10 SpCs applying the aforementioned sorting strategy (Fig. A.6a). αTubulin and histone H3 were both analyzed to roughly compare cytoskeletal and nuclear proteins between OPCs and differentiated OLs. Differentiated OLs were in the large cell fraction judged by the cytometer forward scatter. In line with this, they displayed a qualitatively high content of αTubulin (Fig. 6.1b). In the quantifications, we used αTubulin for normalization. TDP-43 itself was detected in OPCs and differentiated OLs from control mice and was strongly reduced in differentiated OLs from *cnp*-cKO mice compared to controls (Fig. 6.1b,c). In contrast, TDP-43 was only trendwise reduced in *cnp*-cKO OPCs compared to controls. The reduction of TDP-43 was further qualitatively assessed by immunofluorescent analysis in SpCs of *cnp*-cKO and control animals at P10 (Fig. 6.1d). Motor neurons (ChAT^{pos}) and OLs (Olig2^{pos}) were both positive for TDP-43 in control SpCs. While strong TDP-43 positive signals were retained in motor neurons of *cnp*-cKO SpCs, TDP-43 signals in OLs were close to background and only few cells still displayed a weak positive signal. *cnp*-cKO mice were born at mendelian ratios and were not distinguishable from their control littermates in the first weeks of their life. However, they started to shiver after 30-35 days, which was gradually exacerbated over time. Due to animal welfare considerations, the last time-point of analysis was between 50 and 60 days of age (further referred to as P50 throughout the thesis). Altogether, our data reveal that TDP-43 is efficiently reduced in differentiated OLs of *cnp*-cKO mice compared to controls. Our results further suggest that only a fraction of *cnp*-cKO OPCs is recombined, or that the turnover of TDP-43 in OPCs is very slow. Moreover, *cnp*-cKO mice develop pathological symptoms visible at one month of age, which progressively deteriorate over time, indicating a crucial function of TDP-43 in OLs.

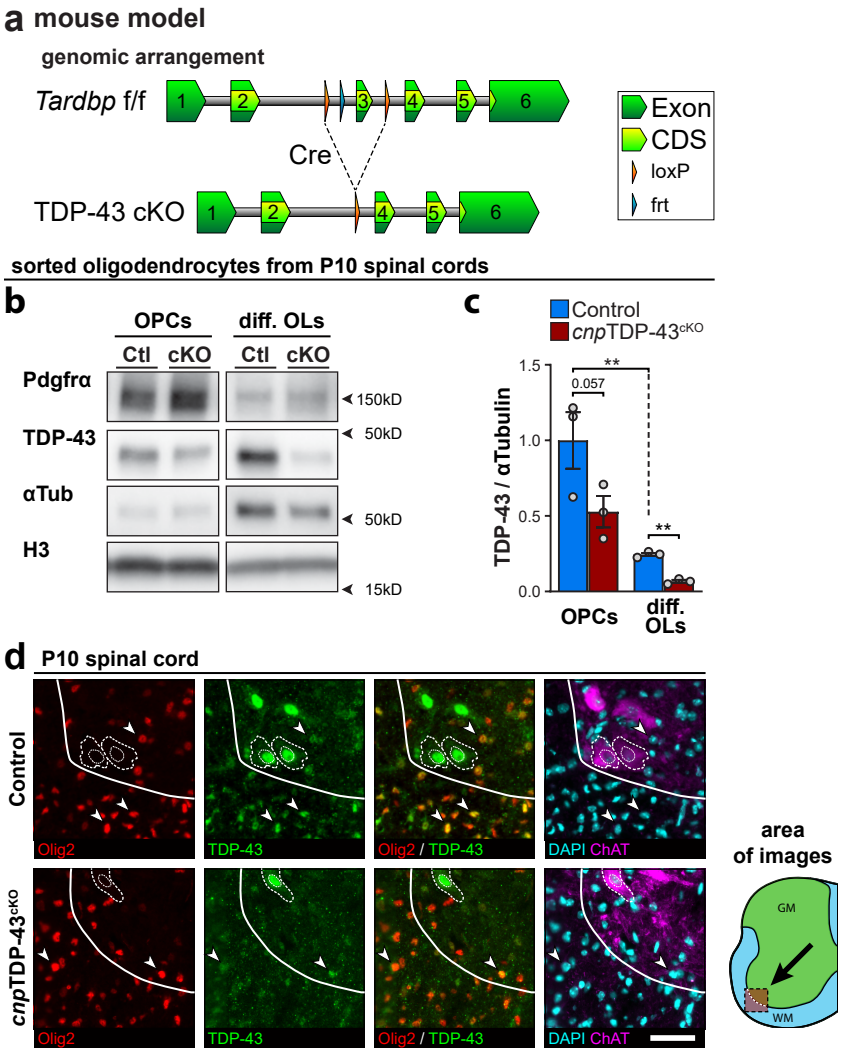

Figure 6.1: Levels of TDP-43 in control and *cnp*-cKO mice. (a) Genetic model. Exon 3 of the *tardbp* gene is floxed and excised upon Cre-mediated recombination. **(b)** Western blot protein analysis of sorted OLs from P10 SpCs split by size. Detection of PDGFRα illustrates the efficient separation between OPCs and differentiated OLs. αTubulin was used for normalization. Comparison of αTubulin with H3 demonstrates the remarkable cellular changes during differentiation, as equal amounts of total protein (3 µg based on µBCA quantification) were loaded in each lane. TDP-43 is detected in OPCs and differentiated OLs, and reduced in *cnp*-cKO mice by qualitative assessment. **(c)** Quantification of TDP-43 in (b) reveals efficient reduction of TDP-43 in differentiated *cnp*-cKO OLs compared to controls (n = 3 mice, mean±SEM, **p<0.01, two-way ANOVA with Tukey's multiple comparisons test). **(d)** Representative immunofluorescent stainings of P10 SpCs. Olig2 (red) marks all cells of the OL lineage (white arrowheads), ChAT (purple) was used to label motor neurons. By qualitative assessment of 3 animals per genotype, TDP-43 (green) is efficiently reduced in most *cnp*-cKO OLs compared to controls. Dashed shapes indicate the soma and nucleus of TDP-43 positive neurons. scalebar: 50 µm.

TDP-43 Is Essential for Developmental Myelination in the Spinal Cord

TDP-43 might be required at any stage in the OL lineage, which would then be translated to the symptomatic defects observed in *cnp*-cKO mice after one month of age. To evaluate the progress and correctness of CNS myelination upon deletion of TDP-43, SpCs from *cnp*-cKO and control mice have been examined at different time-points from P10 to P50, spanning the time from ongoing initiation of myelination to the endpoint of our analysis, when myelination is expected to be largely finished in SpCs. Western blot analysis of MBP, a major myelin protein, revealed less abundance in *cnp*-cKO SpCs than in controls at both P10 and P50, indicating myelination of the whole tissue was reduced (Fig. 6.2a,b). The tissue morphology of lumbar SpCs was studied using electron microscopy of the medial ventral white matter (WM, Fig. 6.2c,d). Myelination was evidently affected in *cnp*-cKO mice at all time-points investigated when compared to controls. Evaluation of the number of myelinated axons per area revealed a clear reduction in *cnp*-cKO SpCs at P10 and P50 when compared to controls (Fig. 6.2e). In contrast, myelinated axon numbers per area were comparable between control and *cnp*-cKO mice at P21 and P30. To further assess the degree of myelination, we also counted non-myelinated axons that are actually large enough to be myelinated (>0.5 µm in diameter, Matthews and Duncan, 1971). Non-myelinated axons larger than 0.5 µm in diameter were significantly enriched in SpCs of *cnp*-cKO mice compared to controls at all time-points except P21 (Fig. 6.2f). The significant elevation of nonmyelinated axons per area at P30, without detectable changes in the density of myelinated axons, might be derived from a generally higher density of all axons (>0.5 µm in diameter), which is only significantly higher at this time-point in *cnp*-cKO mice compared to controls (Fig. A.7a). A higher density of axons would equally elevate the number of myelinated and non-myelinated axons per area in P30 *cnp*-cKO, therefore masking a potential reduction of myelinated axons per area and likewise increasing the number of non-myelinated axons per area. Considering the proportion of myelinated axons per all axons (>0.5 µm in diameter), all timepoints expect P21 reveal a significant reduction in *cnp*-cKO SpCs compared to controls (Fig. A.7b), indicating an initial delay in the onset of myelination on individual internodes and demyelination at P30 and P50. Qualitative appraisal of EM micrographs also suggested generally thinner myelin in *cnp*-cKO compared to controls. To formally evaluate the relation of myelin thickness and axon diameter, the g-ratio was quantified at P30 and P50, confirming a substantial reduction of the average myelin sheath thickness (higher g-ratio) in *cnp*-cKO compared to control SpCs (Fig. 6.2g).

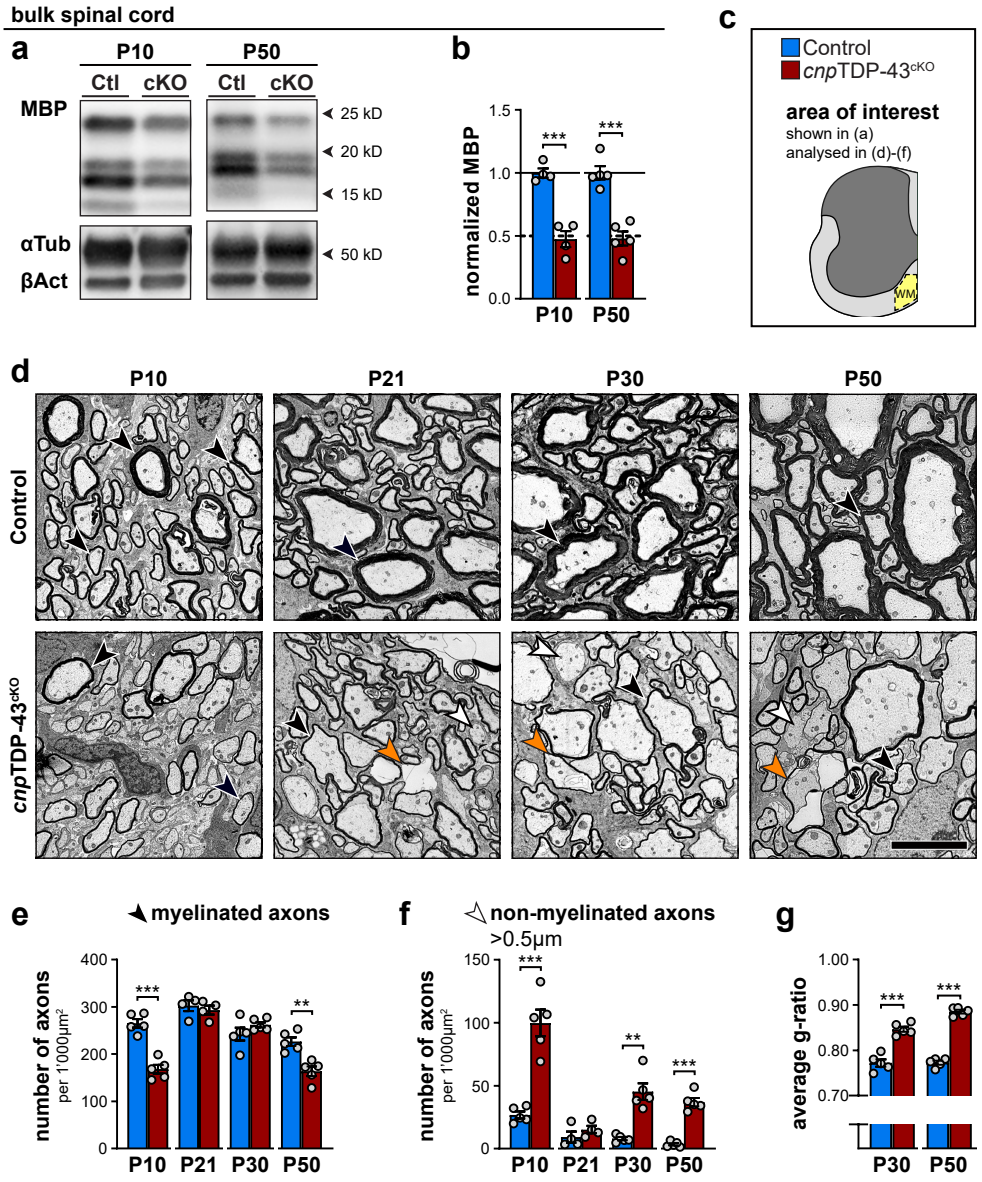

Figure 6.2: Myelination is impaired in *cnp*-cKO spinal cords. Control and *cnp*-cKO SpCs were analysed at various time-points between P10 and P50. **(a)** Western blot protein analysis in bulk SpC lysates at P10/P50 reveal decreased MBP in *cnp*-cKO mice compared to controls. **(b)** Quantification of MBP shown in (b) using αTubulin for normalization. **(c)** Illustration of the region analysed by EM. **(d)** Representative EM micrographs showing the lumbar ventral funiculus in control and *cnp*-cKO mice (see scheme). Myelinated axons (black arrowheads) appear to have thinner myelin at all time-points and more non-myelinated axons (>0.5 µm in diameter, white arrowheads) are observed in *cnp*-cKO SpCs at P30/P50 when compared to controls. Note the occurrence of vacuoles (orange arrowheads) in *cnp*-cKO SpCs at P30/P50. scalebar: 5 µm. **(e,f)** Occurrence of myelinated (e) and non-myelinated axons (>0.5 µm, f) axons per area in the ventral funiculus reveals a delayed onset of myelination and signs of demyelination in *cnp*-cKO mice compared to controls. **(g)** Analysis of myelin thickness quantified as g-ratio shows thinner myelin of axons in the ventral funiculus of *cnp*-cKO SpCs compared to controls. **(Statistics)** Bar graphs represent mean±SEM; **p<0.01, ***p<0.001. (b) P10 n = 4 mice, P50 n = 5 mice; multiple two-tailed, unpaired Student's t-tests corrected using the Holm-Šídák method, (e-g) P21 n = 4 mice, P10,30,50 n = 5 mice; multiple two-tailed, unpaired Student's t-tests corrected using the Holm-Šídák method.

In summary, TDP-43 appears to be essential in OLs for various aspects of CNS myelination. Our data suggests that TDP-43 is required for a timely onset of myelination of individual internodes, which is resolved in *cnp*-cKO SpCs at P21. In addition, myelin sheaths appeared thinner in *cnp*-cKO SpCs compared to controls, which was quantitatively confirmed at P30 and P50, indication that TDP-43 is essential for myelin growth. Furthermore, the reappearance of non-myelinated axons larger than 0.5 µm in diameter at P30 and P50 indicates that TDP-43 is crucial to prevent demyelination in later stages during CNS development.

Loss of TDP-43 Leads to Impaired Tissue Integrity

Apart from the changes in myelination in *cnp*-cKO mice, we also observed vacuoles in *cnp*-cKO animals at P30 and P50 (Fig. 6.2d, orange arrowheads). Hence, we next investigated the prevalence of vacuoles and microgliosis as indicators of disturbed tissue integrity. Vacuoles in myelinated fibers were virtually absent in *cnp*-cKO mice at P10 and started to appear from P21 onwards (Fig. 6.3a,b). Compared to controls, *cnp*-cKO mice displayed a mild enrichment of vacuoles at P21 and P30, of which some were observed between the myelin ring and the axon (see magnified inserts from Fig. 6.3a). In P50 *cnp*-cKO SpCs, vacuoles became more widespread compared to controls, and appeared larger than at earlier timepoints. To investigate whether microgliosis is concomitant with strong vacuolation in *cnp*-cKO SpCs, we analysed Iba1 as marker for microglia. Immunofluorescent staining of Iba1 revealed a pronounced migrogliosis in *cnp*-cKO mice at P50 when compared to controls (Fig. 6.3c,d). Both the white and the grey matter of *cnp*-cKO SpCs were populated by many strongly Iba^{pos} microglia, which were more numerous in the WM. In summary, *cnp*-cKO SpCs display vacuoles along with pronounced microgliosis at P50 when compared to controls. Beyond the impaired onset of myelination and myelin thickening, and defective myelin preservation in *cnp*-cKO mice, these results further highlight the instability of the axon-myelin unit due to the lack of TDP-43 in OLs, altogether emphasizing that TDP-43 is essential for OL biology with strong ramifications for CNS tissue homeostasis.

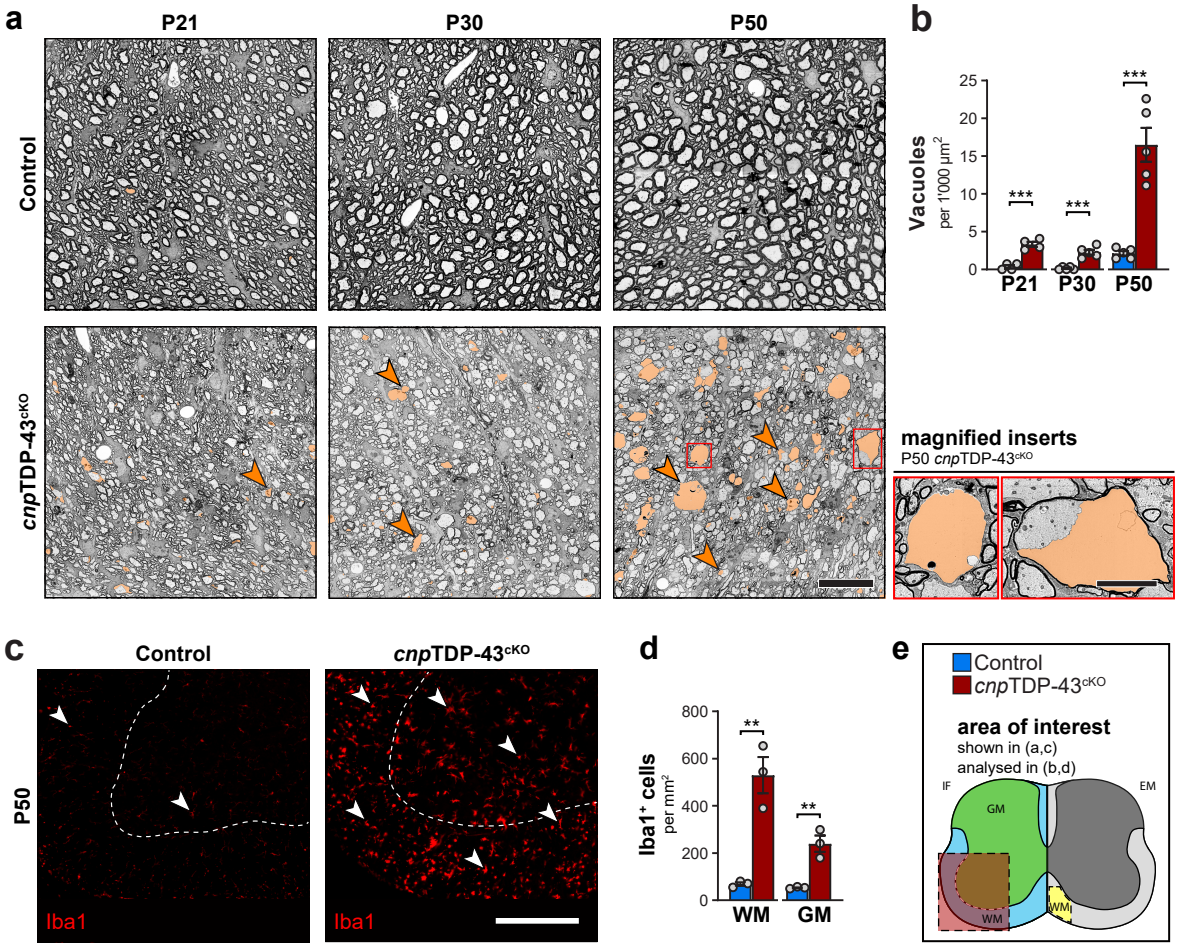

Figure 6.3: ***cnp*-cKO mice display highly vacuolated SpC WM and develop a pronounced microgliosis.** **(a)** Exemplary EM micrographs at low magnification reveal the enriched presence of vacuoles (orange arrowheads, false-colored area) in the WM of *cnp*-cKO SpCs between P21 and P50 when compared to controls. Magnified inserts show exemplary large vacuoles in more detail. scalebar: 20 µm, enlarged examples 5 µm. **(b)** Quantification of vacuoles in the medial ventral WM (see schematic) shows elevated numbers of vacuoles in *cnp*-cKO mice when compared to controls, which is strongly exacerbated in *cnp*-cKO mice at P50. **(c)** Representative immunofluorescence stainings of Iba1^{pos} to mark microglia (white arrowheads) in P50 SpC sections. Note the high signal intensity in *cnp*-cKO mice compared to controls, indicative of microglia activation. scalebar: 250 µm. **(d)** Quantification of Iba1^{pos} cells at P50 reveals a significant enrichment in SpCs of *cnp*-cKO mice compared to controls. Whole spinal cord hemisections were quantified for the white and the grey matter separately (see schematic). **(e)** Illustration of the region analysed by EM and immunofluorescence, including the region shown in (c) is indicated (red square). **(Statistics)** Bar graphs represent mean±SEM; **p<0.01, ***p<0.001. (b) P21 n = 4 mice, P30/50 n = 5 mice; multiple two-tailed, unpaired Student's t-tests corrected using the Holm-Šídák method. (d) n = 3 mice, two-tailed, unpaired Student's t-test.

TDP-43 Is Also Required in Brain Development

So far, we have reported a strong defect in SpCs of *cnp*-cKO mice during development, compatible with a key importance of TDP-43 in OLs in the SpC. Oligodendrogenesis differs between the SpC and the brain. The microenvironment is known to influence OL biology (Vigano et al., 2013), and mature OLs display heterogenous gene expression profiles that are enriched in specific brain regions (Marques et al., 2016). Therefore it was unclear whether OLs in other regions of the CNS also depend on TDP-43. To address this question, we examined the corpus callosum (CC), the cortical grey matter (GM) and the cerebellum (CB) of *cnp*-cKO and control mice at P50 (Fig. 6.4a). A cortical GM region overlaying the CC, including part of the lower layers of the somatosensory and posterior parietal association areas, was included in the analysis. The CC robustly displayed fewer myelinated axons in *cnp*-cKO mice compared to controls (Fig. 6.4a,b). Compared to other regions in the CNS, axons in the CC are considerably smaller relative to the SpC ventral WM, and myelin sheaths are proportionally thinner already in control mice. Therefore, we could not detect a major difference in the myelin sheath thickness between genotypes by qualitative observation. In contrast, vacuoles were evidently enriched in corpora callosa from *cnp*-cKO mice compared to controls, although to a lesser and more variable extent than in the *cnp*-cKO SpCs at P50 (Fig. 6.4a,c). As expected, only very few axons were myelinated in the cortical GM of all animals (Fig. 6.4a). Despite the already few myelinated axons in the cortical GM of control mice, we could still detect a significant reduction in the numbers of myelinated axons in *cnp*-cKO mice (Fig. 6.4a,d). In contrast to the SpC and CC, we could not detect evident signs of vacuolation in the cortical GM of *cnp*-cKO mice. The CB was included in the analysis as a second WM area of the brain. By qualitative inspection, fewer axons appeared to be myelinated, myelin sheaths appeared obviously thinner, and vacuoles were sparsely observed in *cnp*-cKO mice compared to controls (Fig. 6.4a, not quantified). Taken together, the analysed brain regions, which include white and grey matter, were less myelinated in *cnp*-cKO mice compared to controls at P50. Moreover, vacuolation was evident in the *cnp*-cKO CC. These observations are consistent with our analysis of the SpC, suggesting that TDP-43 function is in principle required for OLs resident in different regions of the CNS. However, brain regions of *cnp*-cKO mice at P50 displayed vacuoles to a lesser extent than than in the SpC WM, indicating region-specific differences.

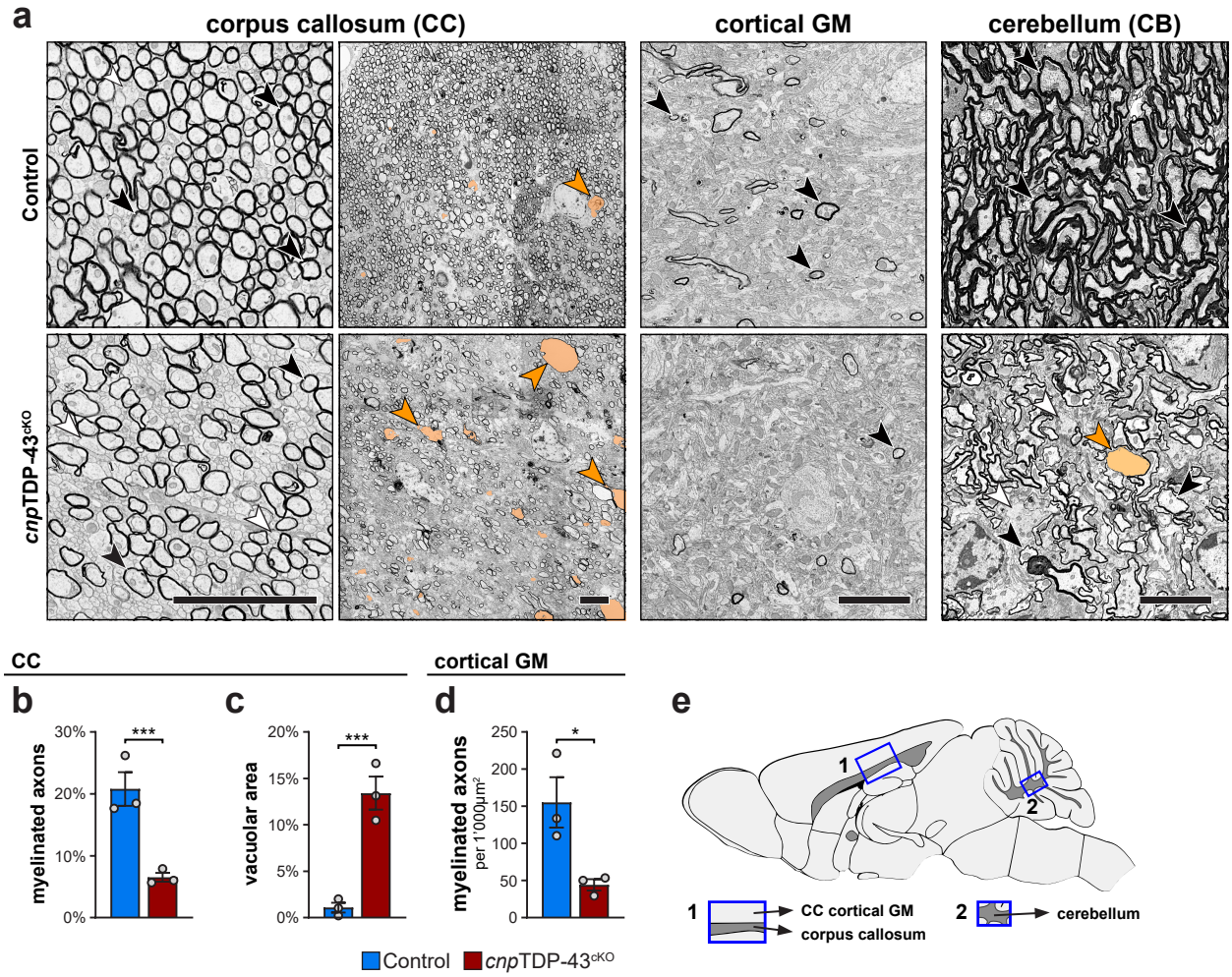

Figure 6.4: Brain areas in *cnp*-cKO mice at P50 display reduced myelination and vacuoles. The corpus callosum (CC), cortical GM and cerebellum (CB) were analysed in control and *cnp*-cKO mice at P50. **(a)** Representative EM micrographs of different brain regions revealed fewer myelinated axons (black arrowhead), more non-myelinated axons (white arrowheads), and vacuolation (orange arrowheads) in *cnp*-cKO mice compared to controls. scalebar: 5 µm. **(b)** Percentage of myelinated axons in the CC showing proportionally fewer myelinated axons in *cnp*-cKO mice compared to controls. **(c)** Relative area covered by vacuoles in the CC was elevated in *cnp*-cKO mice compared to controls. **(d)** Myelinated axons per area in the cortical GM are significantly reduced in *cnp*-cKO mice compared to controls. **(e)** Scheme of analysed brain regions, modified from the GENSAT project. The analysed cortical GM is part of the somatosensory and posterior parietal cortex. **(Statistics)** Bar graphs represent mean±SEM; *p<0.05, **p<0.01. (b-d) n = 3 mice, two-tailed, unpaired Student's t-test.

Differentiated OLs Are Differentially Impacted by Loss of TDP-43 in the SpC WM and GM

Our analysis so far established that TDP-43 is essential in OLs to allow normal CNS development. Even though myelination is clearly impaired in *cnp*-cKO mice, it remained unclear which stage(s) particularly depend on TDP-43 during OL development. It is possible that TDP-43 is essential in OPCs, for example for their proliferation or potential to differentiate. It is also conceivable that differentiated OLs are greatly impaired in a process during maturation, or myelination itself, in the absence of TDP-43. Moreover, TDP-43 may also be essential for survival at any stage of OL development. To experimentally evaluate these possibilities, we quantified the numbers of OLs at different differentiation stages in control and *cnp*-cKO SpCs.

First, we assessed the occurrence and proliferative state of OPCs at P10 using immunofluorescent stainings (Fig. 6.5a,b). Olig2 was used a general OL lineage marker and OPCs were identified by Pdgfrα. OPC numbers were not statistically different in the white or the gray matter from *cnp*-cKO mice compared to controls at P10 (Fig. 6.5a',b'). Mice were injected with EdU one hour before euthanasia, to label cells going through S-phase in that period. The proportion of EdU^{pos} cells among OPCs was comparable between genotypes in the white and the grey matter (Fig. 6.5a'',b'').

$Pdgfr\alpha^{neg}$ OLs were considered to be differentiated, and we used CC1 antibodies at P10 and P50 to analyse these cells. It is of note that OLs during early stages of maturation – a separate process following differentiation – , also known as intermediate or pre-myelinating OLs, are not yet positive for CC1. Numbers of $CC1^{pos}$ differentiated OLs were not significantly different in the WM of *cnp*-cKO SpCs at P10 when compared to controls (Fig. 6.6a,e). Unexpectedly, $CC1^{pos}$ differentiated OLs were much more numerous in the P50 WM of *cnp*-cKO SpCs compared to controls (Fig. 6.6b,f). In contrast, numbers of $CC1^{pos}$ differentiated OLs in the GM were already reduced at P10 in *cnp*-cKO SpCs compared to controls (Fig. 6.6c,g), and this change was still detectable with greater consistency by 50 days of age (Fig. 6.6d,h). Total OL numbers, based on Olig2 positivity, followed a very similar pattern as seen in the $CC1^{pos}$ differentiated OLs in the white and grey matter of *cnp*-cKO SpCs compared to controls (Fig. A.8a-d). We hypothesized that the reduction of $CC1^{pos}$ differentiated OLs in the *cnp*-cKO SpC GM is likely due to cell death, and set out to evaluate apoptosis of OLs in *cnp*-cKO and control mice. However, our attempts with immunostaining for cleaved caspase 3 and with TUNEL assays detected only a minor number of apoptotic OLs in both genotypes at both P10 or P50 (data not shown).

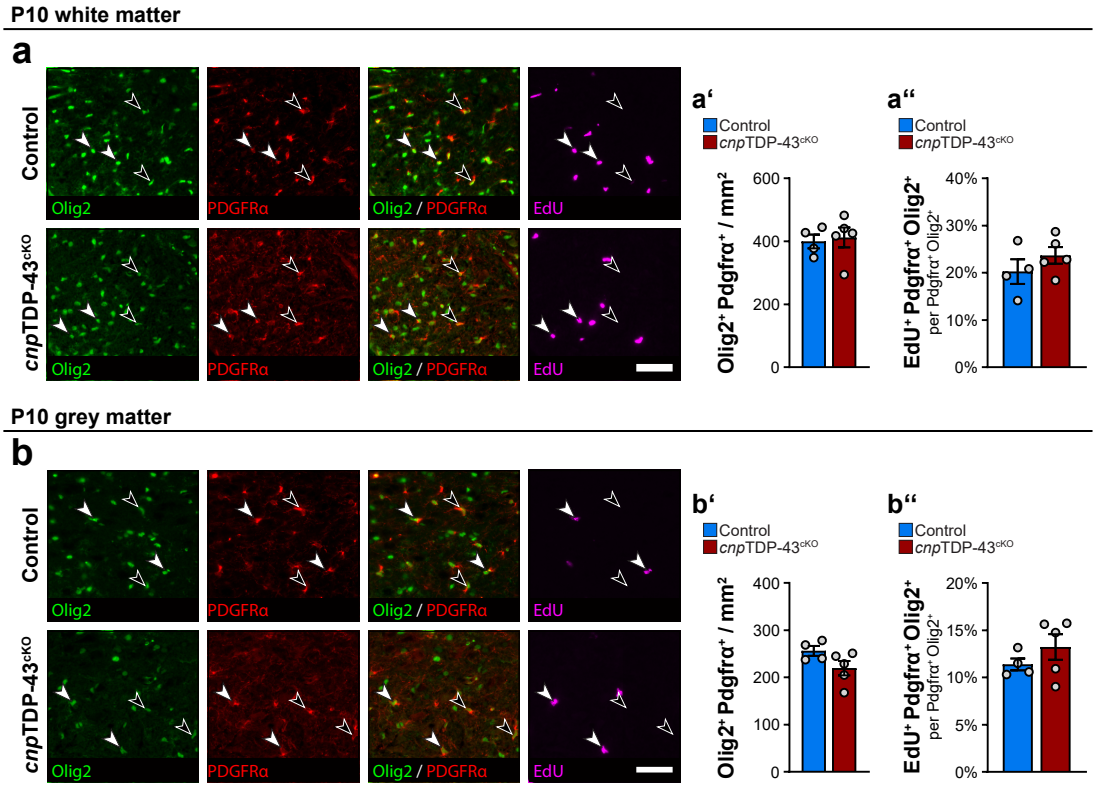

Figure 6.5: OPCs numbers and proliferation are not significantly affected in *cnp*-cKO SpC at P10. **(a,b)** Immunofluorescence stainings with EdU labelling (injected 1h before euthanasia) of SpC cross sections from control and *cnp*-cKO mice at P10. Olig2 was selected to label all OLs. Pdgfrα was selected to label OPCs and EdU was used to identify proliferating cells. scalebar: 50 µm. **(a)** SpC WM. Representative images are shown from the lateral ventral WM. Graphs display the density of OPCs (a') and the percentage of proliferating, EdU^{pos} OPCs (a''). **(b)** SpC GM. Representative images are shown from the ventral horn (see schematic Fig. A.8e). Graphs display the density of OPCs (b') and the percentage of proliferating, EdU^{pos} OPCs (b''). **(Statistics)** Bar graphs represent mean±SEM. (all graphs) n = 4 control and 5 *cnp*-cKO mice, two-tailed, unpaired Student's t-test.

Collectively, our observations disclose a complex picture in which OLs located in the SpC white and grey matter respond differently to the loss of TDP-43. The comparable numbers of $CC1^{pos}$ differentiated OLs in the P10 WM and their increased number at P50 are not able to achieve adequate tissue myelination, which suggests that TDP-43 might regulate maturation of these cells. Conversely, the reduction of $CC1^{pos}$ differentiated OLs in the GM suggests a potential implication in cell death. These results indicate that TDP-43 is required in different, possibly region-specific aspects of differentiated OL biology. Although OPC numbers and proliferation were comparable between genotypes, we cannot rule out an essential function of TDP-43 in OPCs, as the exact time of recombination and loss of TDP-43 protein is unknown and our previous experiments indicated only partial reduction of TDP-43 protein levels.

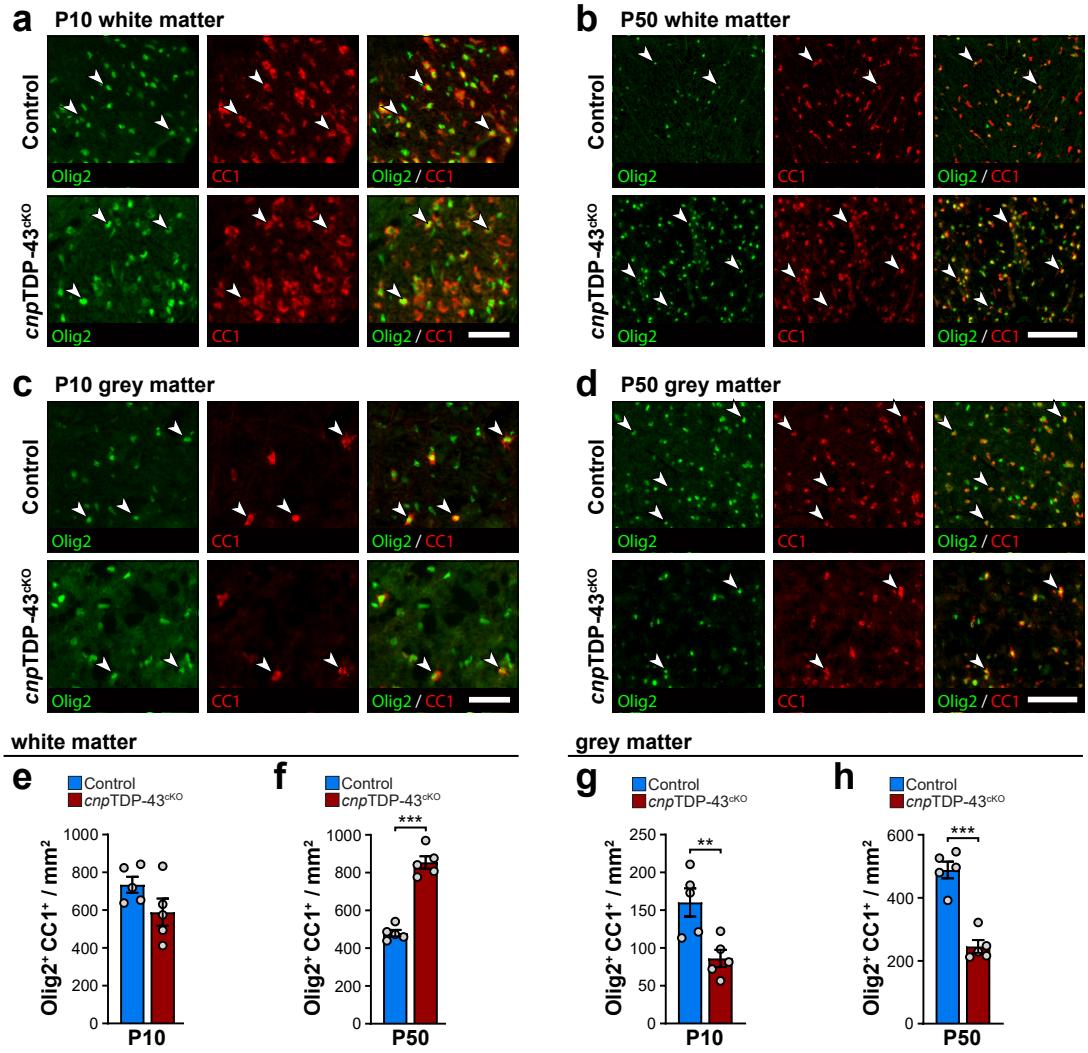

Figure 6.6: Differentiated OLs are divergently affected in white and grey matter of SpCs from *cnp*-cKO. SpC cross sections from control and *cnp*-cKO mice were analysed by immunofluorescence at P10 and P50. Olig2 (green) was selected to label all OLs and CC1 (red) was used as an indicator of their differentiated state. **(a-d)** Exemplary immunofluorescence images of SpC cross sections. Areas shown are the ventral funiculus (a,b) and the ventral horn (c,d), respectively (see schematic Fig. A.8e). SpCs were analyzed in the WM at P10 (a) and P50 (b), and likewise in the GM at P10 (c) and P50 (d). scalebar: (a,c) 50 µm, (b,d) 100 µm. **(e,f)** Density of differentiated OLs in the SpC WM at P10 (e) and P50 (f) reveals strongly elevated numbers of differentiated OLs in P50 *cnp*-cKO mice compared to controls. **(g,h)** Density of differentiated OLs in the SpC GM at P10 (g) and P50 (h) reveals a reduction of differentiated OLs in *cnp*-cKO mice at both timepoints when compared to controls. **(Statistics)** Bar graphs represent mean±SEM; **p<0.01, ***p<0.001. (e-h) n = 5 mice, two-tailed, unpaired Student's t-test.

6.2. Transcriptomic Changes in *cnp*TDP-43^{cKO} OLs

Differentiated *cnp*-cKO OLs Display Loss of TDP-43 Function and a Shift to an Earlier State of Maturation

TDP-43 is a known RNA binding protein involved in splicing (Buratti and Baralle, 2001; Buratti et al., 2001; Polymenidou et al., 2011), which suggests that the main primary effects of its deletion can be observed in the transcriptome. To evaluate the transcriptomic impact upon loss of TDP-43, we performed RNA sequencing from sorted control and *cnp*-cKO OLs. We selected age P10 for the analysis, as we expect to have a minimum of downstream changes compared to later timepoints. We aimed to minimize potential contamination of the OL lineage with other cell types. Therefore, OL cells have been marked by *cnp*Cre-dependent expression of tdTomato and EGFP expression from the endogenous *Pdgfrα* locus (Lappe-Siefke et al., 2003; Madisen et al., 2010; Hamilton et al., 2003; Fig. 6.7a). EGFP is expressed as an H2B-EGFP fusion protein and is apparently highly stable, remaining its signal even when OLs are already differentiated. This orthogonal reporter approach allowed us to sort very pure populations of tdTomato and EGFP double-positive OLs. As in the previous sorting experiments, small and large OLs have been collected separately to enrich for OPCs and differentiated OLs (Fig. 6.7b, Fig. A.6).

First, we assessed the reduction of TDP-43 as whole transcript and exon 3 mRNA, which is excised upon recombination. We observed a clear reduction of both total TDP-43 and exon 3 mRNA in OPCs and differentiated OLs from *cnp*-cKO mice compared to controls, although exon 3 reduction did not reach significance in OPCs (Fig. 6.7c,d). These results are largely in line with the previously performed protein analysis from sorted OLs (Fig. 6.1b,c). As the function of TDP-43 involves the repression of cryptic splicing events (Ling et al., 2015, Fig. 6.7e), we also encountered marked cryptic retention of intronic sequence of various genes in differentiated OLs (Fig. 6.7f). To bolster the assumption that these events are a primary change due to the loss of TDP-43, we re-analyzed TDP-43 UV-CLIP data from 8-week-old mouse brains (Polymenidou et al., 2011). We found strong coverage of TDP-43 binding in close proximity to cryptic exons in many identified cryptic splicing events (Fig. 6.7f). The presence of evident cryptic splicing events in differentiated OLs is coherent with a clear loss of TDP-43 function.

We also detected these cryptic splicing events in OPCs, although retention of cryptic exons was usually to a lesser extent. Considering the partial reduction of TDP-43 mRNA in OPCs, which is consistent with our previous analysis of TDP-43 protein, we consider that TDP-43 function is only abolished in a fraction of OPCs or that some cells collected in the OPC-enriched fractions had already differentiated beyond the OPC stage.

In order to get an overview of the differentiation state of OLs at the mRNA level, marker genes covering all the key lineage progression states have been analyzed (Fig. 6.7g). OPC samples displayed high expression levels for OPC markers and some early differentiation-committed OL precursor (COP) genes, and the levels were not markedly changed in *cnp*-cKO samples compared to controls. Differentiated OL samples displayed high expression of markers of mature and newly formed OLs. This further indicates that, also as judged by the transcript levels, cell size is a robust criterion to distinguish OPCs from differentiated OLs by FACS. Differentiated OLs from *cnp*-cKO animals were similar to differentiated control OLs. However, a lower abundance of mature OL markers and higher levels for markers of newly formed OLs were observed. In addition, myelin genes as well as genes involved in lipid and cholesterol synthesis were markedly less expressed in differentiated *cnp*-cKO OL samples when compared to controls (Fig. 6.7h). Taken together, our transcriptomic analysis reveals a strong reduction of non-recombined TDP-43 mRNA in differentiated OLs, and a less pronounced, non-significant reduction in OPCs. This reduction resulted in cryptic splicing of various genes in intronic regions where TDP-43 is able to interact with the transcript, confirming that TDP-43 guards against cryptic splicing in OLs. As a consequence of TDP-43 deletion, differentiated *cnp*-cKO OLs acquire a less mature transcript signature and display reduced levels of genes associated with myelin proteins and lipid biosynthesis compared to controls, consistent with a key role of TDP-43 in promoting maturation of differentiated OLs.

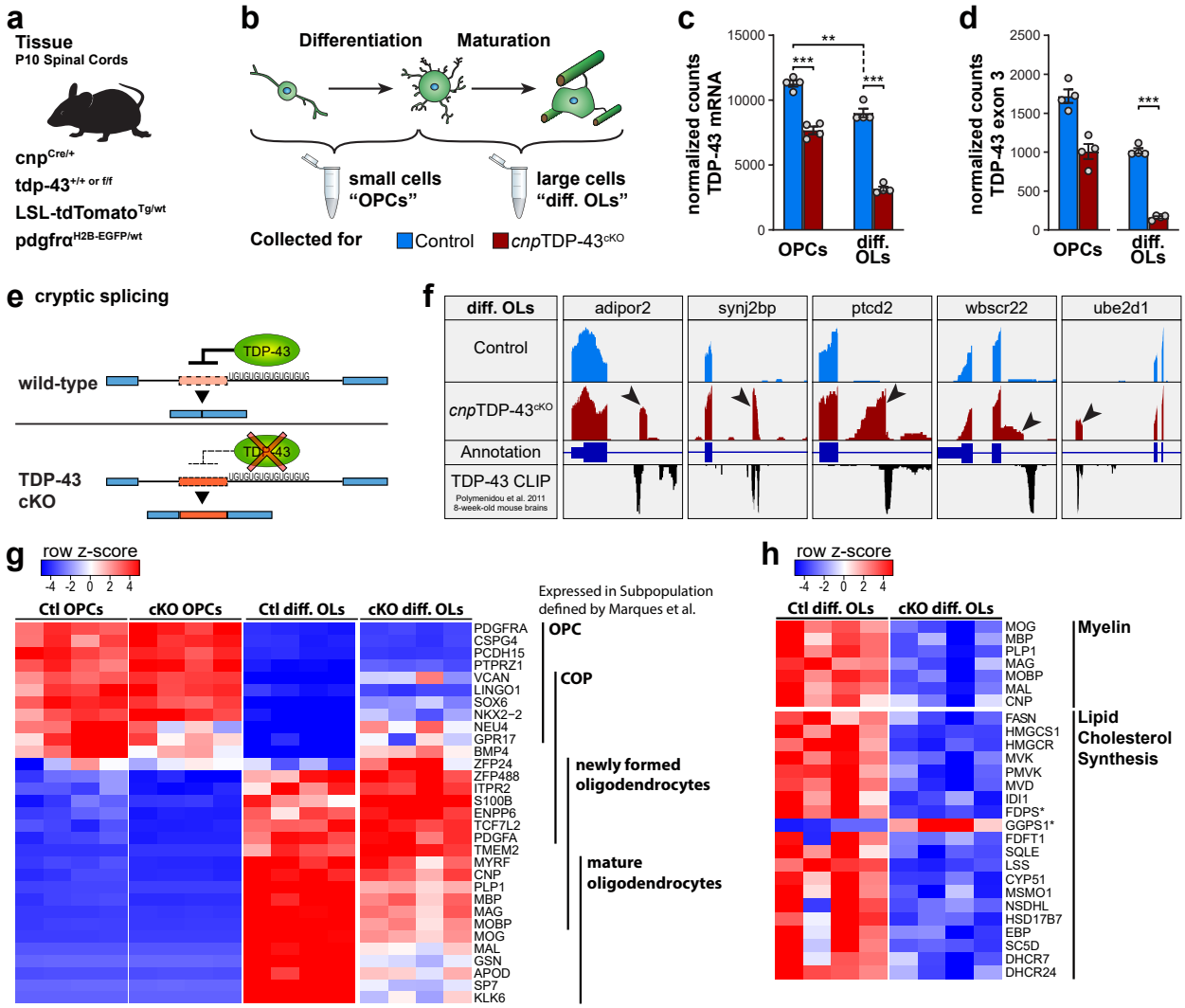

Figure 6.7: Impact of TDP-43 on the transcriptome in OLs from *cnp*-cKO SpC at P10. OL cells from control and *cnp*-cKO mice were collected at P10 by FACS and analysed using RNA sequencing. **(a)** Transgenic mice used for the experiment. Both transgenic reporters, Cre-dependent tdTomato and *pdgfrα*-driven H2B-EGFP, were used in the experiment to maximize the purity of samples. **(b)** Scheme summarizing the sorting strategy. modified from Goldman and Kuypers (2015) **(c)** Total TDP-43 gene quantification displayed as normalized counts (n = 4 samples/condition, **p<0.01, ***p<0.001, pairwise analysis by EdgeR, comparison of *cnp*-cKO OPCs vs OLs has not been performed). **(d)** Quantification of TDP-43 exon 3 mRNA expression as normalized coverage counts (n = 4 samples/condition, ***p<0.001, pairwise comparison using JunctionSeq). **(e)** Schematic of mechanism of TDP-43 mediated repression of cryptic splicing. Blue bars represent canonical exons, orange bars represent cryptic exons in intronic regions. modified from (Ling et al., 2015) **(f)** Identified cryptic splicing events in differentiated *cnp*-cKO OLs. Mouse brain TDP-43 UV-CLIP data (Polymenidou et al., 2011) has been re-analysed and indicates direct interaction between TDP-43 and identified genes in close proximity to the cryptic exons (black arrowheads), which do not display sequencing-coverage in control samples. **(g)** Heatmap of gene normalized counts of various genes expressed during OL differentiation and maturation. The more resolved states of differentiation-committed OL precursors (COP) and newly formed OLs are inferred from a previous single-cell study (Marques et al., 2016). Note the enriched expression levels of genes typical for early states of differentiation in differentiated OLs from *cnp*-cKO samples compared to controls. **(h)** Heatmap of gene normalized counts for genes related to myelin proteins and lipid biosynthesis reveals consistently lower expression in *cnp*-cKO differentiated OLs compared to controls. *fdps* and *ggps1* (asterisks) perform the same enzymatic reactions within the cholesterol biosynthetic pathway. Based on FPKM values, *fdps* is expressed >12-fold than *ggps1* in controls and more than >6-fold in *cnp*-cKO OLs.

Differentiated OLs in *cnp*-cKO Mice Diverge to Different Fates

Bulk RNA sequencing revealed the average transcriptomic state of OPCs and differentiated OLs as a mixture of all cells in each sample, which is dependent on both the transcriptomic state of each cell and the number of cells in each state. The number of cells in each state not only depends on their occurrence *in vivo* (*e.g* more newly differentiated OLs than mature OLs in one genotype versus the other), but is also subjected to individual properties of cells affecting how efficient they are extracted from the tissue and survive the experimental procedure. TDP-43 exon 3 mRNA levels are a sensitive read-out for recombination of the TDP-43 floxed allele. In bulk RNA sequencing, they trend lower in OPCs samples from *cnp*-cKO animals compared to controls (Fig. 6.7d). We reasoned that there are two major factors which could potentially contribute to this observation: *First*, only a fraction of OPCs from *cnp*-cKO mice are recombined at the *Tardbp* locus. *Second*, recombination of TDP-43 may not be taking place in OPCs, but efficiently in newly differentiated OLs, of which some might be collected in the OPC sample. A similar rationale can be applied to provide different possibilities that contribute to the transcriptomic shift observed in differentiated *cnp*-cKO OLs (see Fig. 6.7g). *First*, it is possible that maturation of differentiated OLs is delayed or partially blocked when TDP-43 is deleted. *Second*, *cnp*-cKO OLs might have a reduced capability to mature properly and thereby adopt an aberrant transcriptomic state, which is not present in controls.

To address these possibilities, we collected all OLs from control and *cnp*-cKO SpCs at P10 without further splitting, and analyzed them by single-cell sequencing. Only *cnp*Cre-dependent expression of tdTomato has been used as a reporter, as the lineage identity of each cell is individually determined and non-OL cells can be removed after data acquisition. From all cells measured, we removed those with high content of mitochondrial genes and low read numbers (Fig. A.9a,b). We additionally removed potential doublets using DoubletFinder (McGinnis et al., 2019). Finally, 4'056 control and 4'342 *cnp*-cKO cells were used for analysis. By clustering and subsequent cell type allocation, 96 % and 94 % of cells were identified to be in the OL lineage in the control and *cnp*-cKO samples, respectively. A recent single-cell sequencing study defined various separate states of OL maturation (Marques et al., 2016), and we adhered to this classification for the analysis of our data. Clustering of OLs demarcated different states along OL differentiation and maturation. In addition, OPCs clustered into different groups according to their cell cycle state (Fig. 6.8a,b; Fig. A.9d-f). Based on this clustering, we noted a profound reduction of TDP-43 mRNA in *cnp*-cKO OLs compared to controls (Fig. 6.8a, represented on log scale).

Excitingly, *cnp*-cKO OPCs in the S/G2M phase still expressed TDP-43 to some extent, while it was abolished in the G1 phase cluster of *cnp*-cKO OPCs. These results provide strong evidence that TDP-43 is already recombined in a substantial number of *cnp*-cKO OPCs, which are not actively dividing. The previously performed protein and bulk RNA sequencing analysis of pooled OPCs therefore likely represents a mixed measurement of recombined and non-recombined *cnp*-cKO OPCs, which is in line with the marginal, trendwise reduction observed in these experiments. Cells were further projected using the UMAP dimensionality-reduction projection (Fig. 6.8b). By qualitative assessment, control and *cnp*-cKO samples were comparably distributed except for one *cnp*-cKO-specific population (Fig. A.9c). In this projection, OLs aligned according to their differentiated state and the *cnp*-cKO-specific cluster diverged from the population of early differentiation-committed precursors (COPs), the first *pdgfrα*-negative state of OLs. Due to the lack of *pdgfrα* expression, we considered the COPs as the earliest state of differentiated OLs. The distribution of cells from control and *cnp*-cKO cells in each cluster (Fig. 6.8c) revealed that control cells only contributed to 3 % of all cells in the *cnp*-cKO specific cluster, emphasizing its specificity. Inspection of the distribution of *cnp*-cKO OLs among clusters revealed higher numbers of OPCs and lower numbers of differentiated OLs in comparison with control OLs. *cnp*-cKO cells were least abundant in the most mature cluster of myelinating OLs (MOLs) when compared to control cells. In the subsequent analysis, we focused on the *cnp*-cKO cluster. Preliminary inspection of genes typical for the *cnp*-cKO cluster exposed a set of genes almost uniquely expressed by this cluster (Fig. 6.8d). Among them, we identified genes coding for the PTEN regulating E-3 ubiquitin ligase WWP2 (*wwp2*; Li et al., 2018a), the orphan g-protein coupled receptor LGR4 (*lgr4*; reviewed by Tang et al., 2012), the notch-target HeyL (*heyl*; Maier and Gessler, 2000), prostaglandin D2 synthase PTGDS (*ptgds*), and the lipase/acyltransferase PNPLA3 (*pnpla3*; reviewed by Pingitore and Romeo, 2019). Further investigation will be required to better understand this unique cluster of OLs and their specific profile of expressed genes, including whether it actively contributes to the defective CNS development in *cnp*-cKO mice.

We have previously shown that *cnp*-cKO SpCs persistently display thinner myelin. Therefore, we compared *cnp*-cKO OLs with corresponding control OLs during late stages of maturation with respect to genes required for myelination (Fig. 6.8e,f). Surprisingly, only some genes encoding myelin proteins were significantly changed in an irregular pattern in myelin forming (MFOL) and mature, myelinating (MOL) *cnp*-cKO OLs compared to controls OLs in the same cluster. While *plp1* was decreased in *cnp*-cKO cells in both clusters, *mag* and *cnp* were more abundant in these clusters when compared to controls. Conversely, *fasn* and a number of genes involved in cholesterol biosynthesis are reduced to a significant extent in *cnp*-cKO MFOLs and MOLs compared to controls. In summary, we propose that TDP-43 is already recombined in a subpopulation of OPCs, and that at a very early stage of differentiated OLs some *cnp*-cKO cells sharply diverge transcriptionally from the canonical maturation trajectory. This divergence includes accumulation of transcripts from genes that are normally not expressed to this extent in the OL lineage during development, and particularly not in cells of their closely related canonical stages of early maturation, COPs and NFOLs. The remaining *cnp*-cKO OLs, which are seen along the same maturation trajectory as control OLs, also display efficient reduction of TDP-43 mRNA compared to control. These observations indicate a critical, stage-delimited step for very early differentiated OLs that depends on TDP-43 function. Moreover, myelin forming and mature *cnp*-cKO OLs display lower expression of *plp1* and genes involved in lipid biosynthesis when compared to controls, which is consistent with reduced myelination in SpCs of the same mutants during development.

Figure 6.8 ***(facing page)*****: Single-cell transcriptomics of control and *cnp*-cKO mice.** Oligodendrocytes were collected at P10 from one control and one *cnp*-cKO spinal cord by FACS using Cre-dependent expression of tdTomato. Samples were processed using the 10X genomics DropSeq approach and further analysed. **(a)** Expression of marker genes for different OL stages and TDP-43 mRNA (*tardbp*) are represented as violin plots on an arbitrary log scale. The bold line marks the median of all cells. Abbreviations: early differentiation committed precursor (COP), newly formed OL (NFOL), myelin forming OL (MFOL) and mature, myelinating OLs (MOL). **(b)** UMAP projection. Clusters are labelled and marked by color. The *cnp*-cKO-specific cluster as well as clusters with a majority of cells in the S/G2M phase are marked by the dashed line. The *cnp*-cKO-specific cluster is further divided into two sub-clusters for analysis in (d). **(c)** Proportion of cells in each cluster among all cells from control and *cnp*-cKO samples. Colors match the clusters in the UMAP plot shown in (b). **(d)** Manual selection of candidate genes that are strikingly enriched in the *cnp*-cKO-specific cluster among OL clusters. *Wwp2* displays highest expression in *cnp*-cKO sub-cluster 1 (see b), while *lgr4*, *heyl*, *ptgds* and *pnpla3* are most abundant in sub-cluster 2. **(e,f)** Analysis of significantly differentially expressed genes between control and *cnp*-cKO cells in the MFOL (e) and MOL (f) clusters, represented as volcano plots (average $\log_2$(fold-change$_{\text{Ctl vs cKO}}$) versus -$\log_{10}$(p_{adjusted})). Vertical lines indicate a linear fold-change of 1.5. Genes encoding myelin proteins (yellow) are differently changed between *cnp*-cKO cells and controls, notably *plp1* is decreased and *mag* is expressed at higher levels in *cnp*-cKO cells. *fasn* and several genes involved in cholesterol biosynthesis (red) are less expressed in *cnp*-cKO cells compared to controls in both MFOL and MOL clusters. Analysis of differentially expressed genes was performed using *FindMarkers* by Seurat Butler et al., 2018; Stuart et al., 2019.

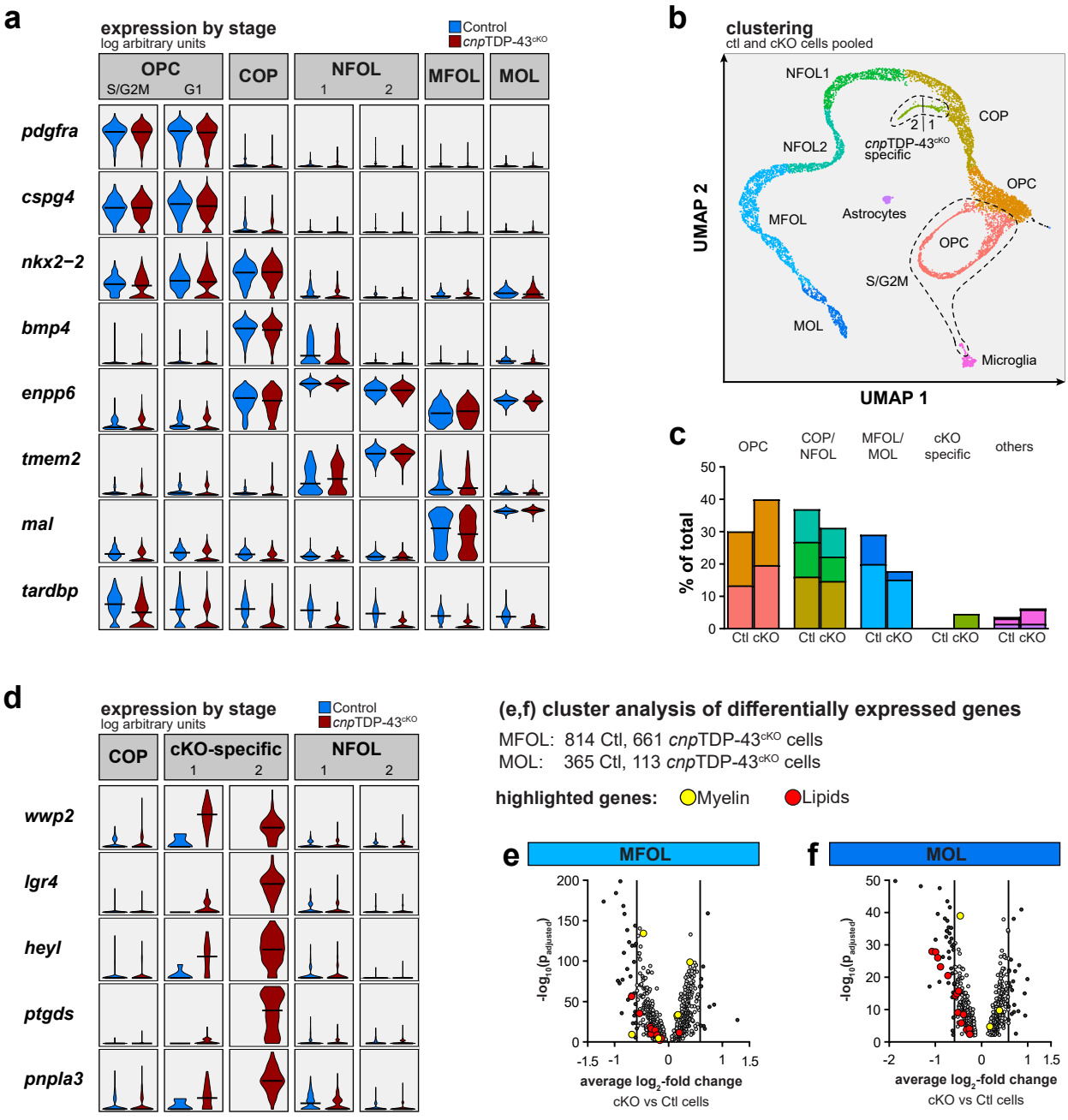
a
expression by stage
log arbitrary units
Control
cnpTDP-43cKO
OPC
S/G2M
G1
COP
NFOL
1
2
MFOL
MOL
pdgfra
cspg4
nkx2−2
bmp4
enpp6
tmem2
mal
tardbp
b
clustering
ctl and cKO cells pooled
NFOL1
COP
2
1
NFOL2
cnpTDP-43cKO specific
OPC
MFOL
Astrocytes
OPC
S/G2M
MOL
Microglia
UMAP 2
UMAP 1
c
OPC
COP/ NFOL
MFOL/ MOL
cKO specific
others
% of total
Ctl cKO
d
expression by stage
log arbitrary units
Control
cnpTDP-43cKO
COP
cKO-specific
NFOL
wwp2
lgr4
heyl
ptgds
pnpla3
(e,f) cluster analysis of differentially expressed genes
MFOL: 814 Ctl, 661 cnpTDP-43cKO cells
MOL: 365 Ctl, 113 cnpTDP-43cKO cells
highlighted genes:
Myelin
Lipids
e
MFOL
f
MOL
-log10(padjusted)
average log2-fold change
cKO vs Ctl cells

Oligodendrocytes in Culture Exhibit a Cell-Autonomous Defect upon Loss of TDP-43

Bulk and single-cell sequencing revealed lower abundance of transcripts encoding some myelin proteins and enzymes of the lipid biosynthesis machinery, and a sub-population of differentiated OLs which diverge from the canonical maturation route. This is in agreement with a potential cell-autonomous requirement for TDP-43 in differentiated OLs to fully mature and reach the myelinating state. Culturing primary OPCs and inducing them to differentiate in culture provides a variety of experimental possibilities to further investigate the molecular function of TDP-43 in line with the hypothesis listed above. However, this involves a completely different, artificial environment, and it is not certain that OLs show the same behaviour as in living mice. In order to establish a cell culture system that recapitulates the main features observed *in vivo*, primary OPCs were extracted by FACS into culture plates, expanded, and induced to differentiate (and further maturation) by replacing Pdgf with thyroid hormone in the culture medium. Cells were finally analyzed by immunofluorescence and RT-qPCR. By direct observation of cell expansion, *cnp*-cKO and control OPC cultures did not show pronounced differences, which suggests that there should not be dramatic differences in the proliferation and survival in these cultures. Analysis of the cells after 4 days under differentiating conditions revealed fewer MBP positive OLs by qualitative assessment (Fig. 6.9a). The expression of *Pdgfrα* remained comparable between *cnp*-cKO and control OPCs, and was heavily reduced after differentiation as expected (Fig. 6.9b). Non-recombined TDP-43 mRNA was reduced to ~25% of control levels in *cnp*-cKO OPCs after expansion, while differentiated OLs had virtually lost it (Fig. 6.9c). *Enpp6* and *tcf7l2*, markers for early differentiated OLs, were 3-fold higher in differentiated *cnp*-cKO cultures compared to differentiated controls (Fig. 6.9d). Conversely, levels of *plp1*, *mag* and *mog*, which are expressed from myelin forming OLs onwards, were evidently reduced in *cnp*-cKO cultures compared to controls (Fig. 6.9d). Collectively, these changes indicate a less mature state of *cnp*-cKO OL cultures after stimulating differentiation. Our transcriptomic analysis of single OL cells uncovered a *cnp*-cKO-specific sub-population, which exhibited high abundance of transcripts that are not typically expressed to this extent in the OL lineage. Four of the 5 specific genes (Fig. 6.8d) were significantly more abundant in differentiated *cnp*-cKO cells (Fig. 6.9e), potentially due to the emergence of a *cnp*-cKO-specific sub-population of OLs also in cell culture. Taken together, the impaired maturation of *cnp*-cKO OLs in culture and the enrichment of most markers from our previously identified *cnp*-cKO-specific

subpopulation in these cells is compatible with the impaired myelination and single-cell transcriptomic analysis in *cnp*-cKO mice, and indicates a cell-autonomous requirement of TDP-43 for OL maturation.

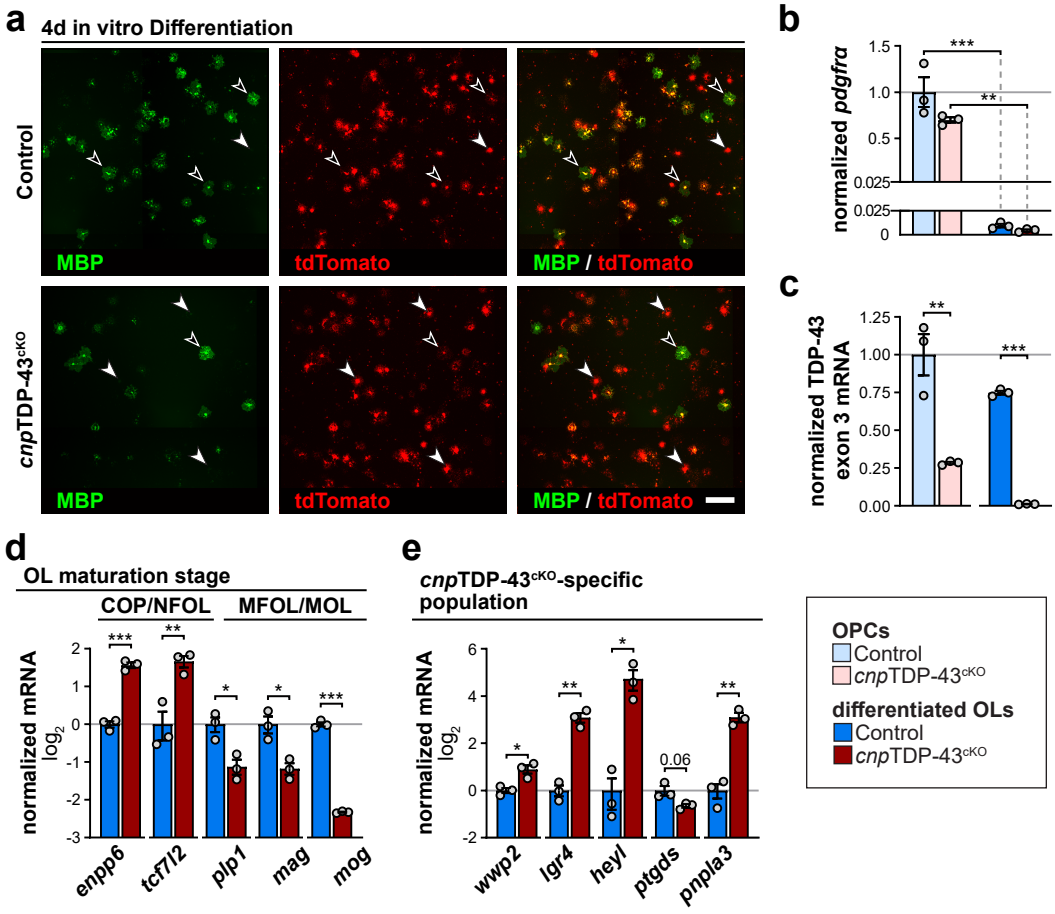

Figure 6.9: Differentiation of cultured *cnp*-cKO OPCs reveals a reduced maturation capacity compared to controls, and an enrichment of some transcripts typical of the *cnp*-cKO-specific subpopulation of differentiated OLs. tdTomato^{pos} OPCs were isolated from P6-P8 control and *cnp*-cKO mice using FACS and cultured for 8 days before switching to differentiating conditions. Differentiated OLs and OPCs were analysed after 4 additional days. **(a)** Exemplary immunofluorescence stainings of MBP to label mature OLs. tdTomato was used to mark all OLs. Note the evident reduction of MBP^{pos} OLs among all tdTomato^{pos} OLs in *cnp*-cKO OLs compared to controls. Scalebar 200 µm. **(b,c)** RT-qPCR of OPCs and differentiated OLs from both control and *cnp*-cKO OLs. (b) Reduction of *pdgfrα* mRNA levels in differentiated OLs compared to OPCs indicates efficient differentiation in both genotypes. (c) TDP-43 exon 3 mRNA levels are already reduced in *cnp*-cKO OPCs compared to controls, and they are reduced to an even more dramatic extent in OLs, indicating that TDP-43 is efficiently deleted in differentiated *cnp*-cKO OLs. **(d)** RT-qPCR analysis of differentiated control and *cnp*-cKO OLs for genes typically expressed in early (COP/NFOL) and late (MFOL/MOL) stages of OL maturation. Levels of *enpp6* and *tcf7l2* are higher in *cnp*-cKO OLs compared to controls, while levels of *plp1*, *mag* and *mog* are reduced, indicating an overall less mature state of the differentiated *cnp*-cKO OLs compared to controls. **(e)** Gene expression analysis of differentiated control and *cnp*-cKO OLs by RT-qPCR for genes highly enriched in the *cnp*-cKO-specific population of OLs (Fig. 6.8d). Except for *ptgds*, all genes displayed higher abundance in differentiated *cnp*-cKO OLs compared controls, suggesting that some differentiated *cnp*-cKO OLs acquired an aberrant transcription state as observed *in vivo*. *heyl* was barely detected in controls, leading to a strong relative enrichment in *cnp*-cKO OLs. **(Statistics)** Bar graphs represent mean±SEM; *p<0.05, **p<0.01, ***p<0.001. (all graphs) n = 3 technical replicates. (b) two-way ANOVA with Tukey's multiple comparisons test. (c-e) two-tailed, unpaired Student's t-test.

Timing of Ablation of TDP-43 is Decisive for the Outcome

OL single-cell sequencing revealed that OPCs partially recombine and lose TDP-43 mRNA in *cnp*-cKO mice compared to controls. We next asked whether development *in vivo* would be more prominently affected when TDP-43 was more widely abolished in OPCs. To this end we used the *olig2*Cre mouse line (Schuller et al., 2008). In these mice (*olig2*TDP-43^{cKO}, hereafter *olig2*-cKO), we expect that TDP-43 should be recombined efficiently in OPCs (Maire et al., 2014; Calabretta et al., 2018). We could not detect embryonic lethality in *olig2*-cKO mice (36 % *olig2*-cKO obtained among 77 pups in *olig2*Cre^{pos} TDP-43$^{f/wt}$ x TDP-43$^{f/f}$ breedings). *olig2*-cKO mice were smaller than their littermates. Due to animal welfare considerations, *olig2*-cKO mice could not be analysed at P50; therefore we restricted our analysis to P10. To compare the phenotype of these mutants with our previous data on *cnp*-cKO mice, we analysed myelination and the number of OLs in control and *olig2*-cKO SpCs. Strikingly, the ventral WM of *olig2*-cKO mice displayed very few myelinated axons (Fig. 6.10a,b).We stained cryosections of control and *olig2*-cKO lumbar SpCs with Olig2 to label OLs and Pdgfrα/CC1 to detect OPCs and differentiated OLs, respectively (Fig. 6.10d,e). By preliminary (as of November 2019), qualitative assessment of 3 animals per genotype, we observed fewer OPCs and almost no CC1^{pos} differentiated OLs. Taken together, deletion of TDP-43 using *olig2*Cre, which should drive efficient recombination in OPCs, resulted in profoundly reduced myelination and a dramatic absence of CC1^{pos} OLs. We reasoned that OPCs might fail to differentiate efficiently, or that loss of TDP-43 detrimentally impaired maturation of early differentiated, Pdgfrα^{neg} CC1^{neg} OLs to the CC1^{pos} stage in *olig2*-cKO mice. Moreover, OPCs *per se* are potentially dependent on TDP-43 function for survival or proliferation. Collectively, these findings indicate an essential function of TDP-43 for OPC biology, differentiation, or early steps of maturation.

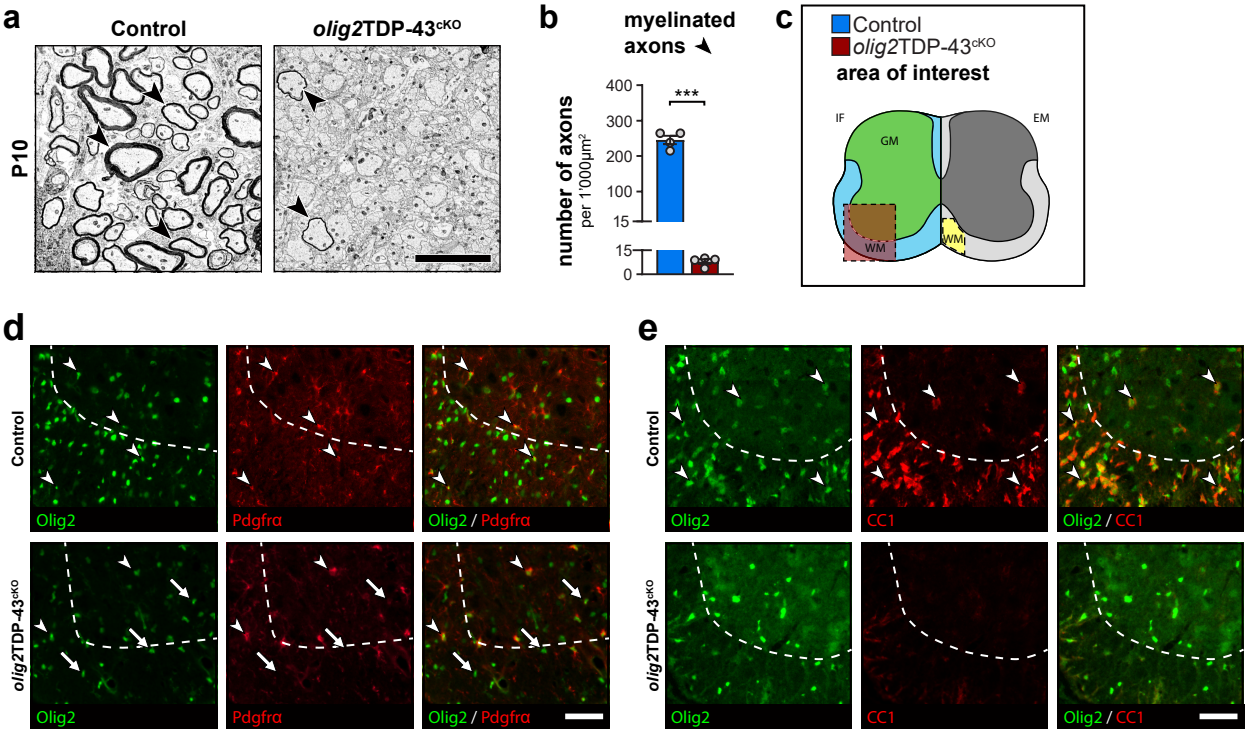

Figure 6.10: Early loss of TDP-43 in the OL lineage is detrimental for myelination. Control and *olig2*-cKO mice were analysed at P10 by EM and immunofluorescence. **(a)** Representative EM micrographs reveal a dramatic reduction of myelinated axons (black arrowheads) in the ventral funiculus of *olig2*-cKO SpCs compared to controls. scalebar: 5 µm. **(b)** Myelinated axons in the ventral funiculus are more than 30-fold reduced in *olig2*-cKO mice when compared to controls. **(c)** Scheme depicting the areas shown in (a) and (d,e). **(d,e)** Immunofluorescence staining of lumbar SpC cryosections at P10. Olig2 (green) labels all OLs, and OPCs were further identified by Pdgfrα (red, white arrowheads, d). Olig2^{pos}, Pdgfrα^{neg} cells potentially represent very early stages of differentiated OLs (white arrows in the *olig2*-cKO image). Differentiated oligodendrocytes were identified by CC1 (red) and almost none were observed in *olig2*-cKO mice compared to controls (e). 3 animals per genotype showed consistent results. scalebar: 50 µm. **(Statistics)** Bar graphs represent mean±SEM; ***p<0.001. (b) n = 4 mice, two-tailed, unpaired Student's t-test.

6.3. Function of TDP-43 in Adult OLs

Induced Loss of TDP-43 in Adult OLs Leads to Demyelination of the Spinal Cord Grey Matter

TDP-43 is essential in OLs for normal CNS development. It remains expressed at lower levels after differentiation and in myelinating oligodendrocytes, suggesting that it is functionally required after development as well. To address the functional relevance of TDP-43 during myelin maintenance, we crossed mice expressing Cre^{ERT2} under control of the *Plp1* promoter with TDP-43 floxed mice (Leone et al., 2003; Chiang et al., 2010; *plp*TDP-43^{iKO}, hereafter *plp*-iKO). Recombination was induced by five consecutive, daily injections of tamoxifen between 8-10 weeks of age (Fig. 6.11a). To mark recombined OLs, we incorporated the Cre-dependent tdTomato reporter (Madisen et al., 2010). For consistency, we used $reporter^{pos}$ control mice (*plp1*Cre^{ERT2+} $R26^{tdTomato/wt}$ TDP-$43^{wt/wt}$) as controls in these experiments. Control and *plp*-iKO mice display no evident differences in free cage behaviour until five weeks post-tamoxifen (wpT). Thereafter, the condition of *plp*-iKO mice progressively worsened at continuously faster pace, until they displayed evident generalized weakness after 6wpT. To address the efficiency of tamoxifen induced recombination, tdTomato expression among OLs was analysed in control and *plp*-iKO SpC cross sections. Unexpectedly, a substantial number of OLs already displayed tdTomato expression without the administration of tamoxifen, which indicates insufficiently confined Cre activity prior to induction in *plp1*Cre^{ERT2+} mice (Fig. 6.11b). It was not clear, however, whether only the loxP-sites in the tdTomato transgene were recombined or also those in the TDP-43 gene. To investigate recombination of TDP-43 in *plp*-iKO mice, we sought to collect tdTomato positive OLs before and one week after tamoxifen injection using FACS. TDP-43 exon 3 expression was measured by qPCR using cDNA from the collected cells (Fig. 6.11c). OLs from control and *plp*-iKO mice did not display statistically different expression of TDP-43 before tamoxifen injection. Only a small number of cells (few hundred to 1'000) could be collected from these mice, which likely contributed to the observed variability. One week post-tamoxifen, non-recombined TDP-43 expression – based on exon 3 – was dramatically reduced only in *plp*-iKO mice compared to controls. These findings indicate that in the vast majority of *plp*-iKO OLs TDP-43 is only recombined after the tamoxifen injection, despite the premature tdTomato expression.

Based on the condition of the *plp*-iKO mice, we set the final timepoint of analysis to 6wpT. At this timepoint, myelination and tissue integrity was analysed in control and *plp*-iKO SpCs using electron microscopy. By qualitative inspection, the ventral WM from *plp*-iKO SpCs did not display widespread differences compared to controls (Fig. 6.11d). Also, the density of myelinated axons or the myelin thickess, quantified as g-ratio, did not reveal statistically significant differences between genotypes (Fig. 6.11e,f). Based on visual inspection of control and *plp*-iKO SpC semithin sections, we noticed a different appearance of the GM between genotypes, and focused on this region for further analysis. Indeed, the number of myelinated axons was strongly reduced in the ventral horn of *plp*-iKO SpCs compared to controls, indicating demyelination in these mutants (Fig. 6.11g,h). Myelination in the dorsal horn was also reduced in *plp*-iKO mice by qualitative inspection, and concentrated patches of myelinated tracts were more scattered and less dense in comparison to controls (Fig. 6.11j, red insert). Nonetheless, there was only a trend to reduction in density of myelinated axons, without statistical significance (Fig. 6.11k). This is potentially in part due to the heterogenous pattern of myelination in this area, which is very challenging for conclusive quantitative analysis. Collectively, these observations strongly indicate active demyelination in the GM of *plp*-iKO mice, as they were allowed to develop normally before deleting TDP-43 in OLs. Vacuolation was observed in *cnp*-cKO SpCs during development, which led us to investigate the presence of vacuoles in SpCs of *plp*-iKO mice. The ventral horn of *plp*-iKO SpCs displayed widespread vacuolation when compared to controls (Fig. 6.11g,i). Vacuoles were also enriched in dorsal horns of *plp*-iKO SpCs compared to controls, although at a much lower density than in the ventral horn of the same mutants (Fig. 6.11j,l; note the difference in scale of the ordinate).

Brain Regions Are Potentially Affected in *plp*TDP-43^{iKO} Mice

Collectively, the SpC white and grey matter reacted very differently to loss of TDP-43 in adult OLs within 6wpT. Other CNS regions may also be affected to various degrees, which led us to inspect the same brain regions as in the *cnp*-cKO mice, namely the corpus callosum (CC), the cortical GM and the cerebellum (CB). It is important to note that at present the brains of control and *plp*-iKO mice have only been qualitatively assessed. Future quantification will deliver statistically reliable results to draw bolstered conclusions.

We could not detect overt vacuolation in the CC. Myelinated axons appeared less numerous and might be slightly reduced in *plp*-iKO mice compared to controls (Fig. 6.12a). The cortical GM above the CC as well as the CB appear to also contain fewer myelinated fibres (Fig. 6.12b,c). In addition, vacuoles were robustly observed in cerebella of all *plp*-iKO but not control mice (Fig. 6.12c).

Figure 6.11 ***(facing page)*****: Loss of TDP-43 leads to demyelination and vacuolation in the SpC GM.** **(a)** Scheme of experimental setup. Control and *plp*-iKO mice were injected with tamoxifen on five consecutive days, when they were between 8-10 weeks of age. *plp*-iKO mice are strongly affected at six weeks after tamoxifen treatment (6wpT). **(b)** Percentage of tdTomato^{pos} cells among all Olig2^{pos} cells (OLs) from lumbar SpC cross sections from control and *plp*-iKO mice at different timepoints. Note the occurrence of tdTomato^{pos} OLs in control and *plp*-iKO mice without tamoxifen administration (Tmx-). No statistical analysis was applied. **(c)** Expression of TDP-43 exon 3 mRNA from sorted OLs using tdTomato-reporter expression. Cells were collected from animals without tamoxifen administration (Tmx-) and at 1wpT. **(d-l)** Analysis of lumbar SpCs from control and *plp*-iKO mice at 6wpT by EM. **(d)** Exemplary EM micrographs of SpC WM are qualitatively comparable between genotypes. scalebar: 5 µm. **(e,f)** Density (e) and myelin thickness (g-ratio, f) of myelinated axons in the SpC WM at 6wpT revealed no significant differences between *plp*-iKO and control mice. **(g)** Representative EM micrographs from control and *plp*-iKO SpC GM in the ventral horn depict a reduction of myelinated axons (white arrowheads) in *plp*-iKO mice compared to controls. Vacuoles (orange arrowheads) are prominent in *plp*-iKO mice. scalebar: 5 µm **(h,i)** Density of myelinated axons (h) and vacuoles (i) in the ventral grey matter showing demyelination and impaired tissue integrity in *plp*-iKO mice compared to controls. **(j)** Representative EM micrographs from control and *plp*-iKO SpC GM in the dorsal horn. Myelinated axons (white arrowheads) appear less frequent in *plp*-iKO mice compared to controls. Inserts (dashed red line) illustrate the changed appearance of densely myelinated patches in the dorsal horns of control and *plp*-iKO mice. Exemplary micrographs at low magnification illustrate the presence of vacuoles (orange arrowheads) in *plp*-iKO mice. scalebar: 5 µm, low magnification 20 µm. **(k,l)** Changes in the density of myelinated axons (k) in the dorsal GM are not statistically significant different between genotypes. Density of vacuoles (l) in the dorsal GM is increased in *plp*-iKO SpCs compared to controls. Note that in contrast to the density of vacuoles in the ventral horn (i), the scale is per 10'000 µm^2. **(m)** Scheme illustrating analysed SpC areas. **(Statistics)** Bar graphs represent mean±SEM; ***p<0.001. (c,e,f,h,i,k,l) n = 5 mice, two-tailed, unpaired Student's t-test.

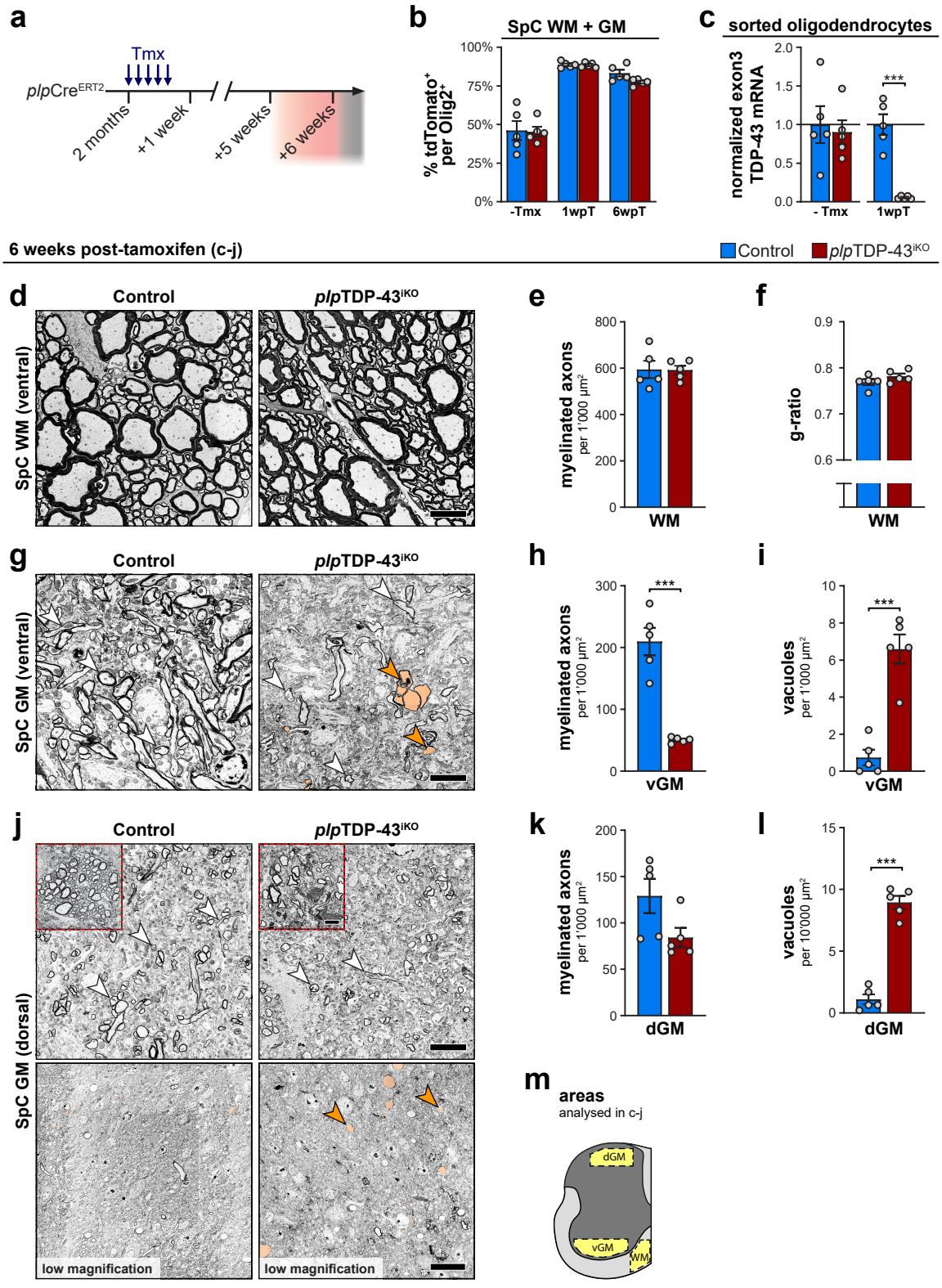
a
Tmx
plpCreERT2
2 months
+1 week
+5 weeks
+6 weeks
b
SpC WM + GM
% tdTomato+ per Olig2+
100%
75%
50%
25%
0%
-Tmx
1wpT
6wpT
c
sorted oligodendrocytes
normalized exon3 TDP-43 mRNA
2.0
1.5
1.0
0.5
0.0
***
- Tmx
1wpT
6 weeks post-tamoxifen (c-j)
Control
plpTDP-43iKO
d
Control
plpTDP-43iKO
SpC WM (ventral)
e
myelinated axons per 1'000 µm²
800
600
400
200
0
WM
f
g-ratio
0.9
0.8
0.7
0.6
WM
g
Control
plpTDP-43iKO
SpC GM (ventral)
h
myelinated axons per 1'000 µm²
300
200
100
0
***
vGM
i
vacuoles per 1'000 µm²
10
8
6
4
2
0
***
vGM
j
Control
plpTDP-43iKO
SpC GM (dorsal)
low magnification
low magnification
k
myelinated axons per 1'000 µm²
200
150
100
50
0
dGM
l
vacuoles per 10'000 µm²
15
10
5
0
***
dGM
m
areas
analysed in c-j
dGM
vGM
WM

In summary, *plp*-iKO mice acquire a detrimental condition around six weeks after induction of recombination. While the SpC WM is largely intact, the GM – especially the ventral horn – is clearly demyelinated. The CC does not seem to be drastically affected, and we further qualitatively observed mild signs of demyelination in the cortical GM as well as the CB. In addition, the SpC GM and the CB displayed evident vacuoles, but not the other regions investigated. From this, we conclude that TDP-43 in mature OLs is essential for myelin maintenance in the SpC GM, and potentially contributes to the myelin maintenance in at least some brain regions.

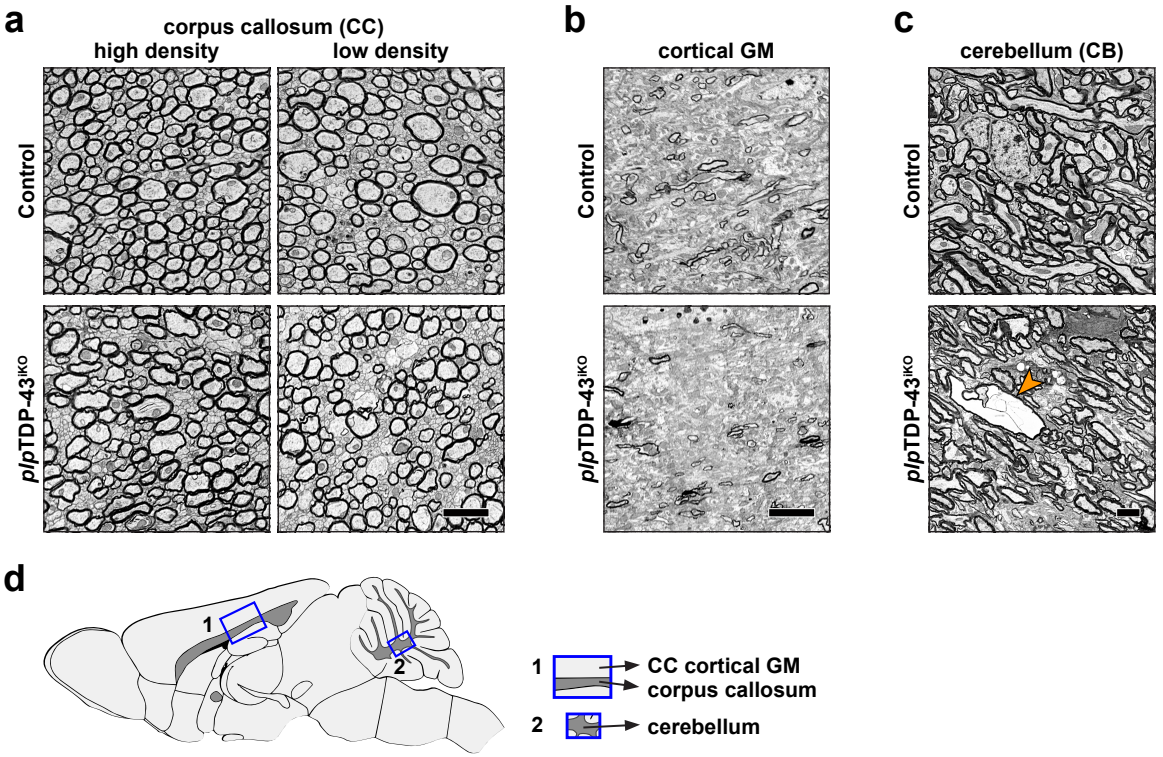

Figure 6.12: Brain areas of control and *plp*-iKO mice at 6wpT.
(a-c) Exemplary EM micrographs of sagittal brain sections from control and *plp*-iKO mice. scalebar: 2 µm. **(a)** Two representative regions of high and low density of myelinated axons in corpora callosa (CC), suggesting a mild reduction of myelinated axons in *plp*-iKO mice compared to controls. **(b)** Representative EM micrographs of cortical GM (located above the analysed CC area) suggesting fewer myelinated axons in *plp*-iKO brains compared to controls. **(c)** Typical EM micrographs from cerebellar white matter tracts. Myelinated axons appear reduced in number in *plp*-iKO mice compared to controls. Note the presence of vacuoles in *plp*-iKO mice. **(d)** Scheme illustrating the location of analysed regions, modified from the GENSAT project. The cortical GM analysed is part of the somatosensory and posterior parietal cortex. Brain regions of 3 mice per condition have been qualitatively assessed.

Survival of Differentiated OLs in the SpC GM Depends on TDP-43

We have previously observed a reduction in OL numbers in the GM of *cnp*-cKO SpCs. Given the pronounced demyelination in the SpC GM of *plp*-iKO mice compared to controls, we hypothesized that numbers of differentiated OLs might also be reduced in *plp*-iKO mice. To this end we analysed SpC cross sections from control and *plp*-iKO mice immediately before tamoxifen, at 1wpT, and 6wpT. Immunofluorescence staining for Olig2 and CC1 were used to label all OLs and their differentiated state, respectively (Fig. 6.13a,d). Statistical analysis of OL numbers in the WM revealed sporadic significant differences (Fig. 6.13b). Our interpretation is that when taken collectively these results do not indicate a coherent change of OL numbers in *plp*-iKO mice compared to controls. Analysis of $CC1^{pos}$ differentiated OLs in the WM was comparable to the analysis of total OLs (Fig. 6.13c), and hence did not denote drastic changes in *plp*-iKO mice compared to controls. In contrast, total OLs in the *plp*-iKO SpC GM already tended to lower numbers at 1wpT and were markedly reduced at 6wpT when compared to controls (Fig. 6.13e), which was also consistently found in the analysis of $CC1^{pos}$ differentiated OLs (Fig. 6.13f). The reduction of differentiated OLs in the GM suggests that TDP-43 may be required for survival of SpC GM-resident OLs. Kang et al. (2013) have reported elevated proliferation and higher numbers of OPCs along with loss of differentiated OLs in the ventral GM from the $SOD1^{G93A}$ mouse, a model for ALS involving motor neuron degeneration (Gurney et al., 1994). We hypothesized that demyelination and reduction of differentiated OLs in the *plp*-iKO GM might similarly result in elevated OPC numbers. While there was no significant difference in the density of OPCs in the SpC WM between *plp*-iKO and control mice at 6wpT, the GM of *plp*-iKO SpCs displayed significantly higher OPC density (Fig. A.10). Based on the demyelination and loss of OLs in the *plp*-iKO GM, we wondered whether these events triggered gliosis in the mutant SpC. As expected, astro-microgliosis in the *plp*-iKO GM was evident as observed by strong $GFAP^{pos}$ (astrocytes) and $Iba1^{pos}$ (microglia) signals compared to controls (Fig. 6.13g). $Iba1^{pos}$ cells displayed not only high levels of Iba1, which is an indicator of their activation, but were also more numerous (Fig. 6.13h). Also the WM of *plp*-iKO mice displayed increased numbers of $Iba1^{pos}$ cells, but to a drastically lower extent than in the GM. The GM displayed an immense density of $Iba1^{pos}$ microglia, and was enriched more than 10-fold when compared to controls, while microglia in the *plp*-iKO WM were only enriched ~1.8-fold in relation to controls. The strong signature of reactive gliosis in the *plp*-iKO SpC GM could potentially create a neurotoxic environment (reviewed by Sochocka et al., 2017) and we quantified

the number of ChAT^{pos} motor neurons using immunofluorescence staining of control and *plp*-iKO SpC cross sections at 6wpT. ChAT^{pos} motor neurons were significantly reduced to a mild extent in *plp*-iKO SpCs compared to controls (Fig. 6.13i). In summary, depletion of TDP-43 in young adult mice particularly affects the SpC GM, resulting in progressive loss of OLs, increased numbers of OPCs, and pronounced reactive gliosis. The SpC WM is only marginally affected in *plp*-iKO mice compared to controls. Collectively, these data suggest that TDP-43 is essential for the survival of differentiated OLs in the adult SpC GM. The pathological signature in the *plp*-iKO GM correlates with a mild but significant reduction of motor neurons at 6wpT, suggesting motor neuron degeneration in these mutants. This might be secondary to changes in the microenvironment due to the ongoing pathology, but there is also the possibility that TDP-43 in differentiated OLs actively contributes towards neuroprotection in the developed CNS.

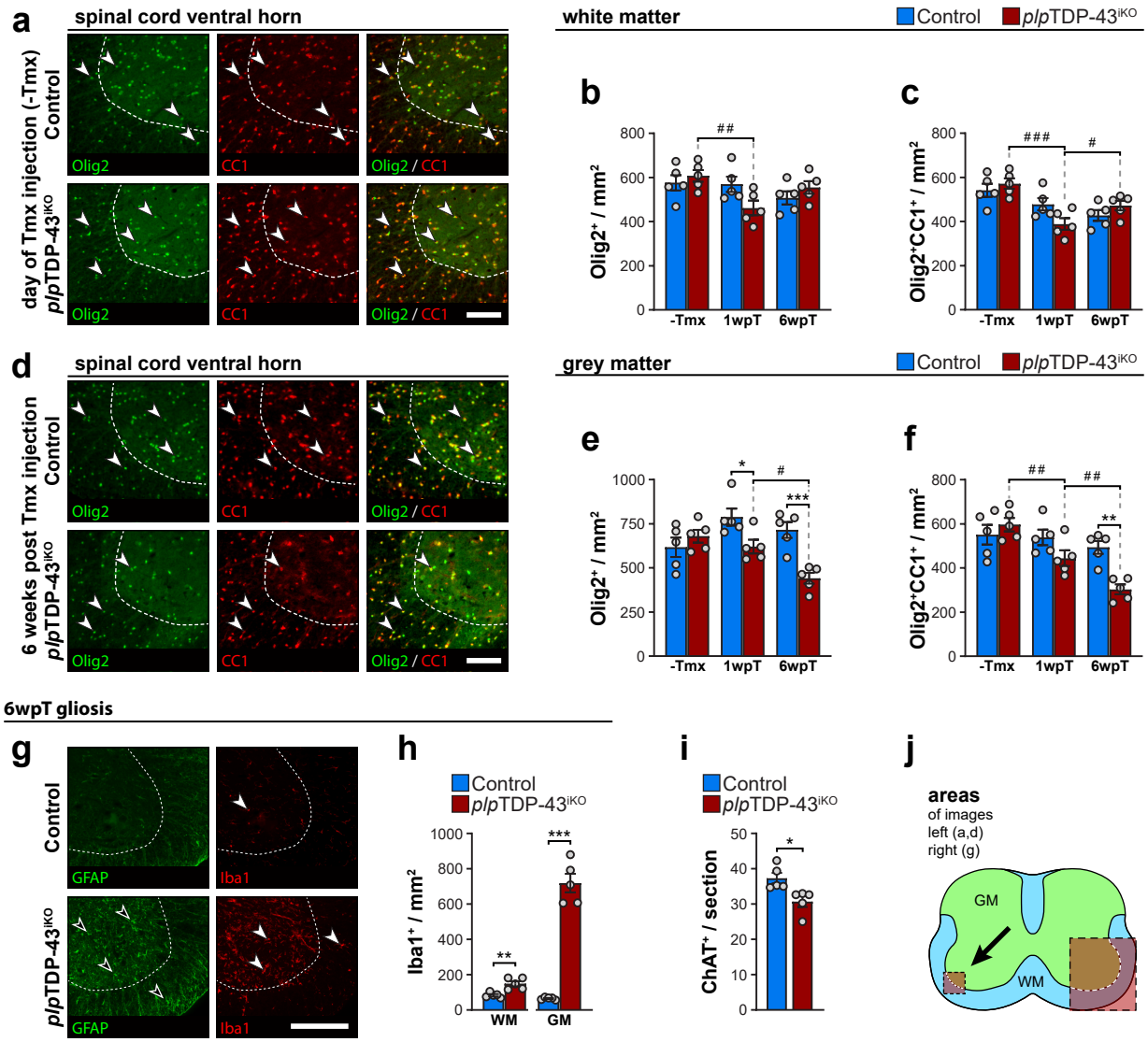

Figure 6.13: Induced deletion of TDP-43 leads to OL loss and reactive gliosis in the SpC at 6wpT. (a-f) Representative immunofluorescence images and analysis of lumbar spinal cord cross sections from control and *plp*-iKO mice before (Tmx-) and after treatment with tamoxifen (1wpT, 6wpT). Olig2 (green) labels all OLs and differentiated OLs are detected by CC1 (red). scalebars: 100 µm. **(a)** Representative staining of non-induced, 8-10 weeks old control and *plp*-iKO mice show no evident differences between genotypes. **(b,c)** Density of total Olig2^{pos} (b) and CC1^{pos} differentiated OLs (c) in the SpC WM showing at most mild changes between genotypes. **(d)** Representative images at 6wpT reveal reduced numbers of differentiated OLs in the GM from *plp*-iKO mice when compared to controls. **(e,f)** Density of total Olig2^{pos} (e) and CC1^{pos} differentiated OLs (f) in the SpC GM reveals a progressive reduction in *plp*-iKO mice compared to controls. **(g)** Exemplary immunofluorescence stainings of SpC cross-sections at 6wpT. Astrocytic marker GFAP (green) and microglial marker Iba1 (red) demonstrate pronounced reactive gliosis in the *plp*-iKO GM compared to controls. scalebar: 250 µm. **(h)** Density of Iba1^{pos} microglia in the SpC at 6wpT revealed increased numbers of microglia in the white and grey matter of *plp*-iKO mice compared to controls. These changes are much greater in the GM when compared to the WM. **(i)** Average number of ChAT^{pos} motor neurons per lumbar SpC cross-section in control and *plp*-iKO mice at 6wpT showing a mild reduction in *plp*-iKO mice. **(j)** Scheme illustrating the areas of representative images shown in (a,d,g). **(Statistics)** Bar graphs represent mean±SEM; (b,c,e,f) n = 5 mice, inter-condition analysis at same timepoint: *p<0.05, **p<0.01, ***p<0.001, two-way ANOVA with Šídák's multiple comparisons test; inter-timepoint analysis within same condition: $^{\#}$p<0.05, $^{\#\#}$p<0.01, $^{\#\#\#}$p<0.001, two-way ANOVA with Holm-Šídák's multiple comparisons test. (h,i) n = 5 mice; *p<0.05, **p<0.01, ***p<0.001, two-tailed, unpaired Student's t-test.

6.4. Summary of the Function of TDP-43 in Oligodendrocytes

We have studied the function of TDP-43 in OLs by conditional deletion during development and in young adult mice. *cnp*-cKO and control mice were analysed at various timepoints between P10 and P50. The *cnp*-cKO mice developed pathological symptoms visible at one month of age, and progressively deteriorated over time. Our data indicate efficient loss of TDP-43 in differentiated OLs and a fraction of not actively dividing OPCs in *cnp*-cKO mice. We have shown that TDP-43 in OLs is essential for the onset of myelination and myelin growth during developmental myelination. In addition, TDP-43 in OLs is required to prevent demyelination, and contributes to the protection of the myelin-axon unit and preservation of tissue integrity during CNS development. Loss of TDP-43 in OLs in *cnp*-cKO mice ultimately leads to widespread vacuolation and microgliosis. OPCs in the P10 SpC were not significantly changed in numbers or proliferation upon deletion of TDP-43. Analysis of $CC1^{pos}$ differentiated OL cell numbers in the SpC painted a complex region-specific picture, in which deletion of TDP-43 in OLs results in reduced numbers of $CC1^{pos}$ differentiated OLs in the GM at both P10 and P50, suggesting that TDP-43 is potentially required in these OLs for survival. Conversely, numbers of $CC1^{pos}$ differentiated OLs in the SpC WM were comparable in *cnp*-cKO and control mice at P10 and later increased in *cnp*-cKO mice at P50. Despite this, *cnp*-cKO mice were not able to achieve adequate tissue myelination, which suggests that TDP-43 might regulate maturation of these cells.

Indeed, detailed transcriptomic analysis of differentiated OLs depicted a less mature transcript signature and reduced levels of expression of genes associated with myelin proteins and lipid biosynthesis in *cnp*-cKO mice compared to controls at P10. Moreover, we have shown that TDP-43 is required in differentiated OLs to guard against cryptic splicing of transcripts. Single-cell transcriptomics of these OLs revealed reduced transcripts of genes associated with lipid biosynthesis in *cnp*-cKO OLs at late stages of maturation. However, genes encoding myelin proteins were not consistently reduced. In addition, some OLs in *cnp*-cKO mice diverge transcriptionally very early after differentiation from the canonical route of maturation, and display accumulation of transcripts from genes that are normally not expressed to this extent in the OL lineage during development, and particularly not in cells of their closely related canonical stages of early maturation, COPs and

NFOLs. We reason that these results suggest the existence of a critical, limited step for very early differentiated OLs that strongly depends on TDP-43 function. We further showed by differentiation of cultured *cnp*-cKO and control OLs that maturation is similarly impaired in culture when TDP-43 is deleted, which advocates for a cell-autonomous requirement of TDP-43 for OL maturation. Preliminary analysis of P10 *olig2*-cKO mice, in which TDP-43 is presumably more efficiently ablated in OPCs, revealed profoundly reduced myelination and a dramatic absence of $CC1^{pos}$ OLs.
We further investigated the function of TDP-43 in OLs using *plp*-iKO mice after induction of recombination between 8-10 weeks of age. The condition of *plp*-iKO mice progressively worsened at a continuously faster pace, until they displayed generalized weakness after 6wpT. Analysis of these mice showed that TDP-43 in mature OLs is essential for myelin maintenance in the SpC GM, and potentially contributes to the myelin maintenance at least in some brain regions. $CC1^{pos}$ OLs were progressively lost and OPCs increased in numbers in the *plp*-iKO SpC GM compared to controls, along with pronounced reactive gliosis. Collectively, these data show that TDP-43 is essential for the survival of differentiated OLs in the adult SpC GM. The pathological signature in the *plp*-iKO GM correlates with a mild but significant reduction of motor neuron numbers at 6wpT, suggesting motor neurodegeneration in these mutants. This might be secondary to changes in the microenvironment due to the ongoing pathology, but there is also the possibility that TDP-43 in differentiated OLs actively contributes towards neuroprotection in the developed CNS.

Part III

Discussion

7. The Multifacetted Functions of TDP-43 in Schwann Cells and Oligodendrocytes

TDP-43 is a well-described regulator of alternative and cryptic splicing (Buratti and Baralle, 2001; Buratti et al., 2001; Polymenidou et al., 2011; Tollervey et al., 2011), and a major disease protein related to ALS. Mutations in TDP-43 are considered causal to the disease in some types of ALS. Strikingly, a main feature of most ALS patients, even when TDP-43 is not mutated, is the appearance of cytoplasmic aggregates incorporating TDP-43, and its concomitant nuclear clearance. This naturally poses the question of whether the main driver of the pathogenesis is a loss of TDP-43 function due to its sequestration in aggregates, or rather a toxic gain of function due to the aggregates or the mutation *per se*. This has not yet been resolved and is still part of recent and ongoing research (Cascella et al., 2016; Sivakumar et al., 2018).

A plethora of ALS disease models have been studied in the last two decades (reviewed by Tsao et al., 2012 and Lutz, 2018). Many models rely on overexpression of wild type human or mutant forms of TDP-43. Even when human TDP-43 is transferred into the mouse genome including its endogenous promoter, both mutant and wild type hTDP-43 lead to mild pathological features in aged mice (Swarup et al., 2011). Since even the mild overexpression of wild type human TDP-43 produces a toxic condition *per se*, most TDP-43-related ALS disease models are highly limited in their potential to unravel the relevant physiological and pathological functions of TDP-43. Congenital loss of TDP-43 is lethal during mouse embryonic development (Kraemer et al., 2010; Sephton et al., 2010; Wu et al., 2010; Yang et al., 2014; Chiang et al., 2010). Few studies have addressed the basic functions of TDP-43 in neurons, and very little is currently known about its functions in Schwann cells (SCs) or oligodendrocytes (OLs). A recent study by Wang et al. (2018b) highlighted the importance of TDP-43 in OLs, but mainly scrutinized events late in development. Strikingly, there are so far no published data on the physiological role of TDP-43 in the context of SCs.

The present study elucidates the multifaceted aspects of TDP-43 in both types of myelination-competent glia. We applied different mouse models to delete TDP-43 at different stages during development and in adult mice. To our surprise, loss of TDP-43 in SCs was rather well tolerated in developmental myelination. In contrast, TDP-43 was required in SCs to correctly express Neurofascin and establish an appropriate architecture around the nodes of Ranvier. Aging mice strictly depend on TDP-43 in SCs for long term myelin maintenance and axonal support.

While myelination was successful in SCs even when TDP-43 was depleted, OLs are strictly dependent on TDP-43 in order to mature and fully myelinate axons. We also encountered a distinct, TDP-43^{cKO}-specific subtype of differentiated OLs, which is transcriptionally divergent from the closely related, canonical stages of maturation, and is apparently not able to follow the typical transcriptional program to become mature myelinating OLs. Finally, we provide evidence that functional TDP-43 is crucial for the formation and survival of OLs in the spinal cord grey matter (SpC GM), in both developing and adult settings. Altogether, our study provides detailed insight into the requirement of TDP-43 in myelination-competent glia along with in-depth transcriptomic data, which together serve as solid basis for future research.

8. Discussion of Individual Aspects

8.1. TDP-43 and Cell Survival

As pointed out by Jeong et al. (2017), loss of TDP-43 function is generally related to cell death. We have shown that TDP-43 is more expressed in SCs and OLs during early postnatal development compared to later timepoints. Unexpectedly, there was no indication of loss of SCs in *dhh*-cKO or *mpz*-cKO SNs, or for loss of OLs in the *cnp*-cKO SpC white matter (WM). We only observed persistently reduced numbers of differentiated OLs in the *cnp*-cKO SpC GM, and a reduction of these cells in the SpC GM after inducible deletion of TDP-43 in young adult *plp*-iKO mice. We conclude that loss of TDP-43 is not inevitably related to widespread cell death in SCs and differentiated OLs.

Experimental and Cellular Context Might Influence the Impact of TDP-43 Deletion

Studies deleting TDP-43 in neurons using different Cre mouse lines highlight that the observed impact depends on the exact experimental setting: Wu et al. (2012a) deleted TDP-43 in motor neurons during embryonic development using Hb9-Cre. Early recombination resulted in a severe phenotype including pronounced loss of motor neurons and a shortened lifespan. Similar results were reported when the ChAT-IRES-Cre mouse line was used (Donde et al., 2019). Conversely, postnatal loss of TDP-43 by the VAChT-Cre.Fast mouse line did not lead to cell death, but rather motor neuron atrophy and muscle denervation (Iguchi et al., 2013). Mutant mice did not display evident motor deficits within the first 50 weeks of life, and these deficits could only be detected in a Rotarod performance test when mice reached 17 months of age. Deletion of TDP-43 in pyramidal forebrain neurons in the adult mouse brain caused brain atrophy along with astrogliosis in one-year-old mice (Wu et al., 2019). These studies emphasize that cells can experience a very different impact due to TDP-43 ablation, depending on the timing of recombination, the specific cell type, and the microenvironmental context of these cells. Concerning the data on OLs in the current study, it might be that TDP-43 plays somewhat different roles in GM compared to WM SpC OLs, or that the GM microenvironment increases the susceptibility of the resident mutant OLs towards cell death. The development of protocols that enable the specific selection of GM and WM OLs should enable a more detailed comparative evaluation of these OL populations in the future.

8.2. Cryptic Splicing of *neurofascin155*

We have identified *neurofascin 155* (*nfasc155*; protein: NF155, glial Neurofascin) as a major target of TDP-43-mediated repression of cryptic splicing in SCs. We also detected cryptic splicing of *nfasc155* in OLs derived from *cnp*-cKO mice, although only to a lesser degree (Fig. A.11). A previous study showed that efficient ablation of Nfasc in both SCs and OLs in *cnp*Cre^{cKO} mice leads to rapid deterioration, and mutant mice die at P16/17 (Pillai et al., 2009). This further suggests that expression of NF155 is unlikely to be meaningfully affected in the CNS of *cnp*-cKO mice. Systematic evaluation of cryptic splicing events in different cell types of mice (excitatory neurons, skeletal myocytes and *in vitro* embryonic stem cells; Jeong et al., 2017) further elucidated the differential impact of TDP-43 in different cellular contexts. Cryptic splicing events were highly variable and in some cases only present in one cell type although the transcript was also expressed in the others. Different repressors of cryptic splicing, such as PTBP1/2, Rbm17 and Hnrnp L, have been described in the past years (Tan et al., 2016; Ling et al., 2016; McClory et al., 2018). It has been demonstrated with PTBP1 and PTBP2 that different proteins can exert a redundant repression of cryptic splicing (Ling et al., 2016). In this context, hitherto undescribed repressors of cryptic splicing could differently modulate the impact of the loss of TDP-43. Overall, we assume that the different cellular context in OLs and SCs may result in a different set of transcripts being affected by loss of TDP-43, or, as in the case of *nfasc155*, in a different extent to which the same transcript is affected. Regarding *nfasc*, this consequently does not allow us to rule out any functional impact of TDP-43-mediated repression of cryptic splicing in OLs, as *in vitro* experiments by Eisenbach et al. (2009) point out different dynamics in the axon-glia interactions involving glial Neurofascin between SCs and OLs. This implies that Neurofascin is required differently by these two cell types, which may therefore be differentially susceptible to reduced or abolished expression of Neurofascin.

Implications of *neurofascin155* Cryptic Splicing in Peripheral Nerve Function

At least in *mpz*-cKO SNs, the efficient cryptic splicing of *nfas155* resulted in profoundly reduced protein levels. NF155 is a well described cell adhesion, ankyrin-binding protein expressed in myelination-competent glia, where it interacts with neuronal Contactin/Caspr1 in the paranodal complex flanking nodes of Ranvier.

Numerous studies have been dedicated to elucidating the functions of these proteins by deleting individual components (Bhat et al., 2001; Boyle et al., 2001; Rios et al., 2003; Sherman et al., 2005; Pillai et al., 2009; Saifetiarova et al., 2017). Remarkably, these studies consistently report a loss or redistribution of the other paranodal components in concert with the elimination of septate-like junctions between the paranodal loop and the axon, as well as a delocalization of juxtaparanodal potassium channels $K_V1.1$ or $K_V1.2$. In line with these findings, we observed loss of Contactin signal in the paranodal region and redistribution of $K_V1.2$ channels closer to the nodes of Ranvier in *mpz*-cKO SNs. We assume that septate-like junctions are equally lost in these nerves. Boyle et al. (2001) formulated a model, in which the loss of adhesion between the paranodal loops and the axolemma leads to reduced paranodal resistance and increased capacitance, which impairs efficient saltatory conduction. Mice genetically missing the axonal components Contactin/Caspr1 (Bhat et al., 2001; Boyle et al., 2001; Saifetiarova et al., 2017), or NF155 (Pillai et al., 2009; Roche et al., 2014) displayed a major reduction in the nerve conduction velocity and in some cases in the nerve compound action potential. Accordingly, *mpz*-cKO mice presented a strong, robust reduction of the conduction velocity *in vivo*. Furthermore, the compound muscle action potential peak-amplitude was decreased in *mpz*-cKO mice, although the compound sensory nerve action potential was highly variable and therefore only illustrates a trend towards reduction. In summary, this emphasizes the likely causative relation between the impaired impulse conduction in *mpz*-cKO mice and the loss of glial Neurofascin due to cryptic splicing upon loss of TDP-43.

Conservation of TDP-43-Mediated Protection of *neurofascin155*

The evolutionary origin of TDP-43-repressed cryptic exons remains to be elucidated. They are not linked to transposable elements and poorly conserved between mouse and human (Humphrey et al., 2017). It must be noted that the intron sequences incorporating the cryptic exon and it's UG-repeats are not conserved in the human genome. Genomic human and mouse *nfasc* intron sequences aligned poorly, and only the sequence of 8 consecutive bases upstream of the cryptic exon appeared in both species in the relevant region. This implies that our findings regarding Neurofascin cannot be directly transferred to a fundamental function of TDP-43 in human SCs or in TDP-43-related diseases such as ALS. However, our findings with *nfasc155* are relevant in the context of TDP-43 studies that employ mouse models, including those addressing molecular pathomechanisms of ALS. A thorough understanding of murine models and their limitations is required to ultimately distill the findings that are more conserved and potentially more relevant to human health.

8.3. Long-Term Requirement of TDP-43

In this work, we aimed to learn more about the function of TDP-43 during development and in adult animals. Studying the latter in OLs was very limited. The welfare of *cnp*-cKO and *plp*-iKO mice deteriorated in a short time, which constrained our analysis in both systems to a few weeks. Nonetheless, by investigating *plp*-iKO mice in this limited time frame we showed that OL survival and/or myelin maintenance in the SpC GM heavily depends on TDP-43 function. There was no evidence in the WM for impaired myelin maintenance or OL survival within the time frame of six weeks, which contrasts with the conclusions in the developmental study by Wang et al. (2018b). However, we cannot rule out that fully mature OLs in the WM also require normal TDP-43 function, and that we might have detected a more pronounced phenotype in the *plp*-iKO SpC WM if it had been feasible to analyze these mutants after a longer time.

In the PNS, deletion of TDP-43 in SCs led to slowly progressing demyelination and loss of myelination of large caliber axons, which translated to motor dysfunction and muscular atrophy from one year of age. When TDP-43 was deleted during development by the *mpz*Cre driver we additionally observed a striking loss of large caliber axons, indicative of axonal degeneration. Although TDP-43-mediated repression of cryptic splicing is at best poorly conserved between different species (as discussed above), the loss of myelinated large caliber axons intriguingly resembles hallmarks of the pathology seen in amyotrophic lateral sclerosis or corresponding mouse models (Bradley et al., 1983; Fischer et al., 2004; Riva et al., 2014).

Developmental Deletion of TDP-43 in SCs Results in a Stronger Long-Term Phenotype

The long-term consequences in *mpz*-cKO mice are more drastic than in *mpz*-iKO mice, particularly concerning the loss of axons that is only detectable in *mpz*-cKO mice. On the one hand, *mpz*-cKO mice already lack TDP-43 during development, which imposes a potential burden that is not shared by *mpz*-iKO mice. On the other hand, incomplete recombination is a common characteristic of inducible knockout models, and non-recombined SCs could potentially compensate to some extent for the recombined cells: *First*, the presence of a non-recombined fraction of SCs in *mpz*-iKO mice could suffice to provide enough support for sustaining axonal protection. *Second*, gradual demyelination, eventually due to the loss of recombined SCs, could lead to remyelination of axons by non-recombined SCs, leading to a proportional shift towards even more non-recombined SCs in *mpz*-iKO nerves.

In this manner, the nerve might therefore further drift away from the progressively worsening condition. However, we found thinly myelinated axons in root nerves of both *mpz*-cKO and *mpz*-iKO mice, indicating some degree of remyelination with both genotypes. It is worth noting that we interpret the reduction in tdTomato-expressing SCs in one-year-old *mpz*-iKO SNs as turnover, meaning loss of recombined SCs replaced by remyelinating non-recombined SCs. However, it is puzzling that we were unable to detect evidently thinner myelin in the g-ratio analysis of these SNs. It might be that not enough recently remyelinated axons were included in this quantification, or that remyelination occurred over long periods of time that allowed myelin to grow towards a thickness similar enough to levels without remyelination. However, the evidently thinner myelin on some axons populating *mpz*-iKO nerve roots, combined with the presence of demyelinated axons, lends further support to occurrence of easily detectable recent remyelination.

Impact of TDP-43 during PNS Regeneration

In the short term remyelination does not seem to be greatly affected by loss of TDP-43, as we have shown in a sciatic nerve crush injury model. It is of note that due to the inducible deletion of TDP-43, non-recombined SCs could have largely replaced the population of recombined SCs during regeneration. Although it remains to be experimentally addressed, we reason that this is an unlikely possibility: *First*, *mpz*-iKO SCs were comparably efficient in myelin breakdown shortly after the nerve crush. *Second*, *mpz*-cKO SNs only displayed a mild delay in the onset of myelination during development, indicating that the engagement of SCs in the myelinating fate is not markedly affected by the absence of TDP-43. *Finally*, the low turnover of recombined SCs in *mpz*-iKO mice without injury demonstrates that there is no major susceptibility leading to cell death on the short term.

Pronounced Susceptibility of Large Caliber Axons in Root Nerves

In both *mpz*-cKO and *mpz*-iKO aged mice, root nerves were generally more affected than the SN, raising the question of the origin of these differences. In contrast to distal peripheral nerves, SCs of the spinal root nerves arise from an intermediate, neural crest-derived multipotent population designated boundary cap cells (BCCs, Maro et al., 2004). BCCs display early Krox20 expression during embryonic development (Schneider-Maunoury et al., 1993; Wilkinson et al., 1989) and have a distinct gene expression pattern relative to SC precursors in distal nerves (Coulpier et al., 2009). Fragmentary observations in the literature also revealed differential impact of mutations, some of

which on proteins mediating ECM-signaling, between nerve roots and SNs (reviewed by Feltri et al., 2016). However, we currently lack a systematic knowledge of potential differences and their functional basis between BCC-derived myelinating SCs compared to myelinating SCs derived from SC precursors in distal nerves. In this context, we currently cannot rule out a specific susceptibility of SCs in spinal root nerves to the deletion of TDP-43.

Among the root nerves, aberrant features were strikingly concentrated in TDP-43$^{cKO/iKO}$ ventral roots, in which especially large caliber axons were heavily affected. We hypothesize two possible explanations for these intriguing observations: *a)* large caliber axons might harbor different intrinsic demands in myelin maintenance and axonal support versus small caliber axons, or *b)* large caliber motor axons might have different demands for SC-mediated support compared to other large caliber axons and to smaller caliber axons. Both aspects may even contribute to the observed phenotype in dorsal and ventral roots, respectively. Nonetheless, the appearance of vacuolated fibers associated with apparently intact axons raises the possibility that a primary failure in myelin maintenance could precede axonal stress and degeneration.

Potential Mechanistic Basis for Myelin Maintenance and Axonal Support Defects in TDP-43$^{cKO/iKO}$ Schwann Cells

Garcia-Fresco et al. (2006) have shown in the CNS that disruption of the paranodal junction by deletion of either Caspr1 or ceramide galactosyltransferase (CGT) can lead to degeneration of Purkinje neuron axons already at P25. Caspr1 and/or Caspr2 null mice were investigated in a long-term study by Saifetiarova et al. (2017), and displayed sparse myelin abnormalities along with a mild reduction of large caliber axons in the SN from six-month-old animals. In addition, one year-old Caspr1^{KO} and Caspr1/2^{KO} mice displayed evident muscular atrophy (Saifetiarova et al., 2017). Disruption of the node of Ranvier itself by postnatally deleting Neurofascin in neurons caused vacuolation and axonal degeneration, which was exacerbated when Neurofascin was additionally deleted in myelination-competent glial cells (Taylor et al., 2017). In our mouse model of TDP-43 deletion in SCs driven by the regulatory sequence of the *mpz* promoter, nodes of Ranvier are apparently intact and glial Neurofascin is only dramatically reduced in SCs, but not OLs. Therefore, paranodal junctions are only disrupted in the peripheral nerves, and we assume that they are not meaningfully affected in the CNS. Accordingly, a potential failure of axonal support by the loss of Neurofascin in SCs could require a substantially longer time to result in axonal degeneration compared to the published studies. We did not observe pronounced alterations in six-month-old *mpz*-cKO mice, and

pathological changes were most prominent in *mpz*-cKO SNs only in 16-month-old mice. *mpz*-cKO mice at this age also displayed pronounced muscular atrophy. We therefore consider that loss of TDP-43-mediated repression of *nfasc* cryptic splicing is likely to contribute, at least in part, to the long-term pathogenesis in our mouse model.

Metabolic homeostasis has been shown to be crucial for developmental myelination and axonal support (Beirowski et al., 2014). The monocarboxylate-transporter 1 (MCT1) is likely to be specifically required during myelin maintenance, as *mpz*MCT1^{cKO} mice displayed prevalent thinner myelin and ultimately demyelination in sural (distal sensory branch of the sciatic nerve) but not root nerves in 1-year-old mice (Jha et al., 2020). However, Morrison et al. (2015) subjected MCT1$^{wt/null}$ mice to SN crush injury, and observed delayed myelin clearance after one week and thinner myelin after six weeks. As MCT1 is expressed at higher levels in SCs compared to MCT2 and 4 (Domenech-Estevez et al., 2015), and myelin clearance as well as myelin growth was not impaired in *mpz*-iKO mice after SN crush injuries, we assume that an impairment of monocarboxylate transport due to deletion of TDP-43 in SCs is unlikely. Failure in myelin maintenance was further reported in mice with impairments of miRNA biogenesis (Lin et al., 2015; Gokbuget et al., 2018; Li et al., 2018b), formation of Cajal bands (Gillespie et al., 2000; Sherman et al., 2012), or maintenance of mitochondrial function (Viader et al., 2011; Funfschilling et al., 2012; Viader et al., 2013). Noteworthily, TDP-43 has been described to influence mitochondrial dynamics and interacts in mouse and human cells with mitochondrial transcripts ND3 and ND6 (Wang et al., 2013; Wang et al., 2016). In ALS patients, and also in experimental models using disease mutations, ND3 and ND6 are both drastically reduced (Wang et al., 2016). Moreover, mitochondrial dysfunction is a potential consequence of mutations in several ALS-associated genes, and is a feature reported to be associated with ALS (reviewed by Smith et al., 2019). Therefore, it remains a possibility that TDP-43 deletion in SCs also leads to some degree of mitochondrial dysfunction. When taken together, we consider that several aspects discussed above could potentially contribute to the failure in myelin maintenance and axonal support observed in TDP-43^{cKO} mice. Specific analysis of SCs derived from aged *mpz*-cKO mice is necessary to experimentally determine which processes are effectively affected. This would need to be coupled to additional manipulations, including genetic mouse models, that could functionally rescue the phenotype and establish a close functional relation between the affected processes and TDP-43. Albeit fascinating, these experiments on aged mice will be very time-consuming and fall beyond the scope of the current thesis.

8.4. Recombination using the Cre/loxP System

There are intrinsic limitations to Cre/loxP-mediated recombination as a research tool. Vooijs et al. (2001) systematically evaluated the recombination frequency of different substrates containing loxP sites, and revealed pronounced differences even within the same cell type. These differences derive from a potential combination of factors, including the genomic location of the alleles flanked by loxP sites, the distance between the loxP sites, the exact sequences that flank the loxP sites, and the level of Cre activity in the cells. Reporter constructs in the Rosa26 locus display remarkably different recombination efficiencies when crossed with the same Cre lines (Tognatta et al., 2017; Liu et al., 2013). Furthermore, Liu et al. (2013) demonstrated that the ai9 tdTomato reporter line (used in our study, Madisen et al., 2010) recombines most efficiently compared to other commonly used reporter lines. A possible explanation is the very short distance of ~0.8kb between the loxP sites. This is in line with our observations using the *plp*Cre^{ERT2} mouse line, in which Cre activity prior to the administration of tamoxifen is sufficient to recombine the tdTomato reporter transgene in some cells, but not the *Tardbp*^{floxed} alleles.

Recombination in the *cnp*Cre Mouse Line

A recent study of TDP-43 in OLs focused on the demyelinating aspect after P21 using *cnp*-cKO mice (Wang et al., 2018b). By assessing the ROSA26-GNZ reporter line, Wang et al. (2018b) reported that *cnp*Cre drives recombination only in differentiated, CC1^{pos} OLs but not in NG2^{pos} OPCs. In contrast, several previous studies have provided accumulating evidence for effective *cnp*Cre-driven recombination in OPCs (Benninger et al., 2006; Bischof et al., 2015; Madsen et al., 2016; Tognatta et al., 2017). Interestingly, Bischof et al. (2015) noted that most *cnp*Cre^{+} mice expressed Cre in OLs when they began to terminally differentiate. Nevertheless, some mice expressed Cre earlier, *i.e.* in OPCs, and transmitted this feature to their progeny. These observations suggest that there might exist *cnp*Cre mouse sub-lines, with inherently different potential for recombination in OPCs. For the *cnp*-cKO mice used in this study, we provide evidence for some recombination in OPCs: *First*, we were able to collect tdTomato^{pos} OPCs from mice using *cnp*Cre. These cells displayed Pdgfrα protein expression and were able to expand *in vitro*. This provides substantial evidence that Cre is expressed to a degree which is at least sufficient to trigger expression of the easy recombinable tdTomato reporter. *Second*, single-cell RNA sequencing of tdTomato^{pos} OLs from

control and *cnp*-cKO SpCs at P10 revealed a substantial reduction of TDP-43 mRNA in non-mitotic OPCs. We conclude that OPCs in our *cnp*-cKO mice are partially recombined for TDP-43. Since we investigated the same transgenic TDP-43$^{fl/fl}$ mouse line as Wang et al. (2018b), we suggest that the TDP-43 recombination we observe on some OPCs might derive from a different subtype of the *cnp*Cre line used in both studies, or due to the possibly lower recombination efficiency of the GNZ reporter line when compared to the TDP-43^{floxed} allele.

8.5. TDP-43 Is required for Different Aspects of CNS and PNS Development

Although SCs and OLs carry out similar functions in the peripheral and central nervous system, respectively, they are inherently different and unique cell types. We have shown with both the *mpz* and the *dhh*Cre-lines that TDP-43 is required for a timely onset of myelination by SCs. By two months of age, control and *mpz*-cKO mice display fully myelinated SNs with comparable g-ratio. Hence, SCs ultimately achieve developmental myelination *per se* even without TDP-43. Conversely, OLs heavily depend on normal TDP-43 function for proper developmental myelination. This is evident in SpCs at P10, in which lack of TDP-43 in OLs results in fewer myelinated internodes. Furthermore, myelin sheaths in *cnp*-cKO SpCs never grow to the required thickness, and we observed signs of demyelination and widespread vacuolation.

TDP-43 Is Required for Appropriate Oligodendrocyte Maturation

This could derive from an impaired progression of TDP-43 depleted-OLs towards transcriptional late-stages of maturation, or to a transcriptional drift of the mutant OLs towards a new state, not typical of control cells and incompatible with achieving or sustaining efficient maturation. To address the transcriptional heterogeneity and maturation fate of TDP-43-depleted OLs, we performed single cell RNA sequencing. We showed that TDP-43 mRNA is already reduced in non-mitotic OPCs and that a *cnp*-cKO-specific population branches off the normal maturation trajectory during a very early differentiated state. This means that, upon deletion of TDP-43, some OLs still proceed with the typical transcriptional program of maturation, whereas others branch away to a transcriptional program not typical of controls. This transcriptional bifurcation of *cnp*-cKO OLs during maturation is an intriguing discovery, and indicates that not all OLs react uniformly to

the ablation of TDP-43, or that the ablation itself is not exactly synchronized with the cell state. We hypothesize that the exact timing of the loss of TDP-43 function may be relevant. It remains open when TDP-43 proteins are lost to a sufficient extent in each individual OL in *cnp*-cKO mice, and whether the timing of protein depletion dictates the consequences for the transcriptome. Possibly, depending on the exact timing of protein depletion, OLs might or might not still progress through a critical TDP-43-dependent step in very early maturation. The latter might then be unable to mature normally and fall into the observed aberrant state. This hypothesis gathers some support by our observations in *olig2*-cKO mice. Recombination in *olig2*Cre mice is reported to occur earlier than in *cnp*Cre mice, which results in the near-complete absence of $CC1^{pos}$ differentiated OLs. It remains to be elucidated to which extent $Pdgfr\alpha^{neg}$ $CC1^{neg}$ OLs (early-differentiated OLs) are present in *olig2*-cKO mice, and whether they are positive for markers of the TDP-43^{cKO}-specific population. Moreover, following the reasoning proposed above, the supposedly later recombining *cnp*Cre line used by (Wang et al., 2018b) would match with their reported absence of a developmental deficit in *cnp*-cKO SpCs.

Potential Contributors to Transcriptional Bifurcation of TDP-43 Oligodendrocytes

The reasoning of protein depletion timing might be further convoluted by the anatomical distribution of the sequenced cells. As we collected OLs from the whole SpC for RNA sequencing, we do not know which cells in the dataset were extracted from the GM and which from the WM. Perhaps only cells of the GM, or only cells of the WM, contribute to the transcriptome-drifting branch in *cnp*-cKO cells. If so, then it might be that the microenvironment around these cell populations strongly influences the transcriptional consequences of TDP-43 deletion, or it might even be that this regional localization impacts how quickly TDP-43 protein levels are depleted. To evaluate the merit of the various possibilities enumerated above, it will be necessary to evaluate the tissue localization of the TDP-43^{cKO}-population which transcriptionally drifted away from controls, through the use of RNA hybridization probes specific to transcripts of this branch. Apart from developmental studies, there are publicly available single cell or single nucleus RNA sequencing data involving OLs derived from EAE mouse models or MS patients (Falcao et al., 2018; Jakel et al., 2019; Schirmer et al., 2019). Genes that were highly expressed in the *cnp*-cKO-specific population, could so far not be related to any reported OL population in these databases. This is not totally unexpected, as the *cnp*-cKO-specific population is apparently composed of early differentiated OLs, whereas MS/EAE etiologies are mainly associated with adult myelinating OLs.

8.6. OL Differentially Require TDP-43 in a Region-Specific Manner

We observed striking differences in how OLs reacted to loss of TDP-43 in the SpC grey versus white matter. In the WM, *cnp*-cKO OLs accumulated over time, and *plp*-iKO OLs were not markedly affected within six weeks post-tamoxifen. Conversely, GM OLs were reduced at P10 and P50 in *cnp*-cKO mice, and they were strongly diminished in *plp*-iKO mice within the short time frame of six weeks post-tamoxifen, indicating involvement of cell death.

Differential Origin of OPCs

Potential differences that underly these observations include intrinsic differences due to the developmental origin of OLs, or extrinsic differences due to the local environment. SpC OLs emerge from two waves of OPC generation (Tripathi et al., 2011). At P13, ventrally derived OLs are distributed in the whole SpC, whereas dorsally derived OLs are concentrated in the dorsal funiculus and only sparsely found in the grey and ventral white matter. In spite of reported differences regarding physiological properties or protein expression among OL lineage cells (Kleopa et al., 2004; Chittajallu et al., 2004; Karadottir et al., 2008), Tripathi et al. (2011) could not link these properties to potentially corresponding developmental origins. Moreover, comprehensive single cell analysis by Marques et al. (2018) reported that OPCs from all developmental origins converge to a similar transcriptional state, based on the analysis of some brain regions.

Different Microenvironment

Extrinsic local cues and demands may also contribute to our observed differential changes. The GM incorporates the motor neurons and a complex network of interneurons, forming a computational network which integrate signals from afferent sensory fibers and corticospinal neurons (Peirs and Seal, 2016; Wang et al., 2017; Ueno et al., 2018). Axons in the GM are only sparsely myelinated. The context of the WM is markedly different, containing mainly myelinated fibers organized in aligned ascending and descending tracts of axons, without resident neuronal cell bodies, and is mainly geared to quickly transporting information between brain and SpC.

These inherent differences are likely to impose distinctive demands on the OLs. Regarding proliferation, Kang et al. (2013) have shown that OPCs in the P21 and P60 SpC GM divided more than 80 % slower than in the WM. Once established, the population of differentiated OLs remains highly stable during adulthood in various regions of the CNS (Yeung et al., 2014; Fard et al., 2017; Tripathi et al., 2017). In addition, no major differences were reported in the generation of new differentiated OLs between the SpC grey and white matter (Lasiene et al., 2009; Young et al., 2013). Although there is no major turnover of mature OLs, myelin is – at least in the brain – plasticly rearranged throughout life (Yeung et al., 2014; Fard et al., 2017). It remains to be addressed whether the complex network in the SpC GM also demands a higher degree of plasticity in myelination and whether turnover rates of OLs or myelin differ in the SpC white versus the grey matter.

Heterogeneity Among Mature OLs

Mature OLs are not a homogenous population of cells (Marques et al., 2016) and might specify during maturation in a region-dependent manner. An ongoing study by Floriddia and Castelo-Branco (2019) is dedicated to elucidating the prevalence and properties of different sets of mature OLs. They focus on subsets of Klk6^{pos} and of Ptgds^{pos} OLs. In two-month-old mice, Klk6^{pos} OLs are more prevalent in the SpC WM and Ptgds^{pos} OLs in the SpC GM. As shown before, these subtypes of OLs are not derived from a specific wave of OPC generation. Instead, the authors suggested that extrinsic cues contribute to their specification. In two axotomy models, Ptgds^{pos} OLs became more numerous at the injury site and Klk6^{pos} OLs were reduced. Nevertheless, this shift was not observed in EAE mice, and the authors of the study suggest that these OL subtypes exhibit pathology-dependent susceptibility. In relation to our model of TDP-43 deletion, mature OL subtypes such as Ptgds^{pos} OLs may be more susceptible than others. It remains to be elucidated whether the accumulating number of differentiated OLs in the WM of P50 *cnp*-cKO mice belongs to a specific transcriptomic subtype of mature OLs.

Impact of Secondary Changes

Finally, the pronounced differences could arise due to secondary changes within the initially most affected regions. For instance, microglia are known to be capable of providing a pro-regenerative environment in demyelinating mouse models, at least in part due to secreted factors that influence OPC recruitment, proliferation and differentiation (Olah et al., 2012; Voss et al., 2012; Miron et al., 2013; secreted factors reviewed by Miron, 2017). In this line, the study by Giera et al. (2018) reported a microglia-derived trans-glutaminase as ligand for the g-protein coupled receptor Adgrg1 (also known as Gpr56) on OPCs, which promotes proliferation. The pronounced microgliosis in the P50 *cnp*-cKO SpC WM and 6wpT *plp*-iKO GM may drive enhanced proliferation and differentiation, which could in part explain why we observed such a high number of differentiated OLs in the P50 *cnp*-cKO WM and such a strong proliferative response of OPCs in the 6wpT *plp*-iKO GM.

9. Limitations and Future Directions

The experiments presented in this thesis have examined the impact of TDP-43 deletion in the myelination-competent cells of mice. Our results underlie a key requirement for TDP-43 at various stages of both SC and OL biology. Despite the wealth of data we have gathered in this project, there are limitations to the interpretation of our data, and open questions that need to be addressed with future experiments and subsequent projects.

TDP-43 in Schwann Cells

Regarding SCs, we have employed different Cre-mouse lines to evaluate the impact of TDP-43 deletion in radial sorting and onset of myelination. The impairment at the onset of myelination was recapitulated in both lines, but no defects in radial sorting could be detected. As both Cre-lines have successfully revealed radial sorting defects upon recombination of numerous genes in the literature[1,2], we consider it likely that TDP-43 is dispensable for radial sorting. However we cannot draw a firm conclusion in this direction, since there is always a chance that residual TDP-43 protein levels are sufficient to drive the process to the end, and further experiments are required to gather evidence for early loss of TDP-43 function in our mouse mutants.

TDP-43 is required for the timely onset of myelination, but we could not resolve the exact molecular mechanisms that are causal for this mild defect. It would be appealing to further investigate changes in RNA splicing or stability for other genes in order to single out candidates that could underlie this impairment (such as incorrect alternative splicing or reduced stability of key transcriptional promoters of myelination). This could be followed by rescue-type of experiments to validate the functional correlation. However, the very mild delay at the onset of myelination may not enable the readout of a partial experimental rescue, leading to inconclusive experiments.

1 *dhh*-Cre: Benninger et al., 2007; Pereira et al., 2009; Guo et al., 2013a; Guo et al., 2013b; Mogha et al., 2013

2 *mpz*-Cre: Feltri et al., 2002; Chen and Strickland, 2003; Yu et al., 2005; Nodari et al., 2007; Berti et al., 2011; Pellegatta et al., 2013; Elbaz et al., 2016; Ommer et al., 2019

A key mechanistic finding of our study is the TDP-43-mediated repression of intronic sequence (cryptic exon) retention in the mature transcript of glial *neurofascin* (*nfasc155*). This intronic region is poorly conserved between the mouse and human genome, and *nfasc* has hitherto not been reported as a target of TDP-43 in human cells (Tollervey et al., 2011; Xiao et al., 2011). Therefore, we reason that TDP-43-mediated repression of *nfasc* may be specific to mice. Despite this reasoning, we cannot exclude that NF155 in human cells is influenced by TDP-43, even if via more indirect mechanisms. This possibility could be further evaluated by studying human Schwann cells (either primary or derived from induced pluripotent stem cells) with silencing of TDP-43 using CRISPR/Cas9 methods.

Concerning the molecular findings in the current study, our results suggest a direct, causative relation between cryptic splicing of *nfasc155* and impaired juxta-/paranodal domain organization and nerve conduction. However, we still lack direct evidence to support this interpretation. Genomic editing to protect *nfasc* from cryptic splicing (*nfasc*^{prot}), *i.e.* through deletion or modification of the cryptic splice junctions, or the cryptic exon itself, would provide a suitable experimental system to evaluate whether the cryptic exon is key to the reduced abundance of NF155 in *mpz*-cKO mice. This would potentially rescue the formation of juxta-/paranodal domains and ameliorate the impaired nerve conduction properties in these mutants. To further evaluate whether the UG repeats in the *Nfasc* intronic region are functionally required to prevent cryptic splicing in control animals, these could be mutated or excised in the mouse genome. According to our hypothesis, this genetic editing would prevent binding of TDP-43 and should alone mimic the impairments in *nfasc155* described in *mpz*-cKO mice. This mimic- and rescue-type of experiments would provide further evidence for a causative relation between TDP-43, correct splicing of *nfasc155*, and appropriate definition of paranodal domains.

The importance of preserving long-term paranodal junction integrity is exemplified in mouse models with deleted paranodal components (Bhat et al., 2001; Rios et al., 2003; Pillai et al., 2009; Saifetiarova et al., 2017) and the existence of human diseases affecting the paranodal domains, such as subtypes of chronic inflammatory demyelinating polyradiculoneuropathy (CIDP) and Guillain-Barré syndrome (reviewed by Mathey et al., 2015). In the current study, we observed evidence of demyelination and reduced protection of axonal health in aged *mpz*-cKO and *mpz*-iKO mice. However, we do not know which molecular mechanisms are causal to the phenotype in these aged

animals, and to which extent diminished expression of NF155 with disruption of the paranodal domain is a contributing factor. Characterization of adult *mpz*-cKO and *mpz*-iKO mice by methods of global analysis, including sequencing of RNA derived from tissue or sorted SCs from SNs or root nerves, might provide more insight into the affected processes. Furthermore, analysis of aged *nfasc*^{prot} (see above) *mpz*-cKO and *nfasc*^{prot} *mpz*-iKO mice would likely reveal the contribution of *nfasc155* deficiency towards the late-onset demyelination and axonal pathology present in adult *mpz*-cKO and *mpz*-iKO mice. In addition, comparative phenotypic and transcriptomic analysis of these four mouse lines might allow the identification of other relevant and possibly conserved mechanisms in the long-term requirement of TDP-43 in SCs, including some potentially masked in *mpz*-cKO and *mpz*-iKO mice alone.

TDP-43 in Oligodendrocytes

By elucidating the impact of TDP-43 in the OL lineage chronology, the earliest defect we observe is an apparent reduction in the numbers of OPCs and a massive decline of abundance of CC1^{pos} mature OLs in *olig2*-cKO mouse SpCs at P10. These defects are not evident in *cnp*-cKO mice, presumably due to the earlier recombination enabled by *olig2*Cre. This results suggest that TDP-43 might contribute to OPC survival, proliferation, or differentiation. These possibilities could be evaluated by bulk RNA sequencing of the OPC-enriched fraction derived from *olig2*-cKO SpCs. The data could be further analyzed to single out candidate targets of TDP-43 that might underlie OPC defects. In addition, the quantitative tissue analysis performed in *cnp*-cKO mice and presented in this thesis should also be carried out on *olig2*-cKO mice. This also includes the direct analysis of protein TDP-43 protein levels, to ascertain whether it is efficiently depleted in OPCs. Beyond the OPC stage, OL maturation apparently depends on TDP-43 function, and we suggest a critical step within early stages of maturation of OLs that requires TDP-43 function. It is possible that earlier recombination with *olig2*-cKO mice allows a greater fraction of early differentiated OLs to diverge to an abnormal branch, which could contribute to the very low numbers of CC1^{pos} OLs in these mice. To experimentally address this possibility and gain more insight into potential differentiation defects in *olig2*-cKO OPCs, single cell RNA sequencing of *olig2*-cKO OLs should be compared to controls and the existing set of *cnp*-cKO mice. This should identify the differential and common aspects of the transcriptome impact on the OL lineage of both mouse lines.

Culturing OLs derived from *cnp*-cKO mice recapitulated key hallmarks of the findings in *cnp*-cKO mice during development. It remains to be experimentally addressed to which extent *olig2*-cKO OLs and OPCs in culture recapitulate the drastic impact we observed in mouse SpCs. Nonetheless, these cultures are a valuable tool that in principle enables the exploration of the mechanistic basis underlying the function of TDP-43 during OL maturation, and the identification of the functionally relevant domains of TDP-43 in this context, *e.g.* by reconstitution of mutated or truncated variants of TDP-43 in TDP-43^{cKO} OLs.

Early deficits in *cnp*-cKO and *olig2*-cKO mice might disguise critical functions of TDP-43 in OLs at later stages during development. To this end, transgenic mice expressing Cre under control of regulatory sequence from a gene typically expressed in later stages of OL maturation (*e.g.* MOG-iCre mice, Hovelmeyer et al., 2005), or tamoxifen-inducible Cre lines (*e.g.* *plp1*Cre^{ERT2}) combined with early postnatal induction, might be investigated to extend our understanding of TDP-43 in OLs at later stages of maturation and myelin growth.

In the scope of this work, we investigated mouse models of TDP-43 deletion in OLs. But currently we lack knowledge of the extent to which TDP-43 function is conserved in human OLs. To fill this gap, and then further extend the knowledge on TDP-43 in human OLs, ensuing experiments should include the analysis of OLs derived from human induced pluripotent stem cells (iPSCs). Deletion of TDP-43 (*e.g.* using CRISPR/Cas9) in IPS-derived human OPCs could be used to analyze the impact of TDP-43 on the capacity of human OLs to differentiate and undergo maturation in culture, and in living MBP-deficient shiverer mice after transplantation (Ehrlich et al., 2017). Incorporation of IPS-derived OLs from ALS patients harboring TDP-43 mutations (Ferraiuolo et al., 2016) will extend the scope of analysis and allow the comparison of mechanistic changes related to disease mutations with a pure loss of function in these cells.

OLs critically depended on TDP-43 function in a region-specific manner during development and in adult mice, and the welfare of *plp*-iKO mice limits our analysis to 6 weeks after recombination. In this time frame, we did not observe overt failure of myelin maintenance or survival of mature OLs in the WM, even though TDP-43 might be critical in these cells on a longer time frame. To investigate this aspect, an optimal experimental system would need to allow induction of TDP-43 recombination in a time-controlled manner only in WM-resident OLs of the SpC, as GM OLs were evidently reduced in *plp*-iKO mice. However, such a system is currently not established. We speculate that incomplete induction of recombination in *plp*-iKO mice could offer an alternative way to

study mature OLs in the WM of adult mice. With incomplete recombination, critically affected regions might eventually cope with the loss or failure of a fraction of OLs, and consequently maintain mutant animals in better welfare conditions to allow analysis at later timepoints. Incomplete recombination of OLs is a double-edged approach, as it might also conceal evidence of a mild impairment in the WM. Moreover, such an approach would demand Cre-dependent expression of reporter proteins to mark recombined OLs, which would require alternatives to the tdTomato-transgene that recapitulate the recombination efficiency of the TDP-43 allele with higher fidelity.

Extending our findings with the experiments proposed in this section should consolidate our mechanistic understanding of TDP-43 in myelinating glia, and ultimately help to determine which aspects are most relevant in the context of human health and disease.

Part IV

Appendix

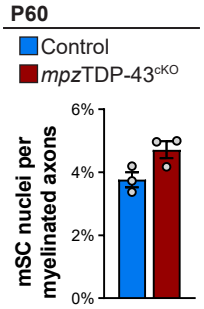

Figure A.1: Deletion of TDP-43 does not lead to significantly more SCs per myelinated internode in nerve cross sections at P60 SN cross sections from control and *mpz*-cKO mice were analysed at P60 by EM. Representative EM images are shown in (Fig. 5.2a). The fraction of observed **nuclei** of myelinating SCs per the total number of myelinated axons (*i.e.* per SC myelinating each internode) was quantified. No significant differences between genotypes were seen, indicating that the overall internodal length cannot be drastically shorter in *mpz*-cKO nerves. **(Statistics)** Bar graphs represent mean±SEM; p = 0.058, n = 3 mice, two-tailed, unpaired Student's t-test.

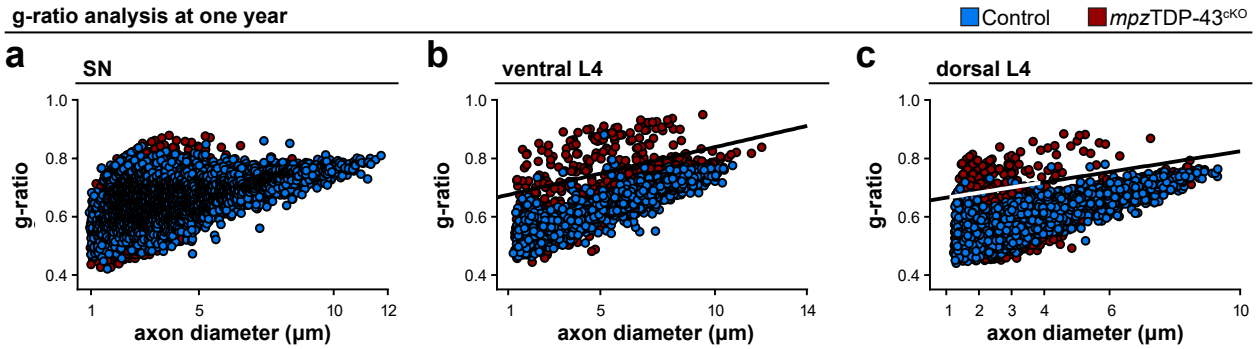

Figure A.2: Control and *mpz*-cKO nerves of 1-year-old mice: scatter plots of g-ratio vs axon caliber Overlay of all measurements of SNs, and dorsal and ventral L4 root nerves from *mpz*-cKO and control mice. n = 5 mice. **(a)** Measurements of *mpz*-cKO SNs largely overlap with those from controls. **(b)** Myelin sheaths of *mpz*-cKO ventral roots are evidently thinner (higher g-ratio) than those of controls in a fraction of myelinated axons across a wide range of axon diameters. **(c)** Plot of g-ratio versus axon diameter of myelinated axons in dorsal root nerves reveals presence of thinly myelinated axons in *mpz*-cKO nerves compared to controls. These are highly prevalent in the small caliber axons of less than 3 µm in diameter.

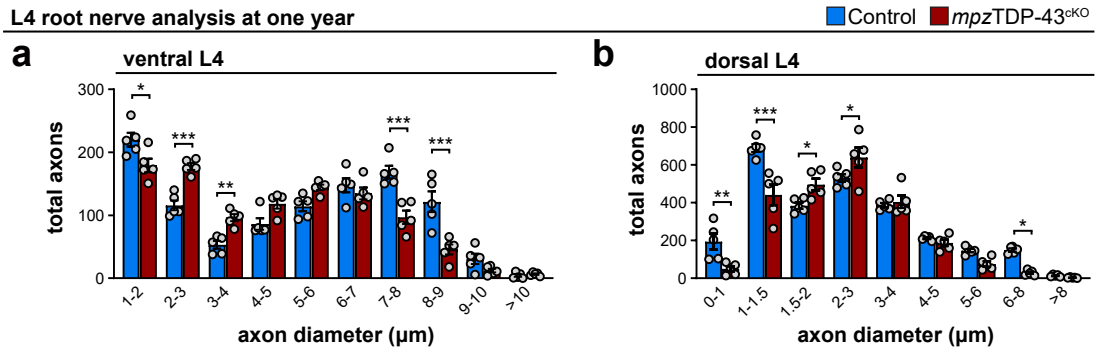

Figure A.3: Diameter-analysis of all axons in L4 root nerves from 1-year-old control and *mpz*-cKO mice. Quantification of diameters from all axons in the ventral **(a)** and dorsal **(b)** root nerves, generally depicts a reduction of axons with large diameters and an increase of axons with small diameters in *mpz*-cKO mice compared to controls. Axons smaller than 1 µm occur only seldom in ventral root nerves (a) and are not displayed. **(Statistics)** Bar graphs represent mean±SEM; *p<0.05, **p<0.01, ***p<0.001. (a,b) n = 5 mice, two-way ANOVA with Šídák's multiple comparisons test.

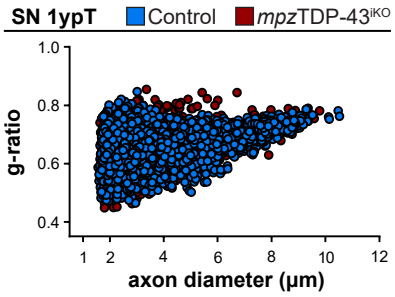

Figure A.4: Control and *mpz*-iKO SNs of mice at 1 year post-tamoxifen: scatter plot of g-ratio vs axon caliber Overlay of all measurements from *mpz*-iKO and control mice do not display a substantial number of myelinated axons with markedly thinner myelin, *i.e.* g-ratio values that are exposed above the cloud of control measurements. n = 5 mice.

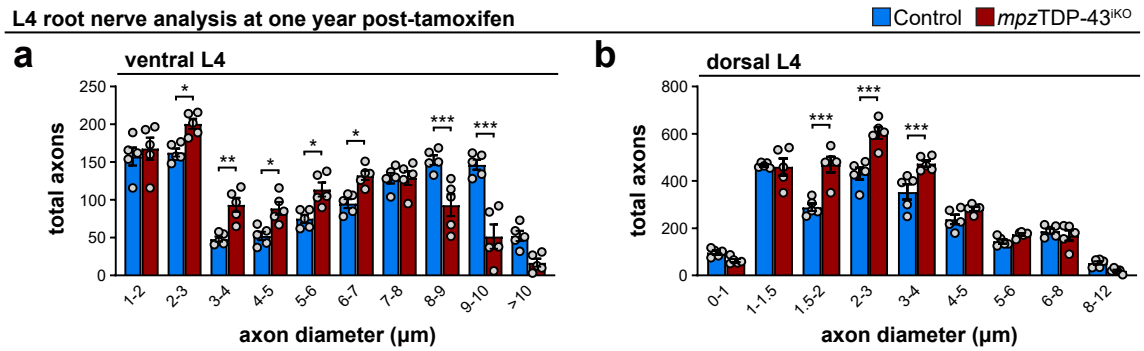

Figure A.5: Diameter-analysis of all axons in L4 root nerves from control and *mpz*-iKO mice at 1 year post-tamoxifen. Quantification of diameters from all axons in the ventral **(a)** and dorsal **(b)** root nerves, depicts a reduction of axons with large diameters in *mpz*-iKO L4 ventral root nerves compared to controls. Axons smaller than 1 µm occur only seldom in ventral root nerves (a) and are not displayed. **(Statistics)** Bar graphs represent mean±SEM; *p<0.05, **p<0.01, ***p<0.001. (a,b) n = 5 mice, two-way ANOVA with Šídák's multiple comparisons test.

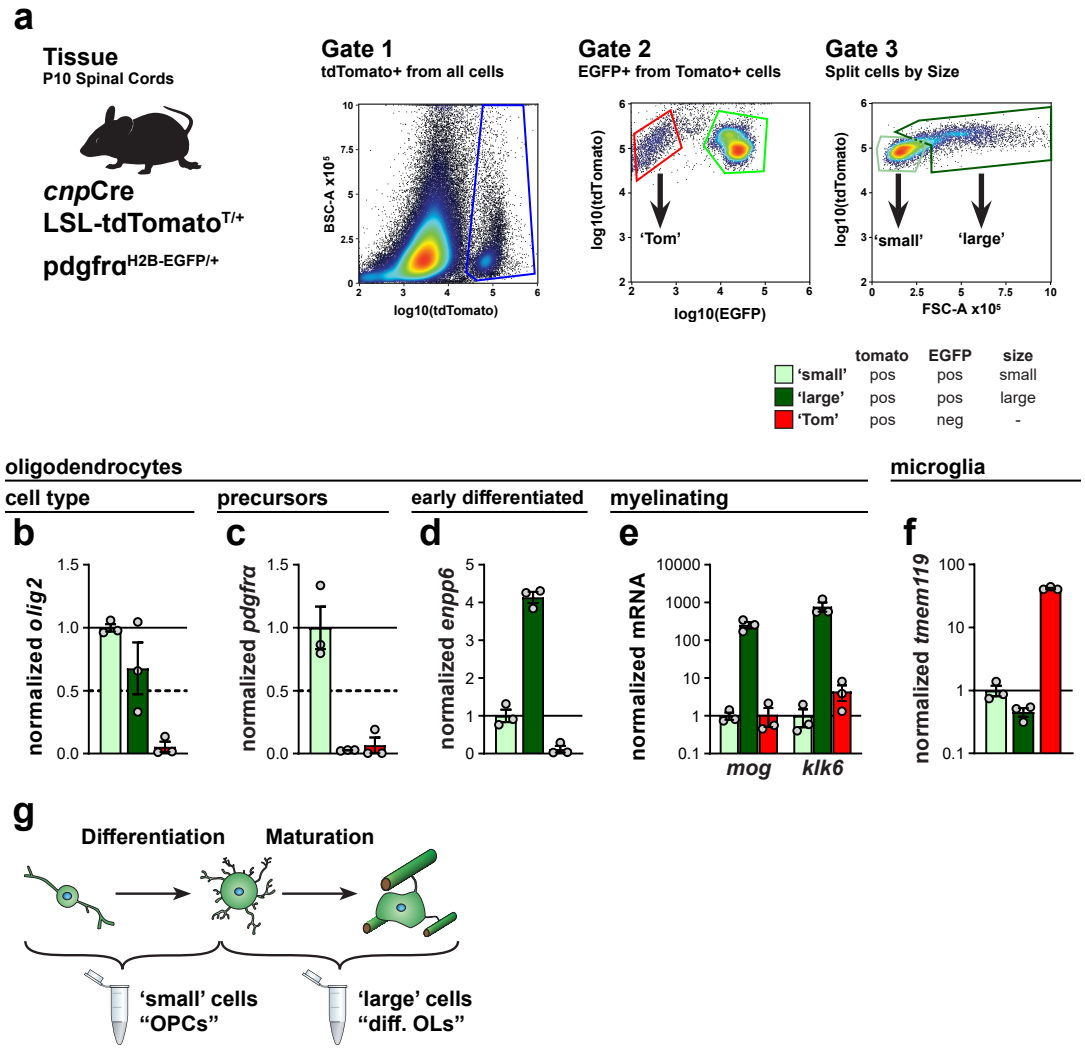

Figure A.6: OPCs and differentiated OLs can be collected separately using cell size as sorting criteria. **(a)** Transgenic mice and sorting strategy. Some experiments were performed using only the tdTomato reporter but not *pdgfrα*H2B-eGFP. In this case all tdTomato^{pos} cells were split by size (FSC-A). **(b-e)** RT-qPCR analysis of different genes expressed in the OL lineage normalized to *βActin*. tdTomato^{pos} GFP^{neg} cells did not display expression of any gene at the expected level (n = 3 mice per sample, mean±SEM, no statistical analysis performed). The OL lineage identity was assessed using *olig2* (b) and *pdgfrα* was used as a marker for OPCs (c). *enpp6* was used as marker for early differentiated, not yet myelinating OLs (d). *mog* and *klk6* are highly expressed in fully mature, myelinating OLs (e). **(f)** RT-qPCR analysis of the microglial marker *tmem119* in the same cells used in (b-e) normalized to *βActin*. *tmem119* was highly expressed only in tdTomato^{pos} GFP^{neg} cells (n = 3 mice per sample, mean±SEM, no statistical analysis performed). **(g)** Inferred separation of OL cells when using their size as indicator for their differentiation state. The two fractions are selectively enriched in either OPCs or OLs. Illustration modified from Goldman and Kuypers (2015).

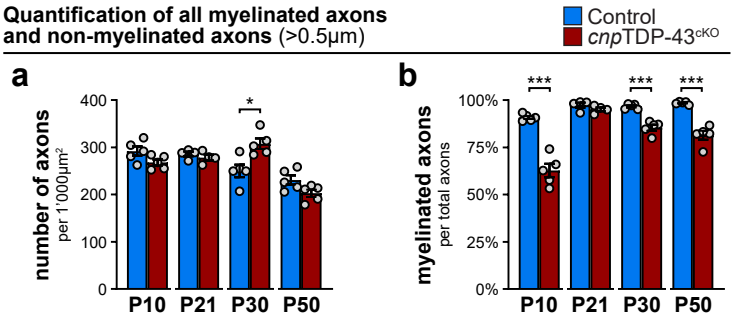

Figure A.7: Total number of axons (non-myelinated axons >0.5 µm in diameter) per area and proportion of myelinated axons in SpCs of *cnp*-cKO and control mice. (a) Total density of myelinated and non-myelinated axons (>0.5 µm in diameter) in analysed fields of ventral WM. Significantly more axons per area were detected in P30 *cnp*-cKO SpCs compared to controls, while other timepoints were not significantly different between genotypes. **(b)** Proportion of myelinated axons among all axons (>0.5 µm in diameter) reveals a significant reduction in the *cnp*-cKO SpC WM compared to controls at P10, P30 and P50, but not P21. (a,b) Individual densities and the schematic of the analysed area is shown in Fig. 6.2. **(Statistics)** Bar graphs represent mean±SEM; *p<0.05, ***p<0.001. (a,b) P21 n = 4 mice, P10,30,50 n = 5 mice; multiple two-tailed, unpaired Student's t-tests corrected using the Holm-Šídák method.

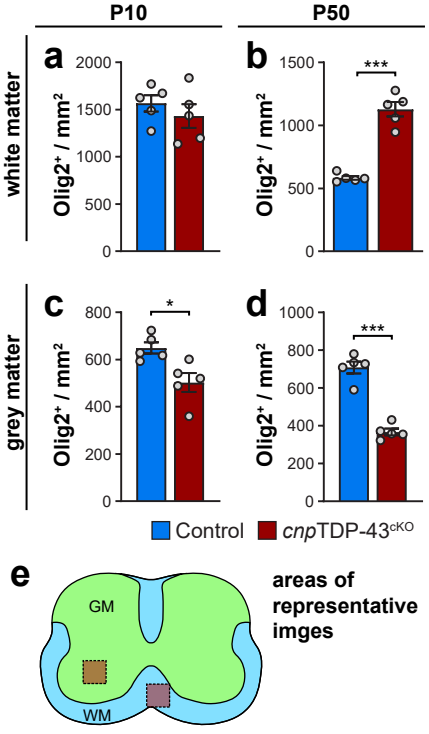

Figure A.8: Total OL numbers in SpCs of control and *cnp*-cKO mice at P10 and P50. Cross-sections of lumbar SpCs were analysed by immunofluorescence using Olig2 to label all OLs. **(a-d)** Densities of OLs in the lumbar SpC white (a,b) and grey matter (c,d) from control and *cnp*-cKO mice at P10 and P50. The number of OLs in the P10 SpC WM was not significantly different between genotypes, whereas OLs were dramatically more numerous in the *cnp*-cKO WM at P50 compared to controls. OL numbers in the SpC GM are reduced in *cnp*-cKO mice at P10 compared to controls, and to a greater extent at P50. **(e)** Scheme of separately analysed areas (WM: blue, GM: green). Squares show areas of exemplary images in Fig. 6.6a-d). **(Statistics)** Bar graphs represent mean±SEM; , *p<0.05, ***p<0.001. (all graphs) n = 5 mice, two-tailed, unpaired Student's t-test.

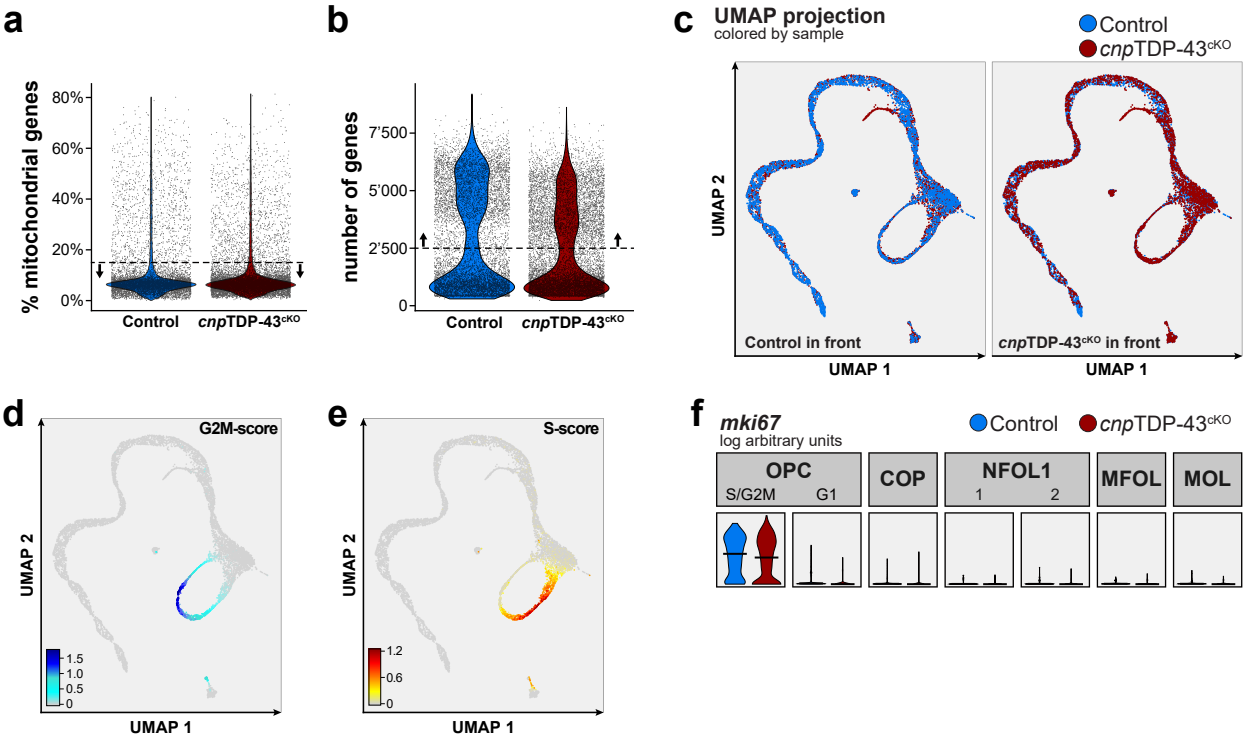

Figure A.9: Quality control and cell cycle analysis on single cell RNA sequencing from control and *cnp*-cKO mice at P10. **(a)** Percentage of mitochondrial genes in *"10X cellranger count"*-processed data. Cells with less than 15% mitochondrial genes were used for further analysis (below dashed line). **(b)** Number of detected genes in *"10X cellranger count"*-processed data. Cells with less than 2'500 genes were used for further analysis (above dashed line). **(c)** UMAP projection of cells that passed the filtering by (a) and (b) and after removing duplicates and clusters with more than 50% classified doublets according to DoubletFinder (McGinnis et al., 2019). Either control cells (left) or *cnp*-cKO cells (right) were moved to the front for better visibility. Apart from a *cnp*-cKO specific cluster, cells are distributed without an evident bias due to the sample origin. **(d,e)** UMAP projections after cell cycle scoring using built in scoring from the Seurat R package (Butler et al., 2018). Scores are separately shown for the G2M phase (d) and the S-Phase (e). **(f)** Violin plot of the expression of *mki67* to represent the proliferating state of the OPC S/G2M cluster.

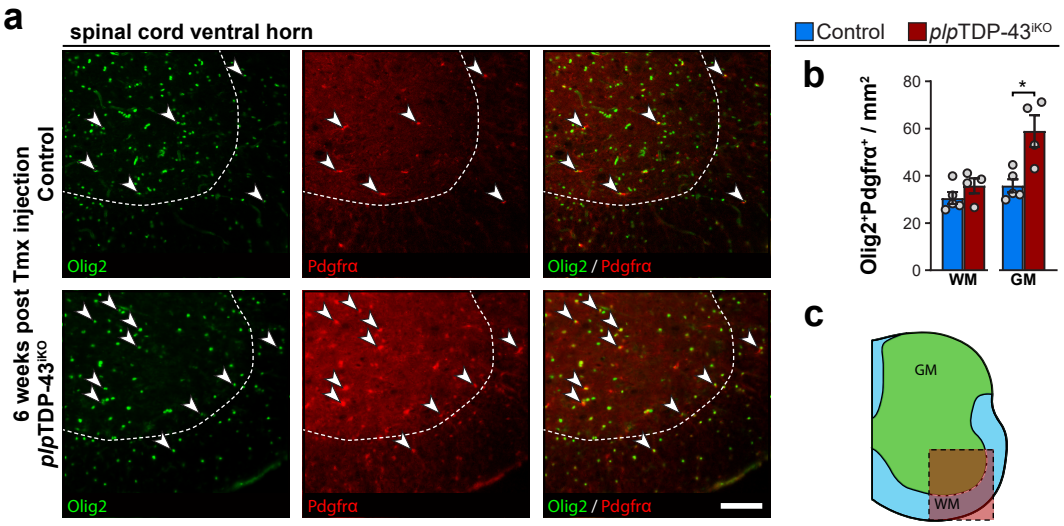

Figure A.10: OPC numbers in SpCs of control and *plp*-iKO mice at 6wpT. (a) Immunofluorescence stainings of Olig2 (green) to label all OLs and Pdgfrα to mark OPCs. Note the reduced number of Olig2^{pos} cells in the GM of *plp*-iKO mice compared to controls. scalebar: 100 µm. **(b)** OPC densities in the lumbar spinal cord white and grey matter from control and *plp*-iKO mice at 6wpT depicts an increase in the GM of *plp*-iKO mice compared to controls. **(c)** Schematic depicting the area of the images shown in (a) and the analysed area (green/blue). **(Statistics)** Bar graphs represent mean±SEM; *p<0.05. (b) n = 5 control and 4 *plp*-iKO mice, two-tailed, unpaired Student's t-test.

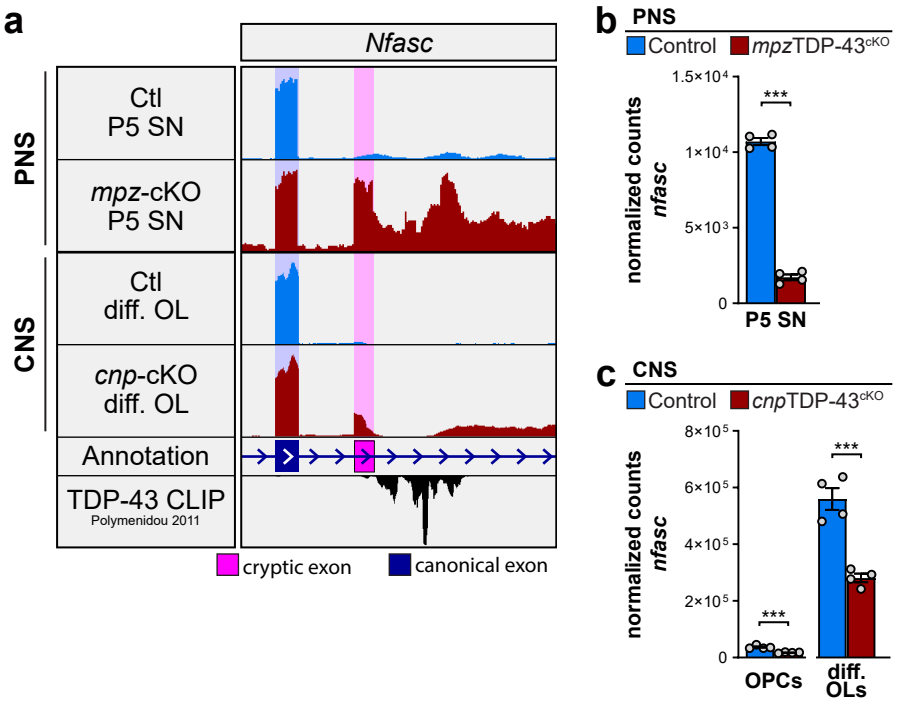

Figure A.11: Cryptic splicing and expression of *nfasc* in SCs and OLs. Cross comparison of transcriptomic data from P5 control and *mpz*-cKO SNs (Fig. 5.5 & 5.6), and sorted OLs enriched for OPCs or differentiated Ols from P10 control and *cnp*-cKO SpCs (Fig. 6.7 & 6.8). **(a)** Coverage of sequencing data around cryptic exon of *nfasc* (purple box) showing proportionally higher coverage in the *mpz*-cKO SN compared to coverage of the neighboring canonical exon (blue box) than in differentiated *cnp*-cKO OLs. The scale was individually adjusted for every sample. TDP-43-coverage is derived from re-analysed mouse brain TDP-43 UV-CLIP data (Polymenidou et al., 2011). **(b,c)** Total *nfasc* quantification of gene expression displayed as normalized counts (n = 4 mice, ***p<0.001, pairwise analysis by EdgeR). (b) Abundance of *nfasc* in *mpz*-cKO SNs is reduced to 16% compared to controls. (c) In OPCs and differentiated OLs from *cnp*-cKO SpC mice, levels of *nfasc* are reduced to 47% and 49% of those in controls, respectively.

Bibliography

Adam SA, Nakagawa T, Swanson MS, Woodruff TK, and Dreyfuss G (1986). "mRNA polyadenylate-binding protein: gene isolation and sequencing and identification of a ribonucleoprotein consensus sequence". *Mol Cell Biol* 6(8):2932–43. DOI: 10.1128/mcb.6.8.2932 (cit. on p. 23).

Adameyko I, Lallemend F, Aquino JB, Pereira JA, Topilko P, Muller T, Fritz N, Beljajeva A, Mochii M, Liste I, Usoskin D, Suter U, Birchmeier C, and Ernfors P (2009). "Schwann cell precursors from nerve innervation are a cellular origin of melanocytes in skin". *Cell* 139(2):366–79. DOI: 10.1016/j.cell.2009.07.049 (cit. on p. 11).

Adlkofer K, Martini R, Aguzzi A, Zielasek J, Toyka KV, and Suter U (1995). "Hypermyelination and demyelinating peripheral neuropathy in Pmp22-deficient mice". *Nat Genet* 11(3):274–80. DOI: 10.1038/ng1195-274 (cit. on p. 10).

Aggarwal S, Snaidero N, Pahler G, Frey S, Sanchez P, Zweckstetter M, Janshoff A, Schneider A, Weil MT, Schaap IA, Gorlich D, and Simons M (2013). "Myelin membrane assembly is driven by a phase transition of myelin basic proteins into a cohesive protein meshwork". *PLoS Biol* 11(6):e1001577. DOI: 10.1371/journal.pbio.1001577 (cit. on p. 10).

Agrawal HC, Sprinkle TJ, and Agrawal D (1990). "2',3'-Cyclic Nucleotide-3'-Phosphodiesterase in the Central-Nervous-System Is Fatty-Acylated by Thioester Linkage". *Journal of Biological Chemistry* 265(20):11849–11853 (cit. on p. 11).

Alami NH, Smith RB, Carrasco MA, Williams LA, Winborn CS, Han SSW, Kiskinis E, Winborn B, Freibaum BD, Kanagaraj A, Clare AJ, Badders NM, Bilican B, Chaum E, Chandran S, Shaw CE, Eggan KC, Maniatis T, and Taylor JP (2014). "Axonal transport of TDP-43 mRNA granules is impaired by ALS-causing mutations". *Neuron* 81(3):536–543. DOI: 10.1016/j.neuron.2013.12.018 (cit. on p. 27).

Anderson P and Kedersha N (2008). "Stress granules: the Tao of RNA triage". *Trends Biochem Sci* 33(3):141–50. DOI: 10.1016/j.tibs.2007.12.003 (cit. on p. 27).

— (2009). "RNA granules: post-transcriptional and epigenetic modulators of gene expression". *Nat Rev Mol Cell Biol* 10(6):430–6. DOI: 10.1038/nrm2694 (cit. on p. 27).

Andres KH (1965). "Uber Die Feinstruktur Besonderer Einrichtungen in Markhaltigen Nervenfasern Des Klienhirns Der Ratte". *Zeitschrift Fur Zellforschung Und Mikroskopische Anatomie* 65(5):701–&. DOI: Doi10.1007/Bf00342591 (cit. on p. 7).

Arai T, Hasegawa M, Akiyama H, Ikeda K, Nonaka T, Mori H, Mann D, Tsuchiya K, Yoshida M, Hashizume Y, and Oda T (2006). "TDP-43 is a component of ubiquitin-positive tau-negative inclusions in frontotemporal lobar degeneration and amyotrophic lateral sclerosis". *Biochem Biophys Res Commun* 351(3):602–11. DOI: 10.1016/j.bbrc.2006.10.093 (cit. on p. 21).

Arthur-Farraj P, Wanek K, Hantke J, Davis CM, Jayakar A, Parkinson DB, Mirsky R, and Jessen KR (2011). "Mouse schwann cells need both NRG1 and cyclic AMP to myelinate". *Glia* 59(5):720–33. DOI: 10.1002/glia.21144 (cit. on p. 12).

Arthur-Farraj PJ, Latouche M, Wilton DK, Quintes S, Chabrol E, Banerjee A, Woodhoo A, Jenkins B, Rahman M, Turmaine M, Wicher GK, Mitter R, Greensmith L, Behrens A, Raivich G, Mirsky R, and Jessen KR (2012). "c-Jun reprograms Schwann cells of injured nerves to generate a repair cell essential for regeneration". *Neuron* 75(4):633–47. DOI: 10.1016/j.neuron.2012.06.021 (cit. on p. 15).

Arthur-Farraj PJ, Morgan CC, Adamowicz M, Gomez-Sanchez JA, Fazal SV, Beucher A, Razzaghi B, Mirsky R, Jessen KR, and Aitman TJ (2017). "Changes in the Coding and Non-coding Transcriptome and DNA Methylome that Define the Schwann Cell Repair Phenotype after Nerve Injury". *Cell Rep* 20(11):2719–2734. DOI: 10.1016/j.celrep.2017.08.064 (cit. on p. 15).

Avendano-Vazquez SE, Dhir A, Bembich S, Buratti E, Proudfoot N, and Baralle FE (2012). "Autoregulation of TDP-43 mRNA levels involves interplay between transcription, splicing, and alternative polyA site selection". *Genes Dev* 26(15):1679–84. DOI: 10.1101/gad.194829.112 (cit. on p. 24).

Ayala YM, De Conti L, Avendano-Vazquez SE, Dhir A, Romano M, D'Ambrogio A, Tollervey J, Ule J, Baralle M, Buratti E, and Baralle FE (2011). "TDP-43 regulates its mRNA levels through a negative feedback loop". *EMBO J* 30(2):277–88. DOI: 10.1038/emboj.2010.310 (cit. on pp. 24, 27).

Ayala YM, Zago P, D'Ambrogio A, Xu YF, Petrucelli L, Buratti E, and Baralle FE (2008). "Structural determinants of the cellular localization and shuttling of TDP-43". *J Cell Sci* 121(Pt 22):3778–85. DOI: 10.1242/jcs.038950 (cit. on p. 24).

Baek D and Green P (2005). "Sequence conservation, relative isoform frequencies, and nonsense-mediated decay in evolutionarily conserved alternative splicing". *Proc Natl Acad Sci U S A* 102(36):12813–8. DOI: 10.1073/pnas.0506139102 (cit. on p. 31).

Bandziulis RJ, Swanson MS, and Dreyfuss G (1989). "RNA-binding proteins as developmental regulators". *Genes Dev* 3(4):431–7. DOI: 10.1101/gad.3.4.431 (cit. on p. 23).

Baraban M, Koudelka S, and Lyons DA (2018). "Ca (2+) activity signatures of myelin sheath formation and growth in vivo". *Nat Neurosci* 21(1):19–23. DOI: 10.1038/s41593-017-0040-x (cit. on p. 19).

Bargmann W and Lindner E (1964). "Über den Feinbau des Nebennierenmarkes des Igels (Erinaceus europaeus L.)" *Zeitschrift für Zellforschung und Mikroskopische Anatomie* 64(6):868–912. DOI: 10.1007/bf00323315 (cit. on p. 7).

Baron W, Shattil SJ, and Constant C ffrench (2002). "The oligodendrocyte precursor mitogen PDGF stimulates proliferation by activation of alpha(v)beta3 integrins". *EMBO J* 21(8):1957–66. DOI: 10.1093/emboj/21.8.1957 (cit. on p. 17).

Barres BA, Burne JF, Holtmann B, Thoenen H, Sendtner M, and Raff MC (1996). "Ciliary neurotrophic factor enhances the rate of oligodendrocyte generation". *Molecular and Cellular Neuroscience* 8(2-3):146–156. DOI: DOI10.1006/mcne.1996.0053 (cit. on p. 17).

Barres BA and Raff MC (1993). "Proliferation of oligodendrocyte precursor cells depends on electrical activity in axons". *Nature* 361(6409):258–60. DOI: 10.1038/361258a0 (cit. on p. 17).

— (1994). "Control of oligodendrocyte number in the developing rat optic nerve". *Neuron* 12(5):935–42. DOI: 10.1016/0896-6273(94)90305-0 (cit. on p. 17).

Barres BA, Raff MC, Gaese F, Bartke I, Dechant G, and Barde YA (1994). "A crucial role for neurotrophin-3 in oligodendrocyte development". *Nature* 367(6461):371–5. DOI: 10.1038/367371a0 (cit. on p. 17).

Barres BA, Schmid R, Sendnter M, and Raff MC (1993). "Multiple extracellular signals are required for long-term oligodendrocyte survival". *Development* 118(1):283–95 (cit. on p. 17).

Barros LF and Weber B (2018). "CrossTalk proposal: an important astrocyte-to-neuron lactate shuttle couples neuronal activity to glucose utilisation in the brain". *J Physiol* 596(3):347–350. DOI: 10.1113/JP274944 (cit. on p. 19).

Bechler ME, Byrne L, and Ffrench-Constant C (2015). "CNS Myelin Sheath Lengths Are an Intrinsic Property of Oligodendrocytes". *Curr Biol* 25(18):2411–6. DOI: 10.1016/j.cub.2015.07.056 (cit. on p. 18).

Bechler ME and Constant C ffrench (2014). "Neuroscience. A new wrap for neuronal activity?" *Science* 344(6183):480–1. DOI: 10.1126/science.1254446 (cit. on p. 9).

Beirowski B, Babetto E, Golden JP, Chen YJ, Yang K, Gross RW, Patti GJ, and Milbrandt J (2014). "Metabolic regulator LKB1 is crucial for Schwann cell-mediated axon maintenance". *Nat Neurosci* 17(10):1351–61. DOI: 10.1038/nn.3809 (cit. on pp. 14, 130).

Beirowski B, Wong KM, Babetto E, and Milbrandt J (2017). "mTORC1 promotes proliferation of immature Schwann cells and myelin growth of differentiated Schwann cells". *Proc Natl Acad Sci U S A* 114(21):E4261–E4270. DOI: 10.1073/pnas.1620761114 (cit. on p. 14).

Benninger Y, Colognato H, Thurnherr T, Franklin RJ, Leone DP, Atanasoski S, Nave KA, Ffrench-Constant C, Suter U, and Relvas JB (2006). "Beta1-integrin signaling mediates premyelinating oligodendrocyte survival but is not required for CNS myelination and remyelination". *J Neurosci* 26(29):7665–73. DOI: 10.1523/JNEUROSCI.0444-06.2006 (cit. on pp. 9, 131).

Benninger Y, Thurnherr T, Pereira JA, Krause S, Wu X, Chrostek-Grashoff A, Herzog D, Nave KA, Franklin RJ, Meijer D, Brakebusch C, Suter U, and Relvas JB (2007). "Essential and distinct roles for cdc42 and rac1 in the regulation of Schwann cell biology during peripheral nervous system development". *J Cell Biol* 177(6):1051–61. DOI: 10.1083/jcb.200610108 (cit. on p. 137).

Berget SM, Moore C, and Sharp PA (1977). "Spliced segments at the 5' terminus of adenovirus 2 late mRNA". *Proc Natl Acad Sci U S A* 74(8):3171–5. DOI: 10.1073/pnas.74.8.3171 (cit. on p. 29).

Bermingham J. R. J, Scherer SS, O'Connell S, Arroyo E, Kalla KA, Powell FL, and Rosenfeld MG (1996). "Tst-1/Oct-6/SCIP regulates a unique step in peripheral myelination and is required for normal respiration". *Genes Dev* 10(14):1751–62. DOI: 10.1101/gad.10.14.1751 (cit. on p. 13).

Berti C, Bartesaghi L, Ghidinelli M, Zambroni D, Figlia G, Chen ZL, Quattrini A, Wrabetz L, and Feltri ML (2011). "Non-redundant function of dystroglycan and beta1 integrins in radial sorting of axons". *Development* 138(18):4025–37. DOI: 10.1242/dev.065490 (cit. on p. 137).

Beyer AL, Christensen ME, Walker BW, and LeStourgeon WM (1977). "Identification and characterization of the packaging proteins of core 40S hnRNP particles". *Cell* 11(1):127–38. DOI: 10.1016/0092-8674(77)90323-3 (cit. on p. 24).

Bhat MA, Rios JC, Lu Y, Garcia-Fresco GP, Ching W, St Martin M, Li J, Einheber S, Chesler M, Rosenbluth J, Salzer JL, and Bellen HJ (2001). "Axon-glia interactions and the domain organization of myelinated axons requires neurexin IV/Caspr/Paranodin". *Neuron* 30(2):369–83. DOI: 10.1016/s0896-6273(01)00294-x (cit. on pp. 126, 138).

Bhuiyan SA, Ly S, Phan M, Huntington B, Hogan E, Liu CC, Liu J, and Pavlidis P (2018). "Systematic evaluation of isoform function in literature reports of alternative splicing". *BMC Genomics* 19(1). DOI: 10.1186/s12864-018-5013-2 (cit. on p. 30).

Bird TD, Farrell DF, and Sumi SM (1978). "Brain lipid composition of the shiverer mouse: (genetic defect in myelin development)". *J Neurochem* 31(1):387–91. DOI: 10.1111/j.1471-4159.1978.tb12479.x (cit. on p. 10).

Bischof M, Weider M, Kuspert M, Nave KA, and Wegner M (2015). "Brg1-dependent chromatin remodelling is not essentially required during oligodendroglial differentiation". *J Neurosci* 35(1):21–35. DOI: 10.1523/JNEUROSCI.1468-14.2015 (cit. on p. 131).

Blokhuis AM, Koppers M, Groen EJ, Heuvel DM van den, Dini Modigliani S, Anink JJ, Fumoto K, Diggelen F van, Snelting A, Sodaar P, Verheijen BM, Demmers JA, Veldink JH, Aronica E, Bozzoni I, Hertog J den, Berg LH van den, and Pasterkamp RJ (2016). "Comparative interactomics analysis of different ALS-associated proteins identifies converging molecular pathways". *Acta Neuropathol* 132(2):175–96. DOI: 10.1007/s00401-016-1575-8 (cit. on p. 27).

Büngner O von (1890). *Über die Degenerations- und Regenerationsvorgänge am Nerven nach Verletzungen*. Fischer (cit. on p. 15).

Bolger AM, Lohse M, and Usadel B (2014). "Trimmomatic: a flexible trimmer for Illumina sequence data". *Bioinformatics* 30(15):2114–20. DOI: 10.1093/bioinformatics/btu170 (cit. on p. 47).

Boutz PL, Bhutkar A, and Sharp PA (2015). "Detained introns are a novel, widespread class of post-transcriptionally spliced introns". *Genes Dev* 29(1):63–80. DOI: 10.1101/gad.247361.114 (cit. on p. 31).

Boyle MET, Berglund EO, Murai KK, Weber L, Peles E, and Ranscht B (2001). "Contactin orchestrates assembly of the septate-like junctions at the paranode in myelinated peripheral nerve". *Neuron* 30(2):385–397. DOI: Doi10.1016/S0896-6273(01)00296-3 (cit. on pp. 63, 126).

Bozzo F, Salvatori I, Iacovelli F, Mirra A, Rossi S, Cozzolino M, Falconi M, Valle C, and Carri MT (2016). "Structural insights into the multi-determinant aggregation of TDP-43 in motor neuron-like cells". *Neurobiol Dis* 94:63–72. DOI: 10.1016/j.nbd.2016.06.006 (cit. on p. 28).

Bradley WG, Good P, Rasool CG, and Adelman LS (1983). "Morphometric and biochemical studies of peripheral nerves in amyotrophic lateral sclerosis". *Ann Neurol* 14(3):267–77. DOI: 10.1002/ana.410140304 (cit. on p. 127).

Braun PE, De Angelis D, Shtybel WW, and Bernier L (1991). "Isoprenoid modification permits 2',3'-cyclic nucleotide 3'-phosphodiesterase to bind to membranes". *J Neurosci Res* 30(3):540–4. DOI: 10.1002/jnr.490300311 (cit. on p. 11).

Braunschweig U, Barbosa-Morais NL, Pan Q, Nachman EN, Alipanahi B, Gonatopoulos-Pournatzis T, Frey B, Irimia M, and Blencowe BJ (2014). "Widespread intron retention in mammals functionally tunes transcriptomes". *Genome Res* 24(11):1774–86. DOI: 10.1101/gr.177790.114 (cit. on p. 31).

Bray NL, Pimentel H, Melsted P, and Pachter L (2016). "Near-optimal probabilistic RNA-seq quantification". *Nat Biotechnol* 34(5):525–7. DOI: 10.1038/nbt.3519 (cit. on p. 47).

Bremer M, Frob F, Kichko T, Reeh P, Tamm ER, Suter U, and Wegner M (2011). "Sox10 is required for Schwann-cell homeostasis and myelin maintenance in the adult peripheral nerve". *Glia* 59(7):1022–32. DOI: 10.1002/glia.21173 (cit. on p. 14).

Brettschneider J, Arai K, Del Tredici K, Toledo JB, Robinson JL, Lee EB, Kuwabara S, Shibuya K, Irwin DJ, Fang L, Van Deerlin VM, Elman L, McCluskey L, Ludolph AC, Lee VM, Braak H, and Trojanowski JQ (2014). "TDP-43 pathology and neuronal loss in amyotrophic lateral sclerosis spinal cord". *Acta Neuropathol* 128(3):423–37. DOI: 10.1007/s00401-014-1299-6 (cit. on p. 22).

Brew HM, Gittelman JX, Silverstein RS, Hanks TD, Demas VP, Robinson LC, Robbins CA, McKee-Johnson J, Chiu SY, Messing A, and Tempel BL (2007). "Seizures and reduced life span in mice lacking the potassium channel subunit Kv1.2, but hypoexcitability and enlarged Kv1 currents in auditory neurons". *J Neurophysiol* 98(3):1501–25. DOI: 10.1152/jn.00640.2006 (cit. on p. 7).

Brew HM, Hallows JL, and Tempel BL (2003). "Hyperexcitability and reduced low threshold potassium currents in auditory neurons of mice lacking the channel subunit Kv1.1". *J Physiol* 548(Pt 1):1–20. DOI: 10.1113/jphysiol.2002.035568 (cit. on p. 7).

Briscoe J and Novitch BG (2008). "Regulatory pathways linking progenitor patterning, cell fates and neurogenesis in the ventral neural tube". *Philos Trans R Soc Lond B Biol Sci* 363(1489):57–70. DOI: 10.1098/rstb.2006.2012 (cit. on p. 16).

Britsch S, Goerich DE, Riethmacher D, Peirano RI, Rossner M, Nave KA, Birchmeier C, and Wegner M (2001). "The transcription factor Sox10 is a key regulator of peripheral glial development". *Genes Dev* 15(1):66–78. DOI: 10.1101/gad.186601 (cit. on p. 13).

Brooks BR, Thisted RA, Appel SH, Bradley WG, Olney RK, Berg JE, Pope LE, and Smith RA (2004). "Treatment of pseudobulbar affect in ALS with dextromethorphan/quinidine". *A randomized trial* 63(8):1364–1370. DOI: 10.1212/01.Wnl.0000142042.50528.2f (cit. on p. 22).

Brown AM, Wender R, and Ransom BR (2001). "Metabolic substrates other than glucose support axon function in central white matter". *J Neurosci Res* 66(5):839–43. DOI: 10.1002/jnr.10081 (cit. on p. 19).

Brugger V, Duman M, Bochud M, Munger E, Heller M, Ruff S, and Jacob C (2017). "Delaying histone deacetylase response to injury accelerates conversion into repair Schwann cells and nerve regeneration". *Nat Commun* 8:14272. DOI: 10.1038/ncomms14272 (cit. on p. 15).

Brugger V, Engler S, Pereira JA, Ruff S, Horn M, Welzl H, Munger E, Vaquie A, Sidiropoulos PN, Egger B, Yotovski P, Filgueira L, Somandin C, Luhmann TC, D'Antonio M, Yamaguchi T, Matthias P, Suter U, and Jacob C (2015). "HDAC1/2-Dependent P0 Expression Maintains Paranodal and Nodal Integrity Independently of Myelin Stability through Interactions with Neurofascins". *PLoS Biol* 13(9):e1002258. DOI: 10.1371/journal.pbio.1002258 (cit. on pp. 9, 14, 78).

Bujalka H, Koenning M, Jackson S, Perreau VM, Pope B, Hay CM, Mitew S, Hill AF, Lu QR, Wegner M, Srinivasan R, Svaren J, Willingham M, Barres BA, and Emery B (2013). "MYRF is a membrane-associated transcription factor that autoproteolytically cleaves to directly activate myelin genes". *PLoS Biol* 11(8):e1001625. DOI: 10.1371/journal.pbio.1001625 (cit. on p. 19).

Bullock PN and Rome LH (1990). "Glass micro-fibers: a model system for study of early events in myelination". *J Neurosci Res* 27(3):383–93. DOI: 10.1002/jnr.490270317 (cit. on p. 18).

Bullock TH, Moore JK, and Fields RD (1984). "Evolution of Myelin Sheaths - Both Lamprey and Hagfish Lack Myelin". *Neuroscience Letters* 48(2):145–148. DOI: Doi10.1016/0304-3940(84)90010-7 (cit. on p. 5).

Buratti E (2018). "TDP-43 post-translational modifications in health and disease". *Expert Opin Ther Targets* 22(3):279–293. DOI: 10.1080/14728222.2018.1439923 (cit. on p. 27).

Buratti E and Baralle FE (2001). "Characterization and functional implications of the RNA binding properties of nuclear factor TDP-43, a novel splicing regulator of CFTR exon 9". *J Biol Chem* 276(39):36337–43. DOI: 10.1074/jbc.M104236200 (cit. on pp. 24, 26, 99, 122).

Buratti E, Brindisi A, Pagani F, and Baralle FE (2004). "Nuclear factor TDP-43 binds to the polymorphic TG repeats in CFTR intron 8 and causes skipping of exon 9: a functional link with disease penetrance". *Am J Hum Genet* 74(6): 1322–5. DOI: 10.1086/420978 (cit. on p. 26).

Buratti E, Dork T, Zuccato E, Pagani F, Romano M, and Baralle FE (2001). "Nuclear factor TDP-43 and SR proteins promote in vitro and in vivo CFTR exon 9 skipping". *EMBO J* 20(7):1774–84. DOI: 10.1093/emboj/20.7.1774 (cit. on pp. 26, 99, 122).

Burrell JR, Kiernan MC, Vucic S, and Hodges JR (2011). "Motor neuron dysfunction in frontotemporal dementia". *Brain* 134(Pt 9):2582–94. DOI: 10.1093/brain/awr195 (cit. on p. 20).

Butler A, Hoffman P, Smibert P, Papalexi E, and Satija R (2018). "Integrating single-cell transcriptomic data across different conditions, technologies, and species". *Nat Biotechnol* 36(5):411–420. DOI: 10.1038/nbt.4096 (cit. on pp. 48, 104, V).

Cai J, Qi Y, Hu X, Tan M, Liu Z, Zhang J, Li Q, Sander M, and Qiu M (2005). "Generation of oligodendrocyte precursor cells from mouse dorsal spinal cord independent of Nkx6 regulation and Shh signaling". *Neuron* 45(1):41–53. DOI: 10.1016/j.neuron.2004.12.028 (cit. on p. 16).

Calabretta S, Vogel G, Yu Z, Choquet K, Darbelli L, Nicholson TB, Kleinman CL, and Richard S (2018). "Loss of PRMT5 Promotes PDGFRalpha Degradation during Oligodendrocyte Differentiation and Myelination". *Dev Cell* 46(4):426–440 e5. DOI: 10.1016/j.devcel.2018.06.025 (cit. on p. 108).

Calver AR, Hall AC, Yu WP, Walsh FS, Heath JK, Betsholtz C, and Richardson WD (1998). "Oligodendrocyte population dynamics and the role of PDGF in vivo". *Neuron* 20(5):869–82. DOI: 10.1016/s0896-6273(00)80469-9 (cit. on p. 17).

Casafont I, Bengoechea R, Tapia O, Berciano MT, and Lafarga M (2009). "TDP-43 localizes in mRNA transcription and processing sites in mammalian neurons". *J Struct Biol* 167(3):235–41. DOI: 10.1016/j.jsb.2009.06.006 (cit. on p. 26).

Cascella R, Capitini C, Fani G, Dobson CM, Cecchi C, and Chiti F (2016). "Quantification of the Relative Contributions of Loss-of-function and Gain-of-function Mechanisms in TAR DNA-binding Protein 43 (TDP-43) Proteinopathies". *J Biol Chem* 291(37):19437–48. DOI: 10.1074/jbc.M116.737726 (cit. on p. 122).

Cassel JA and Reitz AB (2013). "Ubiquilin-2 (UBQLN2) binds with high affinity to the C-terminal region of TDP-43 and modulates TDP-43 levels in H4 cells: characterization of inhibition by nucleic acids and 4-aminoquinolines". *Biochim Biophys Acta* 1834(6):964–71. DOI: 10.1016/j.bbapap.2013.03.020 (cit. on p. 28).

Castelfranco AM and Hartline DK (2016). "Evolution of rapid nerve conduction". *Brain Res* 1641(Pt A):11–33. DOI: 10.1016/j.brainres.2016.02.015 (cit. on p. 5).

Catenaccio A, Llavero Hurtado M, Diaz P, Lamont DJ, Wishart TM, and Court FA (2017). "Molecular analysis of axonal-intrinsic and glial-associated co-regulation of axon degeneration". *Cell Death Dis* 8(11):e3166. DOI: 10.1038/cddis.2017.489 (cit. on p. 15).

Chang CK, Chiang MH, Toh EK, Chang CF, and Huang TH (2013). "Molecular mechanism of oxidation-induced TDP-43 RRM1 aggregation and loss of function". *FEBS Lett* 587(6):575–82. DOI: 10.1016/j.febslet.2013.01.038 (cit. on p. 28).

Chen S, Velardez MO, Warot X, Yu ZX, Miller SJ, Cros D, and Corfas G (2006). "Neuregulin 1-erbB signaling is necessary for normal myelination and sensory function". *J Neurosci* 26(12):3079–86. DOI: 10.1523/JNEUROSCI.3785-05.2006 (cit. on p. 9).

Chen ZL and Strickland S (2003). "Laminin gamma1 is critical for Schwann cell differentiation, axon myelination, and regeneration in the peripheral nerve". *J Cell Biol* 163(4):889–99. DOI: 10.1083/jcb.200307068 (cit. on p. 137).

Chiang PM, Ling J, Jeong YH, Price DL, Aja SM, and Wong PC (2010). "Deletion of TDP-43 down-regulates Tbc1d1, a gene linked to obesity, and alters body fat metabolism". *Proc Natl Acad Sci U S A* 107(37):16320–4. DOI: 10.1073/pnas.1002176107 (cit. on pp. 35, 110, 122).

Chittajallu R, Aguirre A, and Gallo V (2004). "NG2-positive cells in the mouse white and grey matter display distinct physiological properties". *J Physiol* 561(Pt 1):109–22. DOI: 10.1113/jphysiol.2004.074252 (cit. on p. 134).

Chizhikov VV and Millen KJ (2005). "Roof plate-dependent patterning of the vertebrate dorsal central nervous system". *Dev Biol* 277(2):287–95. DOI: 10.1016/j.ydbio.2004.10.011 (cit. on p. 16).

Chomiak T and Hu B (2009). "What is the optimal value of the g-ratio for myelinated fibers in the rat CNS? A theoretical approach". *PLoS One* 4(11):e7754. DOI: 10.1371/journal.pone.0007754 (cit. on p. 9).

Chong SY, Rosenberg SS, Fancy SP, Zhao C, Shen YA, Hahn AT, McGee AW, Xu X, Zheng B, Zhang LI, Rowitch DH, Franklin RJ, Lu QR, and Chan JR (2012). "Neurite outgrowth inhibitor Nogo-A establishes spatial segregation and extent of oligodendrocyte myelination". *Proc Natl Acad Sci U S A* 109(4):1299–304. DOI: 10.1073/pnas.1113540109 (cit. on p. 18).

Chow LT, Gelinas RE, Broker TR, and Roberts RJ (1977). "An amazing sequence arrangement at the 5′ ends of adenovirus 2 messenger RNA". *Cell* 12(1):1–8. DOI: 10.1016/0092-8674(77)90180-5 (cit. on p. 29).

Clement AM, Nguyen MD, Roberts EA, Garcia ML, Boillee S, Rule M, McMahon AP, Doucette W, Siwek D, Ferrante RJ, Brown R. H. J, Julien JP, Goldstein LS, and Cleveland DW (2003). "Wild-type nonneuronal cells extend survival of SOD1 mutant motor neurons in ALS mice". *Science* 302(5642):113–7. DOI: 10.1126/science.1086071 (cit. on p. 22).

Cohen RI, Marmur R, Norton WT, Mehler MF, and Kessler JA (1996). "Nerve growth factor and neurotrophin-3 differentially regulate the proliferation and survival of developing rat brain oligodendrocytes". *J Neurosci* 16(20): 6433–42 (cit. on p. 17).

Cohen TJ, Hwang AW, Unger T, Trojanowski JQ, and Lee VM (2012). "Redox signalling directly regulates TDP-43 via cysteine oxidation and disulphide cross-linking". *EMBO J* 31(5):1241–52. DOI: 10.1038/emboj.2011.471 (cit. on p. 28).

Colombrita C, Onesto E, Megiorni F, Pizzuti A, Baralle FE, Buratti E, Silani V, and Ratti A (2012). "TDP-43 and FUS RNA-binding proteins bind distinct sets of cytoplasmic messenger RNAs and differently regulate their post-transcriptional fate in motoneuron-like cells". *J Biol Chem* 287(19):15635–47. DOI: 10.1074/jbc.M111.333450 (cit. on p. 27).

Colombrita C, Zennaro E, Fallini C, Weber M, Sommacal A, Buratti E, Silani V, and Ratti A (2009). "TDP-43 is recruited to stress granules in conditions of oxidative insult". *J Neurochem* 111(4):1051–61. DOI: 10.1111/j.1471-4159.2009.06383.x (cit. on p. 27).

Compston A and Coles A (2008). "Multiple sclerosis". *The Lancet* 372(9648):1502–1517. DOI: 10.1016/s0140-6736(08)61620-7 (cit. on p. 20).

Cornett KMD, Menezes MP, Shy RR, Moroni I, Pagliano E, Pareyson D, Estilow T, Yum SW, Bhandari T, Muntoni F, Laura M, Reilly MM, Finkel RS, Eichinger KJ, Herrmann DN, Bray P, Halaki M, Shy ME, and Burns J (2017). "Natural history of Charcot-Marie-Tooth disease during childhood". *Ann Neurol* 82(3):353–359. DOI: 10.1002/ana.25009 (cit. on p. 20).

Costessi L, Porro F, Iaconcig A, and Muro AF (2014). "TDP-43 regulates beta-adducin (Add2) transcript stability". *RNA Biol* 11(10):1280–90. DOI: 10.1080/15476286.2014.996081 (cit. on p. 27).

Coulpier F, Le Crom S, Maro GS, Manent J, Giovannini M, Maciorowski Z, Fischer A, Gessler M, Charnay P, and Topilko P (2009). "Novel features of boundary cap cells revealed by the analysis of newly identified molecular markers". *Glia* 57(13):1450–7. DOI: 10.1002/glia.20862 (cit. on p. 128).

Cunningham F, Achuthan P, Akanni W, Allen J, Amode MR, Armean IM, Bennett R, Bhai J, Billis K, Boddu S, Cummins C, Davidson C, Dodiya KJ, Gall A, Giron CG, Gil L, Grego T, Haggerty L, Haskell E, Hourlier T, Izuogu OG, Janacek SH, Juettemann T, Kay M, Laird MR, Lavidas I, Liu Z, Loveland JE, Marugan JC, Maurel T, McMahon AC, Moore B, Morales J, Mudge JM, Nuhn M, Ogeh D, Parker A, Parton A, Patricio M, Abdul Salam AI, Schmitt BM, Schuilenburg H, Sheppard D, Sparrow H, Stapleton E, Szuba M, Taylor K, Threadgold G, Thormann A, Vullo A, Walts B, Winterbottom A, Zadissa A, Chakiachvili M, Frankish A, Hunt SE, Kostadima M, Langridge N, Martin FJ,

Muffato M, Perry E, Ruffier M, Staines DM, Trevanion SJ, Aken BL, Yates AD, Zerbino DR, and Flicek P (2019). "Ensembl 2019". *Nucleic Acids Res* 47(D1):D745–D751. DOI: 10.1093/nar/gky1113 (cit. on pp. 29, 30).

Custer AW, Kazarinova-Noyes K, Sakurai T, Xu X, Simon W, Grumet M, and Shrager P (2003). "The Role of the Ankyrin-Binding Protein NrCAM in Node of Ranvier Formation". *The Journal of Neuroscience* 23(31):10032–10039. DOI: 10.1523/jneurosci.23-31-10032.2003 (cit. on pp. 8, 62).

Dammer EB, Fallini C, Gozal YM, Duong DM, Rossoll W, Xu P, Lah JJ, Levey AI, Peng J, Bassell GJ, and Seyfried NT (2012). "Coaggregation of RNA-binding proteins in a model of TDP-43 proteinopathy with selective RGG motif methylation and a role for RRM1 ubiquitination". *PLoS One* 7(6):e38658. DOI: 10.1371/journal.pone.0038658 (cit. on p. 27).

D'Antonio M, Droggiti A, Feltri ML, Roes J, Wrabetz L, Mirsky R, and Jessen KR (2006). "TGFbeta type II receptor signaling controls Schwann cell death and proliferation in developing nerves". *J Neurosci* 26(33):8417–27. DOI: 10.1523/JNEUROSCI.1578-06.2006 (cit. on p. 13).

Daoud H, Suhail H, Szuto A, Camu W, Salachas F, Meininger V, Bouchard JP, Dupre N, Dion PA, and Rouleau GA (2012). "UBQLN2 mutations are rare in French and French-Canadian amyotrophic lateral sclerosis". *Neurobiol Aging* 33(9):2230 e1–2230 e5. DOI: 10.1016/j.neurobiolaging.2012.03.015 (cit. on p. 28).

David CN (1973). "A quantitative method for maceration of hydra tissue". *Wilhelm Roux Arch Entwickl Mech Org* 171(4):259–268. DOI: 10.1007/BF00577724 (cit. on p. 4).

Davidson Y, Kelley T, Mackenzie IR, Pickering-Brown S, Du Plessis D, Neary D, Snowden JS, and Mann DM (2007). "Ubiquitinated pathological lesions in frontotemporal lobar degeneration contain the TAR DNA-binding protein, TDP-43". *Acta Neuropathol* 113(5):521–33. DOI: 10.1007/s00401-006-0189-y (cit. on p. 21).

Davis AD, Weatherby TM, Hartline DK, and Lenz PH (1999). "Myelin-like sheaths in copepod axons". *Nature* 398(6728): 571. DOI: 10.1038/19212 (cit. on p. 5).

Deacon RM (2013). "Measuring the strength of mice". *J Vis Exp* (76):e2610. DOI: 10.3791/2610 (cit. on p. 37).

Decker L, Desmarquet-Trin-Dinh C, Taillebourg E, Ghislain J, Vallat JM, and Charnay P (2006). "Peripheral myelin maintenance is a dynamic process requiring constant Krox20 expression". *J Neurosci* 26(38):9771–9. DOI: 10.1523/JNEUROSCI.0716-06.2006 (cit. on p. 14).

Deng HX, Chen W, Hong ST, Boycott KM, Gorrie GH, Siddique N, Yang Y, Fecto F, Shi Y, Zhai H, Jiang H, Hirano M, Rampersaud E, Jansen GH, Donkervoort S, Bigio EH, Brooks BR, Ajroud K, Sufit RL, Haines JL, Mugnaini E, Pericak-Vance MA, and Siddique T (2011). "Mutations in UBQLN2 cause dominant X-linked juvenile and adult-onset ALS and ALS/dementia". *Nature* 477(7363):211–5. DOI: 10.1038/nature10353 (cit. on p. 28).

Dewey CM, Cenik B, Sephton CF, Dries DR, Mayer P. r, Good SK, Johnson BA, Herz J, and Yu G (2011). "TDP-43 is directed to stress granules by sorbitol, a novel physiological osmotic and oxidative stressor". *Mol Cell Biol* 31(5): 1098–108. DOI: 10.1128/MCB.01279-10 (cit. on p. 27).

Di Carlo V, Grossi E, Laneve P, Morlando M, Dini Modigliani S, Ballarino M, Bozzoni I, and Caffarelli E (2013). "TDP-43 regulates the microprocessor complex activity during in vitro neuronal differentiation". *Mol Neurobiol* 48(3): 952–63. DOI: 10.1007/s12035-013-8564-x (cit. on p. 27).

Diaper DC, Adachi Y, Lazarou L, Greenstein M, Simoes FA, Di Domenico A, Solomon DA, Lowe S, Alsubaie R, Cheng D, Buckley S, Humphrey DM, Shaw CE, and Hirth F (2013). "Drosophila TDP-43 dysfunction in glia and muscle cells cause cytological and behavioural phenotypes that characterize ALS and FTLD". *Hum Mol Genet* 22(19): 3883–93. DOI: 10.1093/hmg/ddt243 (cit. on p. 28).

Dickey TH, Altschuler SE, and Wuttke DS (2013). "Single-stranded DNA-binding proteins: multiple domains for multiple functions". *Structure* 21(7):1074–84. DOI: 10.1016/j.str.2013.05.013 (cit. on p. 23).

Ding Y and Brunden KR (1994). "The cytoplasmic domain of myelin glycoprotein P0 interacts with negatively charged phospholipid bilayers". *J Biol Chem* 269(14):10764–70 (cit. on p. 10).

Dobin A, Davis CA, Schlesinger F, Drenkow J, Zaleski C, Jha S, Batut P, Chaisson M, and Gingeras TR (2013). "STAR: ultrafast universal RNA-seq aligner". *Bioinformatics* 29(1):15–21. DOI: 10.1093/bioinformatics/bts635 (cit. on p. 47).

Dobson R and Giovannoni G (2019). "Multiple sclerosis - a review". *Eur J Neurol* 26(1):27–40. DOI: 10.1111/ene.13819 (cit. on p. 20).

Domenech-Estevez E, Baloui H, Repond C, Rosafio K, Medard JJ, Tricaud N, Pellerin L, and Chrast R (2015). "Distribution of monocarboxylate transporters in the peripheral nervous system suggests putative roles in lactate shuttling and myelination". *J Neurosci* 35(10):4151–6. DOI: 10.1523/JNEUROSCI.3534-14.2015 (cit. on p. 130).

Donaldson HH and Hoke GW (1905). "On the areas of the axis cylinder and medullary sheath as seen in cross sections of the spinal nerves of vertebrates." *Journal of Comparative Neurology and Psychology* 15(1):1–16. DOI: DOI10.1002/cne.920150102 (cit. on p. 9).

Donde A, Sun M, Jeong YH, Wen X, Ling J, Lin S, Braunstein K, Nie S, Wang S, Chen L, and Wong PC (2019). "Up-regulation of ATG7 attenuates motor neuron dysfunction associated with depletion of TARDBP/TDP-43". *Autophagy*: 1–11. DOI: 10.1080/15548627.2019.1635379 (cit. on p. 124).

Dong Z, Brennan A, Liu N, Yarden Y, Lefkowitz G, Mirsky R, and Jessen KR (1995). "Neu differentiation factor is a neuron-glia signal and regulates survival, proliferation, and maturation of rat schwann cell precursors". *Neuron* 15(3): 585–596. DOI: 10.1016/0896-6273(95)90147-7 (cit. on pp. 11, 12).

Dormann D, Capell A, Carlson AM, Shankaran SS, Rodde R, Neumann M, Kremmer E, Matsuwaki T, Yamanouchi K, Nishihara M, and Haass C (2009). "Proteolytic processing of TAR DNA binding protein-43 by caspases produces C-terminal fragments with disease defining properties independent of progranulin". *J Neurochem* 110(3):1082–94. DOI: 10.1111/j.1471-4159.2009.06211.x (cit. on p. 28).

Dowsing BJ, Morrison WA, Nicola NA, Starkey GP, Bucci T, and Kilpatrick TJ (1999). "Leukemia inhibitory factor is an autocrine survival factor for Schwann cells". *J Neurochem* 73(1):96–104. DOI: 10.1046/j.1471-4159.1999.0730096.x (cit. on p. 12).

Dreyfuss G, Choi YD, and Adam SA (1984). "Characterization of heterogeneous nuclear RNA-protein complexes in vivo with monoclonal antibodies". *Mol Cell Biol* 4(6):1104–14. DOI: 10.1128/mcb.4.6.1104 (cit. on p. 24).

Dreyfuss G, Kim VN, and Kataoka N (2002). "Messenger-RNA-binding proteins and the messages they carry". *Nat Rev Mol Cell Biol* 3(3):195–205. DOI: 10.1038/nrm760 (cit. on p. 23).

Dreyfuss G, Matunis MJ, Pinol-Roma S, and Burd CG (1993). "hnRNP proteins and the biogenesis of mRNA". *Annu Rev Biochem* 62:289–321. DOI: 10.1146/annurev.bi.62.070193.001445 (cit. on p. 23).

Dupre C and Yuste R (2017). "Non-overlapping Neural Networks in Hydra vulgaris". *Curr Biol* 27(8):1085–1097. DOI: 10.1016/j.cub.2017.02.049 (cit. on p. 4).

Dyachuk V, Furlan A, Shahidi MK, Giovenco M, Kaukua N, Konstantinidou C, Pachnis V, Memic F, Marklund U, Muller T, Birchmeier C, Fried K, Ernfors P, and Adameyko I (2014). "Neurodevelopment. Parasympathetic neurons originate from nerve-associated peripheral glial progenitors". *Science* 345(6192):82–7. DOI: 10.1126/science.1253281 (cit. on p. 11).

Ederle H, Funk C, Abou-Ajram C, Hutten S, Funk EBE, Kehlenbach RH, Bailer SM, and Dormann D (2018). "Nuclear egress of TDP-43 and FUS occurs independently of Exportin-1/CRM1". *Sci Rep* 8(1):7084. DOI: 10.1038/s41598-018-25007-5 (cit. on p. 24).

Edgar JM and Garbern J (2004). "The myelinated axon is dependent on the myelinating cell for support and maintenance: molecules involved". *J Neurosci Res* 76(5):593–8. DOI: 10.1002/jnr.20063 (cit. on p. 10).

Edgar JM, McLaughlin M, Werner HB, McCulloch MC, Barrie JA, Brown A, Faichney AB, Snaidero N, Nave KA, and Griffiths IR (2009). "Early ultrastructural defects of axons and axon-glia junctions in mice lacking expression of Cnp1". *Glia* 57(16):1815–24. DOI: 10.1002/glia.20893 (cit. on p. 11).

Eggers R, Tannemaat MR, Ehlert EM, and Verhaagen J (2010). "A spatio-temporal analysis of motoneuron survival, axonal regeneration and neurotrophic factor expression after lumbar ventral root avulsion and implantation". *Exp Neurol* 223(1):207–20. DOI: 10.1016/j.expneurol.2009.07.021 (cit. on p. 15).

Ehrlich M, Mozafari S, Glatza M, Starost L, Velychko S, Hallmann AL, Cui QL, Schambach A, Kim KP, Bachelin C, Marteyn A, Hargus G, Johnson RM, Antel J, Sterneckert J, Zaehres H, Scholer HR, Baron-Van Evercooren A, and Kuhlmann T (2017). "Rapid and efficient generation of oligodendrocytes from human induced pluripotent stem cells using transcription factors". *Proc Natl Acad Sci U S A* 114(11):E2243–E2252. DOI: 10.1073/pnas.1614412114 (cit. on p. 140).

Eisenbach M, Kartvelishvily E, Eshed-Eisenbach Y, Watkins T, Sorensen A, Thomson C, Ranscht B, Barnett SC, Brophy P, and Peles E (2009). "Differential clustering of Caspr by oligodendrocytes and Schwann cells". *J Neurosci Res* 87(15):3492–501. DOI: 10.1002/jnr.22157 (cit. on p. 125).

Elbaz B, Traka M, Kunjamma RB, Dukala D, Brosius Lutz A, Anton ES, Barres BA, Soliven B, and Popko B (2016). "Adenomatous polyposis coli regulates radial axonal sorting and myelination in the PNS". *Development* 143(13):2356–66. DOI: 10.1242/dev.135913 (cit. on p. 137).

Elvira G, Wasiak S, Blandford V, Tong XK, Serrano A, Fan X, Rayo Sanchez-Carbente M del, Servant F, Bell AW, Boismenu D, Lacaille JC, McPherson PS, DesGroseillers L, and Sossin WS (2006). "Characterization of an RNA granule from developing brain". *Mol Cell Proteomics* 5(4):635–51. DOI: 10.1074/mcp.M500255-MCP200 (cit. on p. 27).

Emery B, Agalliu D, Cahoy JD, Watkins TA, Dugas JC, Mulinyawe SB, Ibrahim A, Ligon KL, Rowitch DH, and Barres BA (2009). "Myelin gene regulatory factor is a critical transcriptional regulator required for CNS myelination". *Cell* 138(1):172–85. DOI: 10.1016/j.cell.2009.04.031 (cit. on p. 19).

Emery B and Dugas JC (2013). "Purification of oligodendrocyte lineage cells from mouse cortices by immunopanning". *Cold Spring Harb Protoc* 2013(9):854–68. DOI: 10.1101/pdb.prot073973 (cit. on p. 49).

Eom T, Zhang C, Wang H, Lay K, Fak J, Noebels JL, and Darnell RB (2013). "NOVA-dependent regulation of cryptic NMD exons controls synaptic protein levels after seizure". *Elife* 2:e00178. DOI: 10.7554/eLife.00178 (cit. on p. 31).

Es MA van, Hardiman O, Chio A, Al-Chalabi A, Pasterkamp RJ, Veldink JH, and Berg LH van den (2017). "Amyotrophic lateral sclerosis". *The Lancet* 390(10107):2084–2098. DOI: 10.1016/s0140-6736(17)31287-4 (cit. on pp. 20, 22).

Espinosa-Medina I, Outin E, Picard CA, Chettouh Z, Dymecki S, Consalez GG, Coppola E, and Brunet JF (2014). "Neurodevelopment. Parasympathetic ganglia derive from Schwann cell precursors". *Science* 345(6192):87–90. DOI: 10.1126/science.1253286 (cit. on p. 11).

Falcao AM, Bruggen D van, Marques S, Meijer M, Jakel S, Agirre E, Samudyata, Floriddia EM, Vanichkina DP, Ffrench-Constant C, Williams A, Guerreiro-Cacais AO, and Castelo-Branco G (2018). "Disease-specific oligodendrocyte lineage cells arise in multiple sclerosis". *Nat Med* 24(12):1837–1844. DOI: 10.1038/s41591-018-0236-y (cit. on p. 133).

Fancy SP, Baranzini SE, Zhao C, Yuk DI, Irvine KA, Kaing S, Sanai N, Franklin RJ, and Rowitch DH (2009). "Dysregulation of the Wnt pathway inhibits timely myelination and remyelination in the mammalian CNS". *Genes Dev* 23(13):1571–85. DOI: 10.1101/gad.1806309 (cit. on p. 18).

Fard MK, Meer F van der, Sanchez P, Cantuti-Castelvetri L, Mandad S, Jakel S, Fornasiero EF, Schmitt S, Ehrlich M, Starost L, Kuhlmann T, Sergiou C, Schultz V, Wrzos C, Bruck W, Urlaub H, Dimou L, Stadelmann C, and Simons M (2017). "BCAS1 expression defines a population of early myelinating oligodendrocytes in multiple sclerosis lesions". *Sci Transl Med* 9(419). DOI: 10.1126/scitranslmed.aam7816 (cit. on p. 135).

Fatima M, Tan R, Halliday GM, and Kril JJ (2015). "Spread of pathology in amyotrophic lateral sclerosis: assessment of phosphorylated TDP-43 along axonal pathways". *Acta Neuropathol Commun* 3:47. DOI: 10.1186/s40478-015-0226-y (cit. on p. 22).

Feltri ML, D'Antonio M, Previtali S, Fasolini M, Messing A, and Wrabetz L (1999). "P0-Cre transgenic mice for inactivation of adhesion molecules in Schwann cells". *Ann N Y Acad Sci* 883(1):116–23. DOI: 10.1111/j.1749-6632.1999.tb08574.x (cit. on p. 35).

Feltri ML, Graus Porta D, Previtali SC, Nodari A, Migliavacca B, Cassetti A, Littlewood-Evans A, Reichardt LF, Messing A, Quattrini A, Mueller U, and Wrabetz L (2002). "Conditional disruption of beta 1 integrin in Schwann cells impedes interactions with axons". *J Cell Biol* 156(1):199–209. DOI: 10.1083/jcb.200109021 (cit. on pp. 52, 137).

Feltri ML, Poitelon Y, and Previtali SC (2016). "How Schwann Cells Sort Axons: New Concepts". *Neuroscientist* 22(3):252–65. DOI: 10.1177/1073858415572361 (cit. on pp. 13, 129).

Ferraiuolo L, Meyer K, Sherwood TW, Vick J, Likhite S, Frakes A, Miranda CJ, Braun L, Heath PR, Pineda R, Beattie CE, Shaw PJ, Askwith CC, McTigue D, and Kaspar BK (2016). "Oligodendrocytes contribute to motor neuron death in ALS via SOD1-dependent mechanism". *Proc Natl Acad Sci U S A* 113(42):E6496–E6505. DOI: 10.1073/pnas.1607496113 (cit. on p. 140).

Fica SM, Tuttle N, Novak T, Li NS, Lu J, Koodathingal P, Dai Q, Staley JP, and Piccirilli JA (2013). "RNA catalyses nuclear pre-mRNA splicing". *Nature* 503(7475):229–34. DOI: 10.1038/nature12734 (cit. on p. 29).

Figlia G, Norrmen C, Pereira JA, Gerber D, and Suter U (2017). "Dual function of the PI3K-Akt-mTORC1 axis in myelination of the peripheral nervous system". *Elife* 6. DOI: 10.7554/eLife.29241 (cit. on p. 14).

Finzsch M, Schreiner S, Kichko T, Reeh P, Tamm ER, Bosl MR, Meijer D, and Wegner M (2010). "Sox10 is required for Schwann cell identity and progression beyond the immature Schwann cell stage". *J Cell Biol* 189(4):701–12. DOI: 10.1083/jcb.200912142 (cit. on p. 13).

Fischer LR, Culver DG, Tennant P, Davis AA, Wang M, Castellano-Sanchez A, Khan J, Polak MA, and Glass JD (2004). "Amyotrophic lateral sclerosis is a distal axonopathy: evidence in mice and man". *Exp Neurol* 185(2):232–40. DOI: 10.1016/j.expneurol.2003.10.004 (cit. on pp. 22, 127).

Floriddia EM and Castelo-Branco G (2019). "Distinct oligodendrocyte populations have spatial preference and injury-specific responses". *bioxRV* (cit. on p. 135).

Florio F, Ferri C, Scapin C, Feltri ML, Wrabetz L, and D'Antonio M (2018). "Sustained Expression of Negative Regulators of Myelination Protects Schwann Cells from Dysmyelination in a Charcot-Marie-Tooth 1B Mouse Model". *J Neurosci* 38(18):4275–4287. DOI: 10.1523/JNEUROSCI.0201-18.2018 (cit. on p. 14).

Fogarty M, Richardson WD, and Kessaris N (2005). "A subset of oligodendrocytes generated from radial glia in the dorsal spinal cord". *Development* 132(8):1951–9. DOI: 10.1242/dev.01777 (cit. on p. 16).

Fontana X, Hristova M, Da Costa C, Patodia S, Thei L, Makwana M, Spencer-Dene B, Latouche M, Mirsky R, Jessen KR, Klein R, Raivich G, and Behrens A (2012). "c-Jun in Schwann cells promotes axonal regeneration and motoneuron survival via paracrine signaling". *J Cell Biol* 198(1):127–41. DOI: 10.1083/jcb.201205025 (cit. on p. 15).

Freibaum BD, Chitta RK, High AA, and Taylor JP (2010). "Global analysis of TDP-43 interacting proteins reveals strong association with RNA splicing and translation machinery". *J Proteome Res* 9(2):1104–20. DOI: 10.1021/pr901076y (cit. on p. 27).

Fridman V, Bundy B, Reilly MM, Pareyson D, Bacon C, Burns J, Day J, Feely S, Finkel RS, Grider T, Kirk CA, Herrmann DN, Laura M, Li J, Lloyd T, Sumner CJ, Muntoni F, Piscosquito G, Ramchandren S, Shy R, Siskind CE, Yum SW, Moroni I, Pagliano E, Zuchner S, Scherer SS, and Shy ME (2015). "CMT subtypes and disease burden in patients enrolled in the Inherited Neuropathies Consortium natural history study: a cross-sectional analysis". *J Neurol Neurosurg Psychiatry* 86(8):873–8. DOI: 10.1136/jnnp-2014-308826 (cit. on p. 20).

Friede RL (1986). "Relation between Myelin Sheath Thickness, Internode Geometry, and Sheath Resistance". *Experimental Neurology* 92(1):234–247. DOI: Doi10.1016/0014-4886(86)90137-8 (cit. on p. 9).

Fruttiger M, Montag D, Schachner M, and Martini R (1995). "Crucial role for the myelin-associated glycoprotein in the maintenance of axon-myelin integrity". *Eur J Neurosci* 7(3):511–5. DOI: 10.1111/j.1460-9568.1995.tb00347.x (cit. on p. 11).

Fu XD and Ares M. J (2014). "Context-dependent control of alternative splicing by RNA-binding proteins". *Nat Rev Genet* 15(10):689–701. DOI: 10.1038/nrg3778 (cit. on p. 30).

Fukui H, Diaz F, Garcia S, and Moraes CT (2007). "Cytochrome c oxidase deficiency in neurons decreases both oxidative stress and amyloid formation in a mouse model of Alzheimer's disease". *Proc Natl Acad Sci U S A* 104(35): 14163–8. DOI: 10.1073/pnas.0705738104 (cit. on p. 19).

Funfschilling U, Supplie LM, Mahad D, Boretius S, Saab AS, Edgar J, Brinkmann BG, Kassmann CM, Tzvetanova ID, Mobius W, Diaz F, Meijer D, Suter U, Hamprecht B, Sereda MW, Moraes CT, Frahm J, Goebbels S, and Nave KA (2012). "Glycolytic oligodendrocytes maintain myelin and long-term axonal integrity". *Nature* 485(7399):517–21. DOI: 10.1038/nature11007 (cit. on pp. 19, 130).

Furlan A and Adameyko I (2018). "Schwann cell precursor: a neural crest cell in disguise?" *Dev Biol* 444 Suppl 1: S25–S35. DOI: 10.1016/j.ydbio.2018.02.008 (cit. on p. 11).

Gal-Mark N, Schwartz S, Ram O, Eyras E, and Ast G (2009). "The pivotal roles of TIA proteins in 5' splice-site selection of alu exons and across evolution". *PLoS Genet* 5(11):e1000717. DOI: 10.1371/journal.pgen.1000717 (cit. on p. 32).

Garcia-Fresco GP, Sousa AD, Pillai AM, Moy SS, Crawley JN, Tessarollo L, Dupree JL, and Bhat MA (2006). "Disruption of axo-glial junctions causes cytoskeletal disorganization and degeneration of Purkinje neuron axons". *Proc Natl Acad Sci U S A* 103(13):5137–42. DOI: 10.1073/pnas.0601082103 (cit. on p. 129).

Garratt AN, Britsch S, and Birchmeier C (2000). "Neuregulin, a factor with many functions in the life of a schwann cell". *Bioessays* 22(11):987–96. DOI: 10.1002/1521-1878(200011)22:11<987::AID-BIES5>3.0.CO;2-5 (cit. on p. 12).

Gasser HS and Grundfest H (1939). "Axon diameters in relation to the spike dimensions and the conduction velocity in mammalian A fibers". *American Journal of Physiology* 127(2):393–414. DOI: 10.1152/ajplegacy.1939.127.2.393 (cit. on p. 9).

Gentile F, Scarlino S, Falzone YM, Lunetta C, Tremolizzo L, Quattrini A, and Riva N (2019). "The Peripheral Nervous System in Amyotrophic Lateral Sclerosis: Opportunities for Translational Research". *Front Neurosci* 13:601. DOI: 10.3389/fnins.2019.00601 (cit. on p. 22).

Geuens T, Bouhy D, and Timmerman V (2016). "The hnRNP family: insights into their role in health and disease". *Hum Genet* 135(8):851–67. DOI: 10.1007/s00439-016-1683-5 (cit. on p. 23).

Ghislain J and Charnay P (2006). "Control of myelination in Schwann cells: a Krox20 cis-regulatory element integrates Oct6, Brn2 and Sox10 activities". *EMBO Rep* 7(1):52–8. DOI: 10.1038/sj.embor.7400573 (cit. on p. 13).

Ghosh A, Kling T, Snaidero N, Sampaio JL, Shevchenko A, Gras H, Geurten B, Gopfert MC, Schulz JB, Voigt A, and Simons M (2013). "A global in vivo Drosophila RNAi screen identifies a key role of ceramide phosphoethanolamine for glial ensheathment of axons". *PLoS Genet* 9(12):e1003980. DOI: 10.1371/journal.pgen.1003980 (cit. on p. 28).

Gibson EM, Purger D, Mount CW, Goldstein AK, Lin GL, Wood LS, Inema I, Miller SE, Bieri G, Zuchero JB, Barres BA, Woo PJ, Vogel H, and Monje M (2014). "Neuronal activity promotes oligodendrogenesis and adaptive myelination in the mammalian brain". *Science* 344(6183):1252304. DOI: 10.1126/science.1252304 (cit. on p. 17).

Giera S, Luo R, Ying Y, Ackerman SD, Jeong SJ, Stoveken HM, Folts CJ, Welsh CA, Tall GG, Stevens B, Monk KR, and Piao X (2018). "Microglial transglutaminase-2 drives myelination and myelin repair via GPR56/ADGRG1 in oligodendrocyte precursor cells". *Elife* 7. DOI: 10.7554/eLife.33385 (cit. on p. 136).

Gillespie CS, Sherman DL, Fleetwood-Walker SM, Cottrell DF, Tait S, Garry EM, Wallace VC, Ure J, Griffiths IR, Smith A, and Brophy PJ (2000). "Peripheral demyelination and neuropathic pain behavior in periaxin-deficient mice". *Neuron* 26(2):523–31. DOI: 10.1016/s0896-6273(00)81184-8 (cit. on p. 130).

Gokbuget D, Pereira JA, Opitz L, Christe D, Kessler T, Marchais A, and Suter U (2018). "The miRNA biogenesis pathway prevents inappropriate expression of injury response genes in developing and adult Schwann cells". *Glia* 66(12):2632–2644. DOI: 10.1002/glia.23516 (cit. on p. 130).

Goldman SA and Kuypers NJ (2015). "How to make an oligodendrocyte". *Development* 142(23):3983–95. DOI: 10.1242/dev.126409 (cit. on pp. 17, 101, III).

Gomez-Sanchez JA, Carty L, Iruarrizaga-Lejarreta M, Palomo-Irigoyen M, Varela-Rey M, Griffith M, Hantke J, Macias-Camara N, Azkargorta M, Aurrekoetxea I, De Juan VG, Jefferies HB, Aspichueta P, Elortza F, Aransay AM, Martinez-Chantar ML, Baas F, Mato JM, Mirsky R, Woodhoo A, and Jessen KR (2015). "Schwann cell autophagy, myelinophagy, initiates myelin clearance from injured nerves". *J Cell Biol* 210(1):153–68. DOI: 10.1083/jcb.201503019 (cit. on p. 15).

Gomez-Sanchez JA, Pilch KS, Lans M van der, Fazal SV, Benito C, Wagstaff LJ, Mirsky R, and Jessen KR (2017). "After Nerve Injury, Lineage Tracing Shows That Myelin and Remak Schwann Cells Elongate Extensively and Branch to Form Repair Schwann Cells, Which Shorten Radically on Remyelination". *J Neurosci* 37(37):9086–9099. DOI: 10.1523/JNEUROSCI.1453-17.2017 (cit. on p. 15).

Gonzalez-Fernandez E, Jeong HK, Fukaya M, Kim H, Khawaja RR, Srivastava IN, Waisman A, Son YJ, and Kang SH (2018). "PTEN negatively regulates the cell lineage progression from NG2(+) glial progenitor to oligodendrocyte via mTOR-independent signaling". *Elife* 7. DOI: 10.7554/eLife.32021 (cit. on p. 19).

Gordon DA, Hamm TM, Enoka RM, Reinking RM, Windhorst U, and Stuart DG (1987). "Measurement of axonal conduction velocity in single mammalian motor axons". *Journal of Neuroscience Methods* 19(4):267–284. DOI: 10.1016/0165-0270(87)90070-7 (cit. on p. 7).

Gregory RI, Yan KP, Amuthan G, Chendrimada T, Doratotaj B, Cooch N, and Shiekhattar R (2004). "The Microprocessor complex mediates the genesis of microRNAs". *Nature* 432(7014):235–40. DOI: 10.1038/nature03120 (cit. on p. 27).

Grove M, Kim H, Santerre M, Krupka AJ, Han SB, Zhai J, Cho JY, Park R, Harris M, Kim S, Sawaya BE, Kang SH, Barbe MF, Cho SH, Lemay MA, and Son YJ (2017). "YAP/TAZ initiate and maintain Schwann cell myelination". *Elife* 6. DOI: 10.7554/eLife.20982 (cit. on p. 14).

Gunther J (1976). "Impulse conduction in the myelinated giant fibers of the earthworm. Structure and function of the dorsal nodes in the median giant fiber". *J Comp Neurol* 168(4):505–31. DOI: 10.1002/cne.901680405 (cit. on p. 5).

Guo L, Lee AA, Rizvi TA, Ratner N, and Kirschner LS (2013a). "The protein kinase A regulatory subunit R1A (Prkar1a) plays critical roles in peripheral nerve development". *J Neurosci* 33(46):17967–75. DOI: 10.1523/JNEUROSCI.0766-13.2013 (cit. on pp. 12, 137).

Guo L, Moon C, Zheng Y, and Ratner N (2013b). "Cdc42 regulates Schwann cell radial sorting and myelin sheath folding through NF2/merlin-dependent and independent signaling". *Glia* 61(11):1906–21. DOI: 10.1002/glia.22567 (cit. on p. 137).

Gurney ME, Pu H, Chiu AY, Dal Canto MC, Polchow CY, Alexander DD, Caliendo J, Hentati A, Kwon YW, Deng HX, and Siddique T (1994). "Motor neuron degeneration in mice that express a human Cu,Zn superoxide dismutase mutation". *Science* 264(5166):1772–5. DOI: 10.1126/science.8209258 (cit. on p. 115).

Habelhah H, Shah K, Huang L, Ostareck-Lederer A, Burlingame AL, Shokat KM, Hentze MW, and Ronai Z (2001). "ERK phosphorylation drives cytoplasmic accumulation of hnRNP-K and inhibition of mRNA translation". *Nat Cell Biol* 3(3):325–30. DOI: 10.1038/35060131 (cit. on p. 24).

Hamilton TG, Klinghoffer RA, Corrin PD, and Soriano P (2003). "Evolutionary divergence of platelet-derived growth factor alpha receptor signaling mechanisms". *Mol Cell Biol* 23(11):4013–25. DOI: 10.1128/mcb.23.11.4013-4025.2003 (cit. on pp. 35, 87, 99).

Hammond E, Lang J, Maeda Y, Pleasure D, Angus-Hill M, Xu J, Horiuchi M, Deng W, and Guo F (2015). "The Wnt effector transcription factor 7-like 2 positively regulates oligodendrocyte differentiation in a manner independent of Wnt/beta-catenin signaling". *J Neurosci* 35(12):5007–22. DOI: 10.1523/JNEUROSCI.4787-14.2015 (cit. on p. 18).

Han H, Myllykoski M, Ruskamo S, Wang C, and Kursula P (2013). "Myelin-specific proteins: a structurally diverse group of membrane-interacting molecules". *Biofactors* 39(3):233–41. DOI: 10.1002/biof.1076 (cit. on p. 10).

Hartley SW and Mullikin JC (2016). "Detection and visualization of differential splicing in RNA-Seq data with JunctionSeq". *Nucleic Acids Res* 44(15):e127. DOI: 10.1093/nar/gkw501 (cit. on pp. 47, 59).

Harty BL and Monk KR (2017). "Unwrapping the unappreciated: recent progress in Remak Schwann cell biology". *Curr Opin Neurobiol* 47:131–137. DOI: 10.1016/j.conb.2017.10.003 (cit. on p. 9).

Hasegawa M, Arai T, Nonaka T, Kametani F, Yoshida M, Hashizume Y, Beach TG, Buratti E, Baralle F, Morita M, Nakano I, Oda T, Tsuchiya K, and Akiyama H (2008). "Phosphorylated TDP-43 in frontotemporal lobar degeneration and amyotrophic lateral sclerosis". *Ann Neurol* 64(1):60–70. DOI: 10.1002/ana.21425 (cit. on p. 27).

Hattori N, Yamamoto M, Yoshihara T, Koike H, Nakagawa M, Yoshikawa H, Ohnishi A, Hayasaka K, Onodera O, Baba M, Yasuda H, Saito T, Nakashima K, Kira J, Kaji R, Oka N, Sobue G, and Hereditary Neuropathy in J Study Group for (2003). "Demyelinating and axonal features of Charcot-Marie-Tooth disease with mutations of myelin-related proteins (PMP22, MPZ and Cx32): a clinicopathological study of 205 Japanese patients". *Brain* 126(Pt 1): 134–51. DOI: 10.1093/brain/awg012 (cit. on p. 82).

He Y, Kim JY, Dupree J, Tewari A, Melendez-Vasquez C, Svaren J, and Casaccia P (2010). "Yy1 as a molecular link between neuregulin and transcriptional modulation of peripheral myelination". *Nat Neurosci* 13(12):1472–80. DOI: 10.1038/nn.2686 (cit. on p. 13).

Hebron ML, Lonskaya I, Sharpe K, Weerasinghe PP, Algarzae NK, Shekoyan AR, and Moussa CE (2013). "Parkin ubiquitinates Tar-DNA binding protein-43 (TDP-43) and promotes its cytosolic accumulation via interaction with histone deacetylase 6 (HDAC6)". *J Biol Chem* 288(6):4103–15. DOI: 10.1074/jbc.M112.419945 (cit. on p. 27).

Hergesheimer RC, Chami AA, Assis DR de, Vourc'h P, Andres CR, Corcia P, Lanznaster D, and Blasco H (2019). "The debated toxic role of aggregated TDP-43 in amyotrophic lateral sclerosis: a resolution in sight?" *Brain* 142(5): 1176–1194. DOI: 10.1093/brain/awz078 (cit. on pp. 21, 28).

Herskowitz JH, Gozal YM, Duong DM, Dammer EB, Gearing M, Ye K, Lah JJ, Peng J, Levey AI, and Seyfried NT (2012). "Asparaginyl endopeptidase cleaves TDP-43 in brain". *Proteomics* 12(15-16):2455–63. DOI: 10.1002/pmic.201200006 (cit. on p. 28).

Heuser JE and Doggenweiler CF (1966). "The fine structural organization of nerve fibers, sheaths, and glial cells in the prawn, Palaemonetes vulgaris". *J Cell Biol* 30(2):381–403. DOI: 10.1083/jcb.30.2.381 (cit. on p. 5).

Higgs MH and Spain WJ (2011). "Kv1 channels control spike threshold dynamics and spike timing in cortical pyramidal neurones". *J Physiol* 589(Pt 21):5125–42. DOI: 10.1113/jphysiol.2011.216721 (cit. on p. 7).

Hildebrand C and Hahn R (1978). "Relation between Myelin Sheath Thickness and Axon Size in Spinal-Cord White Matter of Some Vertebrate Species". *Journal of the Neurological Sciences* 38(3):421–434. DOI: Doi10.1016/0022-510x(78)90147-8 (cit. on p. 9).

Hirata K and Kawabuchi M (2002). "Myelin phagocytosis by macrophages and nonmacrophages during Wallerian degeneration". *Microsc Res Tech* 57(6):541–7. DOI: 10.1002/jemt.10108 (cit. on p. 15).

Hodgkin AL (1954). "A note on conduction velocity". *J Physiol* 125(1):221–4. DOI: 10.1113/jphysiol.1954.sp005152 (cit. on p. 4).

Holcomb ER and Friedman DL (1984). "Phosphorylation of the C-proteins of HeLa cell hnRNP particles. Involvement of a casein kinase II-type enzyme". *J Biol Chem* 259(1):31–40 (cit. on p. 24).

Holmes W (1942). "The giant myelinated nerve fibres of the prawn". *Philosophical Transactions of the Royal Society of London. Series B, Biological Sciences* 231(582):293–311. DOI: 10.1098/rstb.1942.0004 (cit. on p. 5).

Hornig J, Frob F, Vogl MR, Hermans-Borgmeyer I, Tamm ER, and Wegner M (2013). "The transcription factors Sox10 and Myrf define an essential regulatory network module in differentiating oligodendrocytes". *PLoS Genet* 9(10): e1003907. DOI: 10.1371/journal.pgen.1003907 (cit. on p. 19).

Horrocks LA (1967). "Composition of myelin from peripheral and central nervous systems of the squirrel monkey". *J Lipid Res* 8(6):569–76 (cit. on p. 10).

Hovelmeyer N, Hao Z, Kranidioti K, Kassiotis G, Buch T, Frommer F, Hoch L von, Kramer D, Minichiello L, Kollias G, Lassmann H, and Waisman A (2005). "Apoptosis of oligodendrocytes via Fas and TNF-R1 is a key event in the induction of experimental autoimmune encephalomyelitis". *J Immunol* 175(9):5875–84. DOI: 10.4049/jimmunol.175.9.5875 (cit. on p. 140).

Howe CL (2006). "Coated glass and vicryl microfibers as artificial axons". *Cells Tissues Organs* 183(4):180–94. DOI: 10.1159/000096509 (cit. on p. 18).

Huang CY, Lee YC, Li PC, Liliang PC, Lu K, Wang KW, Chang LC, Shiu LY, Chen MF, Sun YT, and Wang HK (2017). "TDP-43 proteolysis is associated with astrocyte reactivity after traumatic brain injury in rodents". *J Neuroimmunol* 313:61–68. DOI: 10.1016/j.jneuroim.2017.10.011 (cit. on p. 28).

Hughes EG, Kang SH, Fukaya M, and Bergles DE (2013). "Oligodendrocyte progenitors balance growth with self-repulsion to achieve homeostasis in the adult brain". *Nat Neurosci* 16(6):668–76. DOI: 10.1038/nn.3390 (cit. on p. 18).

Hui S, Ghergurovich JM, Morscher RJ, Jang C, Teng X, Lu W, Esparza LA, Reya T, Le Z, Yanxiang Guo J, White E, and Rabinowitz JD (2017). "Glucose feeds the TCA cycle via circulating lactate". *Nature* 551(7678):115–118. DOI: 10.1038/nature24057 (cit. on p. 19).

Humphrey J, Emmett W, Fratta P, Isaacs AM, and Plagnol V (2017). "Quantitative analysis of cryptic splicing associated with TDP-43 depletion". *BMC Med Genomics* 10(1):38. DOI: 10.1186/s12920-017-0274-1 (cit. on pp. 31, 32, 59, 126).

Hursh JB (1939). "Conduction velocity and diameter of nerve fibers". *American Journal of Physiology* 127(1):131–139. DOI: 10.1152/ajplegacy.1939.127.1.131 (cit. on p. 7).

Hynes RO (2012). "The evolution of metazoan extracellular matrix". *J Cell Biol* 196(6):671–9. DOI: 10.1083/jcb.201109041 (cit. on p. 30).

Igaz LM, Kwong LK, Lee EB, Chen-Plotkin A, Swanson E, Unger T, Malunda J, Xu Y, Winton MJ, Trojanowski JQ, and Lee VM (2011). "Dysregulation of the ALS-associated gene TDP-43 leads to neuronal death and degeneration in mice". *J Clin Invest* 121(2):726–38. DOI: 10.1172/JCI44867 (cit. on p. 28).

Iguchi Y, Katsuno M, Niwa J, Takagi S, Ishigaki S, Ikenaka K, Kawai K, Watanabe H, Yamanaka K, Takahashi R, Misawa H, Sasaki S, Tanaka F, and Sobue G (2013). "Loss of TDP-43 causes age-dependent progressive motor neuron degeneration". *Brain* 136(Pt 5):1371–82. DOI: 10.1093/brain/awt029 (cit. on p. 124).

Inukai Y, Nonaka T, Arai T, Yoshida M, Hashizume Y, Beach TG, Buratti E, Baralle FE, Akiyama H, Hisanaga S, and Hasegawa M (2008). "Abnormal phosphorylation of Ser409/410 of TDP-43 in FTLD-U and ALS". *FEBS Lett* 582(19):2899–904. DOI: 10.1016/j.febslet.2008.07.027 (cit. on p. 27).

Jacob C, Christen CN, Pereira JA, Somandin C, Baggiolini A, Lotscher P, Ozcelik M, Tricaud N, Meijer D, Yamaguchi T, Matthias P, and Suter U (2011). "HDAC1 and HDAC2 control the transcriptional program of myelination and the survival of Schwann cells". *Nat Neurosci* 14(4):429–36. DOI: 10.1038/nn.2762 (cit. on p. 13).

Jaegle M, Ghazvini M, Mandemakers W, Piirsoo M, Driegen S, Levavasseur F, Raghoenath S, Grosveld F, and Meijer D (2003). "The POU proteins Brn-2 and Oct-6 share important functions in Schwann cell development". *Genes Dev* 17(11):1380–91. DOI: 10.1101/gad.258203 (cit. on pp. 13, 35, 56).

Jaegle M, Mandemakers W, Broos L, Zwart R, Karis A, Visser P, Grosveld F, and Meijer D (1996). "The POU factor Oct-6 and Schwann cell differentiation". *Science* 273(5274):507–10. DOI: 10.1126/science.273.5274.507 (cit. on p. 13).

Jagalur NB, Ghazvini M, Mandemakers W, Driegen S, Maas A, Jones EA, Jaegle M, Grosveld F, Svaren J, and Meijer D (2011). "Functional dissection of the Oct6 Schwann cell enhancer reveals an essential role for dimeric Sox10 binding". *J Neurosci* 31(23):8585–94. DOI: 10.1523/JNEUROSCI.0659-11.2011 (cit. on p. 13).

Jahn O, Tenzer S, and Werner HB (2009). "Myelin proteomics: molecular anatomy of an insulating sheath". *Mol Neurobiol* 40(1):55–72. DOI: 10.1007/s12035-009-8071-2 (cit. on pp. 10, 11).

Jakel S, Agirre E, Mendanha Falcao A, Bruggen D van, Lee KW, Knuesel I, Malhotra D, Ffrench-Constant C, Williams A, and Castelo-Branco G (2019). "Altered human oligodendrocyte heterogeneity in multiple sclerosis". *Nature* 566(7745):543–547. DOI: 10.1038/s41586-019-0903-2 (cit. on p. 133).

Jangi M, Boutz PL, Paul P, and Sharp PA (2014). "Rbfox2 controls autoregulation in RNA-binding protein networks". *Genes Dev* 28(6):637–51. DOI: 10.1101/gad.235770.113 (cit. on p. 31).

Jeong YH, Ling JP, Lin SZ, Donde AN, Braunstein KE, Majounie E, Traynor BJ, LaClair KD, Lloyd TE, and Wong PC (2017). "Tdp-43 cryptic exons are highly variable between cell types". *Mol Neurodegener* 12(1):13. DOI: 10.1186/s13024-016-0144-x (cit. on pp. 32, 124, 125).

Jessen KR and Mirsky R (2005). "The origin and development of glial cells in peripheral nerves". *Nat Rev Neurosci* 6(9):671–82. DOI: 10.1038/nrn1746 (cit. on pp. 9, 11).

— (2019). "Schwann Cell Precursors; Multipotent Glial Cells in Embryonic Nerves". *Front Mol Neurosci* 12:69. DOI: 10.3389/fnmol.2019.00069 (cit. on p. 12).

Jessen KR, Mirsky R, and Lloyd AC (2015). "Schwann Cells: Development and Role in Nerve Repair". *Cold Spring Harb Perspect Biol* 7(7):a020487. DOI: 10.1101/cshperspect.a020487 (cit. on p. 12).

Jha MK, Lee Y, Russell KA, Yang F, Dastgheyb RM, Deme P, Ament XH, Chen W, Liu Y, Guan Y, Polydefkis MJ, Hoke A, Haughey NJ, Rothstein JD, and Morrison BM (2020). "Monocarboxylate transporter 1 in Schwann cells contributes to maintenance of sensory nerve myelination during aging". *Glia* 68(1):161–177. DOI: 10.1002/glia.23710 (cit. on p. 130).

Jha MK and Morrison BM (2018). "Glia-neuron energy metabolism in health and diseases: New insights into the role of nervous system metabolic transporters". *Exp Neurol* 309:23–31. DOI: 10.1016/j.expneurol.2018.07.009 (cit. on p. 19).

Jiang LL, Che MX, Zhao J, Zhou CJ, Xie MY, Li HY, He JH, and Hu HY (2013). "Structural transformation of the amyloidogenic core region of TDP-43 protein initiates its aggregation and cytoplasmic inclusion". *J Biol Chem* 288(27):19614–24. DOI: 10.1074/jbc.M113.463828 (cit. on p. 24).

Jiang LL, Xue W, Hong JY, Zhang JT, Li MJ, Yu SN, He JH, and Hu HY (2017). "The N-terminal dimerization is required for TDP-43 splicing activity". *Sci Rep* 7(1):6196. DOI: 10.1038/s41598-017-06263-3 (cit. on pp. 24, 28).

Jiang M, Rao R, Wang J, Wang J, Xu L, Wu LM, Chan JR, Wang H, and Lu QR (2018). "The TSC1-mTOR-PLK axis regulates the homeostatic switch from Schwann cell proliferation to myelination in a stage-specific manner". *Glia* 66(9):1947–1959. DOI: 10.1002/glia.23449 (cit. on p. 14).

Jo BS and Choi SS (2015). "Introns: The Functional Benefits of Introns in Genomes". *Genomics Inform* 13(4):112–8. DOI: 10.5808/GI.2015.13.4.112 (cit. on p. 29).

Joseph NM, Mukouyama YS, Mosher JT, Jaegle M, Crone SA, Dormand EL, Lee KF, Meijer D, Anderson DJ, and Morrison SJ (2004). "Neural crest stem cells undergo multilineage differentiation in developing peripheral nerves to generate endoneurial fibroblasts in addition to Schwann cells". *Development* 131(22):5599–612. DOI: 10.1242/dev.01429 (cit. on p. 11).

Kametani F, Obi T, Shishido T, Akatsu H, Murayama S, Saito Y, Yoshida M, and Hasegawa M (2016). "Mass spectrometric analysis of accumulated TDP-43 in amyotrophic lateral sclerosis brains". *Sci Rep* 6:23281. DOI: 10.1038/srep23281 (cit. on p. 27).

Kang SH, Fukaya M, Yang JK, Rothstein JD, and Bergles DE (2010). "NG2+ CNS glial progenitors remain committed to the oligodendrocyte lineage in postnatal life and following neurodegeneration". *Neuron* 68(4):668–81. DOI: 10.1016/j.neuron.2010.09.009 (cit. on pp. 18, 19).

Kang SH, Li Y, Fukaya M, Lorenzini I, Cleveland DW, Ostrow LW, Rothstein JD, and Bergles DE (2013). "Degeneration and impaired regeneration of gray matter oligodendrocytes in amyotrophic lateral sclerosis". *Nat Neurosci* 16(5):571–9. DOI: 10.1038/nn.3357 (cit. on pp. 22, 115, 135).

Kao SC, Wu H, Xie J, Chang CP, Ranish JA, Graef IA, and Crabtree GR (2009). "Calcineurin/NFAT signaling is required for neuregulin-regulated Schwann cell differentiation". *Science* 323(5914):651–4. DOI: 10.1126/science.1166562 (cit. on p. 13).

Kapeli K, Martinez FJ, and Yeo GW (2017). "Genetic mutations in RNA-binding proteins and their roles in ALS". *Hum Genet* 136(9):1193–1214. DOI: 10.1007/s00439-017-1830-7 (cit. on p. 21).

Karadottir R, Hamilton NB, Bakiri Y, and Attwell D (2008). "Spiking and nonspiking classes of oligodendrocyte precursor glia in CNS white matter". *Nat Neurosci* 11(4):450–6. DOI: 10.1038/nn2060 (cit. on p. 134).

Karn J, Vidali G, Boffa LC, and Allfrey VG (1977). "Characterization of the non-histone nuclear proteins associated with rapidly labeled heterogeneous nuclear RNA". *J Biol Chem* 252(20):7307–22 (cit. on p. 24).

Kaukua N, Shahidi MK, Konstantinidou C, Dyachuk V, Kaucka M, Furlan A, An Z, Wang L, Hultman I, Ahrlund-Richter L, Blom H, Brismar H, Lopes NA, Pachnis V, Suter U, Clevers H, Thesleff I, Sharpe P, Ernfors P, Fried K, and Adameyko I (2014). "Glial origin of mesenchymal stem cells in a tooth model system". *Nature* 513(7519):551–4. DOI: 10.1038/nature13536 (cit. on p. 11).

Kawahara Y and Mieda-Sato A (2012). "TDP-43 promotes microRNA biogenesis as a component of the Drosha and Dicer complexes". *Proc Natl Acad Sci U S A* 109(9):3347–52. DOI: 10.1073/pnas.1112427109 (cit. on p. 27).

Keren H, Lev-Maor G, and Ast G (2010). "Alternative splicing and evolution: diversification, exon definition and function". *Nat Rev Genet* 11(5):345–55. DOI: 10.1038/nrg2776 (cit. on p. 32).

Kessaris N, Fogarty M, Iannarelli P, Grist M, Wegner M, and Richardson WD (2006). "Competing waves of oligodendrocytes in the forebrain and postnatal elimination of an embryonic lineage". *Nat Neurosci* 9(2):173–9. DOI: 10.1038/nn1620 (cit. on p. 16).

Kim D, Choi JO, Fan C, Shearer RS, Sharif M, Busch P, and Park Y (2017). "Homo-trimerization is essential for the transcription factor function of Myrf for oligodendrocyte differentiation". *Nucleic Acids Res* 45(9):5112–5125. DOI: 10.1093/nar/gkx080 (cit. on p. 19).

Kim KY, Lee HW, Shim YM, Mook-Jung I, Jeon GS, and Sung JJ (2015). "A phosphomimetic mutant TDP-43 (S409/410E) induces Drosha instability and cytotoxicity in Neuro 2A cells". *Biochem Biophys Res Commun* 464(1):236–43. DOI: 10.1016/j.bbrc.2015.06.125 (cit. on p. 27).

Kim S, Merrill BM, Rajpurohit R, Kumar A, Stone KL, Papov VV, Schneiders JM, Szer W, Wilson SH, Paik WK, and Williams KR (1997). "Identification of N(G)-methylarginine residues in human heterogeneous RNP protein A1: Phe/Gly-Gly-Gly-Arg-Gly-Gly-Gly/Phe is a preferred recognition motif". *Biochemistry* 36(17):5185–92. DOI: 10.1021/bi9625509 (cit. on p. 24).

Kim W, Bennett EJ, Huttlin EL, Guo A, Li J, Possemato A, Sowa ME, Rad R, Rush J, Comb MJ, Harper JW, and Gygi SP (2011). "Systematic and quantitative assessment of the ubiquitin-modified proteome". *Mol Cell* 44(2):325–40. DOI: 10.1016/j.molcel.2011.08.025 (cit. on p. 27).

Kirby BB, Takada N, Latimer AJ, Shin J, Carney TJ, Kelsh RN, and Appel B (2006). "In vivo time-lapse imaging shows dynamic oligodendrocyte progenitor behavior during zebrafish development". *Nat Neurosci* 9(12):1506–11. DOI: 10.1038/nn1803 (cit. on p. 18).

Kirby L, Jin J, Cardona JG, Smith MD, Martin KA, Wang J, Strasburger H, Herbst L, Alexis M, Karnell J, Davidson T, Dutta R, Goverman J, Bergles D, and Calabresi PA (2019). "Oligodendrocyte precursor cells present antigen and are cytotoxic targets in inflammatory demyelination". *Nat Commun* 10(1):3887. DOI: 10.1038/s41467-019-11638-3 (cit. on p. 19).

Kirschner DA and Ganser AL (1980). "Compact myelin exists in the absence of basic protein in the shiverer mutant mouse". *Nature* 283(5743):207–10. DOI: 10.1038/283207a0 (cit. on p. 10).

Kleopa KA, Orthmann JL, Enriquez A, Paul DL, and Scherer SS (2004). "Unique distributions of the gap junction proteins connexin29, connexin32, and connexin47 in oligodendrocytes". *Glia* 47(4):346–57. DOI: 10.1002/glia.20043 (cit. on p. 134).

Klim JR, Williams LA, Limone F, Guerra San Juan I, Davis-Dusenbery BN, Mordes DA, Burberry A, Steinbaugh MJ, Gamage KK, Kirchner R, Moccia R, Cassel SH, Chen K, Wainger BJ, Woolf CJ, and Eggan K (2019). "ALS-implicated protein TDP-43 sustains levels of STMN2, a mediator of motor neuron growth and repair". *Nat Neurosci* 22(2):167–179. DOI: 10.1038/s41593-018-0300-4 (cit. on p. 32).

Ko HS, Uehara T, Tsuruma K, and Nomura Y (2004). "Ubiquilin interacts with ubiquitylated proteins and proteasome through its ubiquitin-associated and ubiquitin-like domains". *FEBS Lett* 566(1-3):110–4. DOI: 10.1016/j.febslet.2004.04.031 (cit. on p. 28).

Kolb SJ and Kissel JT (2011). "Spinal muscular atrophy: a timely review". *Arch Neurol* 68(8):979–84. DOI: 10.1001/archneurol.2011.74 (cit. on p. 72).

Kondziella W (1964). "[a New Method for the Measurement of Muscle Relaxation in White Mice]". *Arch Int Pharmacodyn Ther* 152:277–84 (cit. on p. 37).

Kraemer BC, Schuck T, Wheeler JM, Robinson LC, Trojanowski JQ, Lee VM, and Schellenberg GD (2010). "Loss of murine TDP-43 disrupts motor function and plays an essential role in embryogenesis". *Acta Neuropathol* 119(4): 409–19. DOI: 10.1007/s00401-010-0659-0 (cit. on p. 122).

Krasnow AM, Ford MC, Valdivia LE, Wilson SW, and Attwell D (2018). "Regulation of developing myelin sheath elongation by oligodendrocyte calcium transients in vivo". *Nat Neurosci* 21(1):24–28. DOI: 10.1038/s41593-017-0031-y (cit. on p. 19).

Laatsch RH, Kies MW, Gordon S, and Alvord E. C. J (1962). "The encephalomyelitic activity of myelin isolated by ultracentrifugation". *J Exp Med* 115(4):777–88. DOI: 10.1084/jem.115.4.777 (cit. on p. 10).

Lalmansingh AS, Urekar CJ, and Reddi PP (2011). "TDP-43 is a transcriptional repressor: the testis-specific mouse acrv1 gene is a TDP-43 target in vivo". *J Biol Chem* 286(13):10970–82. DOI: 10.1074/jbc.M110.166587 (cit. on p. 26).

Lander ES, Linton LM, Birren B, Nusbaum C, Zody MC, Baldwin J, Devon K, Dewar K, Doyle M, FitzHugh W, Funke R, Gage D, Harris K, Heaford A, Howland J, Kann L, Lehoczky J, LeVine R, McEwan P, McKernan K, Meldrim J, Mesirov JP, Miranda C, Morris W, Naylor J, Raymond C, Rosetti M, Santos R, Sheridan A, Sougnez C, Stange-Thomann Y, Stojanovic N, Subramanian A, Wyman D, Rogers J, Sulston J, Ainscough R, Beck S, Bentley D, Burton J, Clee C, Carter N, Coulson A, Deadman R, Deloukas P, Dunham A, Dunham I, Durbin R, French L, Grafham D, Gregory S, Hubbard T, Humphray S, Hunt A, Jones M, Lloyd C, McMurray A, Matthews L, Mercer S, Milne S, Mullikin JC, Mungall A, Plumb R, Ross M, Shownkeen R, Sims S, Waterston RH, Wilson RK, Hillier LW, McPherson JD, Marra MA, Mardis ER, Fulton LA, Chinwalla AT, Pepin KH, Gish WR, Chissoe SL, Wendl MC, Delehaunty KD, Miner TL, Delehaunty A, Kramer JB, Cook LL, Fulton RS, Johnson DL, Minx PJ, Clifton SW, Hawkins T, Branscomb E, Predki P, Richardson P, Wenning S, Slezak T, Doggett N, Cheng JF, Olsen A, Lucas S, Elkin C, Uberbacher E, Frazier M, et al. (2001). "Initial sequencing and analysis of the human genome". *Nature* 409(6822):860–921. DOI: 10.1038/35057062 (cit. on p. 32).

Lappe-Siefke C, Goebbels S, Gravel M, Nicksch E, Lee J, Braun PE, Griffiths IR, and Nave KA (2003). "Disruption of Cnp1 uncouples oligodendroglial functions in axonal support and myelination". *Nat Genet* 33(3):366–74. DOI: 10.1038/ng1095 (cit. on pp. 11, 35, 99).

Lareau LF, Inada M, Green RE, Wengrod JC, and Brenner SE (2007). "Unproductive splicing of SR genes associated with highly conserved and ultraconserved DNA elements". *Nature* 446(7138):926–9. DOI: 10.1038/nature05676 (cit. on pp. 31, 32).

Lasiene J, Matsui A, Sawa Y, Wong F, and Horner PJ (2009). "Age-related myelin dynamics revealed by increased oligodendrogenesis and short internodes". *Aging Cell* 8(2):201–13. DOI: 10.1111/j.1474-9726.2009.00462.x (cit. on p. 135).

Le N, Nagarajan R, Wang JY, Araki T, Schmidt RE, and Milbrandt J (2005a). "Analysis of congenital hypomyelinating Egr2Lo/Lo nerves identifies Sox2 as an inhibitor of Schwann cell differentiation and myelination". *Proc Natl Acad Sci U S A* 102(7):2596–601. DOI: 10.1073/pnas.0407836102 (cit. on p. 14).

Le N, Nagarajan R, Wang JYT, Svaren J, LaPash C, Araki T, Schmidt RE, and Milbrandt J (2005b). "Nab proteins are essential for peripheral nervous system myelination". *Nature Neuroscience* 8(7):932–940. DOI: 10.1038/nn1490 (cit. on p. 13).

Leblanc SE, Srinivasan R, Ferri C, Mager GM, Gillian-Daniel AL, Wrabetz L, and Svaren J (2005). "Regulation of cholesterol/lipid biosynthetic genes by Egr2/Krox20 during peripheral nerve myelination". *J Neurochem* 93(3):737–48. DOI: 10.1111/j.1471-4159.2005.03056.x (cit. on p. 14).

Lee EB, Lee VM, and Trojanowski JQ (2011). "Gains or losses: molecular mechanisms of TDP43-mediated neurodegeneration". *Nat Rev Neurosci* 13(1):38–50. DOI: 10.1038/nrn3121 (cit. on p. 21).

Lee S, Leach MK, Redmond SA, Chong SY, Mellon SH, Tuck SJ, Feng ZQ, Corey JM, and Chan JR (2012a). "A culture system to study oligodendrocyte myelination processes using engineered nanofibers". *Nat Methods* 9(9):917–22. DOI: 10.1038/nmeth.2105 (cit. on p. 18).

Lee Y, Morrison BM, Li Y, Lengacher S, Farah MH, Hoffman PN, Liu Y, Tsingalia A, Jin L, Zhang PW, Pellerin L, Magistretti PJ, and Rothstein JD (2012b). "Oligodendroglia metabolically support axons and contribute to neurodegeneration". *Nature* 487(7408):443–8. DOI: 10.1038/nature11314 (cit. on p. 19).

Lefebvre S, Bürglen L, Reboullet S, Clermont O, Burlet P, Viollet L, Benichou B, Cruaud C, Millasseau P, Zeviani M, Le Paslier D, Frézal J, Cohen D, Weissenbach J, Munnich A, and Melki J (1995). "Identification and characterization of a spinal muscular atrophy-determining gene". *Cell* 80(1):155–165. DOI: 10.1016/0092-8674(95)90460-3 (cit. on p. 20).

Leone DP, Genoud S, Atanasoski S, Grausenburger R, Berger P, Metzger D, Macklin WB, Chambon P, and Suter U (2003). "Tamoxifen-inducible glia-specific Cre mice for somatic mutagenesis in oligodendrocytes and Schwann cells". *Mol Cell Neurosci* 22(4):430–40. DOI: http://dx.doi.org/10.1016/S1044-7431(03)00029-0 (cit. on pp. 35, 75, 110).

Lewis BP, Green RE, and Brenner SE (2003). "Evidence for the widespread coupling of alternative splicing and nonsense-mediated mRNA decay in humans". *Proc Natl Acad Sci U S A* 100(1):189–92. DOI: 10.1073/pnas.0136770100 (cit. on p. 31).

Li H, Zhang P, Zhang Q, Li C, Zou W, Chang Z, Cui CP, and Zhang L (2018a). "WWP2 is a physiological ubiquitin ligase for phosphatase and tensin homolog (PTEN) in mice". *J Biol Chem* 293(23):8886–8899. DOI: 10.1074/jbc.RA117.001060 (cit. on p. 103).

Li Q, Yokoshi M, Okada H, and Kawahara Y (2015). "The cleavage pattern of TDP-43 determines its rate of clearance and cytotoxicity". *Nat Commun* 6:6183. DOI: 10.1038/ncomms7183 (cit. on p. 28).

Li T, Evdokimov E, Shen RF, Chao CC, Tekle E, Wang T, Stadtman ER, Yang DC, and Chock PB (2004). "Sumoylation of heterogeneous nuclear ribonucleoproteins, zinc finger proteins, and nuclear pore complex proteins: a proteomic analysis". *Proc Natl Acad Sci U S A* 101(23):8551–6. DOI: 10.1073/pnas.0402889101 (cit. on p. 24).

Li T, Wang J, Wang H, Yang Y, Wang S, Huang N, Wang F, Gao X, Niu J, Li Z, Mei F, and Xiao L (2018b). "The deletion of dicer in mature myelinating glial cells causes progressive axonal degeneration but not overt demyelination in adult mice". *Glia* 66(9):1960–1971. DOI: 10.1002/glia.23450 (cit. on p. 130).

Li Z, Park Y, and Marcotte EM (2013). "A Bacteriophage tailspike domain promotes self-cleavage of a human membrane-bound transcription factor, the myelin regulatory factor MYRF". *PLoS Biol* 11(8):e1001624. DOI: 10.1371/journal.pbio.1001624 (cit. on p. 19).

Liang XH, Haritan A, Uliel S, and Michaeli S (2003). "trans and cis splicing in trypanosomatids: mechanism, factors, and regulation". *Eukaryot Cell* 2(5):830–40. DOI: 10.1128/ec.2.5.830-840.2003 (cit. on p. 29).

Liao Y, Smyth GK, and Shi W (2019). "The R package Rsubread is easier, faster, cheaper and better for alignment and quantification of RNA sequencing reads". *Nucleic Acids Res* 47(8):e47. DOI: 10.1093/nar/gkz114 (cit. on p. 47).

Lin HP, Oksuz I, Hurley E, Wrabetz L, and Awatramani R (2015). "Microprocessor complex subunit DiGeorge syndrome critical region gene 8 (Dgcr8) is required for schwann cell myelination and myelin maintenance". *J Biol Chem* 290(40):24294–307. DOI: 10.1074/jbc.M115.636407 (cit. on p. 130).

Lin L, Jiang P, Shen S, Sato S, Davidson BL, and Xing Y (2009). "Large-scale analysis of exonized mammalian-wide interspersed repeats in primate genomes". *Hum Mol Genet* 18(12):2204–14. DOI: 10.1093/hmg/ddp152 (cit. on p. 32).

Ling JP, Chhabra R, Merran JD, Schaughency PM, Wheelan SJ, Corden JL, and Wong PC (2016). "PTBP1 and PTBP2 Repress Nonconserved Cryptic Exons". *Cell Rep* 17(1):104–113. DOI: 10.1016/j.celrep.2016.08.071 (cit. on pp. 31, 32, 125).

Ling JP, Pletnikova O, Troncoso JC, and Wong PC (2015). "TDP-43 repression of nonconserved cryptic exons is compromised in ALS-FTD". *Science* 349(6248):650–5. DOI: 10.1126/science.aab0983 (cit. on pp. 26, 31, 32, 59, 61, 99, 101).

Ling SC, Albuquerque CP, Han JS, Lagier-Tourenne C, Tokunaga S, Zhou H, and Cleveland DW (2010). "ALS-associated mutations in TDP-43 increase its stability and promote TDP-43 complexes with FUS/TLS". *Proc Natl Acad Sci U S A* 107(30):13318–23. DOI: 10.1073/pnas.1008227107 (cit. on p. 27).

Ling SC, Polymenidou M, and Cleveland DW (2013). "Converging mechanisms in ALS and FTD: disrupted RNA and protein homeostasis". *Neuron* 79(3):416–38. DOI: 10.1016/j.neuron.2013.07.033 (cit. on p. 20).

Liu A and Niswander LA (2005). "Bone morphogenetic protein signalling and vertebrate nervous system development". *Nat Rev Neurosci* 6(12):945–54. DOI: 10.1038/nrn1805 (cit. on p. 16).

Liu J, Willet SG, Bankaitis ED, Xu Y, Wright CV, and Gu G (2013). "Non-parallel recombination limits Cre-LoxP-based reporters as precise indicators of conditional genetic manipulation". *Genesis* 51(6):436–42. DOI: 10.1002/dvg.22384 (cit. on p. 131).

Lobsiger CS, Boillee S, McAlonis-Downes M, Khan AM, Feltri ML, Yamanaka K, and Cleveland DW (2009). "Schwann cells expressing dismutase active mutant SOD1 unexpectedly slow disease progression in ALS mice". *Proc Natl Acad Sci U S A* 106(11):4465–70. DOI: 10.1073/pnas.0813339106 (cit. on p. 23).

Logroscino G, Traynor BJ, Hardiman O, Chio A, Mitchell D, Swingler RJ, Millul A, Benn E, Beghi E, and Eurals (2010). "Incidence of amyotrophic lateral sclerosis in Europe". *J Neurol Neurosurg Psychiatry* 81(4):385–90. DOI: 10.1136/jnnp.2009.183525 (cit. on p. 21).

Louis JC, Magal E, Takayama S, and Varon S (1993). "CNTF protection of oligodendrocytes against natural and tumor necrosis factor-induced death". *Science* 259(5095):689–92. DOI: 10.1126/science.8430320 (cit. on p. 17).

Lu QR, Yuk Di, Alberta JA, Zhu Z, Pawlitzky I, Chan J, McMahon AP, Stiles CD, and Rowitch DH (2000). "Sonic Hedgehog–Regulated Oligodendrocyte Lineage Genes Encoding bHLH Proteins in the Mammalian Central Nervous System". *Neuron* 25(2):317–329. DOI: 10.1016/s0896-6273(00)80897-1 (cit. on p. 16).

Luders KA, Nessler S, Kusch K, Patzig J, Jung RB, Mobius W, Nave KA, and Werner HB (2019). "Maintenance of high proteolipid protein level in adult central nervous system myelin is required to preserve the integrity of myelin and axons". *Glia* 67(4):634–649. DOI: 10.1002/glia.23549 (cit. on p. 10).

Lundgaard I, Luzhynskaya A, Stockley JH, Wang Z, Evans KA, Swire M, Volbracht K, Gautier HO, Franklin RJ, Charles FC, Attwell D, and Karadottir RT (2013). "Neuregulin and BDNF induce a switch to NMDA receptor-dependent myelination by oligodendrocytes". *PLoS Biol* 11(12):e1001743. DOI: 10.1371/journal.pbio.1001743 (cit. on p. 18).

Lunn KF, Clayton MK, and Duncan ID (1997). "The temporal progression of the myelination defect in the taiep rat". *J Neurocytol* 26(5):267–81. DOI: 10.1023/a:1018548400536 (cit. on p. 9).

Lutz C (2018). "Mouse models of ALS: Past, present and future". *Brain Res* 1693(Pt A):1–10. DOI: 10.1016/j.brainres.2018.03.024 (cit. on p. 122).

Lykke-Andersen S and Jensen TH (2015). "Nonsense-mediated mRNA decay: an intricate machinery that shapes transcriptomes". *Nat Rev Mol Cell Biol* 16(11):665–77. DOI: 10.1038/nrm4063 (cit. on p. 31).

Lyons DA, Pogoda HM, Voas MG, Woods IG, Diamond B, Nix R, Arana N, Jacobs J, and Talbot WS (2005). "erbb3 and erbb2 are essential for schwann cell migration and myelination in zebrafish". *Curr Biol* 15(6):513–24. DOI: 10.1016/j.cub.2005.02.030 (cit. on p. 11).

Lyssiotis CA, Walker J, Wu C, Kondo T, Schultz PG, and Wu X (2007). "Inhibition of histone deacetylase activity induces developmental plasticity in oligodendrocyte precursor cells". *Proc Natl Acad Sci U S A* 104(38):14982–7. DOI: 10.1073/pnas.0707044104 (cit. on p. 18).

Mackenzie IR, Bigio EH, Ince PG, Geser F, Neumann M, Cairns NJ, Kwong LK, Forman MS, Ravits J, Stewart H, Eisen A, McClusky L, Kretzschmar HA, Monoranu CM, Highley JR, Kirby J, Siddique T, Shaw PJ, Lee VM, and Trojanowski JQ (2007). "Pathological TDP-43 distinguishes sporadic amyotrophic lateral sclerosis from amyotrophic lateral sclerosis with SOD1 mutations". *Ann Neurol* 61(5):427–34. DOI: 10.1002/ana.21147 (cit. on p. 21).

Madisen L, Zwingman TA, Sunkin SM, Oh SW, Zariwala HA, Gu H, Ng LL, Palmiter RD, Hawrylycz MJ, Jones AR, Lein ES, and Zeng H (2010). "A robust and high-throughput Cre reporting and characterization system for the whole mouse brain". *Nat Neurosci* 13(1):133–40. DOI: 10.1038/nn.2467 (cit. on pp. 35, 78, 87, 99, 110, 131).

Madsen PM, Motti D, Karmally S, Szymkowski DE, Lambertsen KL, Bethea JR, and Brambilla R (2016). "Oligodendroglial TNFR2 Mediates Membrane TNF-Dependent Repair in Experimental Autoimmune Encephalomyelitis by Promoting Oligodendrocyte Differentiation and Remyelination". *J Neurosci* 36(18):5128–43. DOI: 10.1523/JNEUROSCI.0211-16.2016 (cit. on p. 131).

Maier MM and Gessler M (2000). "Comparative analysis of the human and mouse Hey1 promoter: Hey genes are new Notch target genes". *Biochem Biophys Res Commun* 275(2):652–60. DOI: 10.1006/bbrc.2000.3354 (cit. on p. 103).

Maire CL, Ramkissoon S, Hayashi M, Haidar S, Ramkissoon L, DiTomaso E, and Ligon KL (2014). "Pten loss in Olig2 expressing neural progenitor cells and oligodendrocytes leads to interneuron dysplasia and leukodystrophy". *Stem Cells* 32(1):313–26. DOI: 10.1002/stem.1590 (cit. on p. 108).

Marin-Husstege M, Muggironi M, Liu AX, and Casaccia-Bonnefil P (2002). "Histone deacetylase activity is necessary for oligodendrocyte lineage progression". *Journal of Neuroscience* 22(23):10333–10345. DOI: 10.1523/jneurosci.22-23-10333.2002 (cit. on p. 18).

Maro GS, Vermeren M, Voiculescu O, Melton L, Cohen J, Charnay P, and Topilko P (2004). "Neural crest boundary cap cells constitute a source of neuronal and glial cells of the PNS". *Nat Neurosci* 7(9):930–8. DOI: 10.1038/nn1299 (cit. on p. 128).

Marques S, Bruggen D van, Vanichkina DP, Floriddia EM, Munguba H, Varemo L, Giacomello S, Falcao AM, Meijer M, Bjorklund AK, Hjerling-Leffler J, Taft RJ, and Castelo-Branco G (2018). "Transcriptional Convergence of Oligodendrocyte Lineage Progenitors during Development". *Dev Cell* 46(4):504–517 e7. DOI: 10.1016/j.devcel.2018.07.005 (cit. on p. 134).

Marques S, Zeisel A, Codeluppi S, Bruggen D van, Mendanha Falcao A, Xiao L, Li H, Haring M, Hochgerner H, Romanov RA, Gyllborg D, Munoz Manchado A, La Manno G, Lonnerberg P, Floriddia EM, Rezayee F, Ernfors P, Arenas E, Hjerling-Leffler J, Harkany T, Richardson WD, Linnarsson S, and Castelo-Branco G (2016). "Oligodendrocyte heterogeneity in the mouse juvenile and adult central nervous system". *Science* 352(6291):1326–1329. DOI: 10.1126/science.aaf6463 (cit. on pp. 87, 94, 101, 102, 135).

Marquez Y, Hopfler M, Ayatollahi Z, Barta A, and Kalyna M (2015). "Unmasking alternative splicing inside protein-coding exons defines exitrons and their role in proteome plasticity". *Genome Res* 25(7):995–1007. DOI: 10.1101/gr.186585.114 (cit. on p. 31).

Martini R, Mohajeri MH, Kasper S, Giese KP, and Schachner M (1995). "Mice Doubly Deficient in the Genes for Po and Myelin Basic-Protein Show That Both Proteins Contribute to the Formation of the Major Dense Line in Peripheral-Nerve Myelin". *Journal of Neuroscience* 15(6):4488–4495 (cit. on p. 10).

Mathey EK, Park SB, Hughes RAC, Pollard JD, Armati PJ, Barnett MH, Taylor BV, Dyck PJB, Kiernan MC, and Lin CSY (2015). "Chronic inflammatory demyelinating polyradiculoneuropathy: from pathology to phenotype". *Journal of Neurology, Neurosurgery & Psychiatry* 86(9):973–985. DOI: 10.1136/jnnp-2014-309697 (cit. on p. 138).

Mathis S, Goizet C, Soulages A, Vallat JM, and Masson GL (2019). "Genetics of amyotrophic lateral sclerosis: A review". *J Neurol Sci* 399:217–226. DOI: 10.1016/j.jns.2019.02.030 (cit. on p. 21).

Matthews MA and Duncan D (1971). "A quantitative study of morphological changes accompanying the initiation and progress of myelin production in the dorsal funiculus of the rat spinal cord". *J Comp Neurol* 142(1):1–22. DOI: 10.1002/cne.901420102 (cit. on pp. 18, 90).

Matunis EL, Matunis MJ, and Dreyfuss G (1992). "Characterization of the major hnRNP proteins from Drosophila melanogaster". *J Cell Biol* 116(2):257–69. DOI: 10.1083/jcb.116.2.257 (cit. on p. 23).

McCampbell A, Cole T, Wegener AJ, Tomassy GS, Setnicka A, Farley BJ, Schoch KM, Hoye ML, Shabsovich M, Sun L, Luo Y, Zhang M, Comfort N, Wang B, Amacker J, Thankamony S, Salzman DW, Cudkowicz M, Graham DL, Bennett CF, Kordasiewicz HB, Swayze EE, and Miller TM (2018). "Antisense oligonucleotides extend survival and reverse decrement in muscle response in ALS models". *J Clin Invest* 128(8):3558–3567. DOI: 10.1172/JCI99081 (cit. on p. 22).

McClory SP, Lynch KW, and Ling JP (2018). "HnRNP L represses cryptic exons". *RNA* 24(6):761–768. DOI: 10.1261/rna.065508.117 (cit. on pp. 32, 125).

McDonald KK, Aulas A, Destroismaisons L, Pickles S, Beleac E, Camu W, Rouleau GA, and Vande Velde C (2011). "TAR DNA-binding protein 43 (TDP-43) regulates stress granule dynamics via differential regulation of G3BP and TIA-1". *Hum Mol Genet* 20(7):1400–10. DOI: 10.1093/hmg/ddr021 (cit. on p. 27).

McGinnis CS, Murrow LM, and Gartner ZJ (2019). "DoubletFinder: Doublet Detection in Single-Cell RNA Sequencing Data Using Artificial Nearest Neighbors". *Cell Syst* 8(4):329–337 e4. DOI: 10.1016/j.cels.2019.03.003 (cit. on pp. 48, 102, V).

McKerracher L and Rosen KM (2015). "MAG, myelin and overcoming growth inhibition in the CNS". *Front Mol Neurosci* 8:51. DOI: 10.3389/fnmol.2015.00051 (cit. on p. 11).

Mei F, Fancy SPJ, Shen YA, Niu J, Zhao C, Presley B, Miao E, Lee S, Mayoral SR, Redmond SA, Etxeberria A, Xiao L, Franklin RJM, Green A, Hauser SL, and Chan JR (2014). "Micropillar arrays as a high-throughput screening platform for therapeutics in multiple sclerosis". *Nat Med* 20(8):954–960. DOI: 10.1038/nm.3618 (cit. on p. 18).

Meier C, Parmantier E, Brennan A, Mirsky R, and Jessen KR (1999). "Developing Schwann Cells Acquire the Ability to Survive without Axons by Establishing an Autocrine Circuit Involving Insulin-Like Growth Factor, Neurotrophin-3, and Platelet-Derived Growth Factor-BB". *The Journal of Neuroscience* 19(10):3847–3859. DOI: 10.1523/jneurosci.19-10-03847.1999 (cit. on p. 12).

Melamed Z, Lopez-Erauskin J, Baughn MW, Zhang O, Drenner K, Sun Y, Freyermuth F, McMahon MA, Beccari MS, Artates JW, Ohkubo T, Rodriguez M, Lin N, Wu D, Bennett CF, Rigo F, Da Cruz S, Ravits J, Lagier-Tourenne C, and Cleveland DW (2019). "Premature polyadenylation-mediated loss of stathmin-2 is a hallmark of TDP-43-dependent neurodegeneration". *Nat Neurosci* 22(2):180–190. DOI: 10.1038/s41593-018-0293-z (cit. on p. 32).

Mendell JT, Sharifi NA, Meyers JL, Martinez-Murillo F, and Dietz HC (2004). "Nonsense surveillance regulates expression of diverse classes of mammalian transcripts and mutes genomic noise". *Nat Genet* 36(10):1073–8. DOI: 10.1038/ng1429 (cit. on p. 31).

Merrill BM, LoPresti MB, Stone KL, and Williams KR (1986). "High pressure liquid chromatography purification of UP1 and UP2, two related single-stranded nucleic acid-binding proteins from calf thymus". *J Biol Chem* 261(2):878–83 (cit. on p. 24).

Michailov GV, Sereda MW, Brinkmann BG, Fischer TM, Haug B, Birchmeier C, Role L, Lai C, Schwab MH, and Nave KA (2004). "Axonal neuregulin-1 regulates myelin sheath thickness". *Science* 304(5671):700–3. DOI: 10.1126/science.1095862 (cit. on pp. 9, 13).

Miller RG, Mitchell JD, and Moore DH (2012). "Riluzole for amyotrophic lateral sclerosis (ALS)/motor neuron disease (MND)". *Cochrane Database Syst Rev* (3):CD001447. DOI: 10.1002/14651858.CD001447.pub3 (cit. on p. 22).

Mioshi E, Caga J, Lillo P, Hsieh S, Ramsey E, Devenney E, Hornberger M, Hodges JR, and Kiernan MC (2014). "Neuropsychiatric changes precede classic motor symptoms in ALS and do not affect survival". *Neurology* 82(2):149–55. DOI: 10.1212/WNL.0000000000000023 (cit. on p. 20).

Miron VE (2017). "Microglia-driven regulation of oligodendrocyte lineage cells, myelination, and remyelination". *J Leukoc Biol* 101(5):1103–1108. DOI: 10.1189/jlb.3RI1116-494R (cit. on p. 136).

Miron VE, Boyd A, Zhao JW, Yuen TJ, Ruckh JM, Shadrach JL, Wijngaarden P van, Wagers AJ, Williams A, Franklin RJM, and Ffrench-Constant C (2013). "M2 microglia and macrophages drive oligodendrocyte differentiation during CNS remyelination". *Nat Neurosci* 16(9):1211–1218. DOI: 10.1038/nn.3469 (cit. on p. 136).

Mizoule J, Meldrum B, Mazadier M, Croucher M, Ollat C, Uzan A, Legrand JJ, Gueremy C, and Le Fur G (1985). "2-Amino-6-trifluoromethoxy benzothiazole, a possible antagonist of excitatory amino acid neurotransmission–I. Anticonvulsant properties". *Neuropharmacology* 24(8):767–73. DOI: 10.1016/0028-3908(85)90011-5 (cit. on p. 22).

Mogha A, Benesh AE, Patra C, Engel FB, Schoneberg T, Liebscher I, and Monk KR (2013). "Gpr126 functions in Schwann cells to control differentiation and myelination via G-protein activation". *J Neurosci* 33(46):17976–85. DOI: 10.1523/JNEUROSCI.1809-13.2013 (cit. on p. 137).

Mompean M, Buratti E, Guarnaccia C, Brito RM, Chakrabartty A, Baralle FE, and Laurents DV (2014). ""Structural characterization of the minimal segment of TDP-43 competent for aggregation"". *Arch Biochem Biophys* 545:53–62. DOI: 10.1016/j.abb.2014.01.007 (cit. on p. 24).

Mompean M, Hervas R, Xu Y, Tran TH, Guarnaccia C, Buratti E, Baralle F, Tong L, Carrion-Vazquez M, McDermott AE, and Laurents DV (2015). "Structural Evidence of Amyloid Fibril Formation in the Putative Aggregation Domain of TDP-43". *J Phys Chem Lett* 6(13):2608–15. DOI: 10.1021/acs.jpclett.5b00918 (cit. on p. 24).

Monk KR, Naylor SG, Glenn TD, Mercurio S, Perlin JR, Dominguez C, Moens CB, and Talbot WS (2009). "A G protein-coupled receptor is essential for Schwann cells to initiate myelination". *Science* 325(5946):1402–5. DOI: 10.1126/science.1173474 (cit. on p. 12).

Montag D, Giese KP, Bartsch U, Martini R, Lang Y, Blüthmann H, Karthigasan J, Kirschner DA, Wintergerst ES, Nave KA, Zielasek J, Toyka KV, Lipp HP, and Schachner M (1994). "Mice deficient for the glycoprotein show subtle abnormalities in myelin". *Neuron* 13(1):229–246. DOI: 10.1016/0896-6273(94)90472-3 (cit. on p. 11).

Morgan JT, Fink GR, and Bartel DP (2019). "Excised linear introns regulate growth in yeast". *Nature* 565(7741): 606–611. DOI: 10.1038/s41586-018-0828-1 (cit. on pp. 29, 30).

Morrison BM, Tsingalia A, Vidensky S, Lee Y, Jin L, Farah MH, Lengacher S, Magistretti PJ, Pellerin L, and Rothstein JD (2015). "Deficiency in monocarboxylate transporter 1 (MCT1) in mice delays regeneration of peripheral nerves following sciatic nerve crush". *Exp Neurol* 263:325–38. DOI: 10.1016/j.expneurol.2014.10.018 (cit. on p. 130).

Morrissey TK, Levi AD, Nuijens A, Sliwkowski MX, and Bunge RP (1995). "Axon-induced mitogenesis of human Schwann cells involves heregulin and p185erbB2". *Proc Natl Acad Sci U S A* 92(5):1431–5. DOI: 10.1073/pnas.92.5.1431 (cit. on p. 12).

Muth KN, Piefke S, Weider M, Sock E, Hermans-Borgmeyer I, Wegner M, and Kuspert M (2016). "The Dual-specificity phosphatase Dusp15 is regulated by Sox10 and Myrf in Myelinating Oligodendrocytes". *Glia* 64(12):2120–2132. DOI: 10.1002/glia.23044 (cit. on p. 19).

Narayanan RK, Mangelsdorf M, Panwar A, Butler TJ, Noakes PG, and Wallace RH (2013). "Identification of RNA bound to the TDP-43 ribonucleoprotein complex in the adult mouse brain". *Amyotroph Lateral Scler Frontotemporal Degener* 14(4):252–60. DOI: 10.3109/21678421.2012.734520 (cit. on p. 26).

N'Diaye EN, Debnath J, and Brown EJ (2009a). "Ubiquilins accelerate autophagosome maturation and promote cell survival during nutrient starvation". *Autophagy* 5(4):573–5. DOI: 10.4161/auto.5.4.8312 (cit. on p. 28).

N'Diaye EN, Kajihara KK, Hsieh I, Morisaki H, Debnath J, and Brown EJ (2009b). "PLIC proteins or ubiquilins regulate autophagy-dependent cell survival during nutrient starvation". *EMBO Rep* 10(2):173–9. DOI: 10.1038/embor.2008.238 (cit. on p. 28).

Nelson AD and Jenkins PM (2017). "Axonal Membranes and Their Domains: Assembly and Function of the Axon Initial Segment and Node of Ranvier". *Front Cell Neurosci* 11:136. DOI: 10.3389/fncel.2017.00136 (cit. on p. 8).

Neumann M, Kwong LK, Lee EB, Kremmer E, Flatley A, Xu Y, Forman MS, Troost D, Kretzschmar HA, Trojanowski JQ, and Lee VM (2009). "Phosphorylation of S409/410 of TDP-43 is a consistent feature in all sporadic and familial forms of TDP-43 proteinopathies". *Acta Neuropathol* 117(2):137–49. DOI: 10.1007/s00401-008-0477-9 (cit. on p. 27).

Neumann M, Sampathu DM, Kwong LK, Truax AC, Micsenyi MC, Chou TT, Bruce J, Schuck T, Grossman M, Clark CM, McCluskey LF, Miller BL, Masliah E, Mackenzie IR, Feldman H, Feiden W, Kretzschmar HA, Trojanowski JQ, and Lee VM (2006). "Ubiquitinated TDP-43 in frontotemporal lobar degeneration and amyotrophic lateral sclerosis". *Science* 314(5796):130–3. DOI: 10.1126/science.1134108 (cit. on p. 21).

Ni JZ, Grate L, Donohue JP, Preston C, Nobida N, O'Brien G, Shiue L, Clark TA, Blume JE, and Ares M. J (2007). "Ultraconserved elements are associated with homeostatic control of splicing regulators by alternative splicing and nonsense-mediated decay". *Genes Dev* 21(6):708–18. DOI: 10.1101/gad.1525507 (cit. on pp. 31, 32).

Nishihira Y, Tan CF, Onodera O, Toyoshima Y, Yamada M, Morita T, Nishizawa M, Kakita A, and Takahashi H (2008). "Sporadic amyotrophic lateral sclerosis: two pathological patterns shown by analysis of distribution of TDP-43-immunoreactive neuronal and glial cytoplasmic inclusions". *Acta Neuropathol* 116(2):169–82. DOI: 10.1007/s00401-008-0385-z (cit. on p. 22).

Nodari A, Zambroni D, Quattrini A, Court FA, D'Urso A, Recchia A, Tybulewicz VL, Wrabetz L, and Feltri ML (2007). "Beta1 integrin activates Rac1 in Schwann cells to generate radial lamellae during axonal sorting and myelination". *J Cell Biol* 177(6):1063–75. DOI: 10.1083/jcb.200610014 (cit. on p. 137).

Norrmen C, Figlia G, Lebrun-Julien F, Pereira JA, Trotzmuller M, Kofeler HC, Rantanen V, Wessig C, Deijk AL van, Smit AB, Verheijen MH, Ruegg MA, Hall MN, and Suter U (2014). "mTORC1 controls PNS myelination along the mTORC1-RXRgamma-SREBP-lipid biosynthesis axis in Schwann cells". *Cell Rep* 9(2):646–60. DOI: 10.1016/j.celrep.2014.09.001 (cit. on p. 14).

Norrmen C, Figlia G, Pfistner P, Pereira JA, Bachofner S, and Suter U (2018). "mTORC1 Is Transiently Reactivated in Injured Nerves to Promote c-Jun Elevation and Schwann Cell Dedifferentiation". *J Neurosci* 38(20):4811–4828. DOI: 10.1523/JNEUROSCI.3619-17.2018 (cit. on p. 15).

Norton WT and Autilio LA (1965). "The Chemical Composition of Bovine Cns Myelin". *Ann N Y Acad Sci* 122(A1): 77–85. DOI: 10.1111/j.1749-6632.1965.tb20193.x (cit. on p. 10).

— (1966). "The lipid composition of purified bovine brain myelin". *J Neurochem* 13(4):213–22. DOI: 10.1111/j.1471-4159.1966.tb06794.x (cit. on p. 10).

Notterpek L, Ryan MC, Tobler AR, and Shooter EM (1999). "PMP22 accumulation in aggresomes: implications for CMT1A pathology". *Neurobiol Dis* 6(5):450–60. DOI: 10.1006/nbdi.1999.0274 (cit. on p. 10).

Obrien JS and Sampson EL (1965). "Lipid Composition of Normal Human Brain - Gray Matter White Matter and Myelin". *Journal of Lipid Research* 6(4):537–& (cit. on p. 10).

O'Brien JS, Sampson EL, and Stern MB (1967). "Lipid composition of myelin from the peripheral nervous system. Intradural spinal roots". *J Neurochem* 14(3):357–65. DOI: 10.1111/j.1471-4159.1967.tb09532.x (cit. on p. 10).

Ohuchi K, Funato M, Ando S, Inagaki S, Sato A, Kawase C, Seki J, Nakamura S, Shimazawa M, Kaneko H, and Hara H (2019). "Impairment of oligodendrocyte lineages in spinal muscular atrophy model systems". *Neuroreport* 30(5): 350–357. DOI: 10.1097/WNR.0000000000001206 (cit. on p. 20).

Olah M, Amor S, Brouwer N, Vinet J, Eggen B, Biber K, and Boddeke HW (2012). "Identification of a microglia phenotype supportive of remyelination". *Glia* 60(2):306–21. DOI: 10.1002/glia.21266 (cit. on p. 136).

O'Meara RW, Cummings SE, De Repentigny Y, McFall E, Michalski JP, Deguise MO, Gibeault S, and Kothary R (2017). "Oligodendrocyte development and CNS myelination are unaffected in a mouse model of severe spinal muscular atrophy". *Hum Mol Genet* 26(2):282–292. DOI: 10.1093/hmg/ddw385 (cit. on p. 20).

Ommer A, Figlia G, Pereira JA, Datwyler AL, Gerber J, DeGeer J, Lalli G, and Suter U (2019). "Ral GTPases in Schwann cells promote radial axonal sorting in the peripheral nervous system". *J Cell Biol* 218(7):2350–2369. DOI: 10.1083/jcb.201811150 (cit. on p. 137).

Ostareck-Lederer A, Ostareck DH, Cans C, Neubauer G, Bomsztyk K, Superti-Furga G, and Hentze MW (2002). "c-Src-mediated phosphorylation of hnRNP K drives translational activation of specifically silenced mRNAs". *Mol Cell Biol* 22(13):4535–43. DOI: 10.1128/mcb.22.13.4535-4543.2002 (cit. on p. 24).

Ostareck-Lederer A, Ostareck DH, Rucknagel KP, Schierhorn A, Moritz B, Huttelmaier S, Flach N, Handoko L, and Wahle E (2006). "Asymmetric arginine dimethylation of heterogeneous nuclear ribonucleoprotein K by protein-arginine methyltransferase 1 inhibits its interaction with c-Src". *J Biol Chem* 281(16):11115–25. DOI: 10.1074/jbc.M513053200 (cit. on p. 24).

Ou SH, Wu F, Harrich D, Garcia-Martinez LF, and Gaynor RB (1995). "Cloning and characterization of a novel cellular protein, TDP-43, that binds to human immunodeficiency virus type 1 TAR DNA sequence motifs". *J Virol* 69(6):3584–96 (cit. on p. 24).

Oubridge C, Ito N, Evans PR, Teo CH, and Nagai K (1994). "Crystal structure at 1.92 A resolution of the RNA-binding domain of the U1A spliceosomal protein complexed with an RNA hairpin". *Nature* 372(6505):432–8. DOI: 10.1038/372432a0 (cit. on p. 23).

Oulton MR and Mezei C (1976). "Characterization of myelin of chick sciatic nerve during development". *J Lipid Res* 17(2):167–75 (cit. on p. 10).

Pan Q, Shai O, Lee LJ, Frey BJ, and Blencowe BJ (2008). "Deep surveying of alternative splicing complexity in the human transcriptome by high-throughput sequencing". *Nat Genet* 40(12):1413–5. DOI: 10.1038/ng.259 (cit. on p. 30).

Pareek S, Notterpek L, Snipes GJ, Naef R, Sossin W, Laliberte J, Iacampo S, Suter U, Shooter EM, and Murphy RA (1997). "Neurons promote the translocation of peripheral myelin protein 22 into myelin". *J Neurosci* 17(20):7754–62 (cit. on p. 10).

Parkinson DB, Bhaskaran A, Arthur-Farraj P, Noon LA, Woodhoo A, Lloyd AC, Feltri ML, Wrabetz L, Behrens A, Mirsky R, and Jessen KR (2008). "c-Jun is a negative regulator of myelination". *J Cell Biol* 181(4):625–37. DOI: 10.1083/jcb.200803013 (cit. on p. 15).

Parkinson DB, Bhaskaran A, Droggiti A, Dickinson S, D'Antonio M, Mirsky R, and Jessen KR (2004). "Krox-20 inhibits Jun-NH2-terminal kinase/c-Jun to control Schwann cell proliferation and death". *J Cell Biol* 164(3):385–94. DOI: 10.1083/jcb.200307132 (cit. on p. 15).

Parkinson DB, Dong Z, Bunting H, Whitfield J, Meier C, Marie H, Mirsky R, and Jessen KR (2001). "Transforming Growth Factor β (TGFβ) Mediates Schwann Cell DeathIn VitroandIn Vivo: Examination of c-Jun Activation, Interactions with Survival Signals, and the Relationship of TGFβ-Mediated Death to Schwann Cell Differentiation". *The Journal of Neuroscience* 21(21):8572–8585. DOI: 10.1523/jneurosci.21-21-08572.2001 (cit. on p. 13).

Parmantier E, Lynn B, Lawson D, Turmaine M, Namini SS, Chakrabarti L, McMahon AP, Jessen KR, and Mirsky R (1999). "Schwann cell-derived Desert hedgehog controls the development of peripheral nerve sheaths". *Neuron* 23(4): 713–24. DOI: 10.1016/s0896-6273(01)80030-1 (cit. on p. 11).

Patzig J, Jahn O, Tenzer S, Wichert SP, Monasterio-Schrader P de, Rosfa S, Kuharev J, Yan K, Bormuth I, Bremer J, Aguzzi A, Orfaniotou F, Hesse D, Schwab MH, Mobius W, Nave KA, and Werner HB (2011). "Quantitative and integrative proteome analysis of peripheral nerve myelin identifies novel myelin proteins and candidate neuropathy loci". *J Neurosci* 31(45):16369–86. DOI: 10.1523/JNEUROSCI.4016-11.2011 (cit. on pp. 10, 11).

Peirs C and Seal RP (2016). "Neural circuits for pain: Recent advances and current views". *Science* 354(6312):578–584. DOI: 10.1126/science.aaf8933 (cit. on p. 134).

Pellegatta M, De Arcangelis A, D'Urso A, Nodari A, Zambroni D, Ghidinelli M, Matafora V, Williamson C, Georges-Labouesse E, Kreidberg J, Mayer U, McKee KK, Yurchenco PD, Quattrini A, Wrabetz L, and Feltri ML (2013). "alpha6beta1 and alpha7beta1 integrins are required in Schwann cells to sort axons". *J Neurosci* 33(46):17995–8007. DOI: 10.1523/JNEUROSCI.3179-13.2013 (cit. on p. 137).

Pereira JA, Benninger Y, Baumann R, Goncalves AF, Ozcelik M, Thurnherr T, Tricaud N, Meijer D, Fassler R, Suter U, and Relvas JB (2009). "Integrin-linked kinase is required for radial sorting of axons and Schwann cell remyelination in the peripheral nervous system". *J Cell Biol* 185(1):147–61. DOI: 10.1083/jcb.200809008 (cit. on p. 137).

Pesiridis GS, Tripathy K, Tanik S, Trojanowski JQ, and Lee VM (2011). "A "two-hit" hypothesis for inclusion formation by carboxyl-terminal fragments of TDP-43 protein linked to RNA depletion and impaired microtubule-dependent transport". *J Biol Chem* 286(21):18845–55. DOI: 10.1074/jbc.M111.231118 (cit. on p. 28).

Philips T, Bento-Abreu A, Nonneman A, Haeck W, Staats K, Geelen V, Hersmus N, Kusters B, Van Den Bosch L, Van Damme P, Richardson WD, and Robberecht W (2013). "Oligodendrocyte dysfunction in the pathogenesis of amyotrophic lateral sclerosis". *Brain* 136(Pt 2):471–82. DOI: 10.1093/brain/aws339 (cit. on p. 22).

Philips T and Rothstein JD (2014). "Glial cells in amyotrophic lateral sclerosis". *Exp Neurol* 262 Pt B:111–20. DOI: 10.1016/j.expneurol.2014.05.015 (cit. on p. 22).

Pillai AM, Thaxton C, Pribisko AL, Cheng JG, Dupree JL, and Bhat MA (2009). "Spatiotemporal ablation of myelinating glia-specific neurofascin (Nfasc NF155) in mice reveals gradual loss of paranodal axoglial junctions and concomitant disorganization of axonal domains". *J Neurosci Res* 87(8):1773–93. DOI: 10.1002/jnr.22015 (cit. on pp. 62, 63, 125, 126, 138).

Pinarbasi ES, Cagatay T, Fung HYJ, Li YC, Chook YM, and Thomas PJ (2018). "Active nuclear import and passive nuclear export are the primary determinants of TDP-43 localization". *Sci Rep* 8(1):7083. DOI: 10.1038/s41598-018-25008-4 (cit. on p. 24).

Pingitore P and Romeo S (2019). "The role of PNPLA3 in health and disease". *Biochim Biophys Acta Mol Cell Biol Lipids* 1864(6):900–906. DOI: 10.1016/j.bbalip.2018.06.018 (cit. on p. 103).

Poliak S and Peles E (2003). "The local differentiation of myelinated axons at nodes of Ranvier". *Nat Rev Neurosci* 4(12):968–80. DOI: 10.1038/nrn1253 (cit. on p. 8).

Polymenidou M, Lagier-Tourenne C, Hutt KR, Huelga SC, Moran J, Liang TY, Ling SC, Sun E, Wancewicz E, Mazur C, Kordasiewicz H, Sedaghat Y, Donohue JP, Shiue L, Bennett CF, Yeo GW, and Cleveland DW (2011). "Long pre-mRNA depletion and RNA missplicing contribute to neuronal vulnerability from loss of TDP-43". *Nat Neurosci* 14(4): 459–68. DOI: 10.1038/nn.2779 (cit. on pp. 24, 26, 60, 61, 99, 101, 122, VII).

Privat A, Jacque C, Bourre JM, Dupouey P, and Baumann N (1979). "Absence of the major dense line in myelin of the mutant mouse 'shiverer'". *Neuroscience Letters* 12(1):107–112. DOI: 10.1016/0304-3940(79)91489-7 (cit. on p. 10).

Pumphrey BRJ and Young JZ (1938). "The rates of conduction of nerve fibres of various diameters in cephalopods". *Journal of Experimental Biology* 15(4):453–466 (cit. on p. 5).

Qi Y, Cai J, Wu Y, Wu R, Lee J, Fu H, Rao M, Sussel L, Rubenstein J, and Qiu M (2001). "Control of oligodendrocyte differentiation by the Nkx2.2 homeodomain transcription factor". *Development* 128(14):2723–33 (cit. on p. 18).

Qin H, Lim LZ, Wei Y, and Song J (2014). "TDP-43 N terminus encodes a novel ubiquitin-like fold and its unfolded form in equilibrium that can be shifted by binding to ssDNA". *Proc Natl Acad Sci U S A* 111(52):18619–24. DOI: 10.1073/pnas.1413994112 (cit. on p. 24).

Quintes S, Brinkmann BG, Ebert M, Frob F, Kungl T, Arlt FA, Tarabykin V, Huylebroeck D, Meijer D, Suter U, Wegner M, Sereda MW, and Nave KA (2016). "Zeb2 is essential for Schwann cell differentiation, myelination and nerve repair". *Nat Neurosci* 19(8):1050–1059. DOI: 10.1038/nn.4321 (cit. on p. 13).

Rabdano SO, Izmailov SA, Luzik DA, Groves A, Podkorytov IS, and Skrynnikov NR (2017). "Onset of disorder and protein aggregation due to oxidation-induced intermolecular disulfide bonds: case study of RRM2 domain from TDP-43". *Sci Rep* 7(1):11161. DOI: 10.1038/s41598-017-10574-w (cit. on p. 28).

Raff MC, Barres BA, Burne JF, Coles HS, Ishizaki Y, and Jacobson MD (1993). "Programmed cell death and the control of cell survival: lessons from the nervous system". *Science* 262(5134):695–700. DOI: 10.1126/science.8235590 (cit. on p. 17).

Ranvier L (1878). "Leçons sur l'Histologie du Système Nerveux. Par L. Ranvier, Professeur d'Anatomie générale au College de France, etc. Paris, 1878". *Journal of Mental Science* 24(105):118–122. DOI: 10.1192/bjp.24.105.118 (cit. on p. 7).

Rasband MN and Peles E (2015). "The Nodes of Ranvier: Molecular Assembly and Maintenance". *Cold Spring Harb Perspect Biol* 8(3):a020495. DOI: 10.1101/cshperspect.a020495 (cit. on p. 8).

Rasband MN, Peles E, Trimmer JS, Levinson SR, Lux SE, and Shrager P (1999a). "Dependence of nodal sodium channel clustering on paranodal axoglial contact in the developing CNS". *J Neurosci* 19(17):7516–28. DOI: 10.1523/jneurosci.19-17-07516.1999 (cit. on p. 8).

Rasband MN, Trimmer JS, Peles E, Levinson SR, and Shrager P (1999b). "K+ channel distribution and clustering in developing and hypomyelinated axons of the optic nerve". *J Neurocytol* 28(4-5):319–31. DOI: 10.1023/a:1007057512576 (cit. on p. 8).

Rascovsky K, Hodges JR, Knopman D, Mendez MF, Kramer JH, Neuhaus J, Swieten JC van, Seelaar H, Dopper EG, Onyike CU, Hillis AE, Josephs KA, Boeve BF, Kertesz A, Seeley WW, Rankin KP, Johnson JK, Gorno-Tempini ML, Rosen H, Prioleau-Latham CE, Lee A, Kipps CM, Lillo P, Piguet O, Rohrer JD, Rossor MN, Warren JD, Fox NC, Galasko D, Salmon DP, Black SE, Mesulam M, Weintraub S, Dickerson BC, Diehl-Schmid J, Pasquier F, Deramecourt V, Lebert F, Pijnenburg Y, Chow TW, Manes F, Grafman J, Cappa SF, Freedman M, Grossman M, and Miller BL (2011). "Sensitivity of revised diagnostic criteria for the behavioural variant of frontotemporal dementia". *Brain* 134(Pt 9):2456–77. DOI: 10.1093/brain/awr179 (cit. on p. 20).

Ribeiro S, Napoli I, White IJ, Parrinello S, Flanagan AM, Suter U, Parada LF, and Lloyd AC (2013). "Injury signals cooperate with Nf1 loss to relieve the tumor-suppressive environment of adult peripheral nerve". *Cell Rep* 5(1):126–36. DOI: 10.1016/j.celrep.2013.08.033 (cit. on p. 78).

Rios JC, Rubin M, Martin MS, Downey RT, Einheber S, Rosenbluth J, Levinson SR, Bhat M, and Salzer JL (2003). "Paranodal Interactions Regulate Expression of Sodium Channel Subtypes and Provide a Diffusion Barrier for the Node of Ranvier". *The Journal of Neuroscience* 23(18):7001–7011. DOI: 10.1523/jneurosci.23-18-07001.2003 (cit. on pp. 126, 138).

Rippon GA, Scarmeas N, Gordon PH, Murphy PL, Albert SM, Mitsumoto H, Marder K, Rowland LP, and Stern Y (2006). "An observational study of cognitive impairment in amyotrophic lateral sclerosis". *Arch Neurol* 63(3):345–52. DOI: 10.1001/archneur.63.3.345 (cit. on p. 20).

Riva N, Chaabane L, Peviani M, Ungaro D, Domi T, Dina G, Bianchi F, Spano G, Cerri F, Podini P, Corbo M, Carro UD, Comi G, Bendotti C, and Quattrini A (2014). "Defining peripheral nervous system dysfunction in the SOD-1G93A transgenic rat model of amyotrophic lateral sclerosis". *J Neuropathol Exp Neurol* 73(7):658–70. DOI: 10.1097/NEN.0000000000000081 (cit. on p. 127).

Rivers LE, Young KM, Rizzi M, Jamen F, Psachoulia K, Wade A, Kessaris N, and Richardson WD (2008). "PDGFRA/NG2 glia generate myelinating oligodendrocytes and piriform projection neurons in adult mice". *Nat Neurosci* 11(12):1392–401. DOI: 10.1038/nn.2220 (cit. on p. 18).

Roach A, Takahashi N, Pravtcheva D, Ruddle F, and Hood L (1985). "Chromosomal mapping of mouse myelin basic protein gene and structure and transcription of the partially deleted gene in shiverer mutant mice". *Cell* 42(1):149–55. DOI: 10.1016/s0092-8674(85)80110-0 (cit. on p. 10).

Robaglia-Schlupp A, Pizant J, Norreel JC, Passage E, Saberan-Djoneidi D, Ansaldi JL, Vinay L, Figarella-Branger D, Levy N, Clarac F, Cau P, Pellissier JF, and Fontes M (2002). "PMP22 overexpression causes dysmyelination in mice". *Brain* 125(Pt 10):2213–21. DOI: 10.1093/brain/awf230 (cit. on p. 10).

Robberecht W and Philips T (2013). "The changing scene of amyotrophic lateral sclerosis". *Nat Rev Neurosci* 14(4):248–64. DOI: 10.1038/nrn3430 (cit. on p. 21).

Roberts SL, Dun XP, Doddrell RDS, Mindos T, Drake LK, Onaitis MW, Florio F, Quattrini A, Lloyd AC, D'Antonio M, and Parkinson DB (2017). "Sox2 expression in Schwann cells inhibits myelination in vivo and induces influx of macrophages to the nerve". *Development* 144(17):3114–3125. DOI: 10.1242/dev.150656 (cit. on p. 14).

Robinson MD, McCarthy DJ, and Smyth GK (2010). "edgeR: a Bioconductor package for differential expression analysis of digital gene expression data". *Bioinformatics* 26(1):139–40. DOI: 10.1093/bioinformatics/btp616 (cit. on p. 47).

Robinson MD and Oshlack A (2010). "A scaling normalization method for differential expression analysis of RNA-seq data". *Genome Biol* 11(3):R25. DOI: 10.1186/gb-2010-11-3-r25 (cit. on p. 47).

Roche SL, Sherman DL, Dissanayake K, Soucy G, Desmazieres A, Lamont DJ, Peles E, Julien JP, Wishart TM, Ribchester RR, Brophy PJ, and Gillingwater TH (2014). "Loss of glial neurofascin155 delays developmental synapse elimination at the neuromuscular junction". *J Neurosci* 34(38):12904–18. DOI: 10.1523/JNEUROSCI.1725-14.2014 (cit. on p. 126).

Rohan Z, Matej R, Rusina R, and Kovacs GG (2014). "Oligodendroglial response in the spinal cord in TDP-43 proteinopathy with motor neuron involvement". *Neurodegener Dis* 14(3):117–24. DOI: 10.1159/000362929 (cit. on p. 22).

Romano G, Appocher C, Scorzeto M, Klima R, Baralle FE, Megighian A, and Feiguin F (2015). "Glial TDP-43 regulates axon wrapping, GluRIIA clustering and fly motility by autonomous and non-autonomous mechanisms". *Hum Mol Genet* 24(21):6134–45. DOI: 10.1093/hmg/ddv330 (cit. on p. 28).

Roper CFE and Shea EK (2013). "Unanswered questions about the giant squid Architeuthis (Architeuthidae) illustrate our incomplete knowledge of coleoid cephalopods". *American Malacological Bulletin* 31(1):109–122. DOI: 10.4003/006.031.0104 (cit. on p. 4).

Rosenberg SS, Kelland EE, Tokar E, Torre AR De la, and Chan JR (2008). "The geometric and spatial constraints of the microenvironment induce oligodendrocyte differentiation". *Proc Natl Acad Sci U S A* 105(38):14662–7. DOI: 10.1073/pnas.0805640105 (cit. on p. 18).

Rosenbluth J, Nave KA, Mierzwa A, and Schiff R (2006). "Subtle myelin defects in PLP-null mice". *Glia* 54(3): 172–82. DOI: 10.1002/glia.20370 (cit. on p. 10).

Rothstein JD (2017). "Edaravone: A new drug approved for ALS". *Cell* 171(4):725. DOI: 10.1016/j.cell.2017.10.011 (cit. on p. 22).

Rotshenker S (2011). "Wallerian degeneration: the innate-immune response to traumatic nerve injury". *J Neuroinflammation* 8:109. DOI: 10.1186/1742-2094-8-109 (cit. on p. 15).

Rowitch DH and Kriegstein AR (2010). "Developmental genetics of vertebrate glial-cell specification". *Nature* 468(7321): 214–22. DOI: 10.1038/nature09611 (cit. on pp. 16, 17).

Rushton WA (1951). "A theory of the effects of fibre size in medullated nerve". *J Physiol* 115(1):101–22. DOI: 10.1113/jphysiol.1951.sp004655 (cit. on pp. 5, 9).

Saab AS, Tzvetavona ID, Trevisiol A, Baltan S, Dibaj P, Kusch K, Mobius W, Goetze B, Jahn HM, Huang W, Steffens H, Schomburg ED, Perez-Samartin A, Perez-Cerda F, Bakhtiari D, Matute C, Lowel S, Griesinger C, Hirrlinger J, Kirchhoff F, and Nave KA (2016). "Oligodendroglial NMDA Receptors Regulate Glucose Import and Axonal Energy Metabolism". *Neuron* 91(1):119–32. DOI: 10.1016/j.neuron.2016.05.016 (cit. on p. 20).

Sacheck JM, Hyatt JP, Raffaello A, Jagoe RT, Roy RR, Edgerton VR, Lecker SH, and Goldberg AL (2007). "Rapid disuse and denervation atrophy involve transcriptional changes similar to those of muscle wasting during systemic diseases". *FASEB J* 21(1):140–55. DOI: 10.1096/fj.06-6604com (cit. on p. 72).

Said G, Slama G, and Selva J (1983). "Progressive centripetal degeneration of axons in small fibre diabetic polyneuropathy". *Brain* 106 (Pt 4):791–807. DOI: 10.1093/brain/106.4.791 (cit. on p. 82).

Saifetiarova J, Liu X, Taylor AM, Li J, and Bhat MA (2017). "Axonal domain disorganization in Caspr1 and Caspr2 mutant myelinated axons affects neuromuscular junction integrity, leading to muscle atrophy". *J Neurosci Res* 95(7): 1373–1390. DOI: 10.1002/jnr.24052 (cit. on pp. 63, 126, 129, 138).

Sanders FK and Whitteridge D (1946). "Conduction Velocity and Myelin Thickness in Regenerating Nerve Fibres". *Journal of Physiology-London* 105(2):152–174. DOI: DOI10.1113/jphysiol.1946.sp004160 (cit. on p. 9).

Saporta AS, Sottile SL, Miller LJ, Feely SM, Siskind CE, and Shy ME (2011). "Charcot-Marie-Tooth disease subtypes and genetic testing strategies". *Ann Neurol* 69(1):22–33. DOI: 10.1002/ana.22166 (cit. on p. 20).

Saudemont B, Popa A, Parmley JL, Rocher V, Blugeon C, Necsulea A, Meyer E, and Duret L (2017). "The fitness cost of mis-splicing is the main determinant of alternative splicing patterns". *Genome Biol* 18(1):208. DOI: 10.1186/s13059-017-1344-6 (cit. on p. 30).

Schirmer L, Velmeshev D, Holmqvist S, Kaufmann M, Werneburg S, Jung D, Vistnes S, Stockley JH, Young A, Steindel M, Tung B, Goyal N, Bhaduri A, Mayer S, Engler JB, Bayraktar OA, Franklin RJM, Haeussler M, Reynolds R, Schafer DP, Friese MA, Shiow LR, Kriegstein AR, and Rowitch DH (2019). "Neuronal vulnerability and multilineage diversity in multiple sclerosis". *Nature* 573(7772):75–82. DOI: 10.1038/s41586-019-1404-z (cit. on p. 133).

Schmitt FO and Bear RS (1937). "The optical properties of vertebrate nerve axons as related to fiber size". *Journal of Cellular and Comparative Physiology* 9(2):229–241 (cit. on p. 9).

Schneider-Maunoury S, Topilko P, Seitandou T, Levi G, Cohen-Tannoudji M, Pournin S, Babinet C, and Charnay P (1993). "Disruption of Krox-20 results in alteration of rhombomeres 3 and 5 in the developing hindbrain". *Cell* 75(6): 1199–214. DOI: 10.1016/0092-8674(93)90329-o (cit. on p. 128).

Schuller U, Heine VM, Mao J, Kho AT, Dillon AK, Han YG, Huillard E, Sun T, Ligon AH, Qian Y, Ma Q, Alvarez-Buylla A, McMahon AP, Rowitch DH, and Ligon KL (2008). "Acquisition of granule neuron precursor identity is a critical determinant of progenitor cell competence to form Shh-induced medulloblastoma". *Cancer Cell* 14(2):123–34. DOI: 10.1016/j.ccr.2008.07.005 (cit. on pp. 35, 108).

Scotter EL, Vance C, Nishimura AL, Lee YB, Chen HJ, Urwin H, Sardone V, Mitchell JC, Rogelj B, Rubinsztein DC, and Shaw CE (2014). "Differential roles of the ubiquitin proteasome system and autophagy in the clearance of soluble and aggregated TDP-43 species". *J Cell Sci* 127(Pt 6):1263–78. DOI: 10.1242/jcs.140087 (cit. on p. 28).

Sela N, Mersch B, Hotz-Wagenblatt A, and Ast G (2010). "Characteristics of transposable element exonization within human and mouse". *PLoS One* 5(6):e10907. DOI: 10.1371/journal.pone.0010907 (cit. on p. 32).

Sephton CF, Cenik C, Kucukural A, Dammer EB, Cenik B, Han Y, Dewey CM, Roth FP, Herz J, Peng J, Moore MJ, and Yu G (2011). "Identification of neuronal RNA targets of TDP-43-containing ribonucleoprotein complexes". *J Biol Chem* 286(2):1204–15. DOI: 10.1074/jbc.M110.190884 (cit. on pp. 26, 27).

Sephton CF, Good SK, Atkin S, Dewey CM, Mayer P. r, Herz J, and Yu G (2010). "TDP-43 is a developmentally regulated protein essential for early embryonic development". *J Biol Chem* 285(9):6826–34. DOI: 10.1074/jbc.M109.061846 (cit. on pp. 24, 52, 122).

Seyfried NT, Gozal YM, Dammer EB, Xia Q, Duong DM, Cheng D, Lah JJ, Levey AI, and Peng J (2010). "Multiplex SILAC analysis of a cellular TDP-43 proteinopathy model reveals protein inclusions associated with SUMOylation and diverse polyubiquitin chains". *Mol Cell Proteomics* 9(4):705–18. DOI: 10.1074/mcp.M800390-MCP200 (cit. on p. 27).

Shan X, Chiang PM, Price DL, and Wong PC (2010). "Altered distributions of Gemini of coiled bodies and mitochondria in motor neurons of TDP-43 transgenic mice". *Proc Natl Acad Sci U S A* 107(37):16325–30. DOI: 10.1073/pnas.1003459107 (cit. on p. 28).

Shen S, Li J, and Casaccia-Bonnefil P (2005). "Histone modifications affect timing of oligodendrocyte progenitor differentiation in the developing rat brain". *J Cell Biol* 169(4):577–89. DOI: 10.1083/jcb.200412101 (cit. on p. 18).

Shen S, Lin L, Cai JJ, Jiang P, Kenkel EJ, Stroik MR, Sato S, Davidson BL, and Xing Y (2011). "Widespread establishment and regulatory impact of Alu exons in human genes". *Proc Natl Acad Sci U S A* 108(7):2837–42. DOI: 10.1073/pnas.1012834108 (cit. on p. 32).

Sherman DL, Tait S, Melrose S, Johnson R, Zonta B, Court FA, Macklin WB, Meek S, Smith AJ, Cottrell DF, and Brophy PJ (2005). "Neurofascins are required to establish axonal domains for saltatory conduction". *Neuron* 48(5):737–42. DOI: 10.1016/j.neuron.2005.10.019 (cit. on p. 126).

Sherman DL, Wu LM, Grove M, Gillespie CS, and Brophy PJ (2012). "Drp2 and periaxin form Cajal bands with dystroglycan but have distinct roles in Schwann cell growth". *J Neurosci* 32(27):9419–28. DOI: 10.1523/JNEUROSCI.1220-12.2012 (cit. on p. 130).

Shi Y (2017). "Mechanistic insights into precursor messenger RNA splicing by the spliceosome". *Nat Rev Mol Cell Biol* 18(11):655–670. DOI: 10.1038/nrm.2017.86 (cit. on p. 29).

Shy ME, Shi Y, Wrabetz L, Kamholz J, and Scherer SS (1996). "Axon-Schwann cell interactions regulate the expression of c-jun in Schwann cells". *Journal of Neuroscience Research* 43(5):511–525. DOI: 10.1002/(sici)1097-4547(19960301)43:5<511::Aid-jnr1>3.0.Co;2-l (cit. on p. 15).

Sibley CR, Blazquez L, and Ule J (2016). "Lessons from non-canonical splicing". *Nat Rev Genet* 17(7):407–421. DOI: 10.1038/nrg.2016.46 (cit. on p. 31).

Sivakumar P, Humphrey J, Lo K, Ricketts T, Oliveira H, Kalmar B, Wang E, Housman D, Baralle F, Greensmith L, Buratti E, Plagnol V, Fisher EMC, Arozena AA, and Fratta P (2018). "Dissecting TDP-43 gain- and loss-of-function in neurodegeneration". *Neuromuscular Disorders* 28. DOI: 10.1016/s0960-8966(18)30366-3 (cit. on p. 122).

Smith EF, Shaw PJ, and De Vos KJ (2019). "The role of mitochondria in amyotrophic lateral sclerosis". *Neurosci Lett* 710:132933. DOI: 10.1016/j.neulet.2017.06.052 (cit. on p. 130).

Smith ME (1968). "The turnover of myelin in the adult rat". *Biochim Biophys Acta* 164(2):285–93. DOI: 10.1016/0005-2760(68)90154-9 (cit. on p. 10).

Smith ME and Curtis BM (1979). "Frog sciatic nerve myelin: a chemical characterization". *J Neurochem* 33(2):447–52. DOI: 10.1111/j.1471-4159.1979.tb05174.x (cit. on p. 10).

Snipes GJ, Suter U, Welcher AA, and Shooter EM (1992). "Characterization of a novel peripheral nervous system myelin protein (PMP-22/SR13)". *J Cell Biol* 117(1):225–38. DOI: 10.1083/jcb.117.1.225 (cit. on p. 10).

Sochocka M, Diniz BS, and Leszek J (2017). "Inflammatory Response in the CNS: Friend or Foe?" *Mol Neurobiol* 54(10):8071–8089. DOI: 10.1007/s12035-016-0297-1 (cit. on p. 115).

Sorek R (2007). "The birth of new exons: mechanisms and evolutionary consequences". *RNA* 13(10):1603–8. DOI: 10.1261/rna.682507 (cit. on p. 32).

Sorek R, Ast G, and Graur D (2002). "Alu-containing exons are alternatively spliced". *Genome Res* 12(7):1060–7. DOI: 10.1101/gr.229302 (cit. on p. 32).

Spritz N, Singh H, and Geyer B (1973). "Myelin from human peripheral nerves. Quantitative and qualitative studies in two age groups". *J Clin Invest* 52(2):520–3. DOI: 10.1172/JCI107210 (cit. on p. 10).

Stefanova N and Wenning GK (2016). "Review: Multiple system atrophy: emerging targets for interventional therapies". *Neuropathol Appl Neurobiol* 42(1):20–32. DOI: 10.1111/nan.12304 (cit. on p. 20).

Steitz TA and Steitz JA (1993). "A general two-metal-ion mechanism for catalytic RNA". *Proc Natl Acad Sci U S A* 90(14):6498–502. DOI: 10.1073/pnas.90.14.6498 (cit. on p. 29).

Stierli S, Napoli I, White IJ, Cattin AL, Monteza Cabrejos A, Garcia Calavia N, Malong L, Ribeiro S, Nihouarn J, Williams R, Young KM, Richardson WD, and Lloyd AC (2018). "The regulation of the homeostasis and regeneration of peripheral nerve is distinct from the CNS and independent of a stem cell population". *Development* 145(24). DOI: 10.1242/dev.170316 (cit. on p. 14).

Strong MJ, Volkening K, Hammond R, Yang W, Strong W, Leystra-Lantz C, and Shoesmith C (2007). "TDP43 is a human low molecular weight neurofilament (hNFL) mRNA-binding protein". *Mol Cell Neurosci* 35(2):320–7. DOI: 10.1016/j.mcn.2007.03.007 (cit. on p. 27).

Stuart T, Butler A, Hoffman P, Hafemeister C, Papalexi E, Mauck W. M. r, Hao Y, Stoeckius M, Smibert P, and Satija R (2019). "Comprehensive Integration of Single-Cell Data". *Cell* 177(7):1888–1902 e21. DOI: 10.1016/j.cell.2019.05.031 (cit. on pp. 48, 104).

Sun T, Dong H, Wu L, Kane M, Rowitch DH, and Stiles CD (2003). "Cross-repressive interaction of the Olig2 and Nkx2.2 transcription factors in developing neural tube associated with formation of a specific physical complex". *J Neurosci* 23(29):9547–56 (cit. on p. 18).

Sun T, Echelard Y, Lu R, Yuk DI, Kaing S, Stiles CD, and Rowitch DH (2001). "Olig bHLH proteins interact with homeodomain proteins to regulate cell fate acquisition in progenitors of the ventral neural tube". *Curr Biol* 11(18):1413–20. DOI: 10.1016/s0960-9822(01)00441-9 (cit. on p. 18).

Sun Y and Chakrabartty A (2017). "Phase to Phase with TDP-43". *Biochemistry* 56(6):809–823. DOI: 10.1021/acs.biochem.6b01088 (cit. on p. 25).

Supplie LM, Duking T, Campbell G, Diaz F, Moraes CT, Gotz M, Hamprecht B, Boretius S, Mahad D, and Nave KA (2017). "Respiration-Deficient Astrocytes Survive As Glycolytic Cells In Vivo". *J Neurosci* 37(16):4231–4242. DOI: 10.1523/JNEUROSCI.0756-16.2017 (cit. on p. 19).

Swanson MS, Nakagawa TY, LeVan K, and Dreyfuss G (1987). "Primary structure of human nuclear ribonucleoprotein particle C proteins: conservation of sequence and domain structures in heterogeneous nuclear RNA, mRNA, and pre-rRNA-binding proteins". *Mol Cell Biol* 7(5):1731–9. DOI: 10.1128/mcb.7.5.1731 (cit. on p. 23).

Swarup V, Phaneuf D, Bareil C, Robertson J, Rouleau GA, Kriz J, and Julien JP (2011). "Pathological hallmarks of amyotrophic lateral sclerosis/frontotemporal lobar degeneration in transgenic mice produced with TDP-43 genomic fragments". *Brain* 134(Pt 9):2610–26. DOI: 10.1093/brain/awr159 (cit. on p. 122).

Swinnen B and Robberecht W (2014). "The phenotypic variability of amyotrophic lateral sclerosis". *Nat Rev Neurol* 10(11):661–70. DOI: 10.1038/nrneurol.2014.184 (cit. on pp. 20, 21).

Swiss VA, Nguyen T, Dugas J, Ibrahim A, Barres B, Androulakis IP, and Casaccia P (2011). "Identification of a gene regulatory network necessary for the initiation of oligodendrocyte differentiation". *PLoS One* 6(4):e18088. DOI: 10.1371/journal.pone.0018088 (cit. on p. 18).

Synofzik M, Maetzler W, Grehl T, Prudlo J, Vom Hagen JM, Haack T, Rebassoo P, Munz M, Schols L, and Biskup S (2012). "Screening in ALS and FTD patients reveals 3 novel UBQLN2 mutations outside the PXX domain and a pure FTD phenotype". *Neurobiol Aging* 33(12):2949 e13–7. DOI: 10.1016/j.neurobiolaging.2012.07.002 (cit. on p. 28).

Takeuchi R, Tada M, Shiga A, Toyoshima Y, Konno T, Sato T, Nozaki H, Kato T, Horie M, Shimizu H, Takebayashi H, Onodera O, Nishizawa M, Kakita A, and Takahashi H (2016a). "Heterogeneity of cerebral TDP-43 pathology in sporadic amyotrophic lateral sclerosis: Evidence for clinico-pathologic subtypes". *Acta Neuropathol Commun* 4(1):61. DOI: 10.1186/s40478-016-0335-2 (cit. on p. 22).

Takeuchi R, Toyoshima Y, Tada M, Tanaka H, Shimizu H, Shiga A, Miura T, Aoki K, Aikawa A, Ishizawa S, Ikeuchi T, Nishizawa M, Kakita A, and Takahashi H (2016b). "Globular Glial Mixed Four Repeat Tau and TDP-43 Proteinopathy with Motor Neuron Disease and Frontotemporal Dementia". *Brain Pathol* 26(1):82–94. DOI: 10.1111/bpa.12262 (cit. on p. 22).

Tan CF, Eguchi H, Tagawa A, Onodera O, Iwasaki T, Tsujino A, Nishizawa M, Kakita A, and Takahashi H (2007). "TDP-43 immunoreactivity in neuronal inclusions in familial amyotrophic lateral sclerosis with or without SOD1 gene mutation". *Acta Neuropathol* 113(5):535–42. DOI: 10.1007/s00401-007-0206-9 (cit. on p. 22).

Tan Q, Yalamanchili HK, Park J, De Maio A, Lu HC, Wan YW, White JJ, Bondar VV, Sayegh LS, Liu X, Gao Y, Sillitoe RV, Orr HT, Liu Z, and Zoghbi HY (2016). "Extensive cryptic splicing upon loss of RBM17 and TDP43 in neurodegeneration models". *Hum Mol Genet* 25(23):5083–5093. DOI: 10.1093/hmg/ddw337 (cit. on pp. 32, 125).

Tan RH, Ke YD, Ittner LM, and Halliday GM (2017). "ALS/FTLD: experimental models and reality". *Acta Neuropathol* 133(2):177–196. DOI: 10.1007/s00401-016-1666-6 (cit. on pp. 22, 33).

Tang XL, Wang Y, Li DL, Luo J, and Liu MY (2012). "Orphan G protein-coupled receptors (GPCRs): biological functions and potential drug targets". *Acta Pharmacol Sin* 33(3):363–71. DOI: 10.1038/aps.2011.210 (cit. on p. 103).

Taylor AM, Saifetiarova J, and Bhat MA (2017). "Postnatal Loss of Neuronal and Glial Neurofascins Differentially Affects Node of Ranvier Maintenance and Myelinated Axon Function". *Front Cell Neurosci* 11:11. DOI: 10.3389/fncel.2017.00011 (cit. on p. 129).

Thomas PK (1999). "Overview of Charcot-Marie-Tooth Disease Type 1A". *Ann N Y Acad Sci* 883(1):1–5. DOI: 10.1111/j.1749-6632.1999.tb08560.x (cit. on pp. 10, 72).

Tognatta R, Sun W, Goebbels S, Nave KA, Nishiyama A, Schoch S, Dimou L, and Dietrich D (2017). "Transient Cnp expression by early progenitors causes Cre-Lox-based reporter lines to map profoundly different fates". *Glia* 65(2):342–359. DOI: 10.1002/glia.23095 (cit. on p. 131).

Tollervey JR, Curk T, Rogelj B, Briese M, Cereda M, Kayikci M, Konig J, Hortobagyi T, Nishimura AL, Zupunski V, Patani R, Chandran S, Rot G, Zupan B, Shaw CE, and Ule J (2011). "Characterizing the RNA targets and position-dependent splicing regulation by TDP-43". *Nat Neurosci* 14(4):452–8. DOI: 10.1038/nn.2778 (cit. on pp. 26, 122, 138).

Topilko P, Schneider-Maunoury S, Levi G, Baron-Van Evercooren A, Chennoufi AB, Seitanidou T, Babinet C, and Charnay P (1994). "Krox-20 controls myelination in the peripheral nervous system". *Nature* 371(6500):796–9. DOI: 10.1038/371796a0 (cit. on p. 13).

Toyama BH, Savas JN, Park SK, Harris MS, Ingolia NT, Yates J. R. r, and Hetzer MW (2013). "Identification of long-lived proteins reveals exceptional stability of essential cellular structures". *Cell* 154(5):971–982. DOI: 10.1016/j.cell.2013.07.037 (cit. on p. 87).

Trapp BD (1990). "Myelin-associated glycoprotein. Location and potential functions". *Ann N Y Acad Sci* 605:29–43. DOI: 10.1111/j.1749-6632.1990.tb42378.x (cit. on p. 11).

Trapp BD, Nishiyama A, Cheng D, and Macklin W (1997). "Differentiation and death of premyelinating oligodendrocytes in developing rodent brain". *J Cell Biol* 137(2):459–68. DOI: 10.1083/jcb.137.2.459 (cit. on p. 17).

Trevisiol A, Saab AS, Winkler U, Marx G, Imamura H, Mobius W, Kusch K, Nave KA, and Hirrlinger J (2017). "Monitoring ATP dynamics in electrically active white matter tracts". *Elife* 6. DOI: 10.7554/eLife.24241 (cit. on p. 19).

Trias E, Ibarburu S, Barreto-Nunez R, and Barbeito L (2017). "Significance of aberrant glial cell phenotypes in pathophysiology of amyotrophic lateral sclerosis". *Neurosci Lett* 636:27–31. DOI: 10.1016/j.neulet.2016.07.052 (cit. on p. 22).

Tripathi RB, Clarke LE, Burzomato V, Kessaris N, Anderson PN, Attwell D, and Richardson WD (2011). "Dorsally and ventrally derived oligodendrocytes have similar electrical properties but myelinate preferred tracts". *J Neurosci* 31(18):6809–6819. DOI: 10.1523/JNEUROSCI.6474-10.2011 (cit. on pp. 16, 134).

Tripathi RB, Jackiewicz M, McKenzie IA, Kougioumtzidou E, Grist M, and Richardson WD (2017). "Remarkable Stability of Myelinating Oligodendrocytes in Mice". *Cell Rep* 21(2):316–323. DOI: 10.1016/j.celrep.2017.09.050 (cit. on p. 135).

Tsao W, Jeong YH, Lin S, Ling J, Price DL, Chiang PM, and Wong PC (2012). "Rodent models of TDP-43: recent advances". *Brain Res* 1462:26–39. DOI: 10.1016/j.brainres.2012.04.031 (cit. on p. 122).

Turner MR, Hardiman O, Benatar M, Brooks BR, Chio A, Carvalho M de, Ince PG, Lin C, Miller RG, Mitsumoto H, Nicholson G, Ravits J, Shaw PJ, Swash M, Talbot K, Traynor BJ, Berg LH Van den, Veldink JH, Vucic S, and Kiernan MC (2013). "Controversies and priorities in amyotrophic lateral sclerosis". *The Lancet Neurology* 12(3):310–322. DOI: 10.1016/s1474-4422(13)70036-x (cit. on p. 21).

Ueno M, Nakamura Y, Li J, Gu Z, Niehaus J, Maezawa M, Crone SA, Goulding M, Baccei ML, and Yoshida Y (2018). "Corticospinal Circuits from the Sensory and Motor Cortices Differentially Regulate Skilled Movements through Distinct Spinal Interneurons". *Cell Rep* 23(5):1286–1300 e7. DOI: 10.1016/j.celrep.2018.03.137 (cit. on p. 134).

Ulloa F and Marti E (2010). "Wnt won the war: antagonistic role of Wnt over Shh controls dorso-ventral patterning of the vertebrate neural tube". *Dev Dyn* 239(1):69–76. DOI: 10.1002/dvdy.22058 (cit. on p. 16).

Vabnick I, Trimmer JS, Schwarz TL, Levinson SR, Risal D, and Shrager P (1999). "Dynamic Potassium Channel Distributions during Axonal Development Prevent Aberrant Firing Patterns". *The Journal of Neuroscience* 19(2):747–758. DOI: 10.1523/jneurosci.19-02-00747.1999 (cit. on pp. 8, 62).

Vallstedt A, Klos JM, and Ericson J (2005). "Multiple dorsoventral origins of oligodendrocyte generation in the spinal cord and hindbrain". *Neuron* 45(1):55–67. DOI: 10.1016/j.neuron.2004.12.026 (cit. on p. 16).

Valori CF, Brambilla L, Martorana F, and Rossi D (2014). "The multifaceted role of glial cells in amyotrophic lateral sclerosis". *Cell Mol Life Sci* 71(2):287–97. DOI: 10.1007/s00018-013-1429-7 (cit. on p. 22).

Vaquie A, Sauvain A, Duman M, Nocera G, Egger B, Meyenhofer F, Falquet L, Bartesaghi L, Chrast R, Lamy CM, Bang S, Lee SR, Jeon NL, Ruff S, and Jacob C (2019). "Injured Axons Instruct Schwann Cells to Build Constricting Actin Spheres to Accelerate Axonal Disintegration". *Cell Rep* 27(11):3152–3166 e7. DOI: 10.1016/j.celrep.2019.05.060 (cit. on p. 15).

Vassileva MT and Matunis MJ (2004). "SUMO modification of heterogeneous nuclear ribonucleoproteins". *Mol Cell Biol* 24(9):3623–32. DOI: 10.1128/mcb.24.9.3623-3632.2004 (cit. on p. 24).

Verheijen MH, Camargo N, Verdier V, Nadra K, Preux Charles AS de, Medard JJ, Luoma A, Crowther M, Inouye H, Shimano H, Chen S, Brouwers JF, Helms JB, Feltri ML, Wrabetz L, Kirschner D, Chrast R, and Smit AB (2009). "SCAP is required for timely and proper myelin membrane synthesis". *Proc Natl Acad Sci U S A* 106(50):21383–8. DOI: 10.1073/pnas.0905633106 (cit. on p. 14).

Verheijen MH, Peviani M, Hendricusdottir R, Bell EM, Lammens M, Smit AB, Bendotti C, and Minnen J van (2014). "Increased axonal ribosome numbers is an early event in the pathogenesis of amyotrophic lateral sclerosis". *PLoS One* 9(1):e87255. DOI: 10.1371/journal.pone.0087255 (cit. on p. 22).

Viader A, Golden JP, Baloh RH, Schmidt RE, Hunter DA, and Milbrandt J (2011). "Schwann cell mitochondrial metabolism supports long-term axonal survival and peripheral nerve function". *J Neurosci* 31(28):10128–40. DOI: 10.1523/JNEUROSCI.0884-11.2011 (cit. on p. 130).

Viader A, Sasaki Y, Kim S, Strickland A, Workman CS, Yang K, Gross RW, and Milbrandt J (2013). "Aberrant Schwann cell lipid metabolism linked to mitochondrial deficits leads to axon degeneration and neuropathy". *Neuron* 77(5):886–98. DOI: 10.1016/j.neuron.2013.01.012 (cit. on p. 130).

Vigano F, Mobius W, Gotz M, and Dimou L (2013). "Transplantation reveals regional differences in oligodendrocyte differentiation in the adult brain". *Nat Neurosci* 16(10):1370–2. DOI: 10.1038/nn.3503 (cit. on p. 94).

Vital A, Ferrer X, Lagueny A, Vandenberghe A, Latour P, Goizet C, Canron MH, Louiset P, Petry KG, and Vital C (2008). "Histopathological features of X-linked Charcot-Marie-Tooth disease in 8 patients from 6 families with different connexin32 mutations". *Journal of the Peripheral Nervous System* 6(2):79–84. DOI: 10.1111/j.1529-8027.2001.01011.x (cit. on p. 82).

Vogler TO, Wheeler JR, Nguyen ED, Hughes MP, Britson KA, Lester E, Rao B, Betta ND, Whitney ON, Ewachiw TE, Gomes E, Shorter J, Lloyd TE, Eisenberg DS, Taylor JP, Johnson AM, Olwin BB, and Parker R (2018). "TDP-43 and RNA form amyloid-like myo-granules in regenerating muscle". *Nature* 563(7732):508–513. DOI: 10.1038/s41586-018-0665-2 (cit. on p. 26).

Volkenhoff A, Weiler A, Letzel M, Stehling M, Klambt C, and Schirmeier S (2015). "Glial Glycolysis Is Essential for Neuronal Survival in Drosophila". *Cell Metab* 22(3):437–47. DOI: 10.1016/j.cmet.2015.07.006 (cit. on p. 19).

Vooijs M, Jonkers J, and Berns A (2001). "A highly efficient ligand-regulated Cre recombinase mouse line shows that LoxP recombination is position dependent". *EMBO Rep* 2(4):292–7. DOI: 10.1093/embo-reports/kve064 (cit. on p. 131).

Vorechovsky I (2010). "Transposable elements in disease-associated cryptic exons". *Hum Genet* 127(2):135–54. DOI: 10.1007/s00439-009-0752-4 (cit. on p. 32).

Voss EV, Skuljec J, Gudi V, Skripuletz T, Pul R, Trebst C, and Stangel M (2012). "Characterisation of microglia during de- and remyelination: can they create a repair promoting environment?" *Neurobiol Dis* 45(1):519–28. DOI: 10.1016/j.nbd.2011.09.008 (cit. on p. 136).

Wagner SA, Beli P, Weinert BT, Nielsen ML, Cox J, Mann M, and Choudhary C (2011). "A proteome-wide, quantitative survey of in vivo ubiquitylation sites reveals widespread regulatory roles". *Mol Cell Proteomics* 10(10):M111 013284. DOI: 10.1074/mcp.M111.013284 (cit. on p. 27).

Wahl MC, Will CL, and Luhrmann R (2009). "The spliceosome: design principles of a dynamic RNP machine". *Cell* 136(4):701–18. DOI: 10.1016/j.cell.2009.02.009 (cit. on p. 29).

Wake H, Lee PR, and Fields RD (2011). "Control of local protein synthesis and initial events in myelination by action potentials". *Science* 333(6049):1647–51. DOI: 10.1126/science.1206998 (cit. on p. 19).

Wang A, Conicella AE, Schmidt HB, Martin EW, Rhoads SN, Reeb AN, Nourse A, Ramirez Montero D, Ryan VH, Rohatgi R, Shewmaker F, Naik MT, Mittag T, Ayala YM, and Fawzi NL (2018a). "A single N-terminal phosphomimic disrupts TDP-43 polymerization, phase separation, and RNA splicing". *EMBO J* 37(5). DOI: 10.15252/embj.201797452 (cit. on p. 27).

Wang IF, Chang HY, Hou SC, Liou GG, Way TD, and James Shen CK (2012a). "The self-interaction of native TDP-43 C terminus inhibits its degradation and contributes to early proteinopathies". *Nat Commun* 3:766. DOI: 10.1038/ncomms1766 (cit. on p. 21).

Wang J, Ho WY, Lim K, Feng J, Tucker-Kellogg G, Nave KA, and Ling SC (2018b). "Cell-autonomous requirement of TDP-43, an ALS/FTD signature protein, for oligodendrocyte survival and myelination". *Proc Natl Acad Sci U S A* 115(46):E10941–E10950. DOI: 10.1073/pnas.1809821115 (cit. on pp. 28, 122, 127, 131–133).

Wang L, Pytel P, Feltri ML, Wrabetz L, and Roos RP (2012b). "Selective knockdown of mutant SOD1 in Schwann cells ameliorates disease in G85R mutant SOD1 transgenic mice". *Neurobiol Dis* 48(1):52–7. DOI: 10.1016/j.nbd.2012.05.014 (cit. on p. 22).

Wang W, Li L, Lin WL, Dickson DW, Petrucelli L, Zhang T, and Wang X (2013). "The ALS disease-associated mutant TDP-43 impairs mitochondrial dynamics and function in motor neurons". *Hum Mol Genet* 22(23):4706–19. DOI: 10.1093/hmg/ddt319 (cit. on p. 130).

Wang W, Wang L, Lu J, Siedlak SL, Fujioka H, Liang J, Jiang S, Ma X, Jiang Z, Rocha EL da, Sheng M, Choi H, Lerou PH, Li H, and Wang X (2016). "The inhibition of TDP-43 mitochondrial localization blocks its neuronal toxicity". *Nat Med* 22(8):869–78. DOI: 10.1038/nm.4130 (cit. on p. 130).

Wang X, Liu Y, Li X, Zhang Z, Yang H, Zhang Y, Williams PR, Alwahab NSA, Kapur K, Yu B, Zhang Y, Chen M, Ding H, Gerfen CR, Wang KH, and He Z (2017). "Deconstruction of Corticospinal Circuits for Goal-Directed Motor Skills". *Cell* 171(2):440–455 e14. DOI: 10.1016/j.cell.2017.08.014 (cit. on p. 134).

Webster HD (1971). "The geometry of peripheral myelin sheaths during their formation and growth in rat sciatic nerves". *J Cell Biol* 48(2):348–67. DOI: 10.1083/jcb.48.2.348 (cit. on p. 9).

Weider M, Starost LJ, Groll K, Kuspert M, Sock E, Wedel M, Frob F, Schmitt C, Baroti T, Hartwig AC, Hillgartner S, Piefke S, Fadler T, Ehrlich M, Ehlert C, Stehling M, Albrecht S, Jabali A, Scholer HR, Winkler J, Kuhlmann T, and Wegner M (2018). "Nfat/calcineurin signaling promotes oligodendrocyte differentiation and myelination by transcription factor network tuning". *Nat Commun* 9(1):899. DOI: 10.1038/s41467-018-03336-3 (cit. on p. 18).

Weider M, Wegener A, Schmitt C, Kuspert M, Hillgartner S, Bosl MR, Hermans-Borgmeyer I, Nait-Oumesmar B, and Wegner M (2015). "Elevated in vivo levels of a single transcription factor directly convert satellite glia into oligodendrocyte-like cells". *PLoS Genet* 11(2):e1005008. DOI: 10.1371/journal.pgen.1005008 (cit. on p. 18).

Weiner JA and Chun J (1999). "Schwann cell survival mediated by the signaling phospholipid lysophosphatidic acid". *Proc Natl Acad Sci U S A* 96(9):5233–8. DOI: 10.1073/pnas.96.9.5233 (cit. on p. 12).

Werner HB, Kramer-Albers EM, Strenzke N, Saher G, Tenzer S, Ohno-Iwashita Y, De Monasterio-Schrader P, Mobius W, Moser T, Griffiths IR, and Nave KA (2013). "A critical role for the cholesterol-associated proteolipids PLP and M6B in myelination of the central nervous system". *Glia* 61(4):567–86. DOI: 10.1002/glia.22456 (cit. on pp. 10, 11).

Wilk HE, Angeli G, and Schafer KP (1983). "In vitro reconstitution of 35S ribonucleoprotein complexes". *Biochemistry* 22(19):4592–600. DOI: 10.1021/bi00288a038 (cit. on p. 24).

Wilkinson DG, Bhatt S, Chavrier P, Bravo R, and Charnay P (1989). "Segment-specific expression of a zinc-finger gene in the developing nervous system of the mouse". *Nature* 337(6206):461–4. DOI: 10.1038/337461a0 (cit. on p. 128).

Williams KL, Warraich ST, Yang S, Solski JA, Fernando R, Rouleau GA, Nicholson GA, and Blair IP (2012). "UBQLN2/ubiquilin 2 mutation and pathology in familial amyotrophic lateral sclerosis". *Neurobiol Aging* 33(10):2527 e3–10. DOI: 10.1016/j.neurobiolaging.2012.05.008 (cit. on p. 28).

Williams KR, Stone KL, LoPresti MB, Merrill BM, and Planck SR (1985). "Amino acid sequence of the UP1 calf thymus helix-destabilizing protein and its homology to an analogous protein from mouse myeloma". *Proc Natl Acad Sci U S A* 82(17):5666–70. DOI: 10.1073/pnas.82.17.5666 (cit. on p. 24).

Wilson L and Maden M (2005). "The mechanisms of dorsoventral patterning in the vertebrate neural tube". *Dev Biol* 282(1):1–13. DOI: 10.1016/j.ydbio.2005.02.027 (cit. on p. 16).

Winton MJ, Igaz LM, Wong MM, Kwong LK, Trojanowski JQ, and Lee VM (2008). "Disturbance of nuclear and cytoplasmic TAR DNA-binding protein (TDP-43) induces disease-like redistribution, sequestration, and aggregate formation". *J Biol Chem* 283(19):13302–9. DOI: 10.1074/jbc.M800342200 (cit. on p. 24).

Wittekind M, Gorlach M, Friedrichs M, Dreyfuss G, and Mueller L (1992). "1H, 13C, and 15N NMR assignments and global folding pattern of the RNA-binding domain of the human hnRNP C proteins". *Biochemistry* 31(27):6254–65. DOI: 10.1021/bi00142a013 (cit. on p. 23).

Wobst HJ, Delsing L, Brandon NJ, and Moss SJ (2017). "Truncation of the TAR DNA-binding protein 43 is not a prerequisite for cytoplasmic relocalization, and is suppressed by caspase inhibition and by introduction of the A90V sequence variant". *PLoS One* 12(5):e0177181. DOI: 10.1371/journal.pone.0177181 (cit. on p. 28).

Wong CE and Tsai KJ (2019). "TDP-43 proteinopathy impairs neuronal mRNP granule mediated postsynaptic local translation and mRNA metabolism". *bioRxiv*:589416. DOI: 10.1101/589416 (cit. on p. 27).

Wong JJ, Ritchie W, Ebner OA, Selbach M, Wong JW, Huang Y, Gao D, Pinello N, Gonzalez M, Baidya K, Thoeng A, Khoo TL, Bailey CG, Holst J, and Rasko JE (2013). "Orchestrated intron retention regulates normal granulocyte differentiation". *Cell* 154(3):583–95. DOI: 10.1016/j.cell.2013.06.052 (cit. on p. 31).

Woodhoo A, Alonso MB, Droggiti A, Turmaine M, D'Antonio M, Parkinson DB, Wilton DK, Al-Shawi R, Simons P, Shen J, Guillemot F, Radtke F, Meijer D, Feltri ML, Wrabetz L, Mirsky R, and Jessen KR (2009). "Notch controls embryonic Schwann cell differentiation, postnatal myelination and adult plasticity". *Nat Neurosci* 12(7):839–47. DOI: 10.1038/nn.2323 (cit. on pp. 12, 14, 52).

Wu H, Williams J, and Nathans J (2014). "Complete morphologies of basal forebrain cholinergic neurons in the mouse". *Elife* 3:e02444. DOI: 10.7554/eLife.02444 (cit. on p. 4).

Wu LS, Cheng WC, Chen CY, Wu MC, Wang YC, Tseng YH, Chuang TJ, and Shen CJ (2019). "Transcriptomopathies of pre- and post-symptomatic frontotemporal dementia-like mice with TDP-43 depletion in forebrain neurons". *Acta Neuropathol Commun* 7(1):50. DOI: 10.1186/s40478-019-0674-x (cit. on p. 124).

Wu LS, Cheng WC, Hou SC, Yan YT, Jiang ST, and Shen CK (2010). "TDP-43, a neuro-pathosignature factor, is essential for early mouse embryogenesis". *Genesis* 48(1):56–62. DOI: 10.1002/dvg.20584 (cit. on pp. 24, 122).

Wu LS, Cheng WC, and Shen CK (2012a). "Targeted depletion of TDP-43 expression in the spinal cord motor neurons leads to the development of amyotrophic lateral sclerosis-like phenotypes in mice". *J Biol Chem* 287(33):27335–44. DOI: 10.1074/jbc.M112.359000 (cit. on p. 124).

Wu M, Hernandez M, Shen S, Sabo JK, Kelkar D, Wang J, O'Leary R, Phillips GR, Cate HS, and Casaccia P (2012b). "Differential modulation of the oligodendrocyte transcriptome by sonic hedgehog and bone morphogenetic protein 4 via opposing effects on histone acetylation". *J Neurosci* 32(19):6651–64. DOI: 10.1523/JNEUROSCI.4876-11.2012 (cit. on p. 18).

Wyss MT, Jolivet R, Buck A, Magistretti PJ, and Weber B (2011). "In vivo evidence for lactate as a neuronal energy source". *J Neurosci* 31(20):7477–85. DOI: 10.1523/JNEUROSCI.0415-11.2011 (cit. on p. 19).

Xiao S, Sanelli T, Dib S, Sheps D, Findlater J, Bilbao J, Keith J, Zinman L, Rogaeva E, and Robertson J (2011). "RNA targets of TDP-43 identified by UV-CLIP are deregulated in ALS". *Mol Cell Neurosci* 47(3):167–80. DOI: 10.1016/j.mcn.2011.02.013 (cit. on pp. 26, 138).

Xin M, Yue T, Ma Z, Wu FF, Gow A, and Lu QR (2005). "Myelinogenesis and axonal recognition by oligodendrocytes in brain are uncoupled in Olig1-null mice". *J Neurosci* 25(6):1354–65. DOI: 10.1523/JNEUROSCI.3034-04.2005 (cit. on p. 9).

Yamashita T, Hideyama T, Hachiga K, Teramoto S, Takano J, Iwata N, Saido TC, and Kwak S (2012). "A role for calpain-dependent cleavage of TDP-43 in amyotrophic lateral sclerosis pathology". *Nat Commun* 3:1307. DOI: 10.1038/ncomms2303 (cit. on p. 28).

Yan Q, Weyn-Vanhentenryck SM, Wu J, Sloan SA, Zhang Y, Chen K, Wu JQ, Barres BA, and Zhang C (2015). "Systematic discovery of regulated and conserved alternative exons in the mammalian brain reveals NMD modulating chromatin regulators". *Proc Natl Acad Sci U S A* 112(11):3445–50. DOI: 10.1073/pnas.1502849112 (cit. on p. 31).

Yang C, Wang H, Qiao T, Yang B, Aliaga L, Qiu L, Tan W, Salameh J, McKenna-Yasek DM, Smith T, Peng L, Moore MJ, Brown R. H. J, Cai H, and Xu Z (2014). "Partial loss of TDP-43 function causes phenotypes of amyotrophic lateral sclerosis". *Proc Natl Acad Sci U S A* 111(12):E1121–9. DOI: 10.1073/pnas.1322641111 (cit. on p. 122).

Yap K, Lim ZQ, Khandelia P, Friedman B, and Makeyev EV (2012). "Coordinated regulation of neuronal mRNA steady-state levels through developmentally controlled intron retention". *Genes Dev* 26(11):1209–23. DOI: 10.1101/gad.188037.112 (cit. on p. 31).

Ye F, Chen Y, Hoang T, Montgomery RL, Zhao XH, Bu H, Hu T, Taketo MM, Es JH van, Clevers H, Hsieh J, Bassel-Duby R, Olson EN, and Lu QR (2009). "HDAC1 and HDAC2 regulate oligodendrocyte differentiation by disrupting the beta-catenin-TCF interaction". *Nat Neurosci* 12(7):829–38. DOI: 10.1038/nn.2333 (cit. on p. 18).

Ye J, Coulouris G, Zaretskaya I, Cutcutache I, Rozen S, and Madden TL (2012). "Primer-BLAST: a tool to design target-specific primers for polymerase chain reaction". *BMC Bioinformatics* 13:134. DOI: 10.1186/1471-2105-13-134 (cit. on p. 40).

Ye P, Carson J, and D'Ercole AJ (1995). "In vivo actions of insulin-like growth factor-I (IGF-I) on brain myelination: studies of IGF-I and IGF binding protein-1 (IGFBP-1) transgenic mice". *The Journal of Neuroscience* 15(11):7344–7356. DOI: 10.1523/jneurosci.15-11-07344.1995 (cit. on p. 17).

Yeung MS, Zdunek S, Bergmann O, Bernard S, Salehpour M, Alkass K, Perl S, Tisdale J, Possnert G, Brundin L, Druid H, and Frisen J (2014). "Dynamics of oligodendrocyte generation and myelination in the human brain". *Cell* 159(4):766–74. DOI: 10.1016/j.cell.2014.10.011 (cit. on p. 135).

Young JZ (1938). "The functioning of the giant nerve fibres of the squid". *Journal of Experimental Biology* 15(2): 170–185 (cit. on p. 5).

Young KM, Psachoulia K, Tripathi RB, Dunn SJ, Cossell L, Attwell D, Tohyama K, and Richardson WD (2013). "Oligodendrocyte dynamics in the healthy adult CNS: evidence for myelin remodeling". *Neuron* 77(5):873–85. DOI: 10.1016/j.neuron.2013.01.006 (cit. on p. 135).

Yu WM, Feltri ML, Wrabetz L, Strickland S, and Chen ZL (2005). "Schwann cell-specific ablation of laminin gamma1 causes apoptosis and prevents proliferation". *J Neurosci* 25(18):4463–72. DOI: 10.1523/JNEUROSCI.5032-04.2005 (cit. on pp. 52, 137).

Yu Y, Chen Y, Kim B, Wang H, Zhao C, He X, Liu L, Liu W, Wu LM, Mao M, Chan JR, Wu J, and Lu QR (2013). "Olig2 targets chromatin remodelers to enhancers to initiate oligodendrocyte differentiation". *Cell* 152(1-2):248–61. DOI: 10.1016/j.cell.2012.12.006 (cit. on p. 18).

Zaimi A, Duval T, Gasecka A, Cote D, Stikov N, and Cohen-Adad J (2016). "AxonSeg: Open Source Software for Axon and Myelin Segmentation and Morphometric Analysis". *Front Neuroinform* 10:37. DOI: 10.3389/fninf.2016.00037 (cit. on p. 46).

Zarnack K, Konig J, Tajnik M, Martincorena I, Eustermann S, Stevant I, Reyes A, Anders S, Luscombe NM, and Ule J (2013). "Direct competition between hnRNP C and U2AF65 protects the transcriptome from the exonization of Alu elements". *Cell* 152(3):453–66. DOI: 10.1016/j.cell.2012.12.023 (cit. on p. 32).

Zeger M, Popken G, Zhang J, Xuan S, Lu QR, Schwab MH, Nave KA, Rowitch D, D'Ercole AJ, and Ye P (2007). "Insulin-like growth factor type 1 receptor signaling in the cells of oligodendrocyte lineage is required for normal in vivo oligodendrocyte development and myelination". *Glia* 55(4):400–11. DOI: 10.1002/glia.20469 (cit. on p. 17).

Zhang H and Miller RH (1996). "Density-dependent feedback inhibition of oligodendrocyte precursor expansion". *J Neurosci* 16(21):6886–95 (cit. on p. 18).

Zhang Y, Chen K, Sloan SA, Bennett ML, Scholze AR, O'Keeffe S, Phatnani HP, Guarnieri P, Caneda C, Ruderisch N, Deng S, Liddelow SA, Zhang C, Daneman R, Maniatis T, Barres BA, and Wu JQ (2014). "An RNA-sequencing transcriptome and splicing database of glia, neurons, and vascular cells of the cerebral cortex". *J Neurosci* 34(36): 11929–47. DOI: 10.1523/JNEUROSCI.1860-14.2014 (cit. on p. 87).

Zhang YJ, Caulfield T, Xu YF, Gendron TF, Hubbard J, Stetler C, Sasaguri H, Whitelaw EC, Cai S, Lee WC, and Petrucelli L (2013). "The dual functions of the extreme N-terminus of TDP-43 in regulating its biological activity and inclusion formation". *Hum Mol Genet* 22(15):3112–22. DOI: 10.1093/hmg/ddt166 (cit. on p. 24).

Zhang YJ, Xu YF, Dickey CA, Buratti E, Baralle F, Bailey R, Pickering-Brown S, Dickson D, and Petrucelli L (2007). "Progranulin mediates caspase-dependent cleavage of TAR DNA binding protein-43". *J Neurosci* 27(39):10530–4. DOI: 10.1523/JNEUROSCI.3421-07.2007 (cit. on p. 28).

Zhao C, Deng Y, Liu L, Yu K, Zhang L, Wang H, He X, Wang J, Lu C, Wu LN, Weng Q, Mao M, Li J, Es JH van, Xin M, Parry L, Goldman SA, Clevers H, and Lu QR (2016). "Dual regulatory switch through interactions of Tcf7l2/Tcf4 with stage-specific partners propels oligodendroglial maturation". *Nat Commun* 7:10883. DOI: 10.1038/ncomms10883 (cit. on p. 18).

Zhao M, Kim JR, Bruggen R van, and Park J (2018). "RNA-Binding Proteins in Amyotrophic Lateral Sclerosis". *Mol Cells* 41(9):818–829. DOI: 10.14348/molcells.2018.0243 (cit. on p. 21).

Zhou Q, Choi G, and Anderson DJ (2001). "The bHLH transcription factor Olig2 promotes oligodendrocyte differentiation in collaboration with Nkx2.2". *Neuron* 31(5):791–807. DOI: 10.1016/s0896-6273(01)00414-7 (cit. on p. 16).

Zhou Q, Wang S, and Anderson DJ (2000). "Identification of a novel family of oligodendrocyte lineage-specific basic helix-loop-helix transcription factors". *Neuron* 25(2):331–43. DOI: 10.1016/s0896-6273(00)80898-3 (cit. on p. 16).

Zhu Q, Zhao X, Zheng K, Li H, Huang H, Zhang Z, Mastracci T, Wegner M, Chen Y, Sussel L, and Qiu M (2014). "Genetic evidence that Nkx2.2 and Pdgfra are major determinants of the timing of oligodendrocyte differentiation in the developing CNS". *Development* 141(3):548–55. DOI: 10.1242/dev.095323 (cit. on p. 18).

Zielasek J, Martini R, and Toyka KV (1996). "Functional abnormalities in P0-deficient mice resemble human hereditary neuropathies linked to P0 gene mutations". *Muscle & Nerve* 19(8):946–952. DOI: 10.1002/(sici)1097-4598(199608)19:8<946::Aid-mus2>3.0.Co;2-8 (cit. on p. 38).

Zou ZY, Zhou ZR, Che CH, Liu CY, He RL, and Huang HP (2017). "Genetic epidemiology of amyotrophic lateral sclerosis: a systematic review and meta-analysis". *Journal of Neurology Neurosurgery and Psychiatry* 88(7):540–549 (cit. on p. 21).

Zuchero JB and Barres BA (2013). "Intrinsic and extrinsic control of oligodendrocyte development". *Curr Opin Neurobiol* 23(6):914–20. DOI: 10.1016/j.conb.2013.06.005 (cit. on p. 18).